Structural, stratigraphic and geodynamic controls on the evolution of the Carboniferous succession of northern England and southern Scotland

Thesis submitted for the degree of Doctor of Philosophy

Louis Philip Howell, December 2021, Keele University

Abstract

This thesis helps determine some key structural and geodynamic controls on the evolution of Carboniferous basins in northern England and Scotland. One key control on early Carboniferous (rift) basin evolution in northern England is the role of buoyant and pre-existing granite intrusions in causing localised basement highs. To investigate this relationship, lithosphere-scale numerical modelling and sedimentological approaches are combined. Whereas rift basins are typically considered to be largely normal fault driven systems, lithosphere-scale numerical modelling of the Pennine Basin highlights the role of flexural isostasy in determining basin geometry. Sedimentological-based studies of the Fell Sandstone Formation show that aspects of the basin fill do not conform well with classically depicted models for the region. Highlighted divergences from these models relate to occurrences of granite-cored basement domes or monoclines, whose origins as basement highs are associated with buoyancy and flexural isostatic processes.

Local seismic and borehole-based mapping of the late Carboniferous succession in the Canonbie Coalfield and in the Midland Valley of Scotland provides evidence of repeated episodes of positive inversion and unconformities. Three phases of accelerated intra-basin deformation are identified: during the middle-late Namurian, the Duckmantian-Bolsovian, and Asturian-Stephanian. Regional depositional and subsidence trends and more local depositional and structural trends help inform an original structural and geodynamic model for the late Carboniferous basins of the British Isles. It is suggested that northern England and Scotland formed part of an extensive 'broken' Variscan foreland system during late Carboniferous times.

The regional structural and geodynamic frameworks for the Carboniferous succession of northern England and Scotland presented in this thesis could be used in combination with other tools, such as the regional subsurface temperature modelling methodology presented, to aid deep geothermal exploration and offshore petroleum exploration. More importantly, they may help reinvigorate research into these rocks.

Lead supervisor:

Dr. Stuart Egan, Senior Lecturer, School of Geography, Geology and the Environment, Keele University

Secondary supervisors:

Dr. Graham Leslie, Senior Mapping Geologist, British Geological Survey, Edinburgh

Dr. Stuart Clarke, Senior Lecturer, School of Geography, Geology and the Environment, Keele University

Acknowledgements

Table of contents

Part I

Part III: The late Carboniferous 'broken' Variscan foreland

Part IV: Deep geothermal energy in northern England and thesis synthesis

Part I

Introduction

Carboniferous bedrock forms the backbone of northern England and central Scotland (Fig. 1.1). These sediments accumulated over a period of approximately 60 million years, between 359 and 299 million years ago, in a series of basins and sub-basins that then formed part of the broader North-western European Carboniferous Basin (NWECB). They have been researched extensively over previous centuries, partly because of their economic significance for coal mining and the hydrocarbon industry. In northern England, the basins that accommodated these sediments are collectively referred to as the Pennine Basin. In central Scotland, deposition occurred along the approximately NE-SW trending Midland Valley of Scotland.

The Carboniferous successions of England and Scotland are rarely described collectively. The northern part of the Pennine Basin is characterised by a series of deep extensional half-grabens, troughs and sag basins, within which thick early Carboniferous (Mississippian) successions are preserved (Johnson, 1984). These basins are separated by areas of comparatively uplifted pre-Carboniferous basement (or blocks) (Fig. 1.1), all of which are of partly buoyant granite compositions (Fig. 1.2) (Chadwick *et al.*, 1995). In contrast, there is a pronounced oblique component to basin formation in Scotland. During the early Carboniferous Period, N-S trending depocentres appear to have formed in response to sinistral transtension (Young and Caldwell, 2019). During the middle-late Carboniferous (Pennsylvanian), sinistral transpression appears to have been reversed, causing E-W contraction, reorientation of localised depocentres and overall transpression (Underhill *et al.*, 2008).

Early Carboniferous basins were mostly compartmentalized and bathymetrically varied (Leeder, 1982). The middle-late Carboniferous successions are characterised by increasing siliciclastic influxes derived from the basin exterior (Morton *et al.*, 2001). Fluvio-deltaic sediments blanketed the NWECB throughout this time. A shift towards climatically dryer conditions took place during mid-Westphalian times (Besly, 1988), immediately before widespread (late Carboniferous-early Permian) basin inversion (Corfield *et al.*, 1996). Continued burial during
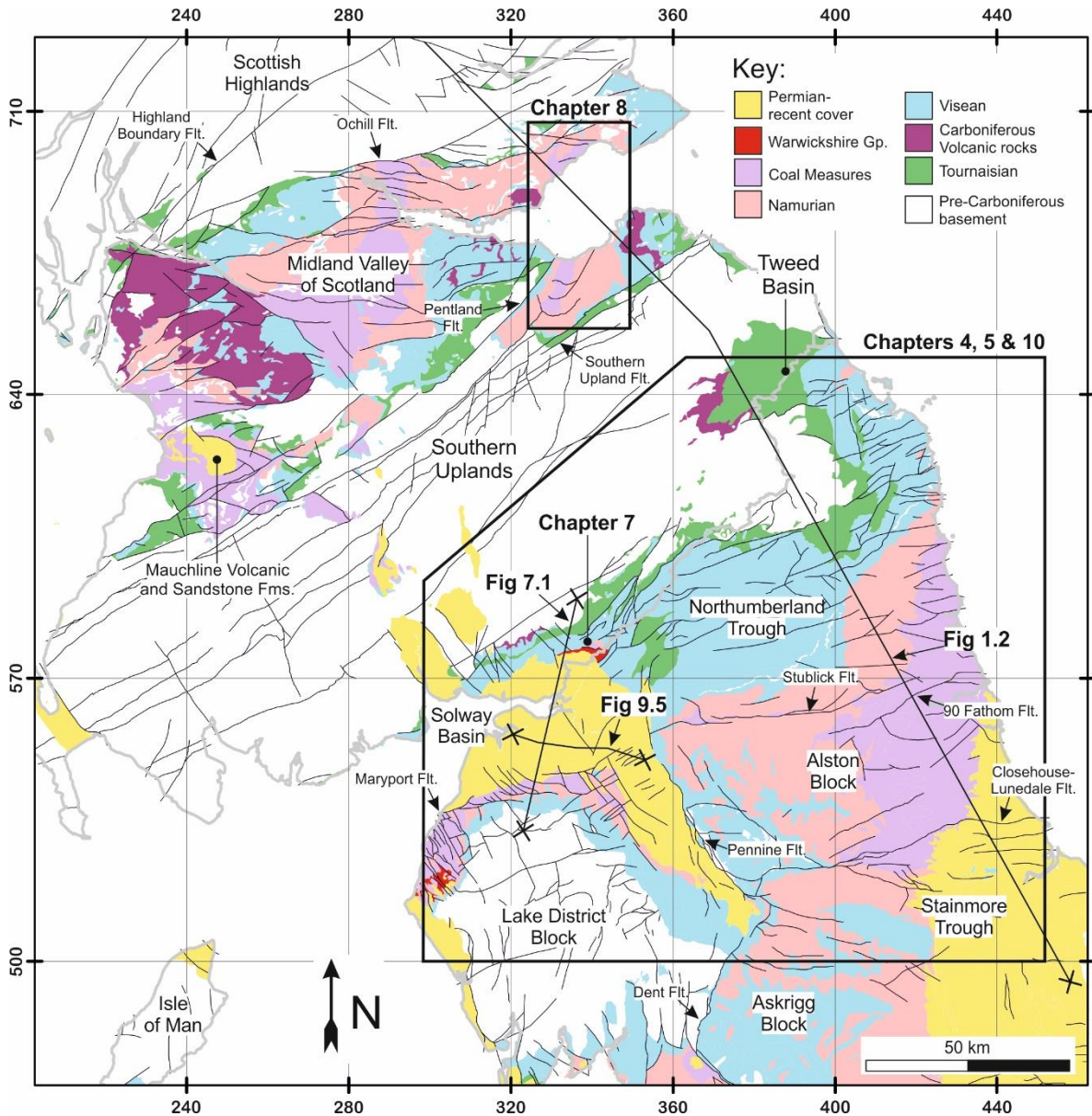
Figure 1.1: Outcropping Carboniferous geology of the northern England and Scotland. Contains BGS DiGmapGB-250 Scale data © UKRI (British Geological Survey, 2008). British National Grid (BNG) co-ordinates are used in this figure and throughout this thesis. Flt. = Fault.

Permian and Mesozoic times preceded widespread exhumation during the Palaeogene (Holford *et al.*, 2008). Consequently, much of the basin's Carboniferous stratigraphy and underpinning basement rock is now exposed or only shallowly buried across the region.

1.2 A history of Carboniferous research

The onshore Carboniferous succession of northern England and Scotland had been extensively researched even before the first published geological map of the UK by William Smith in

1820 (Strachey, 1719; Aikin, 1811; Farey, 1812). 'Carboniferous' translates literally as 'coal-bearing', thus highlighting these rocks' primary economic significance during the 18th to 20th centuries. The mineral resources hosted within Carboniferous strata fuelled the Industrial Revolution of the late 1700s to early 1800s and leave a considerable imprint on British society today (Dunham, 1990; Cann and Banks, 2001). From the mid-1960s, offshore Carboniferous strata constituted the primary gas-prone source rock for the southern North Sea gas fields, which had helped make the UK self-sufficient with regards to energy during the late 20th century (Quirk and Aitken, 1997; Clark and Jacks, 2007; Besly, 2019). More recently, as part of a worldwide effort to combat climate change by reducing our greenhouse gas emissions, Carboniferous strata have been suggested as possible solutions to carbon capture and sequestration (CCS), geothermal energy and underground hydrogen storage problems (Jones *et al.*, 2004; Ellen, 2017; Gluyas *et al.*, 2018; Heinemann *et al.*, 2018; Monaghan *et al.*, 2019).

Moreover, many of the fundamental ways in which we understand and interpret Earth processes and tectonism may still be traced to seminal studies on Carboniferous strata in northern England and Scotland. Some of Martin Bott's pioneering works on Earth gravity, magnetism and isostasy focussed upon the North Pennine Batholith (Weardale Granite) of northern England, which is concealed beneath the Alston Block in the northern Pennine Basin (Bott and Mason-Smith, 1958; Dunham *et al.*, 1961; Bott, 1967, 1978) (Fig. 1.2). The way we understand the Earth's temperature may be traced to temperature measurements made along the Rookhope Borehole (Bott *et al.*, 1972) and observations made by coal miners over a century ago (Gluyas *et al.*, 2018). Leeder and Gawthorpe's (1987, 2000) highly influential models for sedimentation in rift basins are informed by Mike Leeder's earlier work on the early Carboniferous succession of the Northumberland Trough (e.g., Leeder, 1973, 1974, 1975, 1976, 1982; Leeder and Bridges, 1978; Leeder and McMahon, 1988) and Rob Gawthorpe's work on the contemporaneous southern Pennine Basin (Gawthorpe and Clemmey, 1985; Gawthorpe, 1986, 1987; Fraser and Gawthorpe, 1990, 2003).

Research into the onshore Carboniferous basins of the British Isles has stagnated somewhat over the previous 25 years as economic interest in these rocks has waned. However, recent

initiatives such as the British Geological Survey's (BGS) 21st Century Exploration Roadmap (21CXRM): Palaeozoic Project (Monaghan *et al.*, 2017), the NERC CDT in Oil and Gas, and the UKRI GeoNetZero CDT have sought to reinvigorate research in this area. Additionally, with the increasing quantities of accessible subsurface data available through the UK Onshore Geophysical Library (UKOGL) and the BGS, there may not have been a more opportune moment to re-visit the UK Carboniferous.

1.3 Thesis overview, aims and rationale

Despite centuries of researching the onshore Carboniferous succession of the UK, numerous underpinning geodynamic and structural controls on Carboniferous sedimentary basins remain poorly understood (Fraser and Gawthorpe, 2003). More concerning and due in part to the recent partial stagnation in research, other geodynamic and structural controls are assumed well-understood despite not having been thoroughly interrogated for some time (Besly, 2019). In Chapter 2, a brief review of Carboniferous stratigraphy in northern England and Scotland is presented. This review is complemented by a correlation of published borehole sections, and isochore thickness, and palaeogeography maps for the region, which are courtesy of the BGS.

1.3.1 'Block and basin' style rift basins

The early Carboniferous northern Pennine Basin comprises a collection of basins and sub-basins that began subsiding at these times because of lithospheric extension, or rifting (Fig. 1.1). This system has been traditionally depicted as a so-called 'block and basin' style rift basin, within which comparatively elevated basement highs or basin margins are underpinned by low-density, or buoyant, pre-existing granite intrusions (Fig. 1.2) (Johnson, 1967). The use of a predictive 'block and basin' type model for deposition has become somewhat out-dated since its inadvertent inception in the early 20th century (Marr, 1921). Nowadays, rift basins are typically depicted as systems driven by the mechanics and interactions of normal faulting (Gawthorpe and Leeder, 2000). However, because of the influence of 'buoyant' granite intrusions, the northern Pennine Basin provides a unique case study compared with these more widely used examples of rift basin systems. One key aim of this thesis will be to reduce the uncertainties surrounding the early Carboniferous (syn-rift)

evolution of the northern Pennine Basin. Throughout Part II of this thesis, key structural and geodynamic controls on the geometry of the basin and the basin's influence on sedimentation during rifting are investigated.

In Chapter 3, a review of the early Carboniferous evolution of the northern Pennine Basin is presented, focussing on the alleged influence of buoyant granite intrusions on localised uplift, basement highs and depositional trends on rifting. A lithosphere scale numerical modelling approach was considered key to generating generic areas of learning and determining the scope of this part of the thesis. In Chapter 4, this approach is adopted to determine the role of normal faulting, granite intrusions and flexural isostasy on basin geometry. The Fell Sandstone Formation became a target for investigation because of its position within the (middle-late) syn-rift sequence of the northern Pennine Basin (Fraser and Gawthorpe, 1990), the vastness of subsurface data and available outcrop for this interval, and some of the hitherto poorly understood regional trends preserved within the formation, particularly within the Tweed Basin and along the eastern flank of the Cheviot Block, which have been previously described in academic literature (e.g., Turner *et al.*, 1993). In Chapter 5, the influences of basin geometry on the sedimentological characteristics and sedimentary provenance relationships of this unit are investigated. Some of the diachronous and base syn-rift units of the northern Pennine Basin should be considered key to understanding the more dynamic effects of normal faulting, granite intrusions and flexural isostasy on early Carboniferous basin evolution. These units include the Roddam Dene Conglomerate and Ballagan formations of the Inverclyde Group in northern Northumberland, and the Pinksey Gill and Marsett formations of the Ravenstonedale Group in the western Pennine and the Lake District. The omission of a study focussing on these intervals was due to time restrictions. However, such a study is suggested as one potential area of future research interest.

1.3.2 The late Carboniferous 'broken' Variscan foreland

Although the sediments that accumulated in the late Carboniferous basins of northern England and Scotland represent some of the most widely researched stratigraphic intervals in the world, the Scottish and Pennine Coal Measures groups, the origin of these basins remains enigmatic

(Leeder and McMahon, 1988). Despite the small area of comparatively stable basement rock separating contemporaneous basins in northern England and central Scotland, the alleged late Carboniferous evolution of these respective systems contrasts markedly. Whereas the late Carboniferous basins of northern England are believed to have subsided because of post-rift or thermally induced sagging (e.g., Fraser and Gawthorpe, 1990), central Scotland is believed to have been incorporated within a regional NE-trending (dextral) wrench zone (Read and Forsyth, 1989).

In Part III of this thesis, one further aim of this thesis is presented, which is to determine the key structural and geodynamic controls on the late Carboniferous evolution of basins in both northern England and central Scotland. In Chapter 6, several theories concerning late Carboniferous sedimentation in northern England, central Scotland, and the remainder of the British Isles are presented and reviewed (e.g., Leeder, 1982; Dewey, 1982; Besly, 1988). This leads on to Chapters 7 and 8 in which two seismic and borehole-based mapping exercises are presented that help highlight localised controls on the late Carboniferous depocentres, in the Canonbie Coalfield and the eastern part of the Midland Valley of Scotland, respectively. The Canonbie Coalfield was chosen as a potential area of interest because of its extensive preserved (late Carboniferous) stratigraphy (Jones *et al.*, 2011) and the presence of multiple and hitherto unexplained intra-formational unconformities evident from seismic reflection profiles (Picken, 1988). Likewise, the eastern part of the Midland Valley of Scotland was chosen as an area of interest because of its extensive late Carboniferous stratigraphy (Ewing and Francis, 1961), and after brief consultation with vintage coal authority seismic in the Midland Valley, strong and possibly regionally significant similarities were recognised between the seismic characteristics of the late Carboniferous sequence here and in the Canonbie Coalfield. In Chapter 8, subsurface mapping of the Midland Valley of Scotland is integrated with a sedimentological investigation of the late Carboniferous sequence exposed here. It was the intention of the author to continue the sedimentological investigations that began at Prestonpans and Port Seton along the Lothian coastline, towards Joppa, and across the Firth of Forth to the Fife coastline. However, travel restrictions due to the coronavirus pandemic prohibited this. These analyses are integrated further in Chapter 9 with regional subsidence plots, metadata, and reports to determine key tectonic and geodynamic controls on more regional trends.
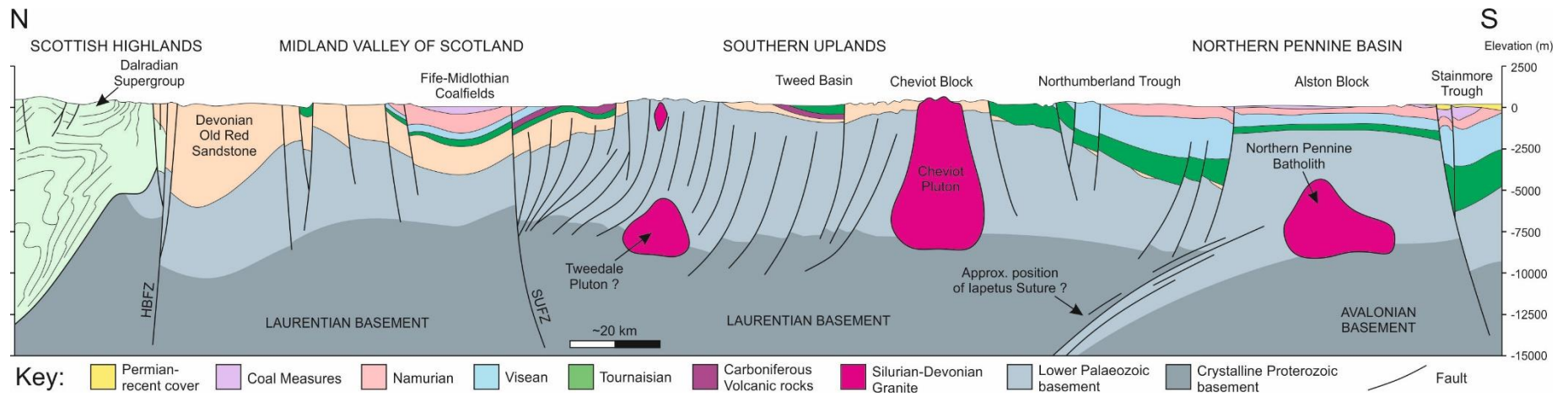
Figure 1.2: A regional cross-section through northern England and Scotland (adapted from Stone, 2008). HBFZ = Highland Boundary Fault Zone; SUFZ = Southern Upland Fault Zone. For cross-section location, see Figure 1.1.

1.3.3 Deep geothermal energy in northern England and thesis synthesis

In the UK and upon its adjacent continental shelf, the mining of Carboniferous strata for coal has mostly diminished and the production of gas sourced from Carboniferous coals in the southern North Sea is declining. However, in the 21st century, the subsurface is increasingly being talked about as one way of combatting climate change. In Part IV of this thesis, a final aim is to help reduce some of the uncertainties surrounding one way in which the subsurface of northern England could be exploited more sustainably to meet energy demands, through deep geothermal energy. Deep geothermal energy was chosen as a further area of interest because of some recent high-profile investments in the region (e.g., Manning *et al.*, 2007; Younger *et al.*, 2016; Watson and Westaway, 2020) and the likely positive role that numerical modelling may yet play in determining the UK's geothermal resource potential. In Chapter 10, an original numerical modelling-based methodology is presented that is designed to help quantify regional subsurface temperature and heat flow density variations. Contoured equivalents to the maps presented in this chapter are amongst the most widely cited in UK geothermal research (e.g., Downing and Gray, 1986a). However, the quality of these maps is often limited by the sparse amounts of reliable subsurface temperature data (Rollin, 1995) and, consequently, depicted subsurface temperatures do not always realistically reflect geological controls. In a closing chapter, Chapter 11, the key findings presented in this thesis are summarised. Key generic learnings are outlined and some possibilities for future research are suggested.

1.4 Data and methods

A wide range of data and contrasting interpretation and analysis techniques have been adopted for this study. The investigations presented in Chapters 4 and 10 are based on numerical modelling approaches. In Chapter 4, a 2D lithosphere scale structural and geodynamic numerical modelling approach is adopted so that several lithospheric extension scenarios can be validated. These methods were first developed and are described in detail by Egan (1992), Egan *et al.* (1999) and Egan and Meredith (2007), amongst others. Java code has been developed to account for the influences of buoyant granite intrusion and flexural isostasy. In Chapter 10, an original numerical

modelling-based method, developed in MATLAB, is presented and used to predict subsurface temperature and heat flow density across northern England. This method implements a rigid 3D finite difference-based technique. However, this technique is amended so that complex geological models can be more accurately incorporated within temperature predictions. Comparisons are made between this model and similar finite element-based or smaller-scale finite difference-based methodologies (e.g., Bayer *et al.*, 1997; Jacquey and Cacace, 2017).

More conventional sedimentological based methods are adopted in Chapters 5 and 8. In these chapters, over 1 km of drillcore and outcrop exposure are logged, documenting grain size, sedimentary structures and palaeocurrent trends, where possible. In Chapter 5, so that gamma ray logs from borehole data within the Northumberland-Solway Basin can be incorporated within these investigations, gamma ray responses of one drillcore succession are recorded. Drillcore and drillcore samples from the Stonehaugh and Harton boreholes were curated and provided by the BGS at Keyworth. These methods are combined further with petrographic and geochemical sedimentary provenance analyses. Sedimentary provenance analyses were performed at Keele University using X-ray fluorescence (XRF) and optical microscope tools. Rock samples and thin sections were taken from drillcore and outcrop samples and prepared at Keele University.

Areas such as the Canonbie Coalfield and the Firth of Forth are associated with high quality seismic data and a dense coverage of deep (>100 m) borehole data (Figs. 1.3a and 1.3b). These areas were considered ideal for the purposes of some study objectives. Further potential areas of interest, such as the Vale of Eden Basin and the western Pennines, are not associated with as much subsurface data and were not investigated as keenly, therefore. Owing to the age of some of the data acquired, specifically for the offshore Solway Firth area and for the southern part of the Solway Basin, data for some regions was in no fit state to be incorporated into this study. Omissions of stratigraphy were made on similar grounds. The Fell Sandstone Formation still constitutes an important aquifer in north-eastern Northumberland and was the primary reservoir target during a short-lived period of onshore hydrocarbon exploration in the late 1980s (Barrett, 1988). Compared to the immediately overlying Scremerston Formation, therefore, the Fell Sandstone Formation has
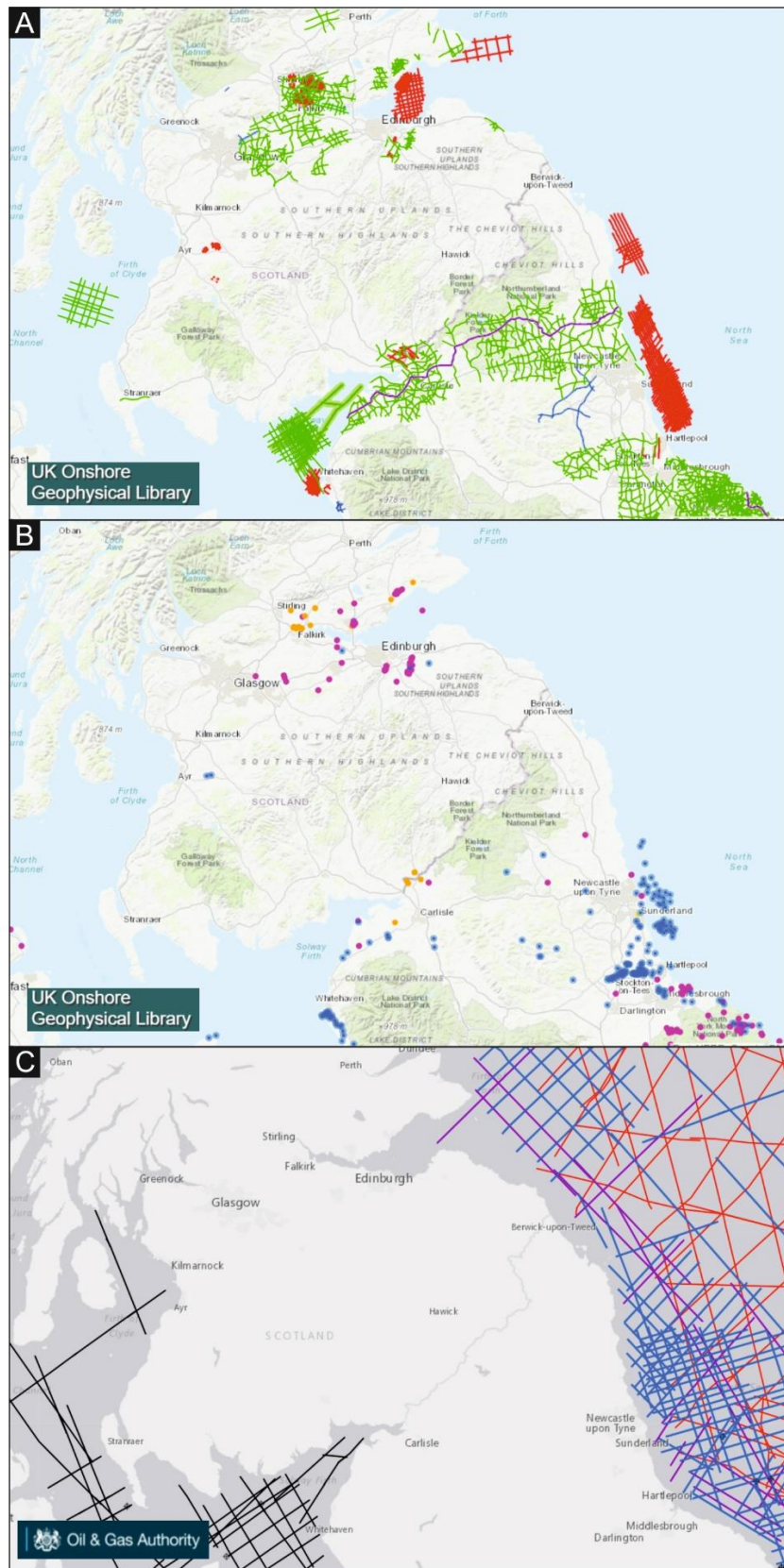
Figure 1.3a: Seismic data available onshore, and for the immediately surrounding offshore area, courtesy of UKOGL. Figure 1.3b: Borehole data available courtesy of UKOGL. Note that further borehole data can be found through the BGS' onshore Geoindex. Figure 1.3c: Seismic data available offshore courtesy of the UK National Data Repository (NDR).

been more frequently documented in academic literature and industry reports and provided a more favourable interval for potential research.

In Chapters 7 and 8, structural trends have been mapped from the interpretation of 2D seismic reflection profiles and borehole data. Borehole data is derived from a variety of sources, including from the BGS' collection of online borehole scans (onshore Geoindex), their physical collection of borehole scans at Keyworth, from UKOGL, or from literature. Seismic reflection profiles were acquired between the 1970s and 1990s for the purpose of coal and hydrocarbon exploration. All seismic data used in this thesis has been curated and is provided by UKOGL. Maps showing all available UKOGL data for the study area is presented in Figures 1.3a and 1.3b, alongside a comparison of all data made available offshore by the UK National Data Repository (NDR) (Fig. 1.3c). The various data and methods adopted for this study are described in greater detail towards the beginning of each chapter.

Carboniferous tectonics and stratigraphy

2.1 Introduction

The diverse lithofacies that are preserved within Carboniferous basins of the UK are partly a consequence of complex tectonic processes and varied subsidence mechanisms. These basins initially formed in response to latest Devonian to early Carboniferous rifting, during which period pre-Carboniferous intra-basin highs separated deeper half-grabens, troughs, or sag basins (Leeder, 1982; Fraser and Gawthorpe, 1990). Following rifting, siliciclastic sediments blanketed north-western Europe and infilled most relict palaeo-relief (Collier, 1989). Despite the economic importance of Carboniferous sediments over recent centuries, a coherent regional basin framework for the Carboniferous succession has thus far alluded geologists (Leeder and McMahon, 1988). This may be partly explained by the, often contradictory, lithostratigraphical frameworks for the Carboniferous succession. Onshore Carboniferous strata of the UK had been locally mined for coal and mineral resources, and construction materials long before the application of any regional lithostratigraphical scheme. Lithostratigraphy for the onshore Carboniferous succession has been traditionally localised, as a result, hindering attempts to understand structural or geodynamic controls on regional depositional trends. There have been notable recent attempts to rectify issues associated with Carboniferous lithostratigraphy (Browne *et al.*, 1999, 2002; Waters *et al.*, 2007; Waters *et al.*, 2011; Dean *et al.*, 2011). The lithostratigraphic nomenclature proposed by these works are adopted throughout this thesis. Prior to these works, there had been no systematic review of Carboniferous stratigraphy for the onshore UK area for some time (e.g., George *et al.*, 1976; Ramsbottom, 1979).

In this chapter, an up-to-date lithostratigraphical framework for the onshore UK Carboniferous succession is outlined and then reviewed along with current chronostratigraphical constraints and plate tectonic setting. A compilation of lithostratigraphic columns, chronostratigraphic correlation schemes, correlation panels, palaeogeography maps, and regional scale isochronous thickness maps is presented. The Carboniferous succession of northern England and Scotland is divided into five units, based on timing of deposition and basin configurations at

these times. Apparent subsidence mechanisms and structural styles during deposition of each of these five units are reviewed, along with the *inherited* pre-Carboniferous basement and post-Carboniferous modification to Carboniferous basins.

2.2 Structural geology of northern England and southern Scotland

Carboniferous deposition post-dated a prolonged episode of widespread mountain building, magmatism and collision referred to as the Caledonian Orogeny (Rickards and Woodcock, 2005). As a result, the pre-Carboniferous basement of northern England and Scotland is characterized by a mosaic of variably deformed and metamorphosed country rock hosting comparatively buoyant intrusive granite bodies and pre-existing faults (Badenszki *et al.*, 2019) (Fig. 1.2).

From the Irish Sea and Lake District regions towards the Northumberland Trough and Mid-North Sea High, the dominant structural (Iapetan and Tornquist) trends rotate clockwise up to 60°. The pre-Carboniferous basement of England and Wales is separated from the Laurentian (Scottish, Norwegian, North American) basement by a north-dipping Iapetus suture line (Freeman *et al.*, 1988) (Fig. 2.1). The suture runs roughly NE-SW across northern England, dipping NW beneath the Southern Uplands (Soper *et al.*, 1992). North of this suture, the Laurentian basement can be subdivided into the metamorphic or orthotectonic Caledonides, north of the Highland border zone, and the paratectonic Caledonides, outcropping in the Southern Uplands (McKerrow *et al.*, 1977) (Fig. 2.1). Ordovician- Lower Devonian (Caledonian) granitoid batholiths strongly influenced deformation throughout the Carboniferous, due to their relative buoyancy, lack of internal deformation, and mechanical strength (Donato, 2020). Examples of these batholiths occur throughout north-western Europe and relatively well constrained onshore because of gravity surveys, outcropping geology, and borehole penetrations (Bott *et al.*, 1967, Kimbell *et al.*, 2010). However, because of the interferences of additional negative gravitational anomalies associated with Zechstein (Permian) salt diapirs and Mesozoic and Carboniferous basins, they are less well constrained offshore (Donato and Tully, 1982; Donato *et al.*, 1983, 1993; Zervos, 1987; Kimbell and Williamson, 2015). They are thought to have resulted from episodic decompressional melting
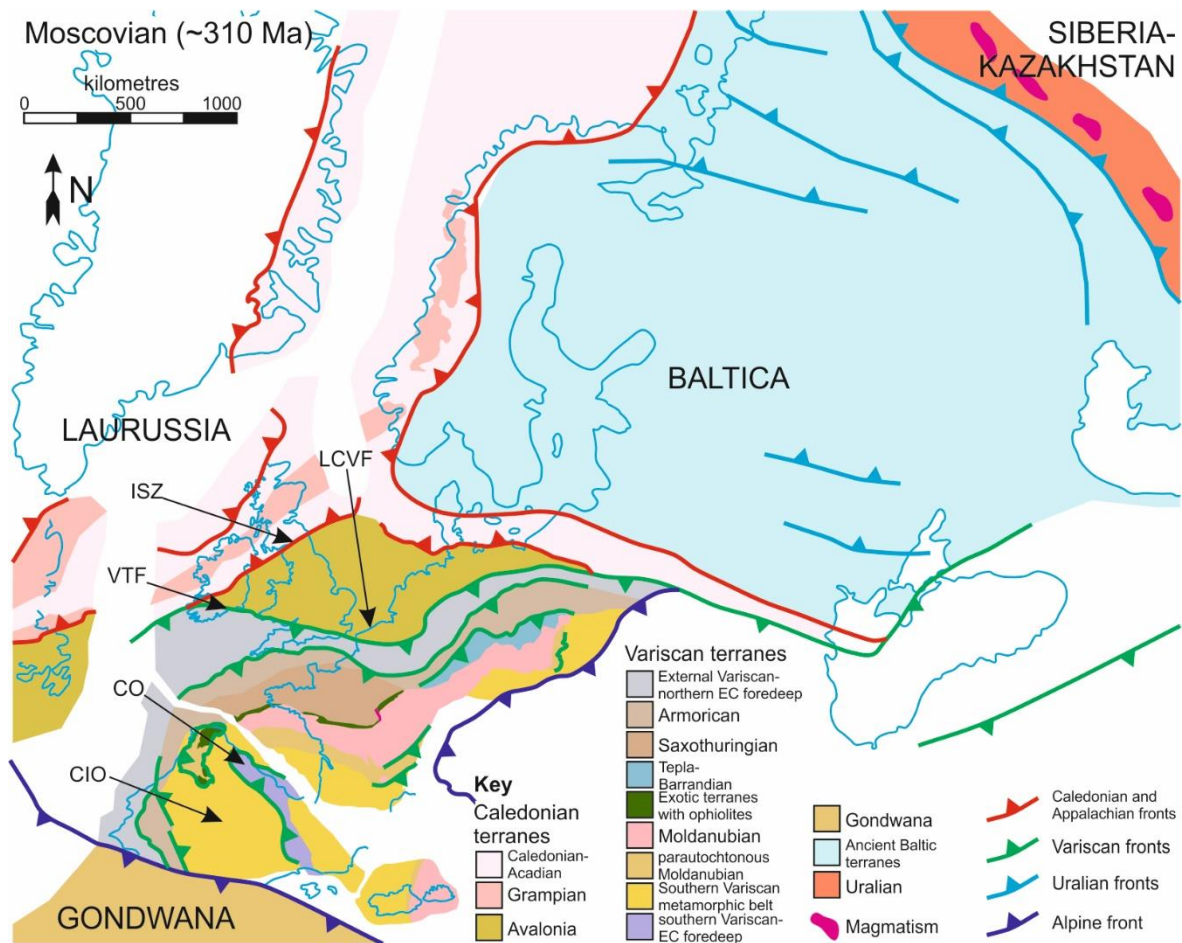
Figure 2.1: Palaeo-tectonic reconstruction of northern and western Europe for the late Carboniferous. Redrawn after Ziegler (1989), Martinez Catalan *et al.* (2007) and Kombrink (2008). ISZ = Iapetus Suture Zone; LCVF = late Carboniferous Variscan foreland; VTF = Variscan thrust-front; CO = Cantabrian orocline; CIO = Central Iberian Orocline.

following the Caledonian Orogeny (Hughes *et al.*, 1996). Brown (1979) documents the decreasing overall bulk densities with younger ages of emplacement. Whereas granite intrusions tend to form widespread clusters of smaller intrusions in Scotland, particularly in the Scottish Highlands, in northern England they form larger but mostly disconnected structures (Brown, 1979) (Fig. 1.2).

The Midland Valley of Scotland is bound to the north-west and south-east by the NE-trending Highland Boundary Fault and (also NE-trending) Southern Upland Fault System, respectively (Fig. 1.1). In the north of the basin, the approximately E-W trending Ochill Fault marks the limit of Carboniferous bedrock. To the south, some major (>50 km in length) faults, such as the Pentland and Crossgateshall faults, splay off the Southern Upland Fault System to the north. All these faults are believed to have been reactivated obliquely during Carboniferous times (Rippon

et al., 1996). The primary accommodating structures in the region were approximately NNE-trending folds, such as the Clackmannan, Midlothian and Leven Synclines (Fig. 1.2) (Underhill *et al.*, 2008). The Midland Valley of Scotland is separated from the northern Pennine Basin of northern England by the Southern Uplands, where pre-Carboniferous bedrock is exposed. The Tweed Basin appears to represent more of a sag than a clear fault-bound graben or half-graben (Millward *et al.*, 2013). The earliest Carboniferous sediments deposited here are suggested to onlap against the Cheviot Block, to the south, like those sediments deposited along the block's eastern margin (Fig. 1.2) (Robson, 1977). The Northumberland Trough is an almost textbook half-graben, which is clearly bound to the south by the vertically displacing Maryport-Ninety Fathom-Stublick Fault System (Chadwick *et al.*, 1995). The trough's western margin is less clearly defined by the approximately NE-trending Bewcastle and Carlisle anticlines, beyond which Carboniferous sediments in the Solway Basin are largely concealed (Picken, 1988). The Lake District and Alston blocks stand proud topographically above the Vale of Eden Basin and preserve thin or no Carboniferous sequences (Johnson *et al.*, 1995). The Vale of Eden is depicted as a Permo-Triassic half-graben (Chadwick et al., 1995). However, the Pennine Fault, along with the Dent and Craven faults, are interpreted as having been reactivated obliquely during Carboniferous times (e.g., Underhill *et al.*, 1988). The Askrigg Block falls just to the south of the study area (Fig. 1.1). The Stainmore Trough is found to the east of the Askrigg Block and is separated from the northerly Alston Block by the vertically displacing Closehouse-Lunedale and Butterknowle fault systems (Collier, 1989).

2.3 Plate tectonic setting

Between the Lower Devonian and the Permian, Gondwana and Gondwana-derived micro-continents collided with Laurussia. This prolonged phase of tectonism is often referred to as the Variscan orogenic cycle, which culminated with the formation of Pangaea (e.g., Grant *et al.*, 2020). Figure 2.1 is a palaeotectonic map for north-western Europe from Kombrink (2008), redrawn after Ziegler (1989), with amendments to Iberia made based on recent works by Shaw *et al.* (2012), Murphy *et al.* (2016) and references therein. The Variscan orogen is classically divided into

numerous tectonostratigraphic zones based on distinct stratigraphic, structural, magmatic, and metamorphic characteristics (e.g., Martinez-Catalan *et al.*, 2007; Shaw *et al.*, 2012; Murphy *et al.*, 2016). These zones represent different aspects of the Early Palaeozoic opening of the Rheic Ocean and the migration of terranes from the Gondwanan margin towards Laurussia.

During the Upper Devonian to early Carboniferous Period, the southern margin of Laurussia is widely depicted as a (Rheic) oceanic subduction zone (Leeder, 1982; Ziegler, 1989; Kombrink, 2008) (see 'exotic terranes with ophiolites' in Fig. 2.1). Within this framework, northern England is believed to have represented a retro-arc basin relative to the Armorican arc, present-day Cornwall, and most of central and northern France (Shail and Leveridge, 2009) (*cf.* modern day stretching in the Aegean or Tyrrhenian Seas). Some authors have depicted Iberia and smaller north African continental fragments as having formed substantial parts of this early Carboniferous arc. However, recent studies suggest that, on the contrary, neither the Cantabrian nor the Iberian oroclines had formed until latest Carboniferous times (*c.* 310 Ma; Murphy *et al.*, 2016 and references therein) (Fig. 2.1). The dominant north-easterly orientated structural grain of Scotland, eastern Greenland, Norway and the Canadian Maritimes is thought to have undergone sinistral transtension during this time (*cf.* Coward, 1993; Calder, 1998; Young and Caldwell, 2019). This is believed to have been a response to Acadian collision to the west, around present-day New York and Newfoundland (*cf.* modern day Himalayan 'escape' tectonics).

Final closure of the Rheic Ocean took place during approximately the middle Visean (Ziegler, 1989, 1990; Ziegler *et al.*, 2004; Kombrink, 2008). Otherwise, the Visean was characterized by northward subduction of the Palaeo-Tethys Ocean beneath southern and central Europe and the encroachment of these European terranes upon the Rheno-Hercynian zone, forming the early Variscan Mountains (Edel *et al.*, 2018). Around the basal Namurian boundary, the Rheno-Hercynian zone was incorporated as an external Variscan collisional zone (Oncken *et al.*, 1999) (Fig. 2.1). Towards the end of the Carboniferous (Westphalian C to Stephanian), Gondwana collided with Europe as the then Variscan foreland of the British Isles contracted (Shaw *et al.*, 2012; Copley and Woodcock, 2016). By this time, sinistral transtension along north-easterly trending structures in

Scotland and the north-western margin of the NWECB had reversed to dextral transpression (De Paola *et al.*, 2005), causing comparatively mild basin shortening in northern Britain (Read, 1988; Ritchie *et al.*, 2003). Some authors argue that this may have been a response to approximately contemporaneous Uralian compressional stresses along the eastern margin of the pre-Caledonian Baltic plate (*cf.* Coward, 1993), despite the large distances to this continental margin (Fig. 2.1).

2.4 Stratigraphic timescales

To adhere with industrial reports and previous literature, the former stratigraphic subdivisions of the Carboniferous succession for north-western Europe are adopted (e.g., Menning *et al.*, 2006). These are illustrated in Figure 2.2 (left) along with a correlation between these stratigraphic subdivisions and global stratigraphic subdivisions for this period (Davydov, 2004; Waldron *et al.*, 2017). In central and western Europe, the Carboniferous had traditionally been divided into the "Lower Carboniferous" or "Dinantian" and the "Upper Carboniferous" or "Silesian", separated at the base of the Namurian. Whilst the formal use of these timescales is now uncommon, throughout this thesis, the former Dinantian Stage is referred to as the "early" Carboniferous, as it approximately distinguishes the syn-rift sequence of northern England from younger and overlaying "late" Carboniferous sequences (e.g., Fraser and Gawthorpe, 1990).

Tournaisian and early Visean stratigraphy is mostly determined by ammonoids or miospores, thanks to work by Neves *et al.* (1973, 1974), Clayton *et al.* (1977), Pearce *et al.* (2005), amongst others. These data are used here as primary means for correlating early Carboniferous strata due to the frequent inclusion of these data within borehole reports. The miospore zonation schemes of Clayton *et al.* (1977, 1978), which were later revised by Clayton *et al.* (1985), are adopted and summarised in Figure 2.3. Where these data are absent, the early Carboniferous succession is traditionally correlated based on lithostratigraphy (Waters *et al.*, 2011). Palynostratigraphic resolution is less than that of marine bands for the Brigantian (late Visean), Namurian and Langsettian (Westphalian A) and Duckmantian (Westphalian B). These marine bands represent the transgressive parts of high amplitude eustatic sea level cycles and typically comprise distinctive fossiliferous assemblages (Ramsbottom, 1979). Thanks to the work of numerous biostratigraphers
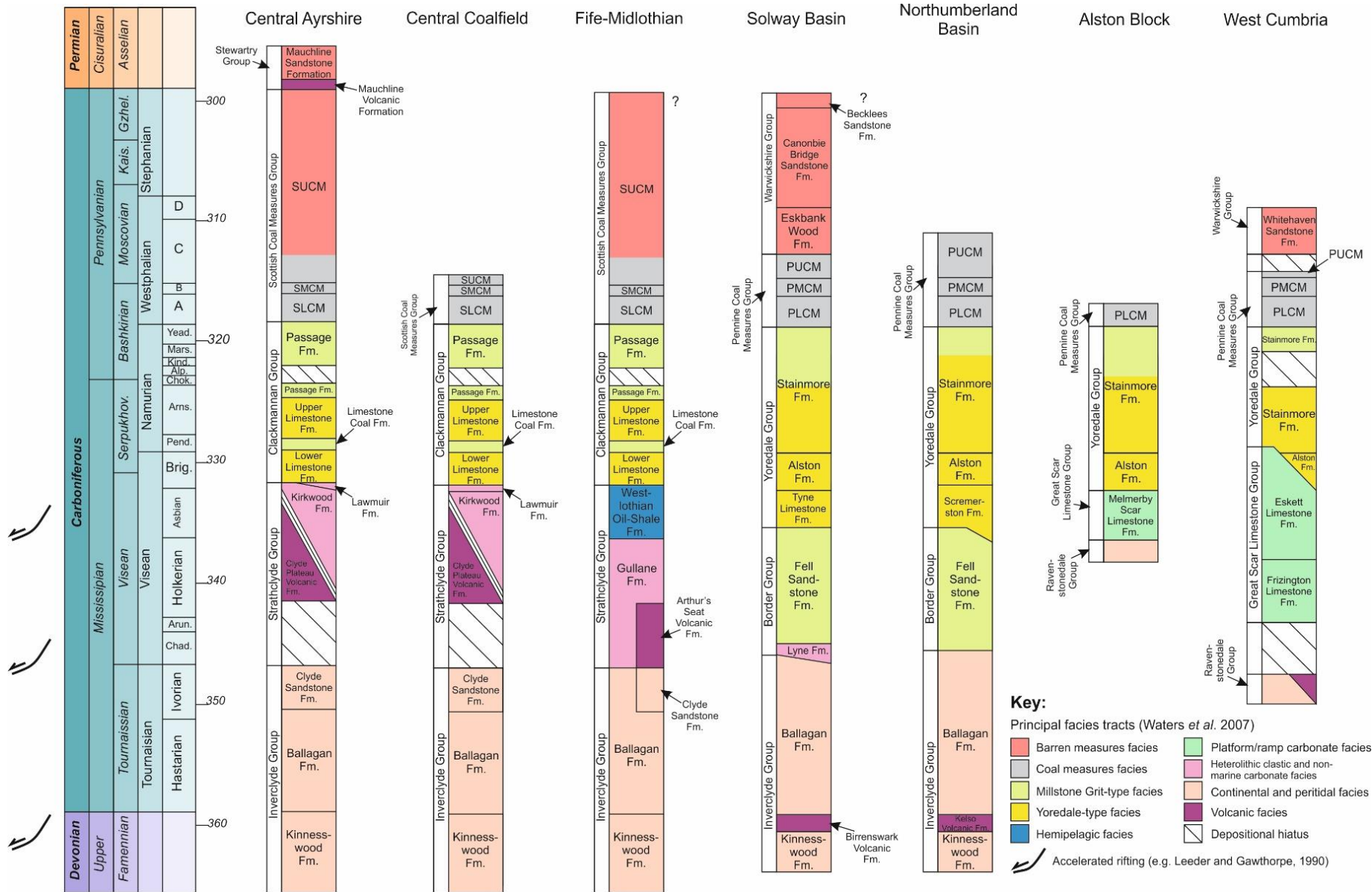
Figure 2.2: Carboniferous lithostratigraphy of the Midland Valley of Scotland and the northern Pennine Basin, modified from Waters *et al.* (2007) with alterations made to latest Carboniferous and early Permian lithostratigraphy of Fife-Midlothian and the Solway Basin based on Howell *et al.* (2020) and other findings presented in Part III of this thesis. Numerical ages and correlation between NW European Carboniferous timescale and international timescale (left) are based on Davydov *et al.* (2004).

on the Carboniferous successions of NW Europe, they provide reliable and uncomplicated means for regional chronostratigraphic correlation (Johnson *et al.*, 2011) (Fig. 2.4). On local scales, lithostratigraphically-defined coal seams may also be used for correlative purposes (e.g., McLean and Murray, 1996; McLean, 2018). In more barren sequences (Bolsovian, or Westphalian C, to Stephanian), chemostratigraphy is applied more readily to gain stratigraphic constraint (Pearce *et al.*, 1999; Powell *et al.*, 1999; Jones *et al.*, 2011). Despite these age constraints, ongoing research in this area is testament to the somewhat controversial nature of Carboniferous stratigraphic timescales (Marshall *et al.*, 2018; Ingrams *et al.*, 2020; Besly and Cleal, 2021).

2.5 Devonian

2.5.1 Frasnian and Famennian

Following Caledonian climax and a Middle Devonian episode of magmatism that resulted in the intrusion of large granitoids such as the North Pennine Batholith, Cheviot Pluton and Criffel-Dalbeattie plutons (Brown, 1979), Upper Devonian red-bed sediments progressively infilled relict palaeorelief (Leeder, 1974). Along the Scottish borders, where these units are thickest in northern England and southern Scotland, these sediments are divided into the Stratheden Group and Kinnesswood Formation (Inverclyde Group) (Browne *et al.*, 2002) (Fig. 2.1), although they are more classically referred to as the Upper Old Red Sandstone Group (Craig and Nairn, 1956; Smith, 1968) Leeder, 1973, 1974). Whilst across much of northern England similarly aged units are largely absent through non-deposition, these sediments are exposed via several classic outcrop localities in southern Scotland including at Pease Bay and Siccar Point (Greig, 1988). During the Upper Devonian (Frasnian and Fammenien), northern Britain occupied a low-lying latitude and climate was suitably arid to semi-arid. Several workers observe a mixture of aeolian, fluvial, deltaic and peri-lacustrine deposits sourced dominantly from a north-eastward flowing fluvial system and from other ill-defined hinterland regions (Leeder, 1973; Bluck, 1977; Hall and Chisholm, 1987). Floodplain deposits are characterised by calcitic or dolomitic concretions or 'cornstones', from which another of these sediments' informal lithostratigraphical names are derived (Donovan, 1982). These concretions are particularly frequent towards the basal Carboniferous boundary, owing to the then

Period	Stage	Substage	Palynozone Index
Permian	Autunian		VC
CARBONIFEROUS	Stephanian	Stephanian C	NBM
		Stephanian B	ST
		Barruelian	
		Cantabrian	OT
	Westphalian	Asturian (D)	SL
		Bolsovian (C)	NJ
		Duckmantian (B)	
		Langsettian (A)	RA
			SS
	Namurian	Yeadonian	FR
		Marsdenian	
		Kinderscoutian	KV
		Alportian	SO
		Chokierian	
		Arnsbergian	
			TK
		Pendleian	CN
	Visean	Brigantian	
			VF
		Asbian	NM
			TC
		Holkerian	TS
		Arundian	
		Chadian	Pu
	Tournaisian	Courceyan	CM
			PC
			BP
			HD
			VI
Devonian	Famenninan		LN

Figure 2.3: Palynomorph correlation scheme for the Carboniferous rocks of NW Europe. Modified from Waters *et al.* (2011), based on Clayton *et al.* (1977, 1978), and later modified by Clayton and Loboziak (1985).

	Standardised names
BOLSOVIAN	Cambriense
	Shafton
	Edmondia
	Aegiranum
DUCKMANTIAN	Sutton
	Haughton
	Clown
	Maltby
	Vanderbeckei
LANGSETTIAN	Burton Joyce
	Langley
	Amaliae
	Meadowfarm
	Parkhouse
	Listeri
	Honley
	Springwood
	Holbrook
	Subcrenatum

Figure 2.4: Empirical nomenclature for Westphalian (A, B and C) fossiliferous marine bands in the British Isles (after Ramsbottom, 1979).

arid climatic conditions and the typically low interpreted rates of sediment reworking and sediment supply prior to rift initiation in northern England (Leeder, 1976; Paterson and Hall, 1986; Marshall *et al.*, 2018).

2.6 Early Carboniferous

2.6.1 Tournaisian

The initiation of early Carboniferous rifting is considered synonymous with the eruption of alkali basalts along the Scottish borders and in the Lake District region (Lumsden *et al.*, 1967; Leeder, 1972, 1975, 1982; Kimbell *et al.*, 1989; Upton *et al.*, 2004). The Birrenswark and Kelso Volcanic Members are believed to have deposited at around the Devonian-Carboniferous boundary along the Scottish Borders (Gale *et al.*, 1979, Gale, 1985; McKerrow *et al.*, 1985; Marshall *et al.*, 2018) (Fig. 1.1). K-Ar dates of 361 ± 7 Ma for the Birrenswark Volcanic Member (de Souza, 1982)

would suggest a latest Famennian age. Similarly, Marshall *et al.* (2018) observe miospores belonging to the Famenninan LL miospore zone (Fig. 2.3) preserved within the Kelso Lavas at Carham, southern Scotland.

An uninterrupted succession transcending the Devonian-Carboniferous pre-rift/syn-rift sequence boundary is rarely observed in northern England or southern Scotland (*cf.* Deegan, 1973 and references therein). Leeder (1975) observed a pronounced north-easterly to southerly switch in palaeocurrent across the basal Carboniferous boundary (Inverclyde Group) around Langholm (Fig. 2.5), which he associated with regional tilting of the Northumberland-Solway Basin in response to movement along the Maryport-Stublick fault systems. Robson (1977) observes conglomerates bearing clasts derived from the Cheviot Granite inter-bedded with the Kelso Volcanic Member along the eastern margin of the Cheviot Block within the Roddam Dene Conglomerate Formation of the Inverclyde Group. Similar 'fan-glomerates' belonging to the Pinksey Gill and Marsett formations of the Ravenstonedale Group are observed sporadically throughout the western Pennines and along the southern and eastern margins of the Lake District Block (Burgess and Holliday, 1979). These deposits show a marked diachroneity, with earliest Tournaisian deposition occurring within basinal areas flanking the Lake District Block (Johnson and Marshall, 1970). Alluvial fan dominated deposits of the Ravenstonedale or Inverclyde groups pass vertically and laterally into deposits characterised by limestones, sandstones and mudstones with calcretes, desiccation structures and evaporite pseudomorphs that are believed to indicate deposition in quiet, nearshore to peritidal restricted marine environment (Holliday *et al.*, 1979), such as the Ballagan Formation (Waters *et al.*, 2007). The youngest Ravenstonedale Group deposits are found unconformably overlying pre-Carboniferous basement rock at the foot of the Rookhope borehole and are believed to be Holkerian-Asbian in age (Johnson *et al.*, 1995).In the western part of the Midland Valley of Scotland and particularly along the margins of this basin, deposition of the Ballagan Formation (Inverclyde Group) appears to have occurred within restricted pull-apart basins linked to sinistral fault movement along the Highland Boundary and Southern Upland fault zones (McLean and Deegan, 1978; Young and Caldwell, 2011, 2019; Jutras, 2017). The conformable base of the late Tournaisian Clyde Sandstone Formation is taken as the transition from the underlying
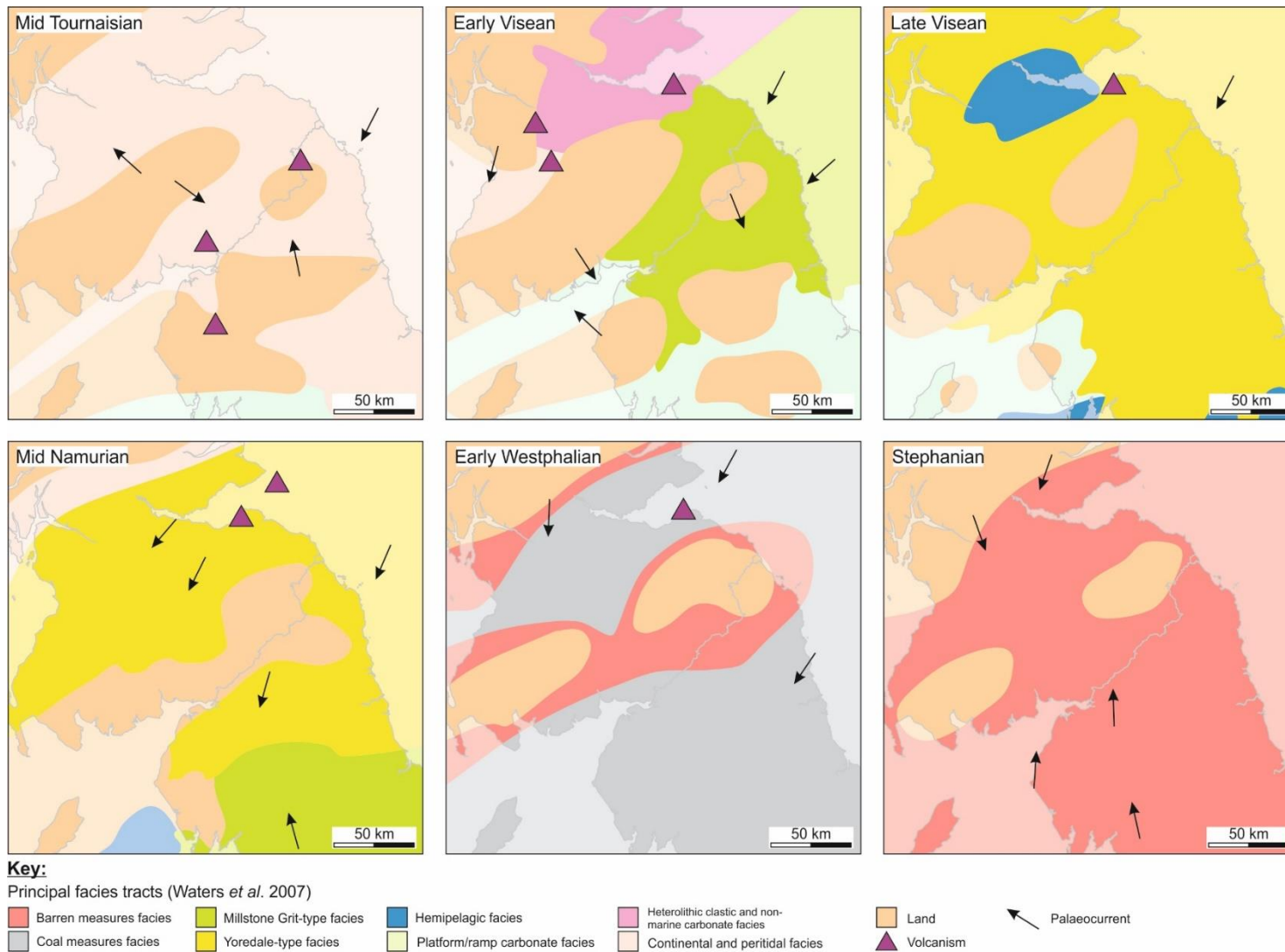
Figure 2.5: Palaeogeographic reconstructions for the Carboniferous succession of northern England and Scotland. Redrawn after Waters *et al.* (2007).

'cementstone' lithofacies group of the Ballagan Formation (*cf.* Waters *et al.*, 2007) to a sandstone-dominated succession (Paterson and Hall, 1986) (Fig. 2.2).

Early Carboniferous sedimentation is confined to broader rift basin depocentres in northern England, such as the Northumberland and Stainmore troughs and the Solway Basin (Gawthorpe, 1986, 1987; Chadwick *et al.*, 1995) (Fig. 2.5). A <4 km thick Tournaisian succession is interpreted in the southern part of the Northumberland Trough (Chadwick *et al.*, 1995) (Fig. 2.6). Alluvial and calcareous sediment was sourced primarily from granite-cored pre-Carboniferous intra-basin fault 'blocks', such as the Southern Uplands Massif and the Cheviot, Alston, Lake District and Askrigg (Nairn, 1956; Leeder, 1974; Gawthorpe, 1986; Wright, 1986; Barret, 1988; Collier, 1991) (Fig. 2.5). Such pre-Carboniferous blocks are thought to have been areas of mostly non-deposition during the early Carboniferous (*cf.* Johnson, 1984, and references therein). However, widespread occurrences of Tournaisian-aged strata in the Lake District area (Johnson and Marshall, 1970; Varker and Higgins, 1979) and the thick (*c.* 500 m) successions of early Carboniferous sediment encountered along the Alston Block's eastern margin (*cf.* Ridd *et al.*, 1970; Younger *et al.*, 2016) contradict this simplistic tectonic framework (Grayson and Oldham, 1986 and references therein).

During the Tournaisian, bathymetrically shallower fluvial and delta-dominated deposits represent geographically limited drainage systems (Leeder, 1974). In the Northumberand Trough, such deposits belong to the Whita Sands Member of the Ballagan Formation (Inverclyde Group) and the Ravenstonedale Group (Craig and Nairn, 1956; Johnson and Marshall, 1970; Varker and Higgins, 1979) (Fig. 2.2). Bathymetrically deeper deposits belong to the age-equivalent lower part of the Lyne Formation (Border Group) (Leeder, 1974; Kearsey *et al.*, 2019; Millward *et al.*, 2019). These deposits are mostly obscured beneath thick sequences of younger basinal Carboniferous successions (Chadwick *et al.*, 1995). Exposed within the core of the Bewcastle Anticline, eastern Solway Basin, these sediments comprise inter-bedded sequences of shallow marine limestones, dolomites, sandstones, siltstones and mudstones deposited in mostly freshwater deltaic-lagoonal environments (Day, 1970). However, the Easton-1 Borehole, which was drilled as an oil exploration well in an adjacent part of the Solway Basin, encountered approximately 700 m of mostly evaporitic sediments
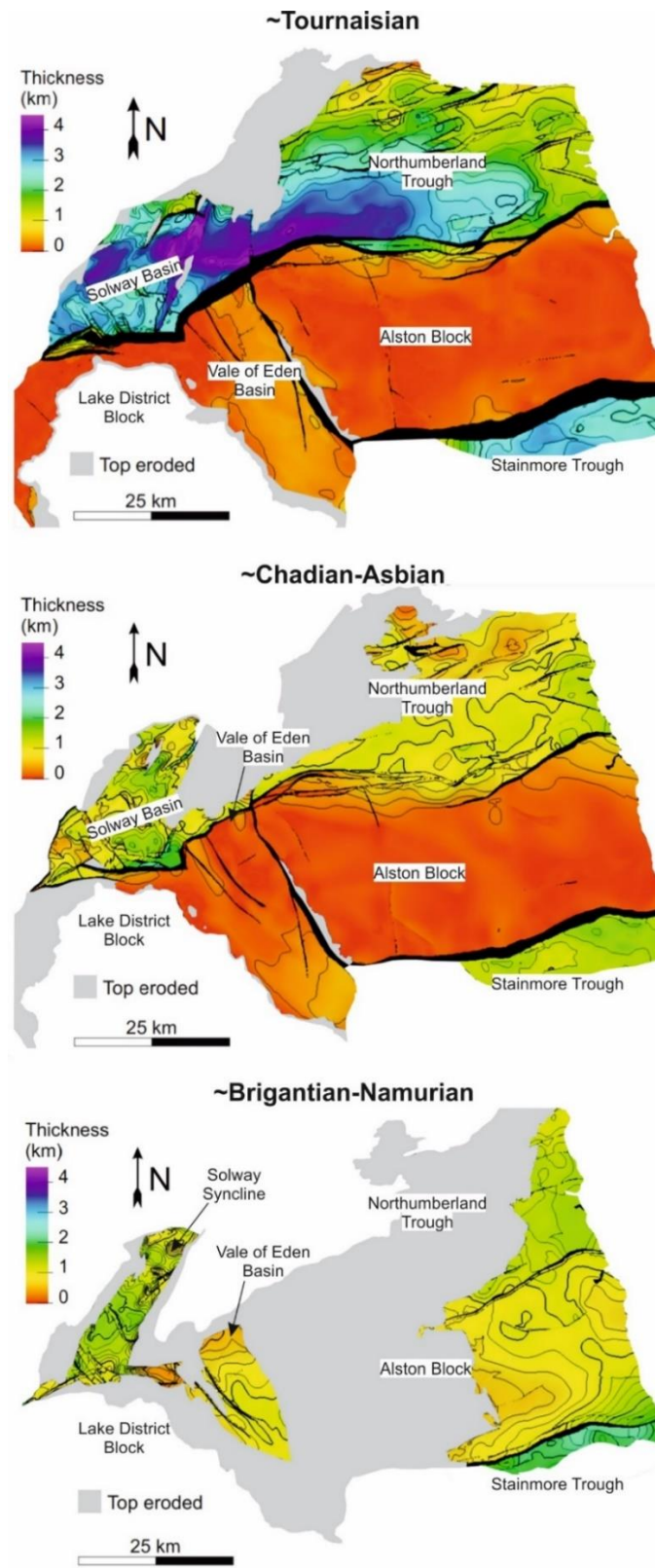
Figure 2.6: Isochronous thickness maps for the early Carboniferous and Namurian successions of northern England. Based on seismic interpretations made by Chadwick *et al.* (1995) and metadata presented in Terrington and Thorpe (2013).

(Ward, 1997), casting doubt on previous depositional models for the Tournaisian succession in northern England (*cf.* Millward *et al.*, 2019) (Fig. 2.7).

2.6.2 Early to middle Visean (Chadian to Holkerian)

From a basin evolutionary perspective, the early to middle Visean succession represents a period when rifting-induced bathymetry became increasingly well-established and major external sources of clastic sediment began to overwhelm more localised ones in Scotland and the northern Pennines (Waters *et al.*, 2007). A second period of basin-wide accelerated rifting is suggested at approximately the base of the Tournaisian-Visean boundary, based on the occurrences of widespread magmatism in Scotland (Monaghan and Parrish, 2004; Upton *et al.*, 2004) and the comparatively thicker sedimentary packages hosted within rifting-induced depocentres in northern England at this time (Fraser and Gawthorpe, 1990) (Fig. 2.6).

The base of the Visean is imperfectly defined across much of northern England and Scotland (Waters *et al.*, 2011). In central and western parts of the Midland Valley of Scotland, the early Visean is represented by a widespread hiatus and later by the eruption of the Clyde Plateau Volcanic Formation (Strathclyde Group) (Browne *et al.*, 1999) (Fig. 2.2). In Fife and the Lothians, this period is represented by the eruption of the Arthur's Seat and Garleton Hills volcanic formations and the variably thick (<560 m) and rarely exposed Gullane Formation (Chisholm *et al.*, 1989), which comprises marine-dominated pale sandstones inter-bedded with siltstones and mudstones (Wilson, 1974) (Fig. 2.2).

Along the Berwickshire coast, an erosional surface separates the Tournaisian Ballagan Formation from the overlying early to middle Visean (Chadian-Holkerian) Fell Sandstone Formation (Border Group) (Smith, 1968; Monro, 1986). Only a brief hiatus is suggested to have occurred between the depositions of these two units, based on recent palynological evidence (Marshall *et al.*, 2018 and references therein). Regionally, mixed fluvial and delta-dominated deposits of the Fell Sandstone Formation represent the western margin of a vast, approximately southward prograding fluvio-deltaic system that extended as far north as offshore Aberdeen in the northern North Sea and towards the Dutch sector in the southern North Sea (Maynard and Dunay, 1999;

Kearsey *et al.*, 2019). In the northern Northumberland Basin, these sediments are typically sandstone dominant, whereas towards the south-west they thicken considerably, from approximately 300 m to greater than 1 km (Chadwick *et al.*, 1995), and incorporate increasing amounts of deltaic siltstones and mudstones (Frost and Holliday, 1980; Turner *et al.*, 1997). The dominantly mixed carbonate-clastic deposits belonging to the Cambeck Member (Lyne Formation) represent age-equivalent strata to the lower part of the Fell Sandstone Formation in the northern Northumberland and Tweed basins (Day, 1970; Armstrong and Purnell, 1987; Mahdi and Butterworth, 1994) (Fig. 2.7).

Based on the absence of early Visean sediments upon the Alston Block, this area appears to have remained an area of mostly non-deposition at this time (Dunham *et al.*, 1961; Johnson and Nudds, 1995). However, the presence of the Fell Sandstone Formation in the Newcastle Science Central Deep Geothermal Borehole (Younger *et al.*, 2016) and a similar 'unnamed sandstone' in the Harton Borehole (Ridd *et al.*, 1970) suggests that sediments were onlapping against and overstepping this structure by the early Visean (Fig. 2.7).

As relative sea level rose in the Pennines during the early Visean, the Lake District, Askrigg and similar blocks or highs to the south of the Alston Block hosted increasingly well-established carbonate platforms and platform lithofacies (e.g., George *et al.*, 1976; Rose and Dunham, 1977; Dunham and Wilson, 1985; Dunham, 1990; Johnson *et al.*, 2001) (Fig. 2.5). The Great Scar Limestone was first used by George *et al.* (1976) to classify shelf carbonate sediments of the Askrigg and Lake District blocks and later formalised by Waters *et al.* (2007) as the Great Scar Limestone Group to encompass many approximately age-equivalent formations hosted upon distinct horst block or tilt-block highs in the region (Fig. 2.2). Sediments belonging to the Great Scar Limestone Group rest conformably on top of sediments belonging to the Ravenstonedale Group in the Stainmore Trough but disconformably upon most comparatively uplifted intra-basin blocks, perhaps because of short-lived marine regressions (Waters *et al.*, 2007; Johnson *et al.*, 2011). They comprise successions of thick limestones and are typically heavily bioturbated, bioclastic with shelly or coral biostromes and algal bands (Burgess and Harrison, 1967). As with most early Visean limestones in
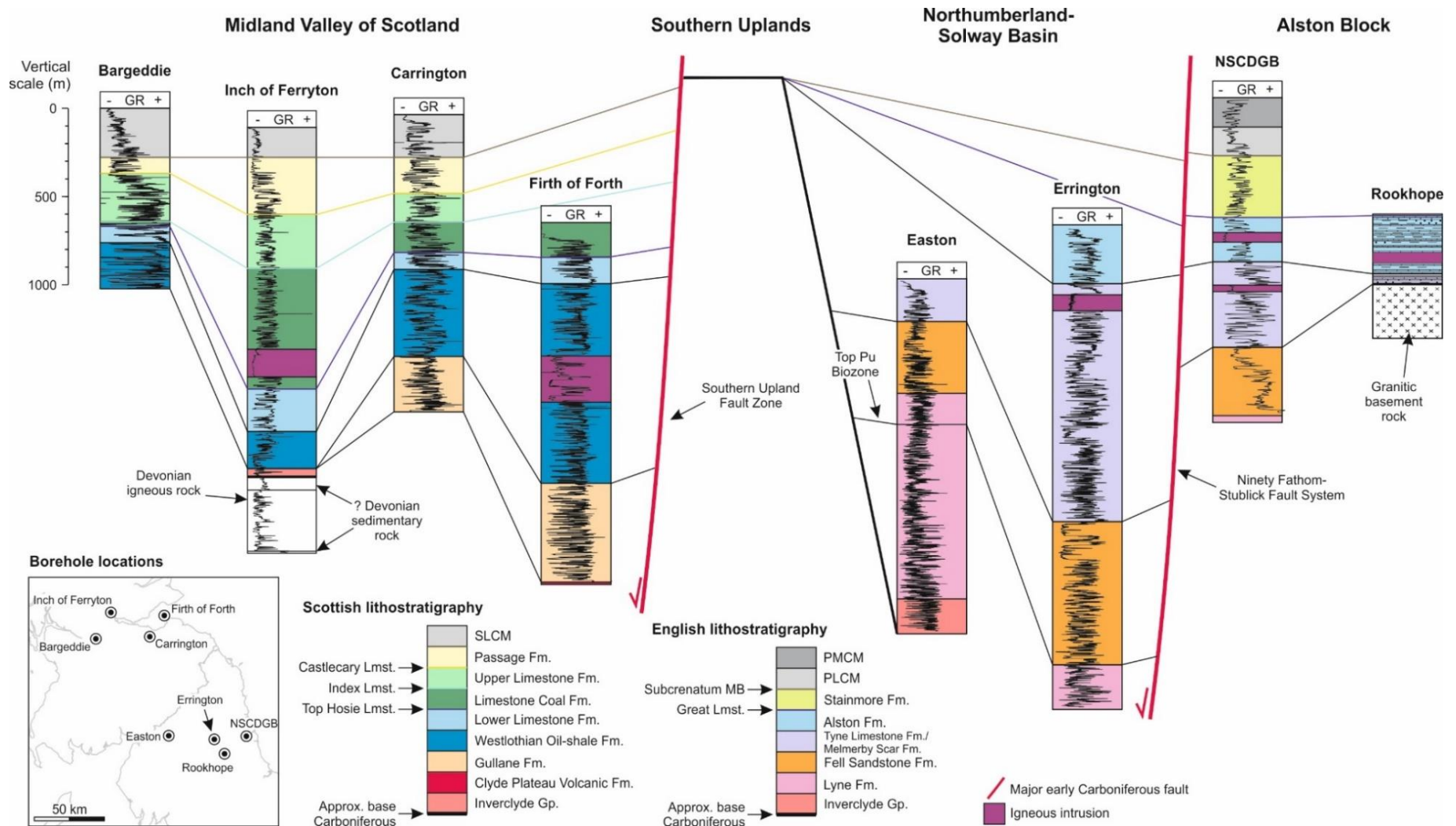
Figure 2.7: A correlation of borehole successions penetrating Carboniferous rocks in northern England and central Scotland. Wireline profiles for the Midland Valley of Scotland are taken from Monaghan (2014). Wireline profile for the Newcastle Science Central Deep Geothermal Borehole (NSCDGB) taken from Younger *et al.* (2016). The lithological log for the Rookhope Borehole is taken from Johnson and Nudds (1995).

the British Isles, these sediments are distinctly dark grey by comparison with younger

Carboniferous limestones in the region (Waltham, 1970).

More so within early Visean basins to the south, the Craven Group has been adopted

lithostratigraphically to distinguish between shelf carbonate sediments belonging to the Great Scar

Limestone Group and deeper water hemipelagic sediments (Waters *et al.*, 2007). These thick (<5000

m) dominantly mudstone and variably organic rich sediments are isolated within some of the deep

rift basins to the south of the study area, such as in the Craven Basin, the Bowland Basin, the

Widmerpool half-graben and across North Wales (Carney, 2001; Davies *et al.*, 2004; Andrews, 2013;

Anderson and Underhill, 2020).

2.6.3 Late Visean (Asbian to Brigantian)

One further early Carboniferous rift pulsation is believed to have occurred at the beginning

of the Asbian Substage (Collier, 1991; Fraser and Gawthorpe, 2003; Monaghan and Pringle, 2004;

Booth *et al.*, 2020). During the Asbian and Brigantian, rifting induced subsidence was combined with

increasingly high amplitude eustatic sea level cycles that persisted throughout the Visean and

Namurian (Maynard *et al.*, 1992) and helped submerge most previously exposed pre-Carboniferous

intra-basin blocks (Collier, 1991) (Fig. 2.5). Towards the end of the Brigantian, subsidence rates

decelerated somewhat and became increasingly uniform laterally, reflected by more uniform unit

thicknesses across northern England, perhaps indicating a period of late syn-rift to post-rift

transition (Leeder and McMahon, 1988; Kimbell *et al.*, 1989; Fraser and Gawthorpe, 1990) (Fig. 2.6).

In the Midland Valley of Scotland volcanism persisted widely, depositing lavas and

dispersing tuffaceous material throughout the basin (Fig. 2.5). Hemipelagic and mostly lacustrine

mudstones, siltstones and inter-bedded limestones belonging to the Westlothian Oil Shale

Formation (Strathclyde Group) accumulated in bathymetrically deeper parts of the Midland Valley

and were fed by geographically restricted deltaic systems (Jones, 2007a) (Fig. 2.7).

The onshore extent of the Holkerian-Asbian Scremerston Formation is restricted to the

north-eastern part of the Northumberland Basin (Jones, 2007b) (Fig. 2.2). By this time, the Tweed

Basin is believed to have no longer been separated from the broader Northumberland-Solway Basin to the south (Johnson, 1984) (Fig. 2.5). In the Northumberland Trough and Solway Basin, the Glencartholme Volcanic Member locally marks the base of the Asbian, upon which shoaling-upwards cycles of limestone, mudstone and sandstone belonging to the Tyne Limestone Formation (Yoredale Group) are deposited (Lumsden *et al.*, 1967). These sediments, along with conformably overlaying sediments belonging to the Alston Formation (also Yoredale Group), are a result of a south-westerly prograding deltaic system, whilst the cyclical nature of these sediments reflects high amplitude eustatic sea level variations (Tucker *et al.*, 2003). Similar sediments began infilling any relict palaeo-relief that resulted from this final Asbian episode of accelerated rifting, allowing for simple correlation of lithostratigraphically defined marine bands (Armstrong and Purnell, 1987; Johnson *et al.*, 2011). Yoredale Group deposits had blanketed the entirety of Alston Block by the early Brigantian (Holliday *et al.*, 1975) (Fig. 2.5).

2.7 Late Carboniferous

2.7.1 Namurian

The beginning of the Namurian marks a decline in localised depocentres (Fig. 2.6), subsidence of intervening highs and the beginning of a period of relative tectonic quiescence (Johnson, 1984; Fraser and Gawthorpe, 1990, 2003; Collier, 1991). There is a reduction in faulting-induced accommodation. However, there are still pronounced thickness contrasts that result from the relict rift basin bathymetry, differential compaction and mild syn-depositional folding (Collier, 1989). In the Midland Valley of Scotland there is a postulated switch from sinistral to dextral movement of the Highland Boundary and Southern Upland Faults, which prompts N-S orientated growth folding thereafter (Ritchie *et al.*, 2003); although the precise timing of this alternation is unclear (*cf.* Caldwell and Young, 2013 and references therein).

Ritchie *et al.* (2003) and Underhill *et al.* (2008) observed an inter-fingering relationship between more sand-prone facies, belonging to the Clackmannan Group, to the east, and the Midlothian Oil Shale Formation, to the west (Fig. 2.5). These units thicken towards the troughs of

approximately NE-trending structures such as the Clackmannan and Midlothian synclines. The Clackmannan Group comprises Yoredale and Millstone Grit-type sequences (e.g., Waters *et al.*, 2007). The oldest Clackmannan Group units are the late Visean Lower Limestone Formation, and the Namurian Limestone Coal and Upper Limestone formations (Forsyth *et al.*, 1996) (Fig. 2.2), which are subdivided according to the laterally extensive limestone horizons at the base of these sequences (Ellen *et al.*, 2019). The Passage Formation, which is punctuated by a widespread Chokeiran-Alportian unconformity and a later more localised and short-lived start Marsdenian unconformity, consists of upward fining sandstone-siltstone fluvio-deltaic facies successions (Goodlet, 1959; Lumsden, 1967; Read, 1981, 1988) (Fig. 2.2). Despite these successions having marine components at their bases, they consist of a proportionally higher alluvial component than earlier Clackmannan Group sequences and the Yoredale sequences exposed in northern England (Dean *et al.*, 2011). The Pendleian Limestone Coal Formation varies from >500 m thick in the Central Coalfield of Scotland and Central Ayrshire to just over 100 m thick along the flanks of the Midlothian Syncline (Cameron and Stephenson, 1985) (Fig. 2.7). Similarly, the Passage Formation in less than 100 m thick in parts of the Midland Valley but is >350 m thick along the Clackmannan Syncline in the Central Coalfield (Ramsbottom, 1979) (Fig. 2.7).

In northern England, the Brigantian Alston Formation is overlain conformably by the Stainmore Formation (Yoredale Group), with the Great Limestone Member forming the base on the Alston Formation (Waters *et al.*, 2011). Both formations are largely indistinguishable from each other save for an upwards decrease in limestone thicknesses and an increasingly dark grey tone to these limestones (Dean *et al.*, 2011). The base of the locally thin Millstone Grit Group is recognised towards the top of the Namurian succession in parts of northern and central England, where inter-bedded limestone horizons are absent (Waters *et al.*, 2007). On the Askrigg Block, the Millstone Grit Group overlays a Lower Pendleian unconformity (Fraser and Gawthorpe, 2003). This interval coincides with an increased concentration of clastic material suggested to have been derived from the Wales-Brabant High as opposed to the SW prograding deltaic systems to the north (Hallsworth *et al.*, 2000) (Fig. 2.5). The introduction of these southerly derived sediments accelerates the rate at which palaeobathymetry is infilled in the southern Pennines (Allen, 1960).

2.7.2 Westphalian (A and B)

During the Namurian and early Westphalian, Britain was at an approximately equatorial palaeo-latitude. As a result, climate was comparatively wetter and coal-bearing continental sequences accumulated in Carboniferous basins (Fielding, 1984) (Fig. 2.5). Sedimentary deposition continues largely unbroken into the Westphalian from the Namurian and becomes increasingly widespread across the NWECB, onlapping and overstepping early Carboniferous basin margins (Ziegler, 1982; Leeder, 1982) (*cf.* A steer head's basin geometry) (Fig. 2.5). The Pennine and Scottish Coal Measures comprise the entirety of the Westphalian A and B successions across northern Britain (Waters *et al.*, 2011). They are characterised by upwards coarsening, vertically stacked, mostly non-marine fluvio-deltaic silts, sands and muds and are often capped by thick coal deposits (Chisholm, 1990), which reach a maximum preserved thickness of approximately 500 m in Northumberland and the central part of the Midland Valley of Scotland (Waters *et al.*, 2011).

The Subcrenatum Marine Band, which marks the base of the Westphalian succession in England (Fig. 2.4), is absent from the Midland Valley of Scotland due to non-deposition (Cameron and Stephenson, 1985). The (Pennine and Scottish) Lower Coal Measures formations consist of several upward coarsening cycles within which coal seams are relatively fewer (Monaghan *et al.*, 2019). Similarly, Picken (1988) reports an absence of the basal Westphalian Subcrenatum Marine Band in the Canonbie Coalfield succession (also see Lumsden *et al.*, 1967 and Jones and Holliday, 2016) and one further localised unconformity in the Westphalian B Pennine Middle Coal Measures Formation succession. The continued progradation of regional deltaic systems keeps pace with the subsiding basin overall, prompting more stable delta-top conditions and thick coal seams (O'Mara and Turner, 1999). There is progressively less marine influence upwards throughout the Westphalian A and B successions and the frequency and thickness of inter-bedded coal seams generally increases upwards (Flint *et al.*, 1995). The Vanderbeckei Marine Band marks the lower limit of the Scottish and Pennine Middle Coal Measures formations (Ramsbottom, 1979) (Fig. 2.4). The Aegiranum Marine Band defines the base of the Westphalian B and the Scottish Upper Coal Measures Formation (Ramsbottom, 1979), formerly referred to as the 'barren' coal measures (Macgregor, 1960). The Westphalian C Cambriense Marine Band separates the Pennine Middle

Coal Measures Formation of northern England from the relatively thin Pennine Upper Coal Measures Formation (Powell *et al.*, 1999).

2.7.3 Westphalian (C and D) to Early Permian

Due to the barren nature of Westphalian C and D sediments in northern England and Scotland and their sparse preservation, these rocks have received comparatively little historical attention (Powell *et al.*, 1999). Therefore, depictions of these rocks are generally informed by previous work on the extensively more studied and thicker late Westphalian to Stephanian successions of the English Midlands (e.g., Poole, 1988). In the English Midlands, a compound or diachronous unconformity locally interrupts the Westphalian succession near the top of the Pennine Coal Measures Group and the base of the Warwickshire Group (Peace and Besly, 1997). This unconformity is known as the 'Symon' unconformity (Clarke, 1901; Besly and Cleal, 1997; Smith *et al.*, 2005; Butler, 2019) and is believed to represent a pre-cursor to the climax of Variscan compression (Pharoah *et al.*, 2020). No lateral equivalent to these unconformities has been formally recognized in northern England or Scotland, although similarly timed phases of deformation have been interpreted in West Cumbria (Akhurst *et al.*, 1997), in the Canonbie Coalfield (Picken, 1988), and in the Firth of Forth area of central Scotland (Ritchie *et al.*, 2003).

The late Westphalian to Stephanian succession of the English Midlands is characterized by a prolonged drying upwards continental transition and the expansion of fluvial red-beds into Carboniferous basins from the south (Besly, 1988; Hallsworth and Chisholm, 2000) (Fig. 2.5), the causes of which Besly (1988) attributes to uplift and a rain shadow effect from the Variscan Mountains to the south. Contemporaneous southerly derived fluvial red-bed sediments are formally recognized beyond the Scottish border in the Canonbie Coalfield (Morton *et al.*, 2010; Jones *et al.*, 2011). These rocks have recently been reclassified as belonging to the Warwickshire Group (Jones and Holliday, 2006), a stratigraphic unit prescribed to Westphalian-early Permian red-bed successions of the Pennine Basin (Powell *et al.*, 1999) (Fig. 2.2). A (lower) Westphalian D age is assigned to the lowermost strata of the Warwickshire Group in the Canonbie Coalfield, based on the occurrence of non-marine bivalves belonging to the *tenuis* biozone (Jones *et al.*, 2011) (Fig. 2.2).

However, 2D seismic reflection profiles for the region indicate <1 km of Carboniferous to early Permian (?) sediment overlying equivalent strata beneath the unconformable base of the St. Bees Sandstone in the Solway Basin (Chadwick *et al.*, 1995). A (lower) Westphalian D age is also assigned to fluvial red-beds encountered at approximately 180 m (MD) in the Firth of Forth Tower No.3 Borehole in the eastern part of the Midland Valley of Scotland (Calver in Ewing and Francis, 1960) (Fig. 2.2) where seismic reflection profiles there reveal a similarly thick (<200 m) Carboniferous to Early Permian (?) succession overlying equivalent strata along the axis of the Leven Syncline (Ritchie *et al.*, 2003).

A Gzhelian-Asselian age is interpreted for the Mauchline Volcanic Formation in Ayrshire based on sparse miospore assemblages (Wagner, 1983) and igneous isotope ages (Monaghan and Parrish, 2006) (Fig. 2.2). This age is not to be confused with the age of the largely Guadalupian-Lopingian Rotliegend Group that rests above the widely recognised, regional and erosive 'base Permian' unconformity, which is observed across most of NW Europe (Ziegler, 1995). Instead, the Mauchline Volcanic Formation is believed to be chronostratigraphically equivalent to the Clent and Kennilworth Sandstone formations of the South Staffordshire and Oxfordshire coalfields (Besly and Cleal, 2021), which lay unconformably over mostly Stephanian sediments belonging to the Halesowen and Tile Hill Mudstone formations (Besly and Cleal, 1997). In South Staffordshire and Oxfordshire, Peace and Besly (1997) attribute this unconformity to the final climax of Variscan compression in the British Isles. However, the lower boundary of the Mauchline Volcanic Formation with the Scottish Upper Coal Measures Formation is considered largely conformable in this part of Scotland (Mykura, 1965; Stephenson, 2003).

2.8 Post-Carboniferous modification

Following Variscan climax in the British Isles, the latest Carboniferous Period and early Permian were characterised by relative relaxation of north-western European tectonic stresses, which resulted in mantle upwelling, widespread magmatism and mild reactivation of pre-existing structures (Edel *et al.*, 2018 and references therein). De Paola *et al.* (2005) observe dextral offset of ENE-orientated structures along the Northumberland coast (*cf.* Coward, 1993) and argue that

Variscan inversion had minimal impact on Carboniferous strata here. Permian and Jurassic extension in north-western Europe reactivated many Carboniferous and pre-existing structures (Bott *et al.*, 1978; Ziegler, 1989). Permian and later Mesozoic sedimentation is believed to have resulted in kilometre-scale burial of Carboniferous basins (Brackenridge *et al.*, 2020). Across much of the British Isles and the adjacent offshore area, the depth of this burial widely surpassed that of initial pre-Variscan burial (*cf.* Vincent *et al.*, 2015 and references therein). Apatite fission track analysis (AFTA) data for the East Midlands, Lake District area and Irish Sea suggest that uplift and erosion of much of the post-Carboniferous cover of northern England and Scotland occurred during the Palaeogene, perhaps as a response to Atlantic break-up and associated magmatism to the west and north-west and Alpine-induced down-tilting to the south-east (Holford *et al.*, 2008). Consequently, the Carboniferous successions of northern England and southern Scotland are now either only shallowly buried, partially exposed, or eroded.

2.9 Summary

This chapter presents an effective scheme that can be used to correlate chrono-stratigraphically much of the Carboniferous succession of northern England and Scotland. This scheme will prove important when considering regional controls on deposition but remains a work in progress for some parts of stratigraphy. The greatest degrees of stratigraphic uncertainty are acknowledged for the latest Carboniferous (to early Permian?) succession of northern England and Scotland, which are discussed in Part III of this thesis. Combinations of previous regional work and more localised studies, which are referenced throughout this chapter, provide excellent platforms upon which some of the key themes outlined in Chapter 1, and expanded upon throughout this thesis, can be investigated.

Part II

'Block and basin' style rift basins

A review of the early Carboniferous northern Pennine 'block and basin' style rift basins

3.1 Introduction

Throughout the second part of this thesis, the early Carboniferous tectono-stratigraphic evolution of the partially exhumed (northern) Pennine rift basin of northern England is interrogated (see Figure 1.1 for location). This system is traditionally depicted as a so-called 'block and basin' style rift basin, within which comparatively elevated intra-basin highs or basin margins are underpinned by low-density, or buoyant, pre-existing granite intrusions (Johnson, 1967). Although predictive 'block and basin' models for deposition and basin structure are now largely redundant in petroleum and mineral exploration, some of the seminal ideas that informed these classic models provide a rare opportunity to study the now largely ignored influences of buoyancy forces and flexural isostasy on rift basins (e.g., Bott and Mason-Smith, 1958; Donato *et al.*, 1993). Whereas now continental rift basins are depicted as dominantly normal fault-driven systems (e.g., Gawthorpe and Leeder, 2000), the early Carboniferous evolution of the northern Pennine Basin is believed to have responded to both normal faulting and basement-bound buoyancy forces (Bott *et al.*, 1967).

Part II of this thesis is split between three chapters. In the succeeding chapter (Chapter 4), a study using a 2D lithosphere-scale modelling technique, investigating the structural and geodynamic controls on these basins, is presented. In the third and final chapter (Chapter 5) of Part II, a study of the early Carboniferous Fell Sandstone Formation in the northern Pennine Basin is presented, in which the influences of this basin system on deposition are considered. The key findings presented in these chapters are discussed separately, at the end of each chapter. A somewhat refined 'block and basin' model for sedimentation in rift basin systems is discussed, which is influenced by buoyancy forces due to granite intrusions, and normal faulting. In addition, key findings are considered in relation to contemporary depictions of generic rift basin systems.

In this chapter, a brief review of the 'block and basin' style rift basin framework is presented. The alleged influences of granite induced buoyancy, and rigidity, on rift basins are discussed, and the structural and sedimentological characteristics of the Pennine rift basin are described within the contexts traditional tectono-stratigraphic 'block and basin' models (e.g., Glennie, 2005). More contemporary depictions of rift basin systems are also considered (e.g., Gawthorpe and Leeder, 2000). A set of aims and objectives for this part of the thesis are presented, based on how a study focussing on the early Carboniferous succession of the northern Pennine Basin may help improve collective understandings of rift basin systems.

3.2 Early Carboniferous 'block and basin' style rifting

Large granite bodies are known to cause both local basement buoyancy and increase mechanical strength (Bott and Mason-Smith, 1958; Bott *et al.*, 1967, 1978; Donato *et al.*, 1982, 1983, 1990, 1993, 2020; Kimbell *et al.*, 2015). Consequently, continental rift basins that are influenced by such intermittent and basement-bound inherited structures are characterised by sporadic and relatively uplifted fault-bound blocks (Leeder, 1982; Chadwick *et al.*, 1995; Corfield *et al.*, 1996). Deep basins, bound by vertically displacing fault systems, where extensional strain localises, often border these blocks (Chadwick *et al.*, 1995). Such rift basins have, therefore, been loosely defined as 'block and basin' style rift basins (Marr, 1921; Trotter and Hollingworth, 1928; Bott, 1967; Johnson, 1967; Leeder, 1982; Kombrink *et al.*, 2010; Besly, 2019). The term 'block and basin' is entrenched particularly in UK Carboniferous geology (Bott, 1967; Johnson, 1967; Leeder, 1982; Johnson, 1984; Smith *et al.*, 1985; Grayson and Oldham, 1987; Gawthorpe, 1987; Pickard *et al.*, 1994). By and large, these studies have focussed on the early Carboniferous northern Pennine rift basin of northern England (Chadwick *et al.*, 1995). The underpinning 'block and basin' tectonic framework of the northern Pennine rift basin is recognised for its influence on localised uplift and subsidence trends, which had led to the popularity of predictive 'block and basin' tectono-stratigraphic models (e.g., Johnson, 1967; Leeder, 1982; Grayson and Oldham, 1987).

3.3 Geodynamic and structural controls of granite intrusions

Bott and Mason-Smith (1958) were first to propose the possible tectonic influences of large granite bodies. Based on similar gravitational responses and mineral deposits to those associated with the Cornubian Batholith in SW England, the authors postulated that a large granite pluton lay beneath the Alston Block of the northern Pennine Basin. Their hypothesis was confirmed by the drilling of the Rookhope Borehole, which encountered the Weardale Pluton (North Pennine Batholith) beneath a condensed early Carboniferous sedimentary succession (Dunham *et al.*, 1961). Based on this discovery, Bott *et al.* (1967) suggested that during periods of tectonic extension, normal faulting around the peripheral regions of granite batholiths permits relatively buoyant and rigid blocks to maintain isostatic equilibrium and resist subsidence, thus forming stable areas during periods of widespread faulting induced subsidence (*cf.* Donato and Megson, 1990). There are now numerous further publications interpreting concealed buoyant granite intrusions using gravity inversion techniques (e.g., Bott, 1962) and documenting the possible tectonic influences of basement-bound granite intrusions, all of which broadly agree with those seminal ideas (e.g., Bott 1967; Bott *et al.* 1978; Chroston *et al.* 1987; Dimitropoulos & Donato 1981; Donato *et al.* 1982, 1983, 1993; Chadwick *et al.*, 1995; de Castro *et al.*, 2008; Kimbell and Williamson, 2015; Arsenikos *et al.*, 2018).

3.4 'Block and basin' style sedimentation

The early Carboniferous northern Pennine rift basin is the archetypal example of a granite-influenced 'block and basin' style rift basin. A prominent negative Bouguer gravitational anomaly is associated with the Alston Block, which is underlain by a suite of large, predominantly cone-shaped and buoyant Early Devonian (Emsian) granitic intrusions, collectively referred to as the North Pennine Batholith (Fig. 3.1) (Kimbell *et al.*, 2010). Directly to the west lies the partially exhumed Lake District Block, which is underlain by the largely Ordovician Lake District Batholith and represented by a further negative Bouguer gravitational anomaly (Fig. 3.1). To the south-west
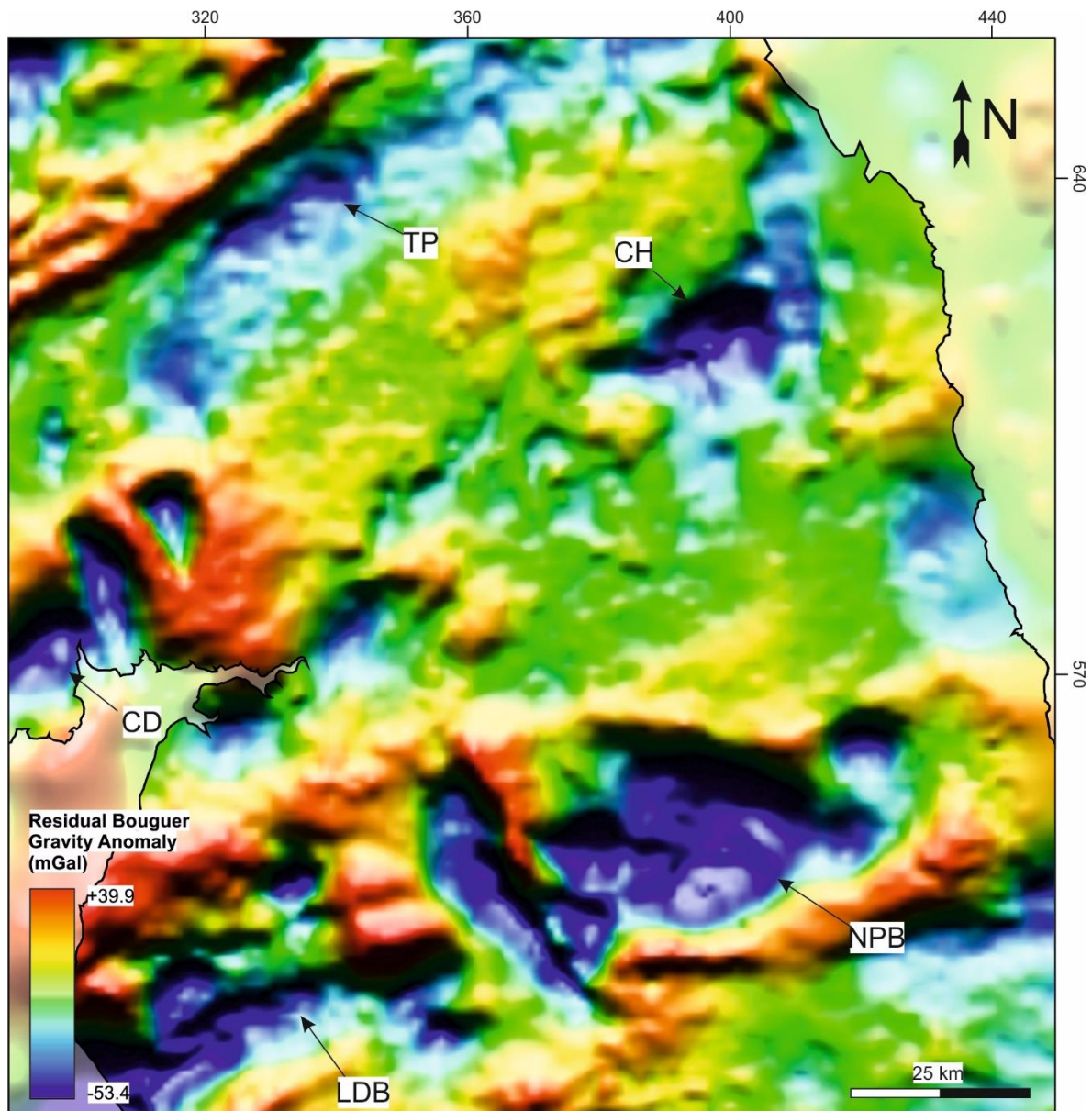
Figure 3.1: Bouguer gravity anomaly map for northern England and southern Scotland (after Kimbell and Williamson, 2015). Negative gravitational anomalies associated with low-density granite intrusions are annotated. TP = Tweedale Pluton; CH = Cheviot Pluton; CD = Criffel-Dalbeattie Pluton; NPB = North Pennine Batholith; LDB = Lake District Batholith.

of the Stainmore Trough, the Wensleydale Granite underpins the Askrigg Block (Fig. 1.1). The Cheviot Block, which is underpinned by the Cheviot Granite, does not form a traditional faulted high but marks the northern limit of the Northumberland Trough.

The implications of tectonic 'block and basin' models for the interpretation of a sedimentary rift basin system are numerous (Fig. 3.2). For example, local drainage systems may be determined by tectonically influenced 'block and basin' topographies (e.g., Gawthorpe and Clemmey, 1985;
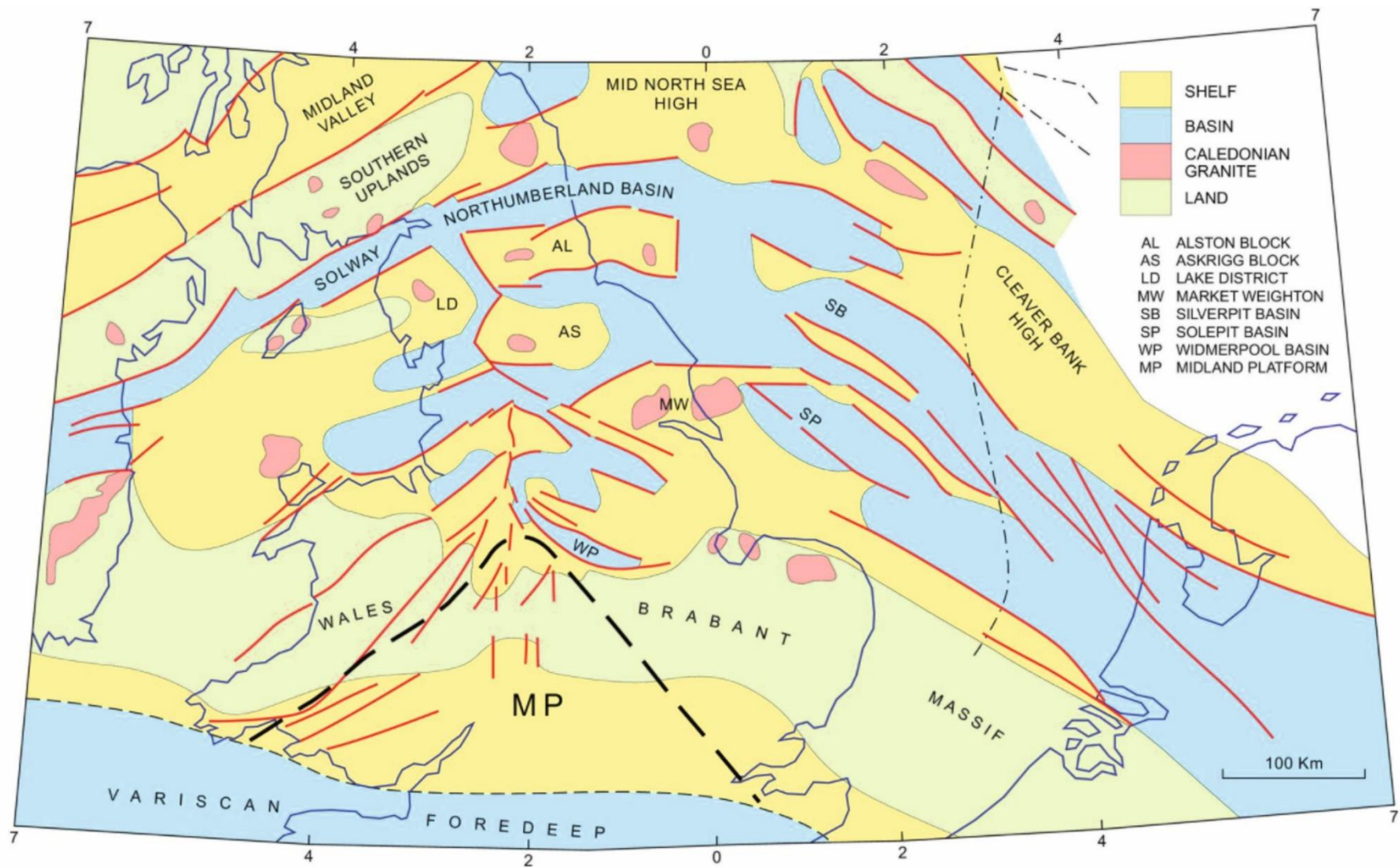
Figure 3.2: Early Carboniferous palaeogeography and structural framework of the Pennine Basin and adjacent offshore areas (after Glennie, 2005).

Leeder and Gawthorpe, 1987), while relatively uplifted granite-cored blocks may comprise localised sediment source areas (e.g., Hallsworth *et al.*, 2000; Hallsworth and Chisholm, 2008) or host shallower water successions (e.g., Pickard *et al.*, 1994; Southern *et al.*, 2010). Even before the acquisition of seismic reflection profiles in northern England, borehole penetrations and geological mapping had long revealed that the early Carboniferous sequences of basinal areas were far thicker than the typically condensed or absent contemporaneous sequences encountered on early Carboniferous blocks (Johnson, 1967). Whereas areas such as the Askrigg Block hosted shallow marine ramp carbonate or platform carbonate facies during early Carboniferous times (Gawthorpe, 1984), the Bowland Basin and Stainmore Trough hosted predominantly deeper water mudstones and calc-turbidites (Newport *et al.*, 2018). Even today, 'block and basin' palaeogeography maps for the early Carboniferous basins of the central and southern North Sea are frequently re-utilised within the contexts of regional petroleum exploration (Fig. 3.2) (Booth *et al.*, 2020).

3.5 Contemporary rift basin models and relevance of 'block and basin' style rifting

As seismic acquisition techniques have improved and better analogues for rift basin systems have emerged, the 'block and basin' rift basin framework has largely become redundant as a tool for hydrocarbon or mineral exploration (Fig. 3.3) (e.g., Grayson and Oldham, 1987). The major shortcomings of the 'block and basin' model relate to its over-simplicity. For example, some of the fault systems that define the major early Carboniferous depocentres of the northern Pennine Basin consist of several complex splays and overlapping relays rather than a simple and laterally persistent fault plane (Chadwick *et al.*, 1995; Manning *et al.*, 2007; Besly, 2019). Despite having been depicted as regions of comparative uplift during early Carboniferous times, the occurrence of Tournaisian and early Visean deeper water facies assemblages are recognised upon several of the intra-basin blocks of the Pennine Basin (Grayson and Oldham, 1987). Many of the basin-bounding structures of the southern Pennine Basin have been re-interpreted as tilted fault blocks (Gawthrope, 1984; Fraser and Gawthorpe, 1990). Within the alleged 'block and basin' framework rift basin system of the northern Pennines, several deep (>500 m) depocentres can be found situated close to pre-Carboniferous highs,

yet unbound by major vertically displacing fault systems. Examples include the eastern margin of the Alston Block (Ridd *et al.*, 1970), within the Vale of Eden Basin (Chadwick *et al.*, 1995), and to the north of the Cheviot Block in the Tweed Basin (Johnson, 1984; Millward *et al.*, 2013).
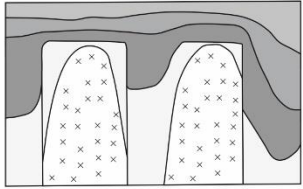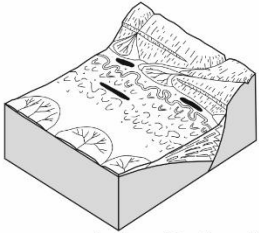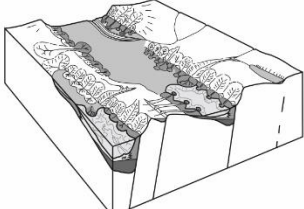
Rift basin models	Key features	Implications for depositional systems	Examples	Schematic illustration
Block and basin model	• Basin-bounding faults form around peripheral margins of comparatively uplifted granite-cored blocks.	• Thick syn-rift successions characterised by deeper water lithofacies accumulate in basins.	Pennine Basin, UK	Leeder (1982)
Tilt-block or half-graben models	• Tilt-block systems are influenced by tectonically induced slopes resulting from HW down-tilting and FW uplift.	• Prompts axial drainage. • Sediment sourced from FW and HW dipslope. • Transgression caused by fault movement and tilting.	Northumberland Trough, UK Rio Grande Rift, Colorado, USA Lower Rhine graben, western Germany	Leeder and Gawthorpe (1987)
Models for active extension	• Evolution of rift basins divided into four parts: *initiation*; *fault interaction and linkage*; *through-going fault stage* and; *fault death*.	• Basin linkage and through fault propagation determine drainage and catchment. • Hydrologically closed rifts evolve into open rifts.	Corinth Rift, central Greece Main Ethiopian Rift Suez Rift, Egypt	Gawthorpe and Leeder (2000)

Figure 3.3: Schematic tectono-stratigraphic models for (top row) 'block and basin' style rift basins (after Leeder, 1982); (middle row) tilt-blocks or half-grabens (after Leeder and Gawthorpe, 1987) and; (bottom row) active rift basins (after Gawthorpe and Leeder, 2000).

In contrast to the traditional depositional models for the early Carboniferous succession of northern England (Leeder, 1982; Johnson, 1984), at present, continental rift basins are now considered largely asymmetrical systems within which subsidence and sedimentary accommodation are controlled dominantly by normal faulting and the interaction of adjacent normal fault systems (Fig. 3.3) (Leeder and Gawthorpe, 1987; Jackson and White, 1989; Roberts and Jackson, 1991; Sharp *et al.*, 2000; Gawthorpe and Leeder, 2000). These relationships are demonstrated by several popular exposed examples of rift basins, such as in the Gulf of Corinth (Moretti *et al.*, 2003; Bell *et al.*, 2009; Cullen *et al.*, 2020), the East African Rift (Ring, 1994; Contreras *et al.*, 2000; Morley, 2010), and many further subsurface examples (Elliott *et al.*, 2017; Phillips *et al.*, 2019). The evolution of a rift

basin system and its influence on drainage (Gawthorpe and Hurst, 1993; Jackson and Leeder, 1994), sediment routing (Schlishce, 1991; Whittaker *et al.*, 2010; Kirby and Whipple, 2012), and sedimentary accommodation (Faulds and Varga, 1998; Gupta *et al.*, 1998; Jackson *et al.*, 2005; Duffy *et al.*, 2015) may be determined by the varying stages of linkage between adjacent fault systems and the corresponding linkages of adjacent rift basin depocentres (Holz *et al.*, 2017). It is perhaps a testament to the relatively little attention the northern Pennine Basin has received in the past 25 years, that the most popular depositional models for the area remain routed to the comparatively out-dated 'block and basin' framework.

The portrayal of the 'block and basin' model as "out-dated" should in no way discredit the work of those previously invested in the early Carboniferous geology of northern England. Many of their observations and ideas are still deeply ingrained within more modern depictions of rift basin systems (e.g., Leeder and Gawthorpe, 1987) and many rift basin systems do respond to underlying structures in the way in which 'block and basin' rift basin models predict, such as the Utsira High and South Viking Graben, offshore Norway (Roe and Steel., 1985; Fazlikhani *et al.*, 2017), the Froya High and Halten Terrace, also offshore Norway (Elliott *et al.*, 2017), the Sugar Loaf High of the Santos Basin, offshore Brazil (Buckley *et al.*, 2015), the Dogger High and North Dogger Basin of the Anglo-Dutch North Sea (Milton-Worsell *et al.*, 2010; Ter Borgh *et al.*, 2019), just to name a few. Although rift basins are now widely considered dominantly normal fault driven systems (e.g., Ford *et al.*, 2013; Holz *et al.*, 2017), Martin Bott's original hypothesis implies that variations in the density of the basement may also influence rift basin evolution. Currently there has been little research carried out to determine the importance of basement density on extensional (rift) basins.

3.6 Summary

For approximately 60 years it has been widely assumed that in basins such as the Carboniferous northern Pennine Basin of northern England, by virtue of their comparative 'rigidity' and 'buoyancy' with respect to accommodating country rock, granite intrusions cause basement rock to be comparatively uplifted during rifting (Bott and Mason-Smith, 1958; Bott *et al.*, 1967, 1978; Donato *et al.*, 1983, 1993; Kimbell *et al.*, 2010; Kimbell and Williamson, 2015). Several authors have

suggested that during periods of tectonic extension, normal faulting around the peripheral regions of granite batholiths permits relatively buoyant and rigid blocks to maintain isostatic equilibrium and resist subsidence, thus forming stable areas during periods of widespread faulting induced subsidence (Donato and Megson, 1990). Yet despite these long-held assumptions, a verifying numerically based forward model for these systems remains elusive. In Chapter 4, basin geometries for the northern Pennine Basin are replicated, using forward 2D lithosphere-scale structural and geodynamic modelling (*cf.* Egan, 1992). A series of viable structural and geodynamic scenarios are proposed, which may help explain why large granitic bodies so often occur in the cores of relatively uplifted intra-rift basin basement blocks.

The underpinning tectonic frameworks of 'block and basin' style rift basins are recognised for their influence on localised uplift and subsidence (Leeder, 1982). However, the way uplift and subsidence within these basins may influence factors that strongly govern the dynamics of depositional systems, such as accommodation, drainage pathways or sediment routing, lacks thorough examination. Moreover, as these relationships lack thorough examination, assumptions regarding the rather primitive 'block and basin' tectonic framework cannot be considered seriously tested. In Chapter 5, the Carboniferous (Visean) fluvio-deltaic Fell Sandstone Formation and age-equivalent stratigraphic units of the northern Pennine Basin in northern England are investigated alongside their interactions with the locally underpinning syn-depositional 'block and basin' style rift basin framework to help determine these relationships.

Structural and geodynamic modelling of the influence of granite bodies during lithospheric extension

This chapter is based on a publication of a similar name. See reference below.

Howell, L., Egan, S., Leslie, G. and Clarke, S., 2019. Structural and geodynamic modelling of the influence of granite bodies during lithospheric extension: application to the Carboniferous basins of northern England. *Tectonophysics, 755*, pp.47-63. https://doi.org/10.1016/j.tecto.2019.02.008

4.1 Introduction

In this chapter, a series of viable structural and geodynamic models are presented that may help to explain why large granite bodies so often occur in the cores of relatively uplifted intra-rift basin basement blocks. A lithosphere-scale numerical modelling approach is adopted to replicate granite emplacement, extensional tectonism, and any changes in the physical state of the lithosphere or basin architecture these processes are likely to incur (*cf.* Egan and Meredith, 2007). A northern England Carboniferous case study is used as both a means of scrutinising the proposed model and as a tool to help analyse the structural trends associated with deeper granite bodies. Some of the implications of these findings are discussed.

4.2 The effects of granite during lithosphere extension: testing long held assumptions

The portrayal of a 'buoyant' and 'rigid' granite body, such as that within the pre-Carboniferous basement beneath the northern Pennine Basin (*cf.* Bott, 1967), appears to have somewhat over-simplified a more complex phenomenon. Rigidity could also perceivably imply brittleness, which may increase the likelihood of fracture nucleation and fault propagation. Perhaps describing younger granite bodies as lacking the same internal heterogeneities and inherited weaknesses as older deformed continental crust (e.g., Chadwick *et al.,* 1991) would be a more

plausible way of accounting for the general absence of significant through-going faults within granite-cored basement, albeit another over-simplification (Bouchez, 1997; de Saint-Blanquat *et al.*, 2001). Buoyancy, in this instance, refers to a crustal mass deficiency associated with crystalline granite by comparison with typically variably metamorphosed basement rock (Lee, 1986). The term 'buoyancy' however, perhaps inadvertently invokes similarities between rather more dynamic salt bodies, which are known to actively resist subsidence via halokinesis. 'Old and cold' granite batholiths are instead fixed entities within a heterogeneous basement which reduce the overall bulk density of the crust.

The assumption that a mass deficiency within a defined volume of the crust can promote stability compared with adjacent crust and an inherent ability to resist subsidence during lithospheric extension contradicts some of the fundamentals of mantle and lithosphere dynamics. During lithospheric extension, regional-scale subsidence occurs in response to net density changes resulting from crustal thinning as well as from thermal re-equilibration (McKenzie, 1978). Fundamental principles of isostasy imply that to maintain equal pressure at a depth of compensation, at and below which the pressures generated from the overlying rock are equal, upwelling asthenosphere compensates for the loss of lithospheric mass due to stretching and thinning (Karner and Watts, 1982). As the compensating asthenosphere is denser than the crust, this results in a negative deflection in surface elevation (e.g., Kooi *et al.*, 1992). Put simply, this negative deflection, S, can be calculated using either equation 4.2.1 or 4.2.2 (see Tables 4.1 and 4.2 for abbreviations). In this instance, subsidence is proportional to the original thickness of the crust (C_o) and the magnitude of extension (β), as well as the density of the crust (ρ_c) and that of the mantle (ρ_m). Note that whilst this calculation applies only to thinning of the crustal lithosphere, it remains valid providing the density of the asthenosphere and mantle lithosphere are assumed equal (ρ_m).

$$S = C_o - \frac{C_o}{\beta} - \left(C_o - \frac{C_o}{\beta}\right) \times \frac{\rho_c}{\rho_m}$$

(Eq. 4.1)

Or $S = \left(C_o - \frac{C_o}{\beta}\right) \times \left(1 - \frac{\rho_c}{\rho_m}\right)$

<div align="right">(Eq. 4.2)</div>

Given that crustal thickness lost due to thinning $= C_o - \frac{C_o}{\beta}$

<div align="right">(Eq. 4.3)</div>

And the isostatic response to this thinning $= (C_o - \frac{C_o}{\beta}) \times \frac{\rho_c}{\rho_m}$

<div align="right">(Eq. 4.4)</div>

Parameters	Abbreviation
Basement elevation (km)	$Basement_{(x)}$
Basin infill density (kg m⁻³)	ρ_i
Constant used for Fast Fourier Transform representing width of model in frequency domain.	N
Crustal thinning due to simple shear (km)	$CTS_{(x)}$
Density of granite-cored crust (kg m⁻³)	ρ_{gc}
Density of granite-cored crust at a given point (kg m⁻³)	$\rho_{gc_{(x)}}$
Depth to fault (km)	$Fd_{(x)}$
Elastic thickness (km)	Te
Magnitude of extension	β
Flexural rigidity (N m)	D
Vertical granite body thickness at a given point (km)	$GR_{(x)}$
Horizontal extension or heave (km)	h
Load at a given point (N)	$Load_{(x)}$
Local isostatic rebound due to granite emplacement (km)	IR
Original granite height/thickness (km)	GR_o
Original lithosphere thickness for granite-cored lithosphere (km)	A_{og}
Subsidence (km)	S
Subsidence of granite-cored crust (km)	S_g
Thermal diffusivity (m² s⁻¹)	i
Thermal time constant (My; Parsons and Sclater, 1977)	τ
Wavenumber of the load in the frequency domain	k

Table 4.1: One-dimensional and two-dimensional modelling variables.

Constants	Abbreviation	Value	Reference
(Non-granite cored/original) crustal density	ρ_c*	2800 kg m^{-3}	Parsons and Sclater (1977)
Acceleration due to gravity	g	9.81 m s^{-2}	
Air density	ρ_a	0 kg m^{-3}	
Brittle-ductile transition (crust)	Zd	20 km	Kusznir and Park (1987)
Granite density	ρ_g	2630 kg m^{-3}	Eskdale granite; Bott and Smithson (1967)
Mantle density (asthenosphere and mantle lithosphere)	ρ_m*	3300 kg m^{-3}	Parsons and Sclater (1977)
Original crustal thickness	C_o	35 km	
Original lithosphere thickness	A_o	125 km	
Poisson's ratio	v	0.25	e.g., Watts et al. (1980)
Sediment density	ρ_s	2500 kg m^{-3}	
Temperature at the base of the lithosphere	T_0	1333^{0}C	Parsons and Sclater (1977)
Volumetric coefficient of thermal expansion	α	3.28×10^{-5}^{0}C^{-1}	Parsons and Sclater (1977)
Water density	ρ_w	1000 kg m^{-3}	
Young's modulus	E	7×10^{10} Pa	e.g., Egan (1992)

Table 4.2: One-dimensional and two-dimensional modelling constants with abbreviations and source. *Densities correct at 0 °C.

Figure 4.1 predicts the depth of two basins in granitic and non-granitic crust when the lithosphere is uniformly stretched (i.e., through pure shear) to twice its original horizontal extent, representing a magnitude of extension (β) of 2. Using the parameters displayed in Table 4.2, the subsidence produced from extending non-granitic crust (ρ_c) is 2.66 km, compared with 3.55 km for a crust composed entirely of granitic material (ρ_g). Net subsidence during extension for less dense crust is greater due to a lesser magnitude of isostatic rebound being required to compensate for thinning of a crust with comparatively lower density.
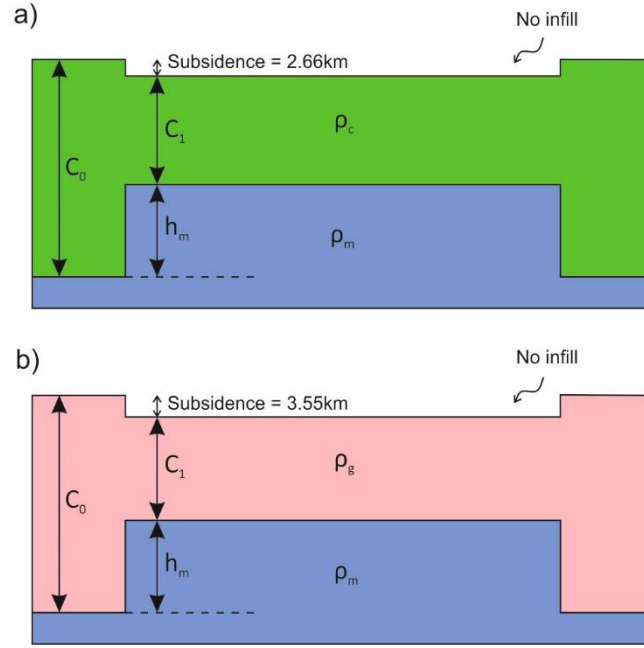
Figure 4.1: Schematic cross-sections through extensional basins within a) non-granitic crust and b) entirely granitic crust. Fully compensated local isostasy is assumed. In other words, $C_0 \times \rho_c = h_m \times \rho_m + C_1 \times \rho_c$. $\rho_m = 3300$ kg m^{-3}, $\rho_c = 2800$ kg m^{-3}, $\rho_g = 2630$ kg m^{-3}.

However, an alteration in overall bulk crustal density causes a separate isostatic adjustment (Fig. 4.2). In the case of density deficiency due to granite emplacement, this implies uplift. When the complete substitution of crustal rock with a granite body of the same volume is assumed (rather than addition to the crust), the uplift, IR, can be given by:

$$IR = GR_o \times \frac{\rho_c - \rho_g}{\rho_m}$$

(Eq. 4.5)

Examples of the isostatic responses to magmatic emplacement are common (e.g., Brodie and White, 1994; Maclennan and Lovell, 2002). Where granite bodies have been inferred based on gravity anomalies, the deficiency in the gravitational field compared with background values has been used to calculate localised isostatic rebound (e.g., Donato *et al.*, 1983). Nonetheless, prior to writing, there had been no fully integrated numerical modelling of the influences of granite induced crustal buoyancy on lithosphere behaviour during lithospheric extension.
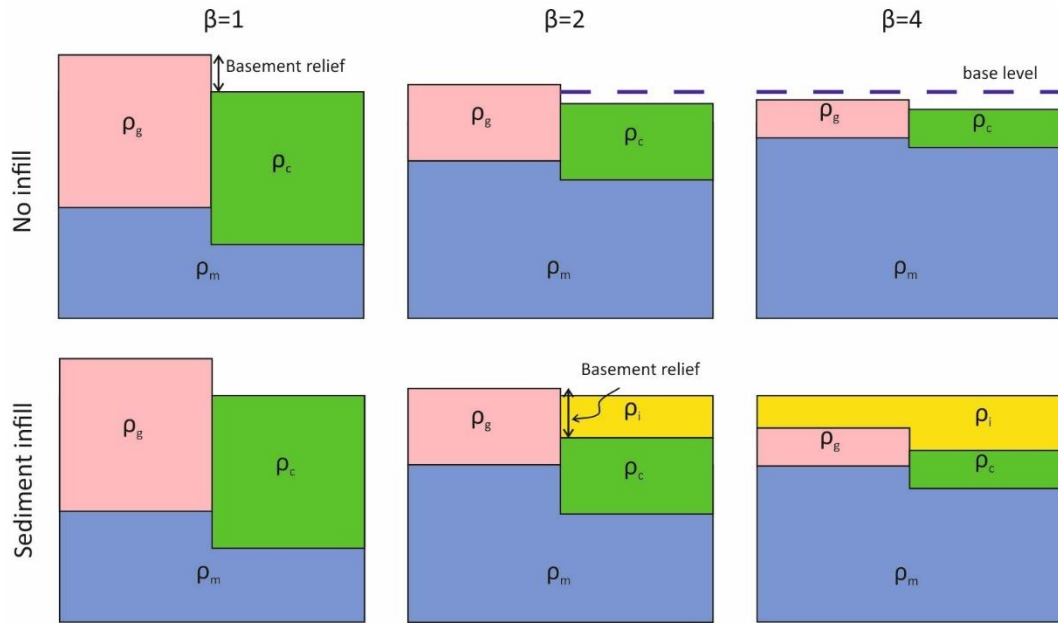
Figure 4.2: Schematic illustration indicating how the influence of a density contrast on basement relief reduces with increased crustal thinning. The pink and green blocks represent granitic and non-granitic crust, respectively. The addition of sediment below base level, represented by yellow shading, exaggerates basement relief (also see Figure 4.3). Fully compensated local isostasy is assumed. To better illustrate the effects of a granitic basement, the density contrast between granite (ρ_g) and 'standard' crustal rock (ρ_c) is exaggerated such that ρ_c = 2800 kg m⁻³ and ρ_g = 2000 kg m⁻³. ρ_m = 3300 kg m⁻³, ρ_i = 2500 kg m⁻³.

4.3 Revised 1D model of lithospheric extension and granite emplacement

Within this chapter, a fully integrated 2D lithosphere scale model that accounts for depth-dependent extension by compound simple shear and pure shear, flexural isostasy, and the thermal perturbations associated with lithospheric deformation is developed (e.g., Kusznir and Egan, 1989; Meredith and Egan, 2002). This 2D model also accounts for the flexural isostatic influences of granite. However, in this section a 1D modelling approach is described, assuming local isostasy (e.g., Airy, 1855; Pratt, 1858), to provide useful approximations for subsidence behaviour in response to extensional tectonics (e.g., McKenzie, 1978) and granite intrusion. Readers should refer to Table 4.2 for a summary of model parameters.

4.3.1 Numerical replication of granite emplacement

Replicating granitic emplacement to quantify isostatic uplift can be performed in several ways. Equation 4.5 assumes the complete substitution of crustal rock with less dense granitic rock and no thermal expansion (e.g., Donato *et al.*, 1983). However, a more accurate portrayal of isostatic uplift due to magmatic emplacement is perhaps achieved by the *addition* of less dense material to the crust; an approach that is like that adopted in the numerical modelling of magmatic underplating (e.g., Maclennon and Lovell, 2002):

$$IR = GR_o - GR_o \times \frac{\rho_c - \rho_g}{\rho_m}$$

(Eq. 4.6)

Both calculations are approximations of the local isostatic adjustment to one of two simplified, end-member magmatic bodies; one derived entirely from partial melting of the crust (Eq. 4.5), and the other derived entirely from the mantle that eventually adds material to the crust (Eq. 4.6). Although the addition of material produces a significantly greater isostatic response, the initial calculation (Eq. 4.5) is deemed more appropriate to the northern Pennine Basin in northern England. Highly acidic, S-type granites such as the North Pennine Batholith typically involve the assimilation of considerable amounts of crustal material (Allsop, 1987). Although the melting of crustal material along with the assumptions of retention of volume combined with an alteration in density is unfeasible, it offers a justifiable simplification of a far more complex process. In addition, a model based on the granitization of the crust is more compatible with the interpretations of the North Pennine Batholith from gravity data and deep seismic imaging, whereby a roughly uniform crustal thickness is observed (Kimbell *et al.*, 2010).

The emplacement of large granite bodies is associated with significant thermal perturbations. These may be in response to the initial upwelling of hot magma, the isostatic compensation of the hotter asthenosphere, or to the elevated radiogenic heat production associated with the resulting granite. However, the one-dimensional model assumes no thermal fluctuations are associated with the granite pluton(s). Essentially, the effects of a thermally re-equilibrated granite

body are modelled. Changes in the elevation of the lithosphere-asthenosphere boundary, due to isostatic adjustment, are transient and not permanent (McKenzie, 1978), so to replicate a thermally re-equilibrated lithosphere profile, the thickness of the entire lithosphere (i.e., the sum of crustal and mantle lithosphere) is adjusted. This can be accounted for by adding the calculated isostatic rebound (Eq. 4.5) to the lithospheric thickness value:

$$A_{og} = A_o + GR_o \times \frac{\rho_c - \rho_g}{\rho_m}$$

(Eq. 4.7)

4.3.2 Numerical replication of lithospheric extension

If uniform lithospheric extension solely via pure shear is assumed, the original height and width of the granite body (GR_o) are altered according to the magnitude of extension (β). Taking this into account, the method for solving the subsidence of granite-cored basement (S_g) can be given one of two ways (Eqs. 4.8 and 4.9). Again, the potential implications of heat flow fluctuations are ignored at this stage.

$$S_g = \left(C_o - \frac{C_o}{\beta}\right) \times \left(1 - \frac{\rho_c}{\rho_m}\right) - \frac{GR_o}{\beta} \times \frac{\rho_c - \rho_g}{\rho_m}$$

$$\text{Or } S_g = \left(C_o - \frac{C_o}{\beta}\right) \times \left(1 - \frac{\rho_{gc}}{\rho_m}\right) - IR$$

(Eq. 4.8)

$$\text{Where } \rho_{gc} = \rho_c - \frac{GR_o}{C_o} \times \left(\rho_c - \rho_g\right)$$

(Eq. 4.9)

Changes in the vertical thicknesses of relatively less dense crust due to stretching or compression prompts relatively less isostatic compensation (e.g., Fig. 4.1). Therefore, with increased extension, the initial uplift of granite-cored crust is cancelled out progressively by extension-driven subsidence when compared with non-granite-cored crust (Figs. 4.2 and 4.3).
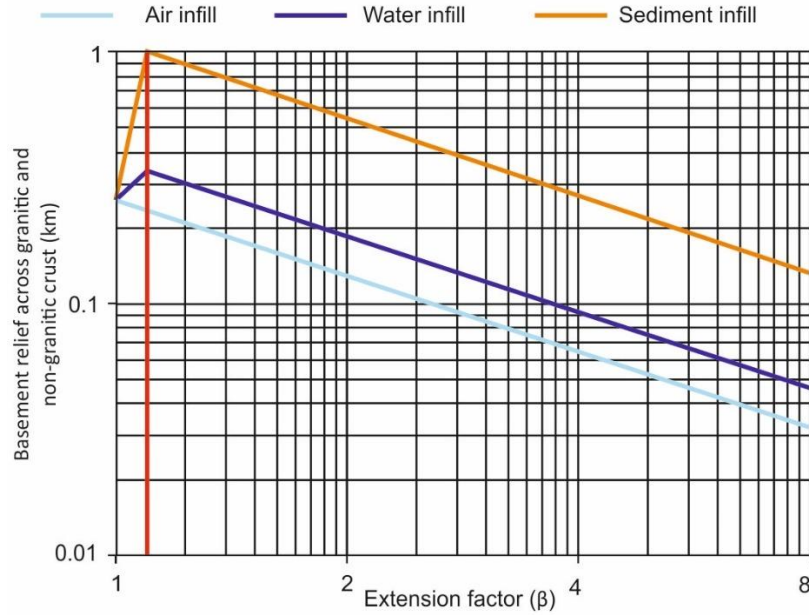
Figure 4.3: The relationship between basement relief across partially granitic and non-granitic crust and extension factor (β) (also see Figure 4.2). The influence of a density contrast on basement relief reduces with increased extension. However, basin infill exaggerates relief. $GR_0 = 5$ km, $C_0 = 35$ km, $\rho_m = 3300$ kg m^{-3}, $\rho_c = 2800$ kg m^{-3}, $\rho_g = 2630$ kg m^{-3}, $\rho_i = 2500$ kg m^{-3}.

4.3.3 Isostatic loading due to basin infill

If the starting elevation of non-granite-cored or granite-cored basement prior to emplacement is assumed to be at infill base level, then providing subsidence is greater than zero such that accommodation space is generated, the subsidence of an infilled basin can be given by the following:

$$S = S_g + \left(S_g \times \frac{\rho_i}{\rho_m - \rho_i}\right)$$

(Eq. 4.10)

The incorporation of basin fill into the model has important implications for generating vertical relief. Where $\beta > 1$, but not sufficient to subside initially uplifted granite-cored crust below base level, differential loading occurs and exaggerates basement relief (e.g., Figs. 4.2 and 4.3). The magnitude of extension (β) required for infill to occur on the granite-cored block can be determined by rearranging equation 4.8:

$$\beta = \frac{C_o \times (\rho_m - \rho_{gc})}{C_o \times (\rho_m - \rho_{gc}) - IR \times \rho_m}$$

<div align="right">(Eq. 4.11)</div>

4.3.4 The effects of erosion of uplifted material

Figures 4.2 and 4.3 suggest that differential loading can have an important role in generating basin relief. However, if the initial uplift due to granite emplacement was met with complete erosion to sea level of the uplifted proportion of the block, producing a flat basement topography prior to extension, then the effects of differential loading would be nullified. Erosion implies an additional negative load and a further positive isostatic response generating additional uplift. The total erosion required to generate a flat surface topography across granite-cored and non-granite cored basement (e) can be defined as:

$$e = \frac{C_o(\rho_c - \rho_{gc})}{\rho_m - \rho_{gc}}$$

<div align="right">(Eq. 4.12)</div>

Given that $C_o \times \rho_c = (C_o - e) \times \rho_{gc} + e \times \rho_m$.

Any erosion implies a reduction in crustal thickness (C_o) prior to stretching. When the uplifted portion of the crust is eroded in its entirety to sea level and the transient asthenosphere-lithosphere boundary re-equilibrates fully, lithospheric thickness remains the same. Less dense crust subsides more than denser crust (Fig. 4.2). However, thinner crust subsides less for any amount of extension as less vertical thickness due to crustal thinning is lost in comparison to thicker crust.

Figure 4.4 presents subsidence in response to the extension of 'standard' lithosphere (i.e., C_0 = 35 km and ρ_c = 2800 kg m⁻³) and a lithosphere which has undergone granite emplacement, isostatic compensation, full thermal re-equilibration and erosion sufficient to generate a flat basement profile. Ignoring any thermal perturbations, which could enhance uplift, when the same stretching factor is applied the calculated subsidence is identical.
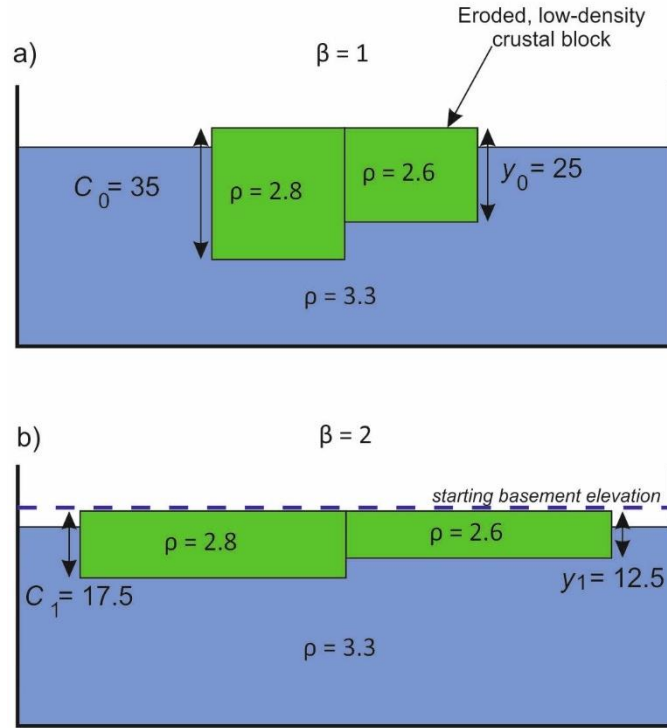
Figure 4.4: Schematic illustration indicating the influence of pre-tectonic denudation of isostatically compensated lithosphere on the basement topography of a) un-extended and b) extended lithosphere. Fully compensated local isostasy is assumed.

In other words, where $z = C_o - e$ is the eroded granite-cored crustal thickness with the same isostatically compensated surface elevation as the original crust (C_o):

$$S = \left(C_o - \frac{C_o}{\beta} \right) \left(1 - \frac{\rho_c}{\rho_m} \right)$$

(Eq. 4.13)

$$= \left(z - \frac{z}{\beta} \right) \left(1 - \frac{\rho_{gc}}{\rho_m} \right)$$

(Eq. 4.14)

For granites to influence basin architecture during lithospheric extension, there needs to be some uplifted basement topography prior to extension. The overall bulk crustal density reduction associated with the emplacement of a 5 km thick granite pluton is ~0.9%. To replicate a flat topography in this scenario requires 1.62 km of erosion. Without considering the mechanics of

58

denudation, it is conceivable that this amount of erosion is achievable over an extended period of tectonic quiescence. Nonetheless, the model presented here will assume no erosion prior to lithospheric extension as ultimately uplift is restricted by lithospheric elasticity (Watts, 2001).

4.3.5 The effects of thermal expansion and contraction

McKenzie (1978) states that compensation of the asthenosphere in response to crustal thinning invokes elevation of the lithosphere-asthenosphere boundary and thus reduces overall initial subsidence. For the sake of mathematical simplicity, instantaneous deformation and thermal expansion is assumed here. After extension, the lithospheric temperature field undergoes gradual thermal recovery back to an equilibrated state. Crustal density has no *direct* influence on thermal expansion or decay (McKenzie, 1978) and thus the severity of uplift in response to thermal perturbations does not vary significantly between granite-cored and non-granite cored crust. In increasing the total lithospheric thickness (e.g., Equation 4.7), the volume increase due to thermal expansion is marginally greater. When a denudated, flat basement topography is modelled (e.g., equation 4.12), lithospheric thickness remains the same yet the ratio of crustal to mantle lithosphere changes. In each instance, the contrast in thermal expansion is insignificant. An additional alteration to Parsons and Sclater's (1977) thermal time constant (τ) is made (see equation 4.13), which helps govern the rate of thermal decay. Despite this, following extension, granite-cored basement and non-granite-cored basement subside at largely the same rate, providing basement fill is laterally consistent.

$$\tau = \frac{A_o{}^2}{\pi^2 \times i}$$

(Eq. 4.13)

One-dimensional numerical modelling does not support the suggestion that a granite-cored crust can isostatically 'resist' subsidence during lithospheric extension. Instead, in a lithosphere with no rigidity, the generation of a basement high is a result of initial isostatic compensation in response to granite emplacement prior to lithospheric extension. The addition of sediment exaggerates any pre-existing topography.

4.4 2D modelling of lithospheric extension and granite emplacement

The one-dimensional models presented above give an indication of the isostatic and subsidence behaviour in response to granite emplacement and lithospheric extension. In reality, the lithosphere has significant elastic strength or flexural rigidity; sufficient to prevent localised features from being *completely* compensated for (*cf.* Watts, 2001). The conceptual 2D pure shear model presented here calculates the flexural response to the various loads imposed on the lithosphere. These loads include tectonically derived loads, sediment infill and the loading imposed due to granite emplacement. Both lateral and vertical heat fluxes due to conduction are calculated within the model (e.g., Meredith and Egan, 2002).

4.4.1 The flexural isostatic implications of granite emplacement

Assuming the lithosphere has a finite flexural rigidity, Figure 4.5 illustrates the flexural responses to the emplacement of a 5 km deep by 15 km wide granite body into a lithosphere with varying elastic thicknesses (Te). The local (Airy) isostatic response represents a lithosphere with an elastic thickness of zero kilometres. The resulting topography imitates that of the granite body at depth. To incorporate lithospheric flexure, the solution representing the local isostatic response of the lithosphere presented previously (Eq. 4.5) is rearranged and solved using a Fast Fourier Transform technique (Cooley and Tukey, 1965; Watts, 2001). Where the flexural response to a density deficiency in the crust, and not thermal expansion, due to granite emplacement is modelled, the load at a given point (x) can be given by:

$$Load_{(x)} = \left(GR_{(x)} \times 1000\right) \times \left(\rho_g - \rho_c\right) \times g$$

<div align="right">(Eq. 4.14)</div>

Before calculating the flexural response to this load, the flexural rigidity of the lithosphere must be defined. Flexural rigidity (D) is proportional to the elastic thickness (Te) of the lithosphere (*cf.* Watts, 2001):

$$D = \frac{E \times Te^3}{12(1 - v^2)}$$

<div align="right">(Eq. 4.15)</div>

Where E is Young's modulus and v represents Poisson's ratio.

Within the frequency domain, the flexural response ($resp$) to this load can be determined by:

$$resp = \frac{Load_{(x)}}{(\rho_m \times g) + (D + resp_1)}$$

<div align="right">(Eq. 4.16)</div>

$$resp_1 = \left(\frac{2 \times \pi \times k}{N \times 2 \times 1000}\right)^4$$

<div align="right">(Eq. 4.17)</div>

Where k is the wave number and N is the width of the profile.

As elastic thickness (Te) increases, maximum uplift decreases at a rapid rate at first which then decays exponentially with increased Te. However, the width or wavelength of the flexural deflection increases (Fig. 4.5). With an elastic thickness of 10 km, maximum uplift is approximately 64 metres compared with an Airy isostatic response of approximately 258 metres. However, the width of the flexural uplift increases to approximately 120 km for an elastic thickness of 10 km compared to 15 km for Airy isostasy, which matches the width of the granite body. Various authors have pointed out that flexural stress can be relaxed over time since the lithosphere often behaves *visco-elastically* (Stein *et al.*, 1989; Watts and Zhong, 2000), and elastic thickness can vary according to the thermal state of the lithosphere (Burov and Diament, 1995). Nevertheless, the incorporation of flexure within a two-dimensional model significantly limits the influence of a granite body on basement topography. Therefore, the implications of incorporating flexure include limiting isostatic uplift and therefore, also limiting the potential influence of pre-extensional erosion and differential loading.
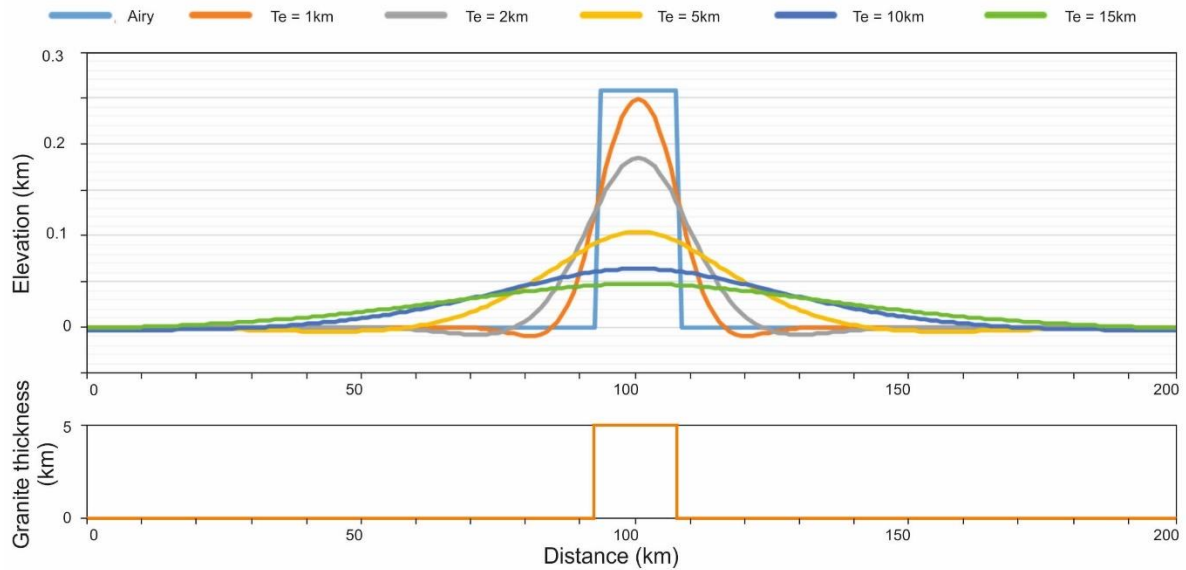
Figure 4.5: The varying flexural responses to an added granite body, 15km wide x 5km high, into a lithosphere with different elastic thicknesses (Te). When the lithosphere is assumed to have elastic strength, isostatic compensation is reduced in amplitude but increased in width with respect to Airy (local) isostatic compensation. $C_0 = 35$ km, $\rho_m = 3300$ kg m^{-3}, $\rho_c = 2800$ kg m^{-3}, $\rho_g = 2630$ kg m^{-3}.

Two-dimensional numerical modelling suggests that initial isostatic compensation due to granite emplacement is incomplete when lithospheric rigidity is incorporated (Fig. 4.5). Depending on the flexural rigidity and effective elastic thickness (Te) of the lithosphere, a regional flexural profile is generated prior to lithospheric extension. As isostatic compensation is incomplete, a likely residual under-compensated 'buoyancy force' remains beyond granite emplacement and the subsequent thermal re-equilibration of the lithospheric temperature profile along with forces related to flexural tension (both of which are referred to as 'second-order forces' by Sonder, 1990 and Zoback, 1992). To investigate the relationship between low-density granite bodies and rift basin geometry further, a 2D lithosphere-scale geodynamic modelling approach is adopted. Constraint and input parameters for the models are obtained from the case study area in northern England.

4.5 Case study: Carboniferous basins of northern England

Modern studies of the Carboniferous succession of the UK benefit from the volume of widely available regional geophysical data and prior interpretations of deeper lying structures (e.g., Brewer *et al.*, 1983; Kimbell *et al.*, 2006). Figure 1.1 shows the distribution of mapped, surface exposed faults

in northern England at 1: 250,000 scale (British Geological Survey, 2008). Figure 3.2 shows the distribution of negative gravitational anomalies associated with concealed and low-density granite intrusions (also see Fig. 1.2). Without considering the various ages and styles of these exposed faults or the distribution of superficial cover, within areas of older outcrop there is a considerably higher fault population density. However, this observation does not accurately describe areas underlain by granite batholiths. The Alston Block, with its predominantly Visean-Westphalian cover (Dean *et al.*, 2011), is a prime example of this. A detailed quantitative analysis of the major basin bounding faults of northern England is beyond the scope of this work. Nevertheless, the faults with the greatest displacement within the region strongly correlate with the margins of the concealed, or partially concealed, granite bodies (Fig. 4.6).

The two cross-sections displayed in Figures 4.6a and 4.6b incorporate the structural interpretations of the Carboniferous-recent succession made by Chadwick *et al.* (1995), based on seismic and well data constraints. Both sections appear only mildly deformed, by Variscan compression, in comparison with the Carboniferous sub-basins further south (Corfield *et al.*, 1996). However, more recent modifications due to Permian-Mesozoic subsidence events are apparent in the thin veneer of Permian succession preserved in the Vale of Eden Basin and to the east of the Alston Block (Fig. 4.6b). Thickening of Carboniferous stratigraphy across the Pennine Fault is minimal, suggesting most displacement along this fault post-dated the Carboniferous Period. The local effects of widely observed, but generally poorly understood, Palaeogene regional south-eastwards tilting, which contributed to kilometre-scale erosion in the Irish Sea (e.g., Green, 2002; Holford *et al.*, 2008), are best illustrated in Figure 4.6b.
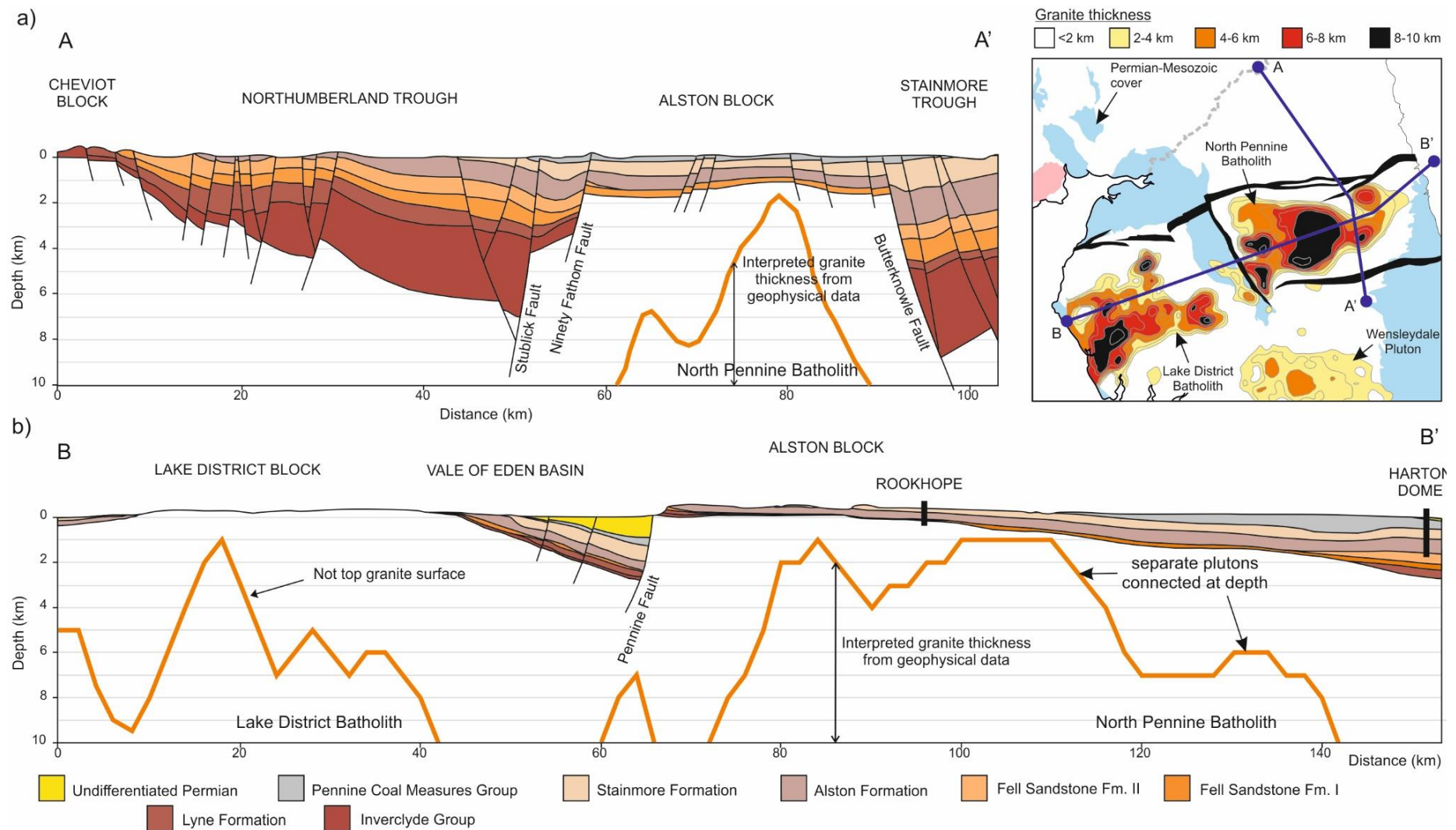
Figure 4.6: Cross-sections of the northern Pennine Basin, based on the structural interpretations of Chadwick *et al.* (1995). Granite thicknesses based on interpretations of gravity and magnetic anomaly data by Kimbell *et al.*, 2006. 3D shapefiles courtesy of Terrington and Thorpe (2013). For cross-section locations, see inset.

4.6 Application of the modelling of lithospheric extension and granite emplacement

A two-dimensional forward modelling methodology is applied to replicate interpreted basin geometries (Fig. 4.6). The effects of the underlying igneous bodies are investigated by simulating extensional basin profiles with and without the granite-induced density contrast. In so doing, some of the ideas previously outlined in the preceding chapter are tested to help gain a greater understanding of the deeper processes that ultimately govern basin architecture.

4.6.1 Two-dimensional modelling principles

The structural and geodynamic modelling approach used in this study represents a section of lithosphere as a numerical model and then simulates its deformation by a variety of processes. A typical starting condition for the modelling is a regional cross-section of undeformed lithosphere. The crustal component of this lithosphere is assumed to be 35 km thick with a density of 2800 kg m^{-3}, whilst the mantle lithosphere is assumed to be 90 km thick with a density of 3300 kg m^{-3}. The modelled lithosphere is thermally conditioned with a geotherm, which has a surface temperature of 0 °C and a temperature at the lithosphere-asthenosphere boundary of 1333 °C. These parameters can be varied. Once the lithosphere is defined it is then possible to model its deformation via a variety of geological and geodynamic processes. These processes can be numerically defined as loads, to which the responses of the lithosphere are calculated (Eqs. 4.14 to 4.17). More comprehensive descriptions of the modelling approach utilised here are presented in Kusznir and Egan (1989), Egan (1992), Egan and Urquhart (1993) and Meredith and Egan (2002) and will not be repeated here.

The model assumes a brittle-ductile transition at a depth of 20 km within the crust (e.g., Kusznir and Park, 1987). Above this boundary, the lithosphere is brittle and deforms by simple shear with subsidence controlled by fault heave and the underlying fault geometry. In the brittle crust, crustal thinning is calculated using the Chevron or vertical shear construction (Verrall, 1982; White *et al.*, 1986). All faults are assumed to have a common detachment depth coinciding with the so-called brittle-ductile transition. The locations and horizontal displacements of faults (see Table 4.3)

are based on the interpretations of Chadwick *et al.* (1995) (Fig. 4.6). As the models are purely 2D, the orientation of maximum extension is assumed to be parallel to the cross-section. Over the length of the modelled section (Fig. 4.7), the total heave is 8.5 km, equating to an overall magnitude of extension (β) of 1.09. This value is lower than that cited by Kimbell *et al.* (1989: $\beta = 1.19$) for the same basin as their magnitude of extensional deformation also accounted for the effects of inclined simple shear. The extension factor is also lower than that proposed by the same authors ($\beta = 1.3$) based on the magnitude of post-rift thermal subsidence. It is very unlikely, however, that the model cross-section presented in Figure 4.7a includes all the fault-controlled deformation in the area, which may explain this mismatch.

Modelling assumes that the lithosphere deforms via pure shear extension below a brittle-ductile transition at 20 km. Both the lateral position and magnitude of pure shear can be defined independently of the overlying simple shear deformation to simulate depth-dependent extension (e.g., Royden and Keen, 1980). To compensate for a low value of upper crustal extension and widely postulated regional out of plane extension (Dewey, 1982; Coward, 1993), a maximum pure shear extension value of $\beta = 1.25$ is applied. Pure shear is unevenly distributed across the model, subsiding laterally from the maximum value at 75 km to $\beta = 1$ (i.e., no deformation) at 0 km and 150 km. The isostatic responses to the thinning of the lithosphere due to simple and pure shear are calculated.

The geometry of the modelled basement and syn-rift fill is mainly a product of the underlying fault geometry and heave (Egan *et al.*, 1999). The basement profiles portrayed in Figure 4.7a and b are based upon the interpretation of deep and relatively low-resolution seismic data (Chadwick *et al.*, 1995), and are not necessarily structurally balanced. Nonetheless, this basement profile is replicated best by incorporating listric faults with a near surface dip of 55° (Fig. 4.7) (Table 4.3). Such structures may reflect inheritance from the pre-Carboniferous Caledonian basement, which is exposed to the north of the study area in the Southern Uplands of Scotland (Pharoah *et al.*, 1995). Much of the Carboniferous structure in northern England is believed to have been derived

66
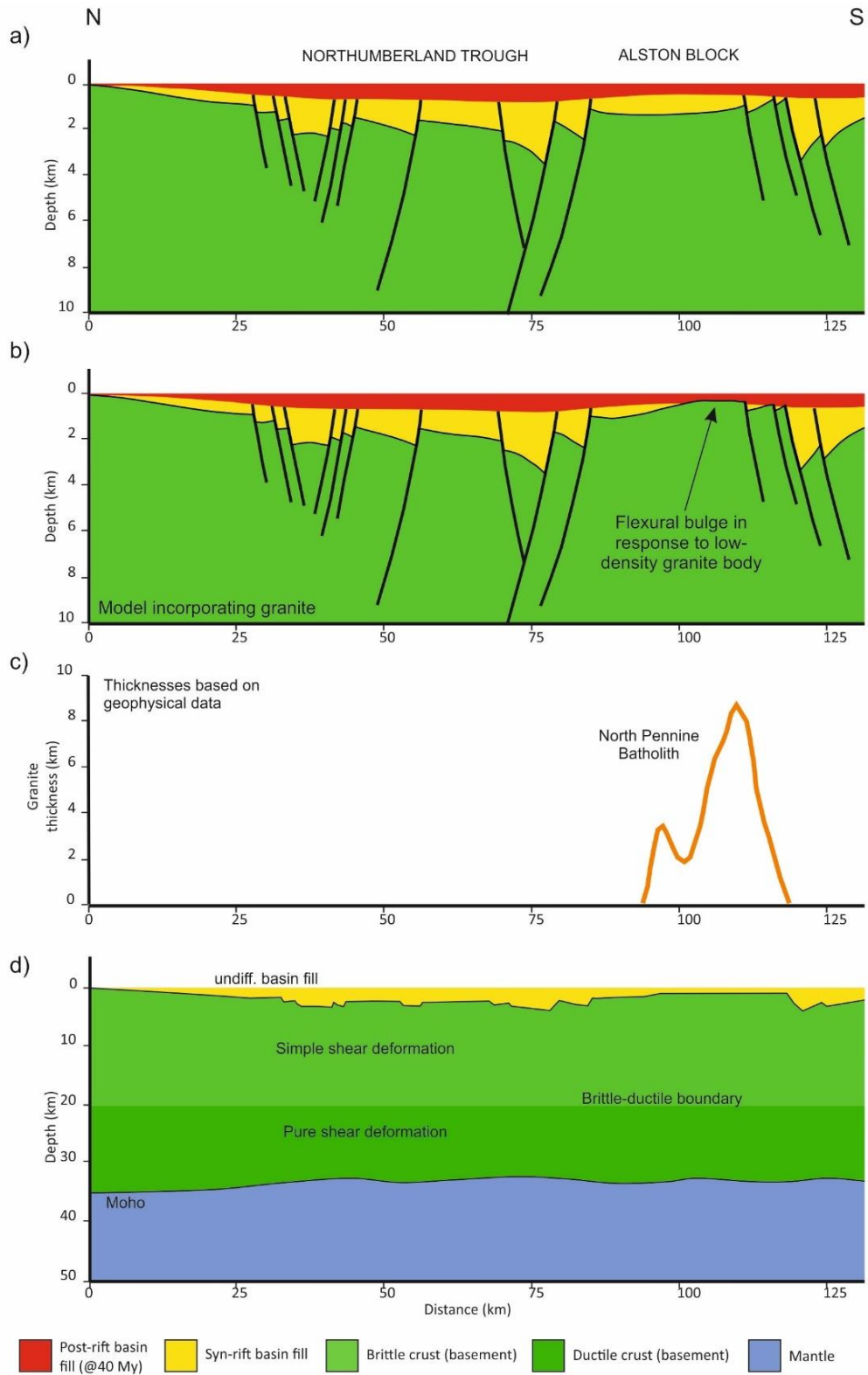
Figure 4.7: Model generated along the line of the cross-section presented in Fig. 4.6a across the Northumberland Trough and Alston Block. Fault locations and offsets (4.7a and b) are displayed in Table 4.3 and are based upon the deep structural interpretations made by Chadwick *et al.* (1995). 4.7b incorporates a granite thickness profile (4.7c) based upon the interpretations of gravity and magnetic anomaly data (Kimbell *et al.*, 2006). 4.7d shows the modelled lithosphere scale profile.

from the reactivation of late Caledonian compressional structures and the shallowly dipping, deep Iapetus suture zone (Fig. 1.2) (Soper *et al.*, 1992).

Fault	x-coordinate (km)	Antithetic/ Synthetic	Heave (km)	Dip (°)
1	28	S	0.25	55
2	32	S	0.25	55
3	34	S	0.5	55
4	41	A	0.25	55
5	43	A	0.25	55
6	45	A	0.25	55
7	56	A	0.5	55
8	70	S	0.25	55
9	79	A	1.5	55
10	85	A	1.0	55
11	111	S	0.25	55
12	116	S	0.25	55
13	118	S	2.5	55
14	124	S	0.5	55

Table 4.3: Coordinates, orientation, horizontal displacement (heave) values and dip values for faults used in two-dimensional modelling (Fig. 4.7; from left to right of section).

Following the rift phase, the models include 40 My of post-rift, thermally induced subsidence (e.g., McKenzie, 1978). If deformation is assumed to have begun during the latest Devonian (~360 Ma; as suggested by Chadwick *et al.*, 1995; Monaghan and Parrish, 2006), the model then effectively calculates sedimentation until the late Namurian or early Bashkirian (~320 Ma) Stage, after which the rate of sedimentation increases during the Westphalian or late Bashkirian stages (Peace and Besly, 1997). Post-rift basin fill is more uniformly distributed than syn-rift basin fill. Whereas syn-rift subsidence is controlled predominantly by faulting, post-rift subsidence is controlled by more uniformly distributed pure shear, which is responsible for thinning the lower lithosphere and raising the lithosphere-asthenosphere boundary (White and McKenzie, 1988).

The modelled maximum basin thickness is ~3.5 km (Fig. 4.7d), which is less than the ~5 km succession of preserved early Carboniferous succession observed in the Northumberland Trough

(Fig. 4.7a) (Day, 1970). Incorporating greater heave within the model would dishonour the interpretations of Chadwick *et al.* (1995), utilising greater pure shear values would invoke perhaps unrealistic depth-dependent extension and 'space issues' (e.g., Egan and Meredith, 2007). This discrepancy could be attributed to several factors: 1) fault heave beyond model resolution (250 m); 2) out-of-plane extension (e.g., Coward, 1993); 3) possible misinterpretation of the poorly imaged top Caledonian basement; or 4) the likely uneven nature of the post-Caledonian, thrusted palaeo-topography. Although a discrepancy in basin depth is recognised, the model is deemed satisfactory for the purposes of this study.

As expected, the differences between the modelled basin geometries with and without incorporating granite-induced density contrasts (Fig. 4.7a and b, respectively) can be observed on the Alston Block. When no granite is incorporated within the model (Fig. 4.7a), top basement forming the Alston Block is characterised by two inwardly dipping margins. This geometry represents the flexural response to lithosphere unloading along regions of crustal thinning due to the two dominant fault systems, which have opposing dip directions (Kusznir *et al.*, 1991). In the absence of granite, the modelled thickness of the sedimentary succession on the Alston Block is ~1500 m. This is significantly greater than the ~700 m-thick Viséan–Namurian succession preserved along the western extent and centre of the Alston Block, despite a lower magnitude of extension being utilised in the modelled example.

4.6.2 Modelling the effects of granite emplacement (cross-line)

The model presented in Figure 4.7b incorporates a 2D granite thickness profile (Figs. 4.7c) based on prior interpretation of geophysical data (Kimbell *et al.*, 2006). The granite thickness value is used to calculate the overall bulk crustal density at a given point, $\rho_{gc_{(x)}}$ (Eq. 4.9), and the imposed load on the lithosphere (Eq. 4.5).

A relatively low elastic thickness (Te) value of 5 km is assumed. This is partly justified to replicate the generally low elastic thicknesses estimated in extensional tectonic settings, which relate in part to the associated elevated geotherm (Kusznir *et al.*, 1991). Additionally, a low elastic

thickness value is adopted to approximate the partial detachment and failure of the lithosphere associated with faulting. Prior to faulting, a more cohesive and cooler lithosphere is likely to limit the isostatic compensation due to the granite body (Fig. 4.5). As basin scale faults propagate, the crust becomes less cohesive and the ability of the lithosphere to limit localised isostatic uplift reduces.

The most obvious difference observed when granite is incorporated into calculations (Fig. 4.7b) is the significantly thinner sedimentary succession (~400 metres) modelled over the centre of the Alston Block, which better replicates the thin Carboniferous succession that is observed (Day, 1970; Stone *et al.*, 2010). This coincides with the thickest part of the North Pennine Batholith. A further significant difference observed in the granite model is the drape-like, broad monocline shape of the top basement along the north of the block (Fig. 4.7b). This geometry is likely exaggerated in the model compared with the cross-section because of the solely two-dimensional nature of the model. The inset granite thickness and fault offset map in Figure 4.6 shows the adopted trend-line intersecting two cupolas of the North Pennine Batholith towards the north-east of the block which are likely to have invoked further out-of-plane uplift and flexure.

Interestingly, the basement monocline observed when incorporating granite (Fig. 4.7b) echoes the north-eastern and offshore margins of the Alston Block (Fig. 4.6b) (Murchison, 2004). Various authors have stated that the margins of the granite-cored highs are characterised by 'hinge-lines' onto which early Carboniferous strata onlap (George, 1958; Bott, 1967; Johnson, 1967; Leeder, 1975). These hinge lines are commonly faulted but are also locally characterised by monoclines like those observed in Figure 4.6 and replicated in Figure 4.7b. Both types of structure are believed to form in crust relatively free from granite that is immediately adjacent to granite-cored crust (Leeder, 1975). Constraints on the deeper concealed stratigraphy of the Alston Block are sparse so perhaps the best illustration of this basement monocline are some of the early-mid Carboniferous thickness trends of the northern Pennine Basin (also see Fig. 2.7). Despite anticipating a thin cap of mid-late Carboniferous stratigraphy akin to the ~390 metres encountered in the Rookhope borehole (Dunham *et al.*, 1965), ~1800 metres of Visean-Westphalian (Bashkirian) stratigraphy were

encountered at Harton Dome without reaching basement and before drilling finally ceased (Fig. 4.6) (Ridd *et al.*, 1970).

4.6.3 In-line

The effects of granite emplacement have been further investigated by the generation of an additional forward model (Fig. 4.8) representing the approximately E-W in-line section across the Lake District Block, Vale of Eden Basin and Alston Block (see inset of Fig. 4.6). As the section is oriented roughly parallel to the dominant structural trend, the effects of faulting are largely removed. A uniform pure shear beta-value of 1.25 is applied that is consistent with the cross-line section. Permian fill of the Vale of Eden Basin is bound to the east by the Pennine Fault. However, as Carboniferous strata shows no significant thickening across the fault, only 0.25 km of horizontal displacement is modelled. Forty million years of post-rift thermal subsidence is included in the model which produces an evenly distributed, uniformly thick succession of approximately 1.3 km due to a combination of assuming a uniform beta-value, no crustal density variations, and a single fault with small displacement (Fig. 4.8a).

When crustal density is varied according to the thickness of the underlying granite bodies (Fig. 4.6), an undulose basement topography is generated (Fig. 4.8b). Despite modelling limited faulting, the general absence of low-density granite underlying the Vale of Eden compared with the surrounding Alston Block and Lake District Block predicts a narrow, trough-shaped basin. Along the eastern extent of the model, syn-rift basin fill thickness increases significantly, again mimicking the thickness trends encountered in the Harton Dome well compared with the Rookhope well (Fig. 4.6). As only minimal amounts of crustal thinning are calculated due to the absence of large Carboniferous faults along the section, post-rift basin fill thickness is largely uniform except for where syn-rift subsidence alone is not sufficient to lower the basement elevation below sea level.

Top basement monoclines and significant sediment thickness variations related to the underlying thicknesses of granite bodies are predicted in numerical modelling experiments. It is suggested therefore that early Carboniferous thickness discrepancies in the northern Pennine Basin
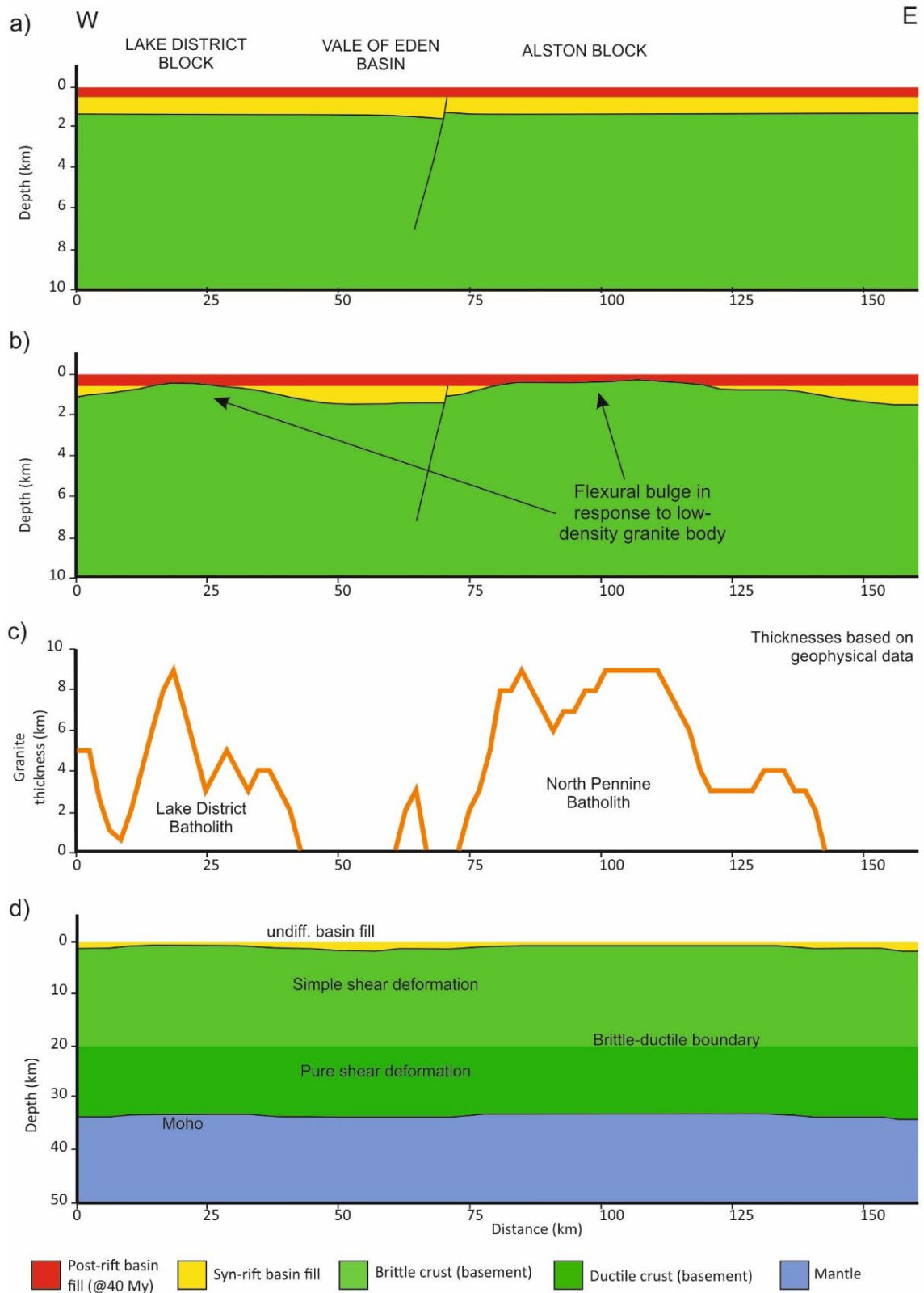
Figure 4.8: Model generated along the line of the cross-section presented in Figure 4.6b. The only fault included within the model is the Pennine Fault, across which the Carboniferous strata barely thicken, suggesting little displacement during this period. Profile b incorporates a granite thickness profile (c) based upon the interpretations of gravity and magnetic anomaly data (Kimbell *et al.*, 2006). Profile d shows the modelled lithosphere-scale profile.

are, in part, due to the flexural isostatic response of the lithosphere to low density granite bodies and the later superimposed effects of lithospheric extension.

4.7 Discussion

Numerical modelling of lithospheric extension and basin formation has provided evidence that large basement granite bodies can strongly influence basin architecture and form areas of strong relief through their buoyancy, as was first proposed by Bott *et al.* (1958). By accounting for large, low-density granite bodies, it is possible to replicate some of the geometries observed in the northern Pennine Basin (Figs. 4.7 and 4.8). However, contrary to common perception, relatively buoyant granite-cored crust is not capable of resisting subsidence during lithospheric extension.

The emplacement of typically low-density granite prompts an incomplete isostatic response; even when associated temperature fluctuations are ignored (Fig. 4.5). This generates a regional flexural profile prior to lithospheric extension and leaves residual second-order stresses associated with the under-compensated buoyancy of the granite and flexural tension (e.g., Sonder, 1990; Zoback et al., 1992). The pre-existing structural framework of the region probably plays an important role in determining the geometry of the granite body and effective elastic thickness of the lithosphere (Te), both of which have a direct influence on numerical simulations of this flexural profile.

The depth of emplacement of a granitic body is likely to influence subsidence and structural partitioning within the crust. The incorporation of a bulk crustal density value, such as is the case here, effectively assumes the proportion of granitic and non-granitic crustal material deforming by simple and pure shear is equal. However, if the granite body were to reside solely within the upper crust, then the granite body would not deform via the mechanism of pure shear at all (e.g., Royden and Keen, 1980). Crustal material removed from the lower lithosphere overburden by means of pure shear would, therefore, have the same density as 'standard' crustal material, regardless of the presence or absence of granite in the upper crust. The calculated subsidence in response to pure shear would be identical to that of 'standard' lithosphere. Alternatively, if a granite body were to

reside solely within the lower, more ductile crust, thinning of the granite body due to pure shear would be underestimated when utilising a bulk crustal density value (ρ_{gc}), as would subsidence.

Regional-scale extensional faulting is another feature strongly linked with this tectonic framework. There is a strong link between the flexural response to granite and the localisation of extensional strain along the hinges of the flexural profile (e.g., Fig. 4.5) or peripheral margins of the granite body at depth (Fig. 4.6). Figure 4.9 illustrates how tectonic stresses due to extensional tectonism and second-order stresses, due to the incomplete isostatic compensation of the low-density granite body and flexural tension, could constructively interfere. However, at the regional scale, large basin-bounding faults, particularly their orientation, are not so apparently guided by the subsurface granite extent. With the northern England case study for example, it is likely that older inherited Caledonian lineaments are more important here (e.g., Coward, 1993; Corfield *et al.*, 1996). Nonetheless, the interaction of these stress fields could perceivably impose the localisation of stress conditions more favourable to the normal reactivation of ancient lineaments within basement surrounding intruded granite.

Where exposed, crystalline granite bodies of northern England lack the internal inconsistencies of the ancient orogenic basement (Allsop, 1987). The granite-cored blocks do not easily develop normal faults during extension because they have an undeformed, relatively homogenous mid-crust. The lateral continuity of the North Pennine Batholith of the Alston Block, and that of the batholiths underpinning the Lake District and Askrigg blocks, at around 10 km depth inhibits the local connectivity of pre-existing structures between the upper- and midlevel crust and limits displacement. Conversely, the surrounding crust that lacks this intruded granite sealant has uninterrupted connecting lineaments which are more easily reactivated.

Second-order stresses can drive preferential propagation of basin-bounding faults during the early stages of extension, which, along with the likely decrease of the effective elastic thickness of the lithosphere, is likely to prompt more complete isostatic compensation of granite-cored blocks and relax these stresses. Figure 4.9 shows a schematic illustration of how these stress fields may interact before and during lithospheric extension. The absence of faults surrounding the largest fault

structures may be explained by a 'strain shadow' effect (e.g., Nicol *et al.*, 2005), whereby tensile stress is relieved by large fault structures, negating the need for further brittle failure in the immediately surrounding area.
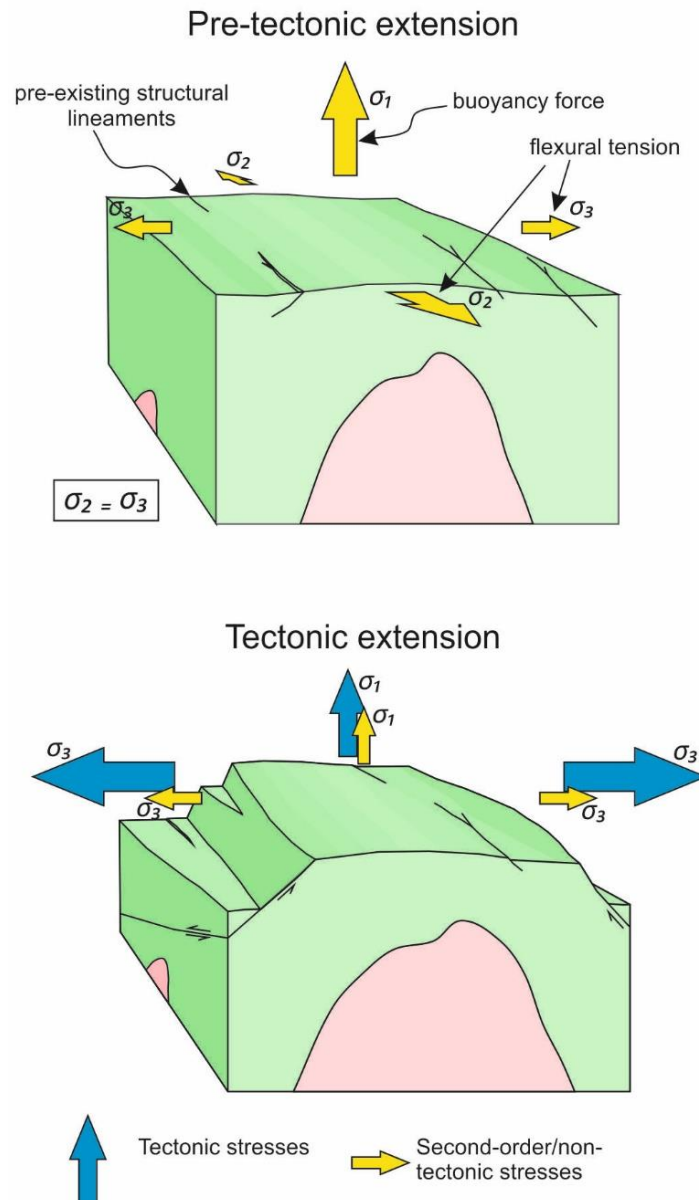
Figure 4.9: A schematic illustration of the stress conditions before (top) and after (bottom) tectonically induced extensional faulting. Yellow arrows indicate 'second-order' stresses (e.g., Sonder, 1990; Zoback, 1992) whilst blue arrows indicate tectonic stresses. It is proposed that the combination of 'buoyancy' forces, flexural tensile stress and horizontal tectonically induced extensional stress constructively interfere during extensional tectonism, creating localised stress conditions favourable to the reactivation of inherited (i.e., Caledonian) lineaments. Buoyancy-related second-order stresses are at least partially relieved during tectonic extension, which permits more complete isostatic compensation of the granite-cored block.

This geodynamic and structural framework has several potentially important implications for predicted depositional trends. The relief of a granite-cored high during the early stages of rifting has important implications for sediment routing, whereas the predicted subsidence of this high during later stages of rifting (e.g., Figs. 4.2 and 4.3) is more likely to influence palaeo-basin topography and the distribution of potential high permeability reservoir facies. The depth to top basement has a significant impact on a region's thermal structure (Bayer *et al.*, 1997) which, even without considering the typically high radiogenic heat production of granite bodies, such as those modelled (Busby *et al.*, 2011), is likely to have a pronounced impact on source rock maturation as well as geothermal potential. Several of the succeeding chapters within this thesis will investigate these relationships.

4.8 Conclusions

In this chapter, a study using lithospheric scale numerical modelling of extensional tectonics is presented to help investigate the possible effects of granite emplacement. It is possible to generate basement relief by incorporating density contrasts within the crust such as those created by the emplacement of a granitic body. However, contrary to common beliefs, the relative buoyancy of granite bodies with respect to accommodating crust is not capable of resisting subsidence during lithospheric extension. Lithospheric flexure reduces the initial isostatic compensation in response to a less dense granite body, in terms of amplitude, but increases the wavelength of the isostatic deflection (Watts, 2001). A regional flexural profile is generated prior to lithospheric extension and residual second-order stresses associated with the under-compensated buoyancy of the granite and flexural tension remain. There is a strong correlation between the distribution of large extensional faults and concealed granite bodies. These faults generally coincide with areas of non-granite cored crust immediately adjacent to concealed granite bodies. The interaction of tectonic forces, second-order isostatic or flexural forces, and inherited basement structure, are suggested to justify this relationship. It is proposed that the interaction of three factors ultimately dictate the tectonic framework within a partially granitic, brittle-ductile lithosphere and the occurrence of intra-basin highs: 1) non-tectonic, 'second-order' stresses such as the flexural response of the lithosphere and

residual, under-compensated buoyancy forces in relation to granite bodies; 2) extensional tectonic stress and; 3) inherited basement fabric.

'Block and basin' style rift basins: sedimentological insights from the early Carboniferous Fell Sandstone Formation

5.1 Introduction

In this chapter, sedimentological characteristics of the early Carboniferous (Visean) fluvio-deltaic Fell Sandstone Formation and age-equivalent stratigraphy of the partially exhumed northern Pennine Basin in northern England are examined, focussing on the interaction of these sediments with the locally underpinning (syn-rift) 'block and basin' style rift basin framework. In doing so, insights into how this, until now, poorly defined tectonic framework may influence basin dynamics during rifting are gained. Field and borehole-based lithological, petrographical, petrochemical and petrophysical observations and sedimentological and provenance analyses are described. This chapter forms the third and final chapter of this part (Part II) of the thesis, which is focussed on the classically interpreted 'block and basin' rift basin style of the early Carboniferous northern Pennine Basin. Key variances between these findings, classic 'block and basin' tectono-stratigraphic models, and more recent depictions of rift basin systems are scrutinised.

5.2 The Fell Sandstone Formation and stratigraphically equivalent units in the northern Pennine Basin

Early Carboniferous half-grabens and sag basins, such as the Northumberland-Solway Basin and more minor Tweed Basin, are separated by pre-Carboniferous intra-basin basement highs, such as the Lake District and Alston Blocks, as well as the Cheviot Block and the remainder of the Southern Uplands, on to which the Carboniferous succession onlaps unconformably (Chadwick and Holliday, 1991) (Fig. 5.1). In Northumberland, Durham and Cumbria, these basins are collectively referred to as the northern Pennine Basin. Many of these basement highs are bound by major (>100 m) vertically displacing faults, such as the Alston and Lake District Blocks and are thus referred to as 'blocks' (e.g., Leeder, 1982) (Fig. 1.2). However, other basement highs, such as the Cheviot Block,

79
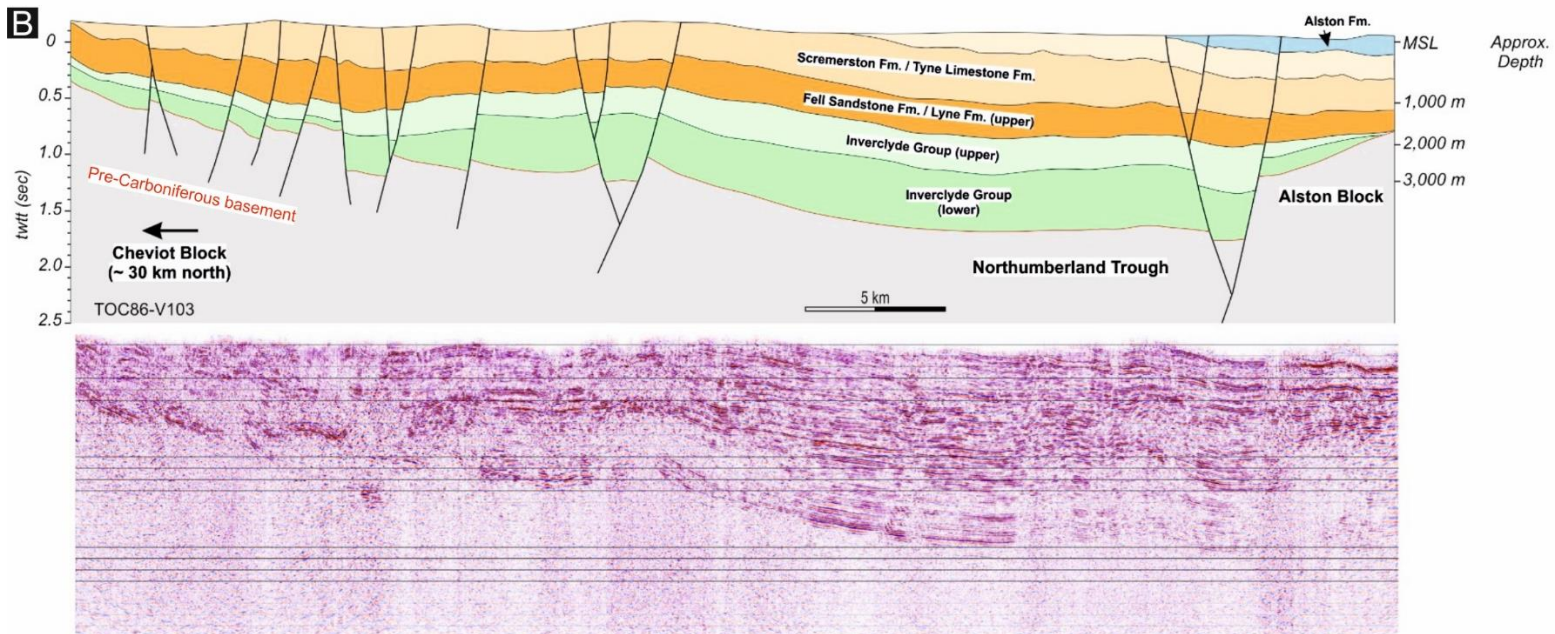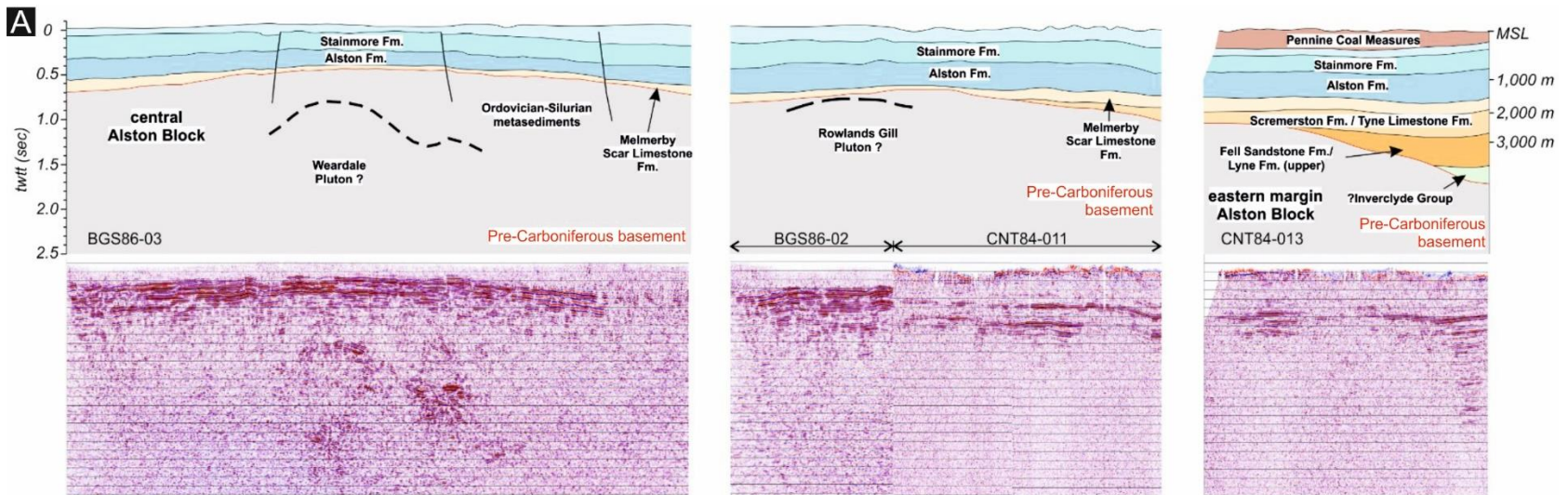
Figure 5.1: Uninterpreted and interpreted seismic sections from the northern Pennine Basin, northern England. Seismic reflection profiles are courtesy of the UK Onshore Geophysical Library (UKOGL). See Figure 5.3 for locations. Figure 5.1a shows an E-W transect from the central and granite-cored part of the Alston Block to the Alston Block's eastern margin. Carboniferous sediments are penetrated by deep boreholes and can be seen onlapping against the Alston Block in response to the low-density North Pennine Batholith. Figure 5.1b shows a N-S transect from the Alston Block to the central part of the Northumberland Trough. The Northumberland Trough forms a tilted half-graben, with Carboniferous sediments thickening to the north.

are not and can be characterised more accurately as regional (tens of kilometres wide) domes (Shiells, 1963). Ordovician-Devonian low-density granitic intrusions underpin all pre-Carboniferous basement highs in the northern Pennine Basin and along the Scottish Borders and are evident from both outcropping surface geology and Bouguer gravity anomalies (Fig. 3.1) (Bott, 1967). The geometry of these basins was successfully replicated in the preceding chapter of this thesis (Chapter 4), by adopting a 2D lithosphere scale structural and geodynamic numerical modelling methodology and by incorporating subsidence in response to normal faulting and lithospheric extension, and uplift in response to the emplacement of low-density granite intrusions and flexural isostasy.

The onshore Fell Sandstone Formation (Middle Border Group) is typified by sand-rich fluvial deposits that are buried across the northern Pennine Basin and crop out across northern Northumberland (Turner *et al.*, 1987). These deposits span the Chadian-Asbian substages (Fig. 2.2) (Waters *et al.*, 2011). The Fell Sandstone Formation pinches out down-system towards the southwest where deposits are mixed clastic-carbonate sediments of deltaic and shallow marine origin (Day, 1970). These mixed, age-equivalent deposits belong partly to the Cambeck Member of the Lyne Formation (also Middle Border Group) as well as partly to the Fell Sandstone Formation itself (Armstrong and Purnell, 1987). These sediments were deposited during a period of prolonged early Carboniferous (Mississippian) rifting (Fraser and Gawthorpe, 1990). The occurrence of 'seismites' and the Glencartholm Volcanic Beds immediately above the Fell Sandstone Formation in Northumberland is believed to represent one pulse of accelerated basin extension (Booth *et al.*, 2020).

In the northern Pennine Basin, successions belonging approximately to this stratigraphic interval have been informally grouped together as the 'Fell Sandstone succession' (Day, 1970; Turner *et al.*, 1993; Dean *et al.*, 2011; Bell *et al.*, 2017) (Fig. 5.2). The informal 'Fell Sandstone succession' is adopted here to describe the Fell Sandstone Formation and Cambeck Member in the central Northumberland and Solway Basins and age-equivalent successions in the broader northern Pennine Basin, deposited by dominantly fluvial or deltaic processes (e.g., Day, 1970). As a result, this succession can effectively be constrained within the upper and lower boundaries of the TS miospore zone with the TC and Pu zones, respectively (Fig. 5.2). Biostratigraphic studies from literature (Day,

Figure 5.2: Latest Devonian-Early Carboniferous (Mississippian) stratigraphy of the northern Pennine Basin. The miospore zonation scheme of Waters *et al.* (2011), based on Clayton *et al.* (1977, 1978) and revised later by Clayton *et al.* (1985), and the onshore Carboniferous lithostratigraphic framework of Waters *et al.* (2007) are used. The former Carboniferous stratigraphic subdivisions of NW Europe are adopted, and a comparison is made with current international stratigraphic nomenclature based on Davydov *et al.* (2004, 2012). Note that the Tournaissian, Visean and Serpukhovian Stages constitute the Mississippian Series under the current International stratigraphic subdivisions and the Tournaissian, Visean and Namurian Stages constituted the Dinantian Series under the former Carboniferous stratigraphic subdivisions of NW Europe. NPB = North Pennine Batholith; CP = Cheviot Pluton; SL = Sixth Limestone; CB = Clattering Band (Knightsbridge Limestone); LAB = Lower Antiquatonia Beds; K/B = Kelso Lavas and Birrenswark Volcanics; GV = Glencartholm Volcanics.

1970; Neves *et al.*, 1973; Armstrong and Purnell, 1987; Mahdi and Butterworth, 1994; Johnson *et al.*, 2011; Waters *et al.*, 2011) and borehole reports are summarised in more detail in Figure 5.2. Where biostratigraphic data are absent, such as for the Newcastle Science Central (deep geothermal) borehole, the top of the Fell Sandstone succession is taken, as far as this study is concerned, as the top of the lithostratigraphically defined Fell Sandstone Formation, as per the Northumberland Basin (Day, 1970). For the Harton borehole succession, the top of the Fell Sandstone succession is taken at the top of the 'unnamed sandstone' unit (Ridd *et al.*, 1970), based on similarities with the nearby Newcastle Science Central succession (Younger *et al.*, 2016).

5.3 Data and Methods

This study combines both field and borehole-based sedimentological, petrographical, petrochemical and petrophysical observations and analyses of the Fell Sandstone succession in the northern Pennine Basin. The localities of borehole and outcrop successions used as part of this study are shown in Figure 5.3, as well as the types of data analysed or collected at each locality. Borehole data were accessed via the British Geological Survey (BGS) core store in Keyworth, online via the BGS onshore Geoindex (bgs.ac.uk/geoindex/) or the UK Onshore Geophysical Library (UKOGL; ukogl.org.uk/), by hard copy through the UK Oil and Gas Authority or via published literature. A more detailed account of borehole data used as part of this study is summarised in Table 5.1. Borehole and outcrop data vary from intact drillcore to drillcore samples, borehole chippings, petrophysical and petrochemical (gamma ray, density, lithology) borehole logs, biostratigraphic data, rock samples for petrographical (thin-section) and petrochemical (handheld XRF) analysis, and outcrop-based sedimentary logs and images.

Lithological and petrochemical facies and facies association schemes are based on conventional sedimentary (grain size, sedimentary structures) and spectral gamma ray logging of the Fell Sandstone succession exposed in the field and borehole successions. Gamma ray responses for the Stonehaugh Borehole succession were collected with the RS 230 Super-Spec BGO spectrometer. Total radioelement abundance was measured for 90 seconds every 50 cm. Net to gross (sand %) map and interpreted facies trends are based on borehole data. Boreholes with over 100 m of
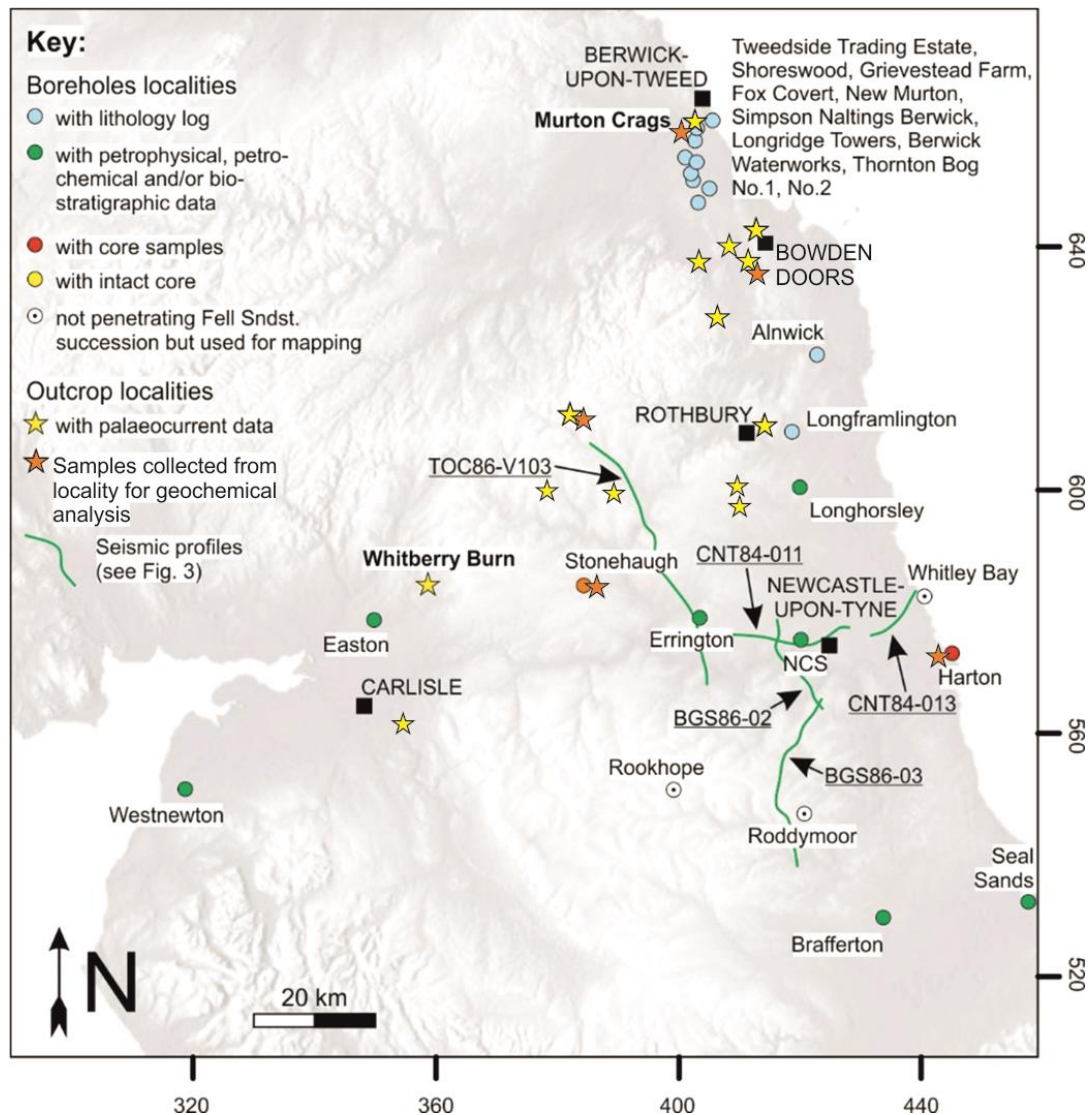
Figure 5.3: A map of the northern Pennines indicating borehole and outcrop localities used as part of this study and the data associated with each locality. Refer to Table 5.1 for a further list of borehole data used as part of this study. The locations of seismic lines displayed in Figure 5.1 are also indicated. Terrane map is modified after maps-for-free.com/.

penetration through the Fell Sandstone succession are included for the sake of the net to gross map's completeness. Palaeocurrent measurements were taken across 13 field localities to construct a map of regional palaeocurrent.

Sandstones from the Stonehaugh and Harton boreholes and the field were cut as thin sections so that their mineralogical assemblages and textural characteristics could be analysed. Fine to medium-grained sandstones collected from drillcore and from the field were analysed using a Niton XL3t energy dispersive spectrometer at Keele University. The instrument was calibrated

using a range of international standard lithological reference materials. Data quality and instrumental drift was evaluated via regular analysis of secondary international reference materials. Precision (2 sigma), determined via repeat analysis of standards and samples, was < 6 % for major elements (SiO_2, TiO_2, Al_2O_3, Fe_2O_3, CaO, K_2O) and < 7 % for trace elements (Nb, Zr, Sr, Rb). The mean deviation from the accepted standard values was typically < 5 % for major elements (excluding $Al_2O_3 - 8$ %) and < 5 % for trace elements. Hand specimen samples were analysed between 3 and 5 times, moving the analysis spot each time, to compensate for sample heterogeneity. The most homogeneously distributed elements within single samples included Sr and Rb; the concentration of these elements varied typically between 10 % and 15 % within single samples. Elements associated strongly with rarer minerals and were therefore less homogenously distributed included Zr, whose concentration varied around 60 % within single samples. The average of these readings was calculated to ensure representative measurements.

Borehole name	BGS reference	Easting (BNG)	Northing (BNG)	Year drilled	Derivation (web link)
Alnwick	NU11SW10	414620	612100	–	Turner *et al.* (1997) BGS Geoindex Onshore (scans.bgs.ac.uk/)
Berwick Waterworks	NT95SE6	399770	652110	1904	BGS Geoindex Onshore (scans.bgs.ac.uk/)
Brafferton	NZ22SE105	428432	521493	1989	OGA
Easton	NY47SW15	344124	571694	1990	OGA
Errington	NY97SE50	397740	571350	2004	OGA
Fox Covert	NT95SE201	397294	650597	1993	BGS Geoindex Onshore (scans.bgs.ac.uk/)
Grievestead Farm (1)	NT94NW19	393062	645057	2010	BGS Geoindex Onshore (scans.bgs.ac.uk/)
Harton (Dome)	NZ36NE80	439660	565620	1960	BGS Core Store Ridd *et al.* (1970) BGS Geoindex Onshore (scans.bgs.ac.uk/)
Longframlington	NU10SW11	413285	600860	1964	Turner *et al.* (1993) BGS Geoindex Onshore (scans.bgs.ac.uk/)

Longhorsley	NZ19SW6	414441	592548	1986	OGA
Longridge Towers	NT95SE11	395850	650010	1942	BGS Geoindex Onshore (scans.bgs.ac.uk/)
New Murton	NT94NE14	396640	648950	1972	BGS Geoindex Onshore (scans.bgs.ac.uk/)
Newcastle Science Central (Deep Geothermal Borehole)	NZ26SW3569	424010	564330	2011	Younger *et al.* (2016)
Seal Sands	NZ52SW308	453796	523805	1974	BGS Core Store Johnson *et al.* (2011)
Shoreswood	NT94NW12	394527	646667	1990	BGS Geoindex Onshore (scans.bgs.ac.uk/)
Simpson Naltings Berwick	NT95SE4	398800	651920	1961	BGS Geoindex Onshore (scans.bgs.ac.uk/)
Stonehaugh	NY77NE2	378990	576190	1975	BGS Core Store Smith and Holliday (1991) BGS Geoindex Onshore (scans.bgs.ac.uk/)
Thorton Bog	NT94NE22	395500	647900	-	BGS Geoindex Onshore (scans.bgs.ac.uk/)
Tweedside Trading Estate	NT95SE200	398714	652078	2018	BGS Geoindex Onshore (scans.bgs.ac.uk/)
Westnewton	NY14SW32	312300	543550	1989	OGA

Table 5.1: Borehole data with derivation and web links.

5.4 Facies and facies tracts

For lithofacies and architectural element descriptions of the Fell Sandstone succession of the northern Pennine Basin, the reader should refer to Tables 5.2 and 5.3, and Figure 5.4, respectively. In this section, two broad facies tracts are summarised. These are: *fluvial-dominated deposits* and *delta-dominated deposits*.

5.4.1 Fluvial-dominated deposits

Description

This association comprises five architectural elements: fluvial channels (FC), sheets (S), lateral and downstream accretion (LA and DA) and floodplain (FP) (see Table 5.3 for architectural element descriptions). Sandy channels and accretionary elements dominate the association with minimal floodplain deposits preserved within outcrop. The channels are typically stacked and amalgamated with minor conglomeratic bases and generally show a progressive fining upwards fill. Most channels are dominated by planar or trough cross-bedded sandstones, whereas some are structureless or contain heterolithic clasts. Sheet-like elements make up a very small proportion of the association and are dominated by structureless to parallel-laminated sandstone. The lateral accretion elements have a lensoidal geometry with internal second and third-order bounding surfaces, with the dip of the internal cross-bedding approximately parallel to the strike of the higher order bounding surfaces. The downstream accretionary elements also have a lensoidal geometry and contain internal third order bounding surfaces, but the internal cross-bedding dips approximately perpendicular to the strike of the higher order bounding surfaces. Floodplain elements are rarely preserved within observed field sections. However, from core analysis, floodplain elements may constitute up to 50 % of the succession locally. The floodplain elements are dominated by structureless to parallel-laminated siltstone, are often heavily bioturbated and typically contain pedogenic facies and minor coal fragments.

Interpretation

This association represents the development and build-up of a fluvial channel belt in a dominantly low sinuosity and bedload dominant fluvial system. The progressively fining upward fill of the channels is interpreted as the gradual abandonment of channels with a steady rate of flow (Bromley, 1991), with the basal conglomeratic units representing channel lag deposits formed from bedload transport within high-energy flows (Bridge, 1993; Fielding *et al.*, 2018). Structureless channels are interpreted to have been produced from marginal sandbank collapse (Turner *et al.*, 1987). The heterolithic channel elements represent channel abandonment (Martin & Turner, 1998).

Figure 5.4: Photoplate showing facies of the Fell Sandstone Fm. and contemporaneous sediments from the northern Pennine Basin (see Figure 5.3 for outcrop locations). 5.4a: Orthorecitified image of the Bowden Doors section showing amalgamated channel sets. 5.4b: Thick tabular cross-bedded sandstone overlying structureless concave-up sandstone from Bowden Doors, interpreted as bank collapse (*cf.* Turner *et al.*, 1987). 5.4c: Trough-cross-bed sandstone showing soft sediment deformation at Long Crag, near Rothbury. 5.4d: Very coarse, poorly sorted sandstone with andesitic and lithic clasts suggesting additional minor local provenance for the Fell Sandstone at Byrness. 5.4e: Fine sandstone-siltstone overbank deposits at Long Crag with overlying coarse-grained trough cross-bedded sandstone. 5.4f: Mudstone and siltstone facies from Whiteberry Burn, note bedding is near vertical. 5.4g: Algal-bound limestone from the Whiteberry Burn section. 5.4h: Bioturbated shallow marine sandstone bedding plane from Whiteberry Burn.
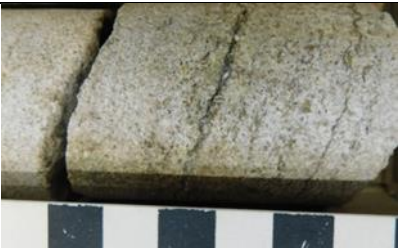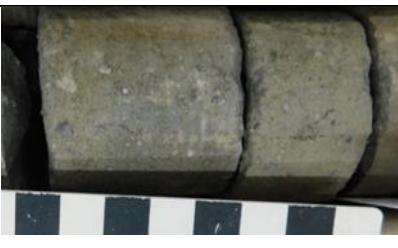
Lateral accretionary elements are interpreted as bank-attached point bars/macroforms deposited on the inside of the channel bend and indicate a moderate degree of sinuosity (Miall, 1977), whereas downstream accretionary elements are interpreted as the deposits of mid-channel bars within the channel belt representing an intermediate channel sinuosity (Miall, 1985; Ashworth *et al.*, 2000). Pedogenesis and coal development within the floodplain element suggests a terrestrial origin of the structureless to parallel-laminated siltstones; forming in a humid to semi-humid environment (Kraus *et al.*, 1999; Spears, 2012). Seatearth (gleyed) and coal provide evidence of cohesive, vegetated overbank material with permanently waterlogged soils.
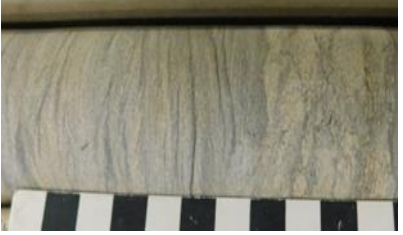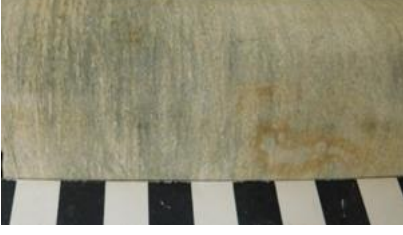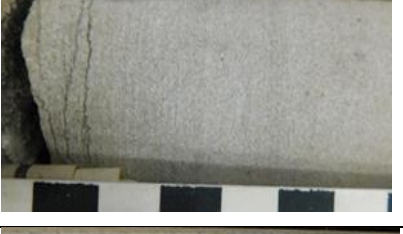
5.4.2 Delta-dominated deposits

Description

This association comprises five architectural elements: delta top distributary channels (DC), delta front bars (DB), delta slope (DS), pro-delta (PD) and floodplain (FP). Coarsening upwards successions of pro-delta sediments through to delta front channels dominate this association. The pro-delta siltstones are typically interbedded with sporadic carbonate lenses, and with thin sandstone lenses that increase in frequency upwards. The siltstones are typically weakly bioturbated and contain shell and crinoid fragments as well as marine ostracods. Delta slope elements also coarsen upwards and are dominantly composed of parallel-laminated siltstone with minor sandstone lenses which increase in abundance upwards through the association. The delta front bars have lensoidal geometries and are dominantly composed of coarsening upwards successions of planar cross-bedded sandstones with flaser to lenticular sandstones and siltstones which are sporadically bioturbated. The delta front channels have an erosional basal bounding surface and progressively fining upwards fills. The channels are dominated by planar and trough cross-bedded sandstones with minor gravel lenses and conglomeratic foresets. Floodplain elements are rarely preserved within outcrop. They are dominated by structureless to parallel-laminated siltstone, are often heavily bioturbated and typically contain pedogenic facies and minor coal fragments.

Code	Photo	Lithology & Texture	Structure & Other Features	Interpretation
C		Black, bituminous to anthracitic coal.	Thinly laminated.	Plant and tree growth in swamps or shallow pools.
Fb		Grey to dark grey, carbonaceous siltstone.	Structureless to crudely parallel-laminated frequent bioturbation and sporadic wood/plant fragments/coal.	Suspension fall out from stationary waters. Stabilization for vegetation to develop and pedogenesis removing any of the lamination.
Ffb		Grey to dark grey, carbonaceous siltstone.	Structureless, heavily bioturbated, with sporadic wood/plant fragments.	Suspension fall out from stationary waters. Stabilization for vegetation to develop.
Fm		Dark grey, carbonaceous mudstone to siltstone.	Structureless with frequent plant debris.	Suspension fall out from stationary waters. Stabilization for vegetation to develop and pedogensis removing any of the lamination.
Fpl		Grey to dark grey siltstone.	Parallel-laminated.	Suspension fall out from stationary waters.
Gm		Grey, granule to pebble sized, poorly sorted, sub-rounded to sub-angular, clast supported conglomerate.	Structureless.	Sub-aqueous, high energy Newtonian flow under high sediment load conditions, with suppressed bedform development.

Gt		Grey, granule to pebble sized, poorly sorted, sub-angular to angular, clast supported conglomerate.	Trough cross-bedded.	Sub-aqueous lower flow regime conditions with high sediment load, intermittent development and migration of dune-forms.
Lc		Light grey, sparitic limestone.	Structureless.	Sub-aqueous precipitation and crystallisation of carbonate.
Lm		Grey to dark grey, carbonate mudstone to wackestone.	Fossiliferous laminations with frequent Ostracods, shell and Crinoid fragments.	Sub-aqueous reworking of allochthonous carbonate
Pg		Grey to dark grey siltstone with brown mottling and up to pebble grade angular clasts.	Structureless to crudely laminated with frequent plant debris.	Suspension fall out from stationary waters. Stabilization for vegetation to develop. Alteration and weathering leading to the pedogenesis of siltstone.
Pn		Dark grey siltstone with rusty brown nodules.	Structureless to crudely laminated with occasional siderite nodules, plant debris and root traces.	Suspension fall out from stationary waters. Stabilization for vegetation to develop. Alteration and weathering leading to the pedogenesis of siltstone.

Sf		Grey siltstone to fine-grained, poorly sorted, sub-rounded sandstone.	Flaser laminations with sporadic roots and bioturbation.	Alternation between oscillatory and unidirectional currents with periods of slack water.
Sgt		Grey, medium to coarse-grained, poorly sorted, sub-angular sandstone with gravel grade clasts.	Gravel lined planar cross-bedding.	Sub-aqueous lower flow regime conditions with high sediment load, intermittent development and migration of dune-forms.
Sh		Light grey to dark grey mudstone to fine-grained, sub-rounded sandstone with bimodal sorting.	Heterolithic bedding with occasional soft sediment deformation.	Oscillatory and unidirectional currents with rapidly fluctuating energy conditions.
Sl		Light grey to grey, siltstone to fine-grained, sub-rounded sandstone, with bimodal sorting.	Lenticular lamination.	Alternation between oscillatory and unidirectional currents with periods of slack water.
Sla		Light grey, very fine to fine-grained, moderate to well sorted, sub-rounded sandstone.	Parallel-laminated.	Sub-aqueous aggrading upper flow regime flat beds.
Sm		Light grey to grey, medium to coarse-grained, moderate to well sorted, sub-rounded sandstone.	Structureless.	Rapid deposition in high sediment load suppressing bedform development.

Sp		Light grey to grey, very fine to medium-grained, moderately sorted, sub-rounded sandstone.	Planar cross-bedded.	Migration of straight-crested dune-scale bedforms and dune trains sub-aqueously under lower flow regime conditions.
Sr		Light grey to grey, very fine to fine-grained, moderately sorted, sub-rounded sandstone.	Asymmetrical ripple-laminated.	Migration of ripple-scale bedforms in lower flow regime.
St		Light grey, fine to coarse-grained, moderately sorted, sub-rounded sandstone.	Trough cross-bedded with sporadic slumping.	Migration of sinuous-crested dune-scale bedforms and dune trains sub-aqueously under lower flow regime conditions.

Table 5.2: Facies for the Fell Sandstone Formation and contemporaneous deposits across the northern Pennine Basin. The photographed scale bars are in centimetre increments.

Interpretation

This dominantly coarsening upwards association represents the progradation of deltaic deposits into a marginal marine environment (Mount, 1984; Smith and Holliday, 1991). The presence and type of bioturbation and marine fossiliferous assemblages suggest deposition in shallow marine conditions (Turner *et al.*, 1997). Siltstones are likely to have been deposited through suspension settling away from the sediment source (Stow and Shanmugam, 1980), whilst inter-bedded parallel and ripple-laminated sandstones are likely to have been transported from up-dip deltaic systems (Blair and McPherson, 2008). Minor carbonate lenses within the parallel-laminated siltstones suggest periods of temporarily low clastic supply accommodating the production of carbonate in shallow water (Mount, 1984). Cross-bedded sandstones indicate the deposition of channel fill material, as dune-scale bedform trains fill distributary channels (Bristow *et al.*, 1993). Thin floodplain deposits with seatearth suggests prolonged periods of non-deposition and sub-aerial exposure, perhaps due to the up-dip avulsion of alluvial feeder systems (Nemec and Postma, 1993).

Element	Code	Facies	Description	Gamma Ray Response	Association
Fluvial Channel	FC	Gm, Gt, Sgt, St, Sp, Sm, Sh, Sr	'U' shaped, fining upwards association with an erosional basal bounding surface. The association is dominated by planar (Sp) and trough (St) cross-bedded, well-sorted sandstones with minor basal conglomerates.	Low response overall, increasing upwards, suggestive of a fining upwards trend.	Fluvial-dominated
Sheet	S	Sm, Sla	Tabular, sheet-like, fining upwards association with an erosional basal bounding surface. The association in dominated by structureless (Sm) to parallel-laminated (Sla) sandstones.	Very low response overall, showing no disernable variation.	Fluvial-dominated
Lateral Accretion	LA	St, Sp, Sr	Lensoidal, fining upwards association dominantly composed of cross-bedded sandstone (St & Sp) with palaeocurrents of accretionary surfaces between 60° to 120° different to the local palaeoflow.	Low overall, shallow bell-shaped curve, slight increase in gamma response upwards.	Fluvial-dominated
Downstream Accretion	DA	Gt, Gm, Sgt, St, Sp, Sr	Lensoidal, fining upwards association dominantly composed of cross-bedded sandstone (St & Sp) with palaeocurrents of accretionary surfaces less than 60° different to the local palaeoflow.	Low overall, shallow bell-shaped curve, slight increase in gamma response upwards.	Fluvial-dominated
Floodplain	FP	Fpl, C, Fb, Ffb, Fm, Pg, Pn	Tabular association of structureless (Fm) to parallel-laminated (Fpl) siltstone with minor coal (C) and pedogenic facies (Pg & Pn).	High overall, shallow peaks corresponding to coal beds.	Both
Delta Top Distributary Channel	DC	Sgt, Sh, St, Sp, Sr	'U' shaped, fining upwards association with an erosional basal bounding surface. The association is dominated by planar (Sp) and trough (St) cross-bedded sandstones.	Typically higher response than fluvial channel, steep bell-shaped curve. A distinct low value at the base due to rapid change in grainsize.	Delta-dominated

Delta Front Bar	DB	Sp, Sr, Sl, Sf	Lensoidal, coarsening upwards association dominantly composed of planar cross-bedded sandstones (Sp) with flaser (Sf) to lenticular (Sl) sandstones and siltstones.	Moderate response overall, cylindrical to funnel shaped curve, some evidence of coarsening upwards, not always present.	Delta-dominated
Delta Slope	DS	Fpl, Fm, Fb	Lensoidal, coarsening upwards association dominantly composed of parallel-laminated siltstone (Fpl) with minor sandstone lenses.	Moderate-high response overall. Funnel-shaped curve, suggestive of a coarsening upwards succession.	Delta-dominated
Pro-delta	PD	Fpl, Lc, Lm	Tabular, coarsening upwards association dominantly composed of parallel-laminated siltstone (Fpl) with minor carbonate lenses.	High response overall. Cylindrical curve with high peaks corresponding to more organic-rich horizons.	Delta-dominated

Table 5.3: Architectural elements for the Fell Sandstone Formation and contemporaneous deposits across the northern Pennine Basin.

5.5 Facies and palaeocurrent trend analysis

5.5.1 Facies trends

Poor surface bedrock exposure limits the scope of detailed facies analyses. However, a decrease of craggy hillside features in the landscape from the north-eastern Northumberland Basin south-westwards reflects decreased concentrations of weathering-resistant sandy fluvial channel and lateral to downstream accretionary facies within the succession. Two logged borehole successions from the north-eastern Northumberland Basin and the central Northumberland-Solway Basin further substantiate these spatial facies trend (Fig. 5.5). In the north-eastern Northumberland Basin, the Alnwick borehole succession comprises over 100 m of stacked, typically erosive, and fluvial-dominated channel and accretionary sand facies with subsidiary inter-bedded silty to very-fine sand floodplain facies. The presence of rooted structures within these finer-grained units indicates their deposition under dominantly terrestrial conditions; although Turner *et al.* (1997) reported a brief, approximately 30 cm thick, ostracod-bearing mudstone interval within this succession at approximately 68 m (MD) that indicates a short-lived marine incursion. Conversely, the Stonehaugh
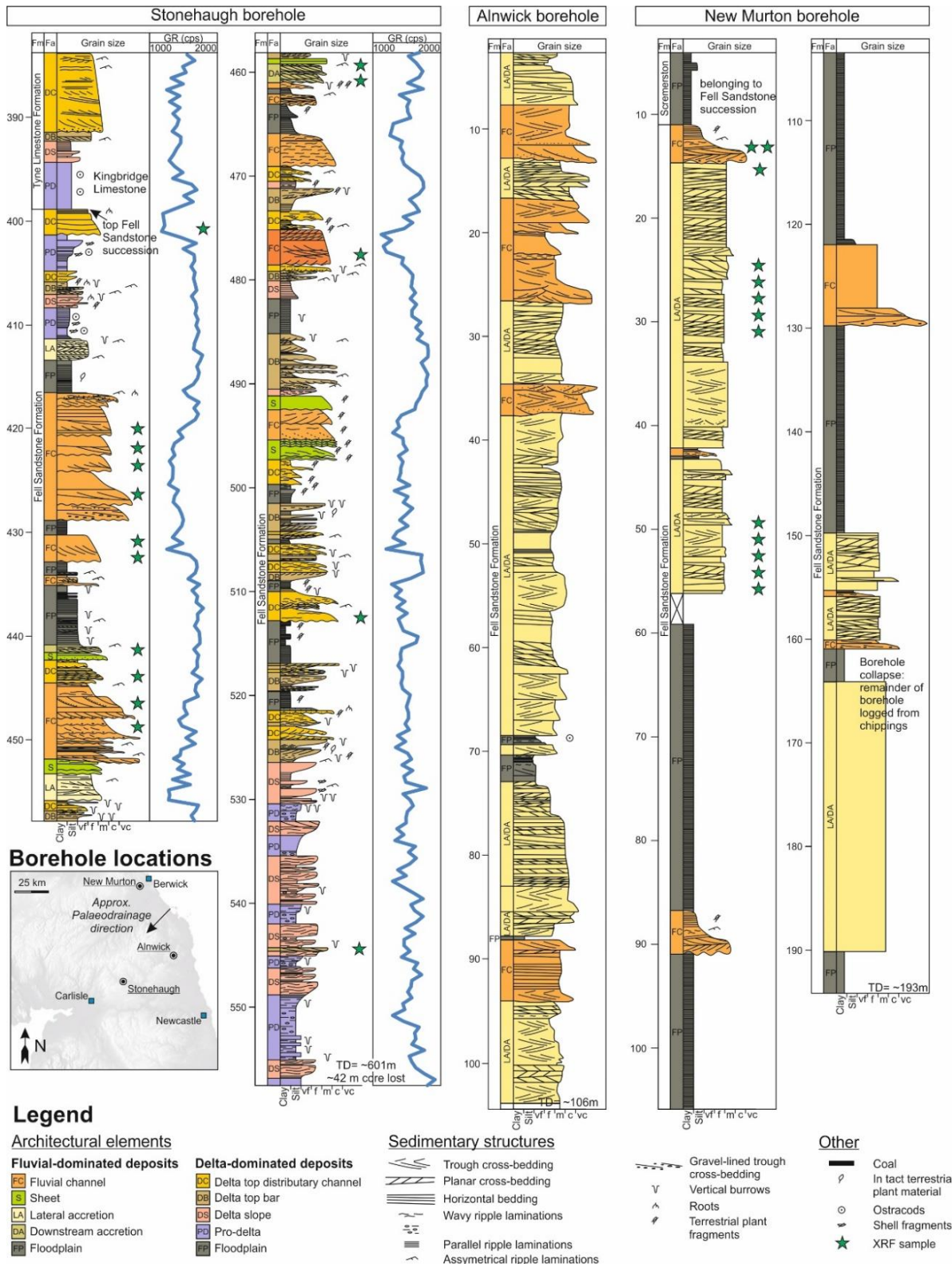
Figure 5.5: Sedimentary logs for the Fell Sandstone succession across the northern Pennine Basin. Each log captures the uppermost Fell Sandstone succession and the succession immediately below it. The Stonehaugh borehole succession was logged directly from drillcore at the BGS core store in Keyworth. The Alnwick and New Murton boreholes were drawn up based on field logs and records by B. Turner (scans.bgs.ac.uk/; also see Turner *et al.*, 1997) and A. Hodgson (scans.bgs.ac.uk/).

borehole succession in the central Northumberland-Solway Basin, comprises a higher proportion of finer-grained delta-dominated facies inter-bedded with coarser fluvial-dominated facies.

The distribution of gamma ray (GR) facies echoes those trends observed at outcrop and through drillcore. For the most proximal borehole penetration, with respect to palaeodrainage, for which there is a GR log associated, the Longhorsley borehole, GR response is largely subdued (Fig. 5.6). Based on the facies and facies tracts analysis presented in Section 5.5 (also see Table 5.3), the overall blocky response of this GR log indicates the presence of fluvial-dominated deposits. 'Cleaning upwards' gamma ray trends (i.e., gamma ray responses that decrease upwards) inter-dispersed within this succession are interpreted as representing inter-bedded delta-dominated deposits. The proportion of these cleaning upwards trends observed within stratigraphically equivalent GR successions increases progressively towards the faulted southerly basin margin of the Northumberland-Solway Basin. In the Westnewton borehole succession, drilled in the western part of the Solway Basin, blocky and more subdued GR responses again comprise a higher proportion of the Fell Sandstone succession. However, much of these facies are comprised predominantly of fossiliferous or crystalline marine limestones, rather than sandstone-rich fluvial-dominated deposits. Outcropping or drillcore equivalents to these deposits were not encountered in the study area. The uppermost part of the contemporaneous succession penetrated by the Brafferton borehole, in the Stainmore Basin, is comprised almost entirely of these carbonate deposits. Lithological logs for boreholes penetrating the Fell Sandstone Formation along the largely unfaulted eastern margin of the Alston Block indicate a mixed sandstone-siltstone succession here, with few inter-bedded limestones.

5.5.2 Net to gross (sand %) trends

Although not all boreholes sunk into the Fell Sandstone succession across the study area now provide intact drillcore or detailed records of sedimentary facies, an analysis of net to gross (sand %) trends apparent from borehole records with brief lithological descriptions further illustrates regional depositional trends, which are not shown in Figure 5.7. Around the Berwick-upon-Tweed area (Fig. 5.3), a cluster of boreholes drilled predominantly for water resource purposes
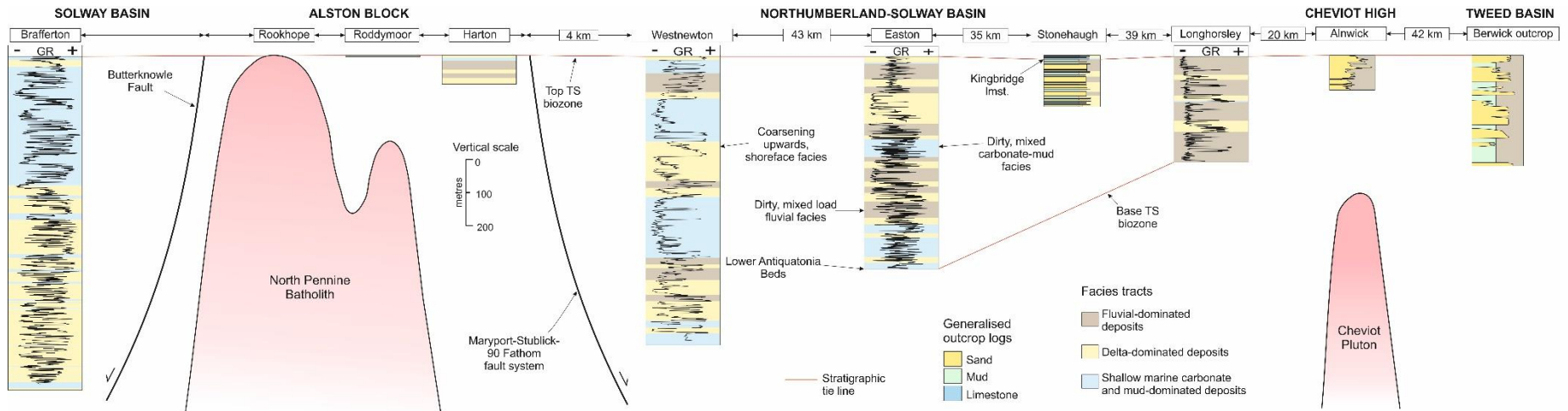
Figure 5.6: Regional correlation of the Fell Sandstone and contemporaneous deposits across the northern Pennine Basin (Tweed Basin, the eastern margin of the Cheviot Block, Northumberland-Solway Basin, Alston Block and Stainmore Trough). See Figure 5.2 and Table 5.1 for borehole locations and data derivation. The Berwick outcrop succession is after Turner *et al.* (1993).

penetrate the Fell Sandstone succession and reveal variable net sand contents of between 40 % and 80 % (see inset Fig. 5.7). These values are consistent with observations made by several previous authors who have reported a more heterolithic Fell Sandstone succession in this area (Hodgson and Gardiner, 1971; Bell, 1978; Turner *et al.*, 1993). Many of these boreholes were drilled at ground level in basal Scremerston Formation strata and therefore penetrate the upper 100 m and more of the Fell Sandstone succession; the latter is believed to be approximately 330 m thick in the vicinity of Berwick-upon-Tweed (Turner *et al.*, 1993). Further to the south, down-system and along the unfaulted eastern margin of the Cheviot Block, documented boreholes penetrations are sparse. In the Rothbury area, the succession in the Alnwick borehole reveals 99 % net sand within a 104 m succession (Fig. 5.7) (also see Fig. 5.5). The Longframlington borehole, which was drilled approximately 7 km south- westwards, reveals a similarly high 95 % net sand content in a 92 m thick succession. Equally, observations of the exposed Fell Sandstone succession here and several tens of kilometres to the north also suggest locally high or entirely sand-bearing compositions (Monro, 1986). A series of sparsely distributed boreholes through the Northumberland-Solway Basin, drilled predominantly during a short-lived period of hydrocarbon exploration in the area (Barrett, 1988), reveal a gradual down-system decrease in preserved net sand content. In the western part of the Solway Basin, the Fell Sandstone succession comprises only 14 % sand. Along the eastern margin of the Alston Block, 46 % and 74 % overall net sand contents are encountered in the Newcastle Science Central and Harton boreholes, respectively. In the Stainmore Trough, immediately to the south, the Seal Sands and Brafferton Fell Sandstone successions comprise 48 % and 26 % net sand respectively; although in the Brafferton borehole succession, less than 10 % net sand is encountered in the uppermost 400 m of the Fell Sandstone succession.

5.5.3 Palaeocurrent trends

In basins that have suffered little post-depositional structural modification, palaeocurrent measurements provide direct indications of palaeo-drainage systems. Around the Berwick-upon-Tweed area and in concurrence with previous literary reports (Turner *et al.*, 1993), the dominant palaeocurrent direction for the Fell Sandstone succession is to the south-west (Fig. 5.8). However, between 10 and 20 km to the south and along the eastern margin of the Cheviot Block, there is a
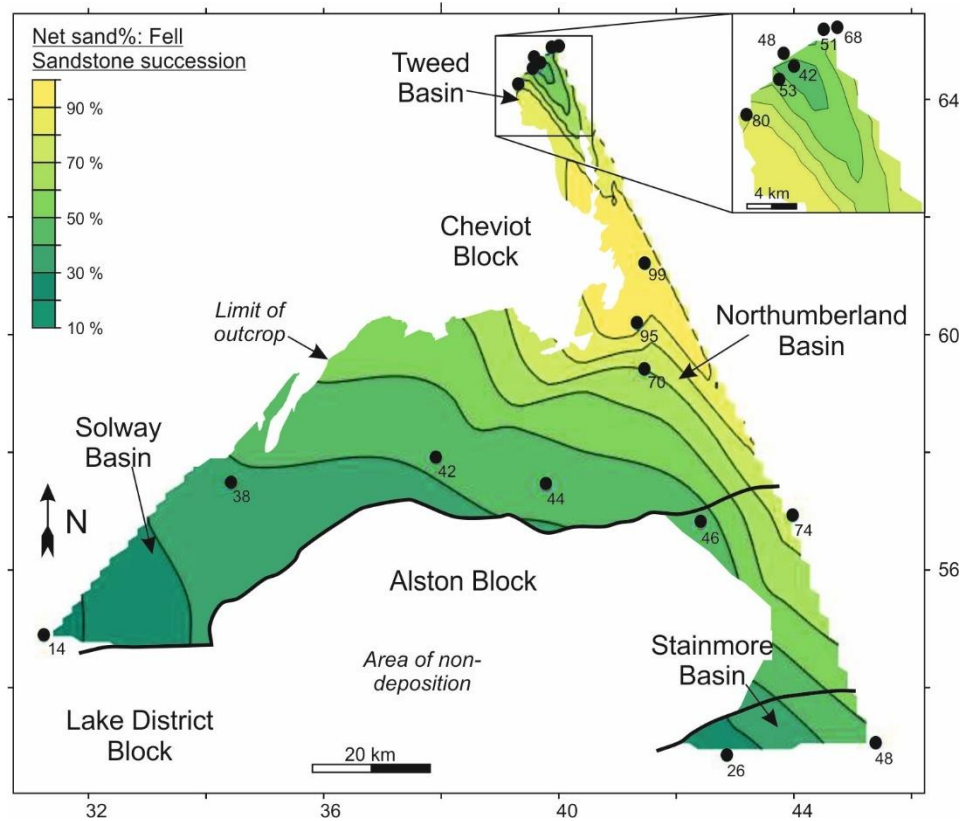
Figure 5.7: Net to gross (sand %) trends for the Fell Sandstone Formation and contemporaneous deposits across the northern Pennine Basin, based on annotated borehole recordings and cubic interpolation in MATLAB. For more detailed descriptions of borehole locations, the reader may refer to Figure 5.3 or Table 5.1.

roughly 90 ° anticlockwise rotation in the dominant palaeocurrent direction. The dominant south to south-eastwards palaeocurrent direction here is roughly parallel with the unfaulted eastern margin of the granite-cored Cheviot Block and approximately consistent with the area of increased downstream net sand composition for the Fell Sandstone succession. The dominant SSE palaeocurrent trend continues down-system towards the Rothbury area where, in meeting the north-eastern apex of the onshore Northumberland-Solway Basin, palaeocurrent rotates back, roughly towards the west and south-west so that it is parallel with the dominant local structural trend in that region. In the Northumberland Trough, and in the eastern part of the Solway Basin, the dispersion in palaeocurrent direction is generally greater than along the eastern margin of the Cheviot Block. Here the dominant palaeocurrent 'doglegs' slightly, varying between subparallel and perpendicular to the dominant trend of normal faults. Progressively towards the south and south-
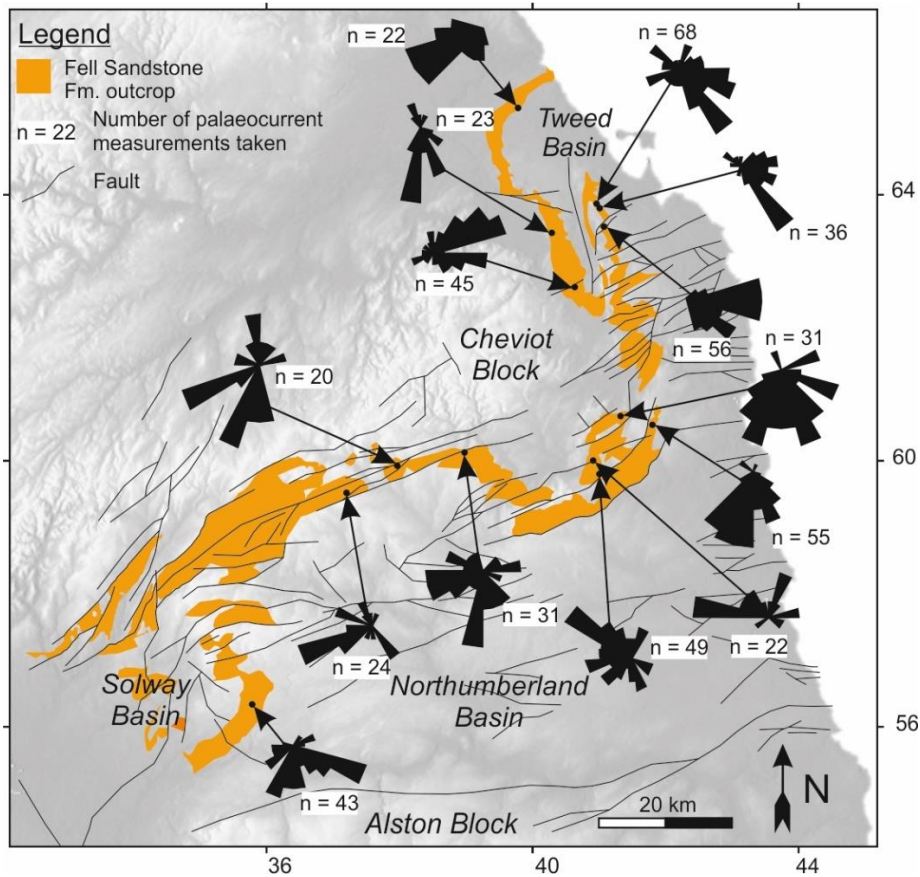
Figure 5.8: Palaeocurrent trends for the Fell Sandstone Formation and contemporaneous deposits across the northern Pennine Basin. Outcrop localities, at which palaeocurrent data were taken, are indicated by black dots. Extent of Fell Sandstone Formation and faulting outcrop is also indicated. Contains BGS DiGmapGB-250 Scale data © UKRI (British Geological Survey, 2008). See also palaeocurrent trends for the Fell Sandstone Formation presented by Monro (1986) and Turner *et al.* (1993).

west, and ultimately towards the key basin-bounding faults of the Northumberland-Solway basins, palaeocurrent direction rotates more dominantly towards the south.

5.6 Sedimentary provenance analysis

Localised aberrancies from regional trends often relate to the complex source-to-sink relationships present within some accommodating sedimentary basins, particularly for fluvio-deltaic systems (Mikesell *et al.*, 2010). In this next section, elemental and mineralogical composition trends are examined for sandstones belonging to the Fell Sandstone succession across the northern Pennine Basin. Compositional trends are compared progressively downstream between immediately adjacent sub- basins or depocentres. Basement rock compositions are plotted against measured
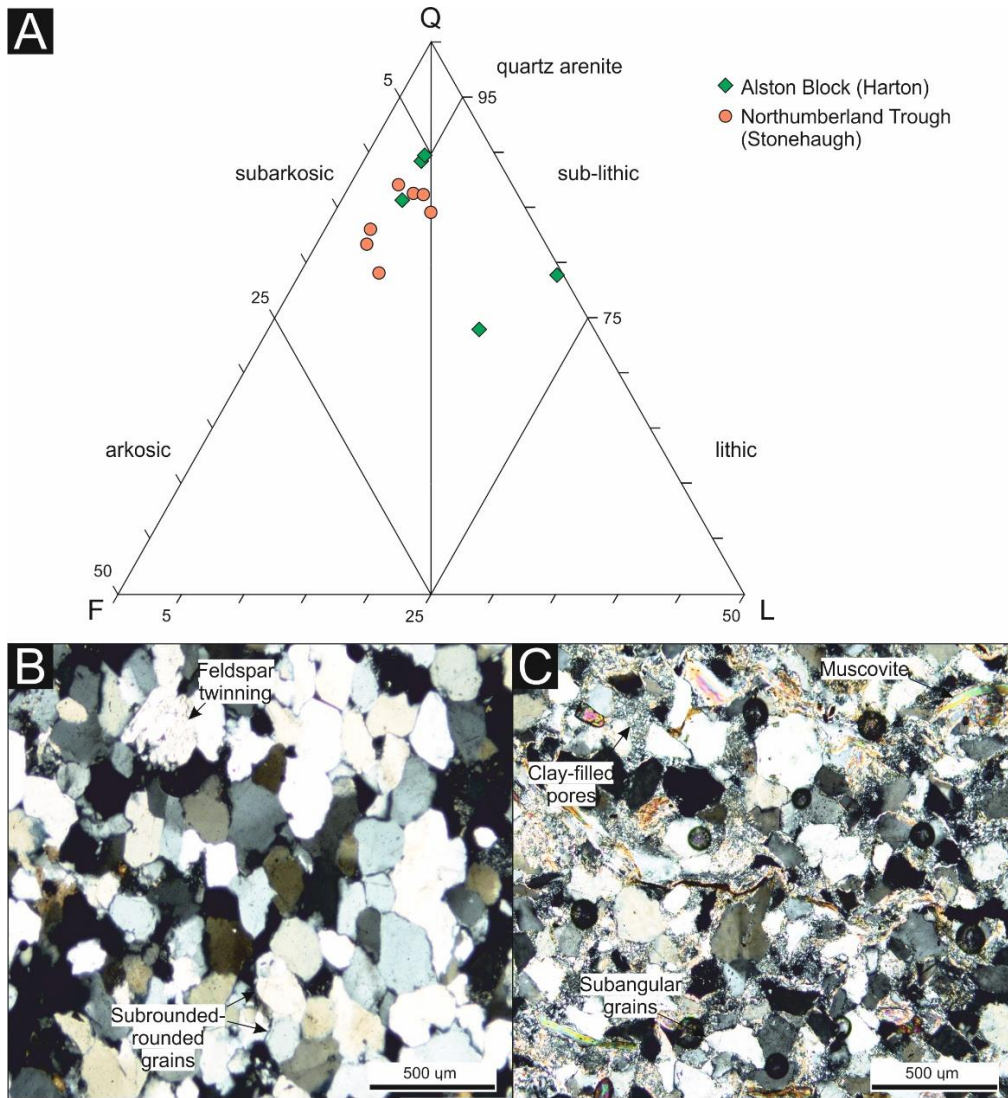
Figure 5.9a: Ternary diagram of mineral composition for sandstones (arenites) belonging to the Fell Sandstone Formation in the northern Pennine Basin. 5.9b: Representative cross-polarised (XPL) photomicrographs of mineral assemblage and texture for the Fell Sandstone Formation sandstones in the northern Northumberland Basin. 5.9c: Representative cross-polarised (XPL) photomicrographs of mineral assemblage and texture for the Fell Sandstone Formation sandstones along the eastern margin of the Alston Block.

compositions for the Fell Sandstone succession to determine the degree to which potential source lithologies may have provided clastic sediment to the various depocentres that together comprise the study area. For a full list of geochemical data, the reader may refer to Supplementary Data Tables 1 and 2 in the Appendix.

5.6.1 Tweed Basin

The detrital components of sandstones taken from the Tweed Basin are typically rounded-subrounded. Sandstones encountered here are compositionally orthoquartzitic-subarkosic (Fig. 5.9). As concentrations of major oxides such as CaO and SiO_2 appear to vary greatly in response to cement and weathering, rather than detrital composition, the concentrations of less soluble oxides and trace elements such as Fe (expressed as Fe_2O_3), K (expressed as K_2O), Ti (expressed as TiO_2), Sr, Rb and Zr are focussed upon here (Fig. 5.10a). Such trace elemental concentrations are generally sparse, particularly in the Tweed Basin, reflecting the comparatively pure compositions of the sandstones. Rb/Sr ratios, a common reference point for the chemical evolution of igneous material (Halliday *et al.*, 1991), are generally between 0.5 and 1.5 around Berwick and reduce downstream. Excluding samples with measurements below the limit of detection, Sr compositions average 10.19 ppm whilst Rb averages 9.87 ppm. Zirconium and TiO_2 concentrations vary between 40 and 240 ppm, and 0.05 and 0.18 % respectively. Iron coated grains appear frequently in the Tweed Basin suite in thin section. However, the detrital components of these sandstones appear lower with respect to Fe_2O_3 compared with the remainder of the samples with average overall concentrations of 0.34 %. K_2O concentrations for the Tweed Basin are also reduced with respect to downstream areas of the northern Pennine Basin.

5.6.2 Northumberland Trough

Samples taken from the Northumberland Basin show greater proportions of typically andesitic lithic material, as well as quartz pebbles, although they are still orthoquartzitic-subarkosic in composition and comprise mostly subrounded clasts. There is a striking downstream Sr increase for samples taken from the Northumberland Basin, averaging 37.5 ppm overall, compared with samples from the Tweed Basin, and little overlap in this regard (Fig. 5.10). This relationship is further substantiated when also considering the samples from the comparatively Sr depleted Tweed Basin suite that were below the limit of detection for this this element (see Table 4). Rb/Sr ratios decrease further downstream, with respect to the Tweed Basin suite, to between 0.1 and 0.9. For K_2O, Rb and Zr, there is little downstream variation. For Fe_2O_3, there is an overall downstream
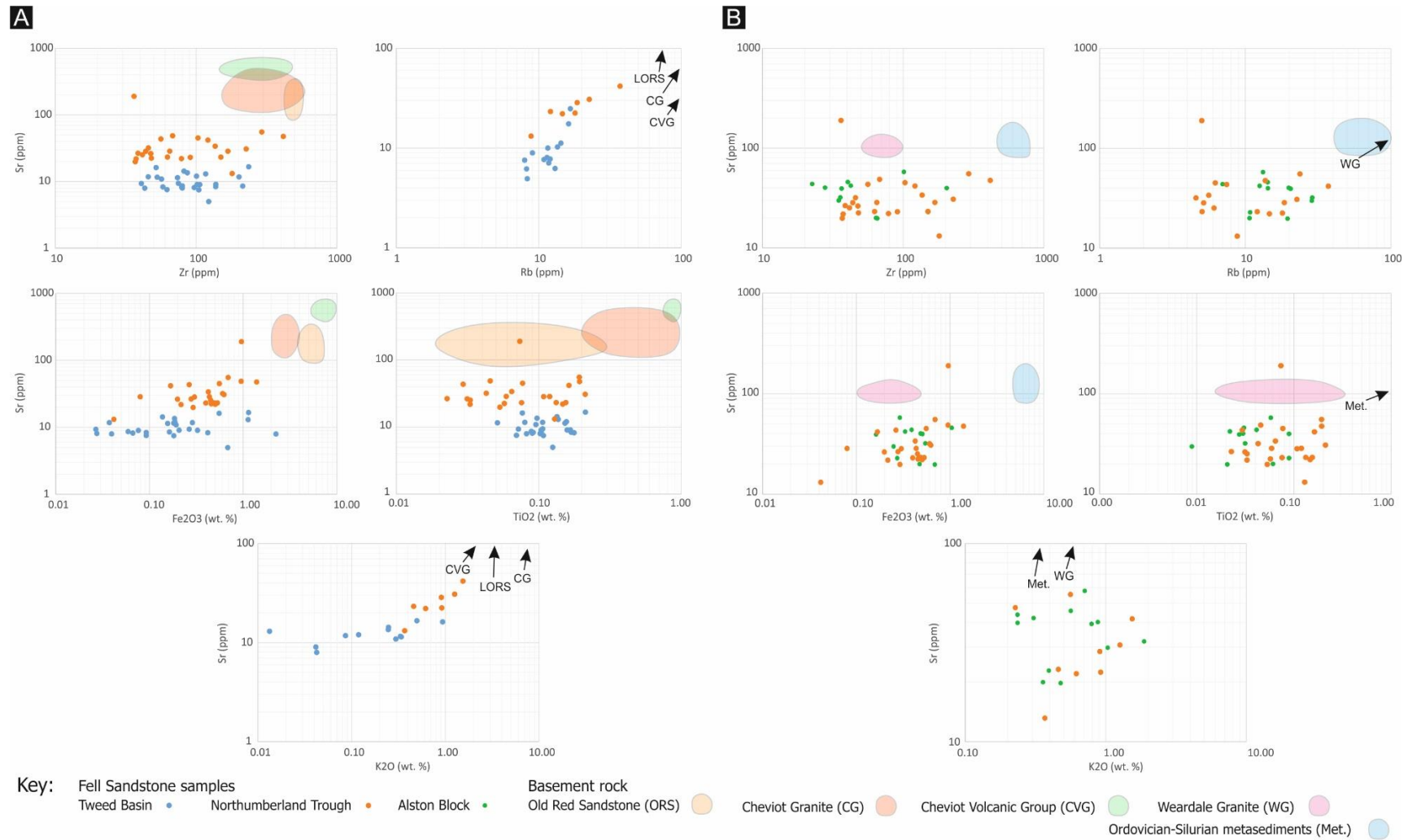
Figure 5.10a: Selected trace and major element compositions for medium-grained and well-sorted sandstones across the Tweed and Northumberland Basins and basement rock compositions for the Cheviot Block. 5.10b: Selected trace element compositions for medium-grained and well-sorted sandstones across the Northumberland and the Alston Block's eastern margin and basement rock compositions for the Alston Block. Geochemical values for potential source rock lithologies taken from Breward (2004), Everett *et al.* (2019), Thirlwall (1988), Al-Hafdh (1985), Dunham *et al.* (1965), BGS (1992) and Everett *et al.* (2019) respectively.

increase whilst for TiO_2, there is slight decrease, although given the small magnitude of this depletion, the sampling number is perhaps too small to consider comparative downstream concentrations for this compound in this region of the case study area.

5.6.3 Alston Block (eastern margin)

Samples taken from remnants of drillcore belonging to the Harton borehole have variable but slightly greater subarkosic compositions with muscovite being prominent and incorporate greater proportions of angular-subangular clasts (Figs. 5.9a and 5.9c). Strontium concentrations do not vary significantly between Fell Sandstone samples taken from the Northumberland Basin and from the eastern margin of the Alston Block (Fig. 5.10b). Likewise, no notable variations in the concentrations of Fe_2O_3, K_2O, Zr or TiO_2 are observed based on the dataset acquired in this region. Rubidium increases downstream along the eastern margin of the Alston Block with respect to the Northumberland Basin, increasing in concentration from an average of 12.2 ppm, to 16.7 ppm. Between these two depocentres, Rb/Sr ratios increase accordingly, on average, from 0.40 to 0.52. These contrasts are close to the limit of detection. Unlike with comparative Sr increases for the Tweed and Northumberland Basins further upstream, however, there is far more overlap in K_2O and Rb enrichments between the Northumberland Basin and the Alston Block.

5.7 Sedimentary provenance interpretations

Based on textures, and mineralogical and geochemical compositions of sandstones taken from the Tweed Basin (Fig. 5.9), it is suggested that these sediments were derived from a mature, either reworked or far-travelled, sediment source. Given the dearth of clay material associated with this suite, it is suggested further that the elevated Rb/Sr ratios of these sandstones may be attributed to a more chemically evolved, perhaps granitic, source rock lithology. In the absence of more sophisticated provenance analysis methods, it is postulated that Caledonian granites of northern Scotland, Norway or western Greenland may have constituted potential source rock lithologies, as they are suggested to have done for overlying strata (e.g., Morton *et al.*, 2002).

Although through-going palaeocurrent trends suggest that the Tweed and Northumberland Basins were not entirely separate systems (Fig. 5.8), chemical composition variances suggest there was an additional sediment source supplying the Northumberland Basin (Fig. 5.11). Given the slight downstream enrichment in Fe_2O_3 and the pronounced Sr enrichment for Fell Sandstone samples taken (downstream) in the northern Northumberland Basin (Fig. 5.10a), it is anticipated that this additional sediment source rock was enriched in these elements. Igneous basement rocks exposed within the Cheviot Block, namely the Cheviot Volcanic Group (Thirwall, 1988) and the Cheviot Granite (Al-Hafdh, 1985), are comparatively enriched in Sr (between 134 and 530 ppm) and Fe_2O_3 (between 1.45 and 7.31 %) compared with sandstones collected from the Tweed Basin. Despite encountering andesite lithic clasts and reports of subordinate granite lithics (Robson, 1977), the comparative TiO_2 enrichments of these basement units (between 0.29 and 1.17 %) casts doubts on their potential as dominant sediment source rocks.

Despite the following units now being largely absent from the Southern Uplands (Browne *et al.*, 2002), eroded stratigraphic equivalents to the unconformable Silurian-Devonian Old Red Sandstone Group may have represented a remobilised Sr and Fe_2O_3 enriched, yet less TiO_2 enriched, potential sediment source lithology (Fig. 5.10a) (Breward, 2004; Everett *et al.*, 2019). An abundance of incorporated volcaniclastic detritus in these basement units (e.g., McKellar *et al.*, 2020) suggests that similar detritus incorporated within the Fell Sandstone need not have been derived solely from the Cheviot Volcanic Group. Moreover, previous petrological studies on underlying parts of the Carboniferous syn-rift succession of the Northumberland-Solway Basin imply a prolonged history of orthoquartzitic material derived from the Southern Uplands (Nairn, 1958). It is suggested, therefore, that comparative downstream enrichments in Sr and Fe_2O_3 in the Northumberland Trough may have been due to supply from Devonian Old Red Sandstone Group basement rock from the Southern Uplands. The Southern Uplands, which were underpinned by low-density granite intrusions such as the Cheviot Pluton, may have undergone progressive un-roofing during deposition of the Fell Sandstone succession (Fig. 5.11).
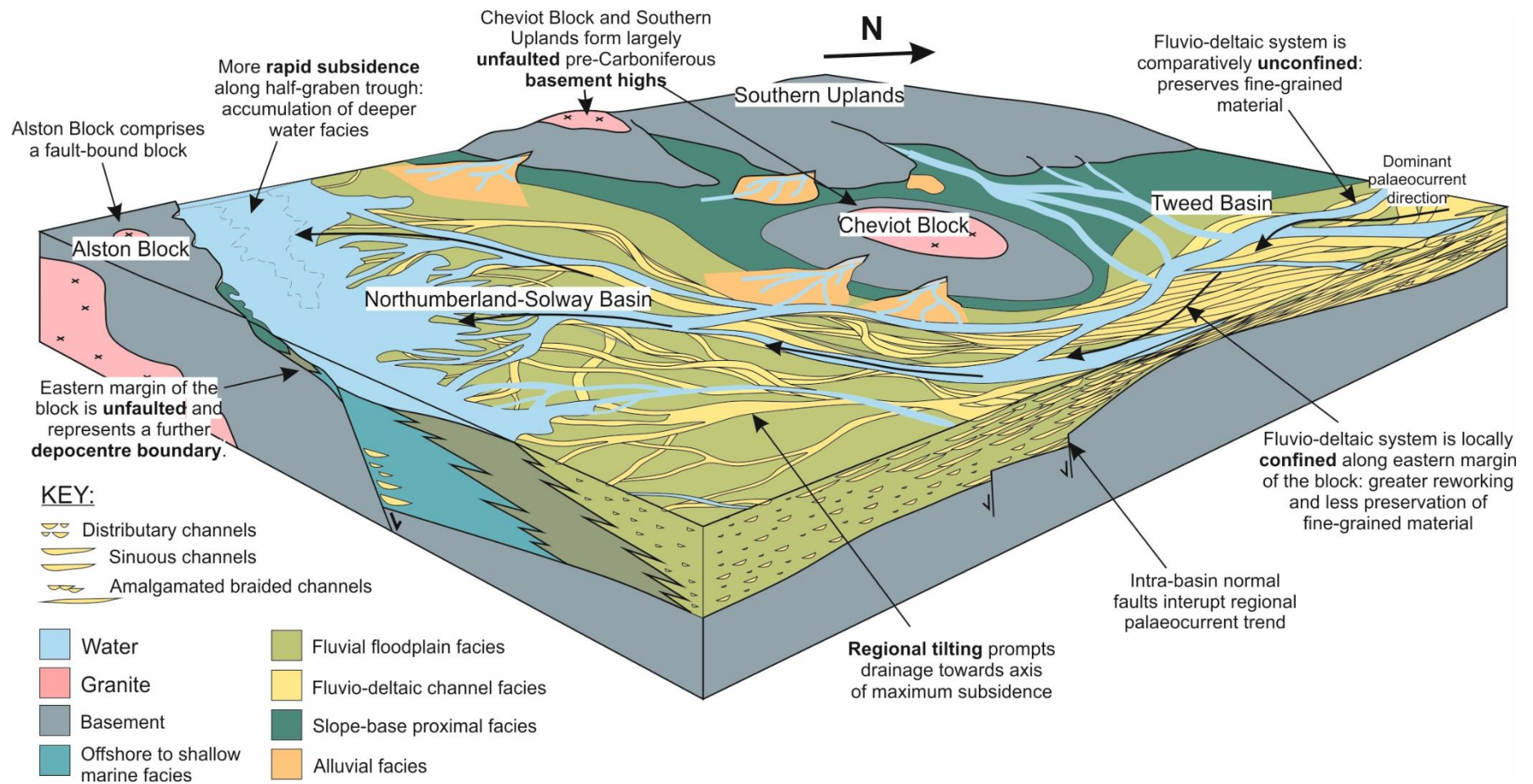
Figure 5.11: A depositional model for the Fell Sandstone Formation and stratigraphically equivalent deposits in the northern Pennine Basin.

Slight downstream petrographical and geochemical deviations between samples taken from the Northumberland Basin, and the eastern margin of the Alston Block, suggest a continuous palaeo-drainage system in this region of the northern Pennine Basin with mixing from an additional clastic sediment source. Based on downstream geochemical deviations between the Northumberland Basin and Alston Block, an additional sediment source enriched in Rb, and slightly depleted in TiO_2 is anticipated. Given the textural immaturity of sandstones taken along the eastern margin of the Alston Block (Fig. 5.9c), it is postulated that this additional source lithology was local. Unconformably underlaying younger Carboniferous strata upon the central part Alston Block and sampled only via the Rookhope and Eastgate boreholes, the chemically evolved Weardale Granite, which is connected at depth to the remainder of the North Pennine Batholith, may represent one such Rb enriched and TiO_2 depleted basement source lithology (Fig. 5.10b) (Dunham *et al.*, 1965). Ordovician-Silurian turbiditic metasediments, like those of the Lake District (Stone *et al.*, 2010), comprise one further component of basement rock along the western margin Alston Block (Dunham *et al.*, 1962). By comparison, the latter is enriched with major oxides such as Fe_2O_3 and TiO_2 with respect to sandstones taken from the Northumberland Basin (British Geological Survey, 1992). Based on the downstream TiO_2 depletion of sandstones between the Northumberland Trough and the Alston Block, and enrichments in Rb, it is suggested that the Weardale Granite was exposed during deposition of the Fell Sandstone succession and comprised one additional sediment source lithology for the eastern margin of the Alston Block (Fig. 5.11). Based on seismic reflection profiles (Fig. 5.1), no accommodating fault system is suggested to have separated this comparative high, upon the central part of the Alston Block, from the depocentre along the block's eastern margin.

5.8 Facies and palaeocurrent trend interpretations

Within the Northumberland-Solway Basin, the preservation of greater amounts of finer-grained sediments and coal towards the south-west (Fig. 5.5) suggests progressively less sediment reworking (*cf.* Ghinassi *et al.*, 2016), perhaps because of greater rates of accommodation space creation (Fig. 5.11). Greater overall thicknesses in the south and south-west of the Northumberland-Solway Basin for early Carboniferous sediments support this idea (Fig. 5.6) (Chadwick *et al.*, 1995).

Such facies trends are consistent with distributive fluvial systems, within which coarse sediment is dispersed radially from an apex (e.g., Weissman *et al.*, 2010), or classic fluvio-deltaic tectono-stratigraphic tilt-block models, within which alluvial fans prograde downslope from an upper hangingwall dipslope towards an axis of maximum subsidence (Gawthorpe and Leeder, 2000). Similarly, palaeocurrent is directed towards the south-west within the Northumberland-Solway Basin. The Northumberland and Solway basins appear to have formed one coherent depocentre during deposition of the Fell Sandstone Formation, given that there is no obvious interruption in regional palaeocurrent trend (Fig. 5.8). Within the Northumberland-Solway Basin, any localised interruptions to this dominant trend are localised and perhaps related to the influences of intra-basin normal faulting (*cf.* Turner *et al.*, 1993). The accumulation and preservation of greater amounts of deeper water facies assemblages towards the south may be a response to asymmetric, basin-bounding normal faulting induced subsidence (*cf.* Leeder and Gawthorpe, 1987). In such systems, sedimentation may react to normal faulting or tilting by causing transgression (Barrett *et al.*, 2019).

Within the Tweed Basin and along the eastern margin of the Cheviot Block that is unbound by major (>100 m) vertically displacing normal faults, palaeocurrent and preserved facies trends suggest a more complicated basin geometry influenced sedimentation (Fig. 5.11). The overall south-eastwards deflection in palaeocurrent and coarser preserved fluvial-dominated deposits along the eastern margin of the Cheviot Block, suggesting greater reworking, indicate local confinement of palaeodrainage because of this topographic feature. The preservation of greater finer grained sediments up dip, towards the Tweed Basin, may indicate progressively less reworking, perhaps due to the greater rates of accommodation in this part of the broader basin system. Sedimentary provenance analyses, and palaeocurrent and facies trend analyses, suggest that the Cheviot Block had been at least partly exposed during deposition of the Fell Sandstone Formation. In contrast, borehole penetrations reveal that the Tweed Basin had accumulated at least hundreds of metres of older (Ballagan Formation) Carboniferous sediments (Millward *et al.*, 2013). Whilst no 2D seismic reflection profiles have been acquired in this part of the UK, there are few suggestions of major (>100 m) vertically displacing fault systems here to accommodate subsidence along the eastern margin of the Cheviot Block (e.g., Fig. 1.1), see also Shiells (1963). Based on the presence of a low-

density granite intrusion within the core of the Cheviot Block, it is suggested that the Tweed Basin and the Cheviot Block together may have resembled a regional monocline, as appears to be the case for the central and eastern parts of the Alston Block (Fig. 5.1a). Facies based comparisons cannot be made between the Tweed Basin and the eastern part of the Alston Block, due to burial. However, both the central part of the Alston Block and the Cheviot Block are suggested to have been exposed and providing sediment during deposition of the Fell Sandstone Formation.

5.9 Influences of low-density granite intrusions and flexural isostasy on basin geometry and sedimentation

In the preceding chapter of this thesis, it was suggested that the origin of basement monoclines in the northern Pennine Basin can be associated with the buoyant composition of their uplifted limbs and flexural isostatic processes. In the same way that regional basement synclines form as a flexural isostatic response to positive lithospheric loads imposed by the mass of volcanic islands (e.g., Watts, 1978), monoclines can form in response to flexurally compensated negative loads imposed by local basement buoyancy, and perhaps the locally thickened crust (Fig. 5.12). Two-dimensional lithosphere scale numerical modelling experiments show that such structures may form irrespectively of normal faulting but depend more so on the rigidity or effective elastic thickness (T_e) of the lithosphere. Lateral subsidence variations may occur in response to differential sediment loading, and perhaps differential compaction of the underlying sedimentary sequence (*cf.* Collier, 1989). The sedimentological and provenance-based studies presented in this chapter, suggest that the uplifted limbs of these monoclines, or basement domes, associated with buoyant granite intrusions can influence sediment preservation, palaeodrainage and local sediment supply (Fig. 5.11). The findings thus presented are not just at variance with classically depicted depositional models for the 'block and basin' style northern Pennine rift basin (e.g., Johnson, 1967), within which faulted blocks are bound by major vertically displacing normal faults, but also with more modern depictions of dominantly normal fault driven rift basins (e.g., Gawthorpe and Leeder, 2000) (Fig. 3.3).
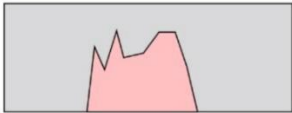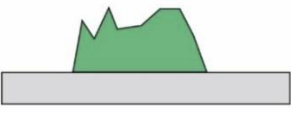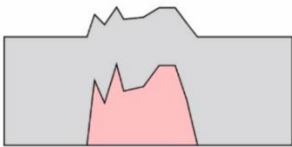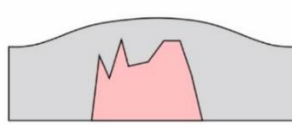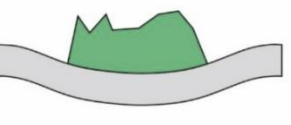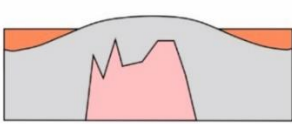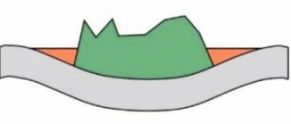
Low-density granite	Volcanic island	Isostatic response
		No isostasy (rigid lithosphere)
		Local (Airy) isostasy
		Regional (flexural) isostasy
		Regional isostasy with sediment fill

Figure 5.12: Schematic illustrations of isostatic responses to subsurface low-density (buoyant) granite intrusions and a comparison with the lithosphere's isostatic response to a volcanic island (after Watts, 1978).

5.10 Discussion

Thanks in part to the success of many recent studies on the kinematics of basin-bounding normal fault systems and their influences on sedimentation (e.g., Elliott *et al.*, 2017; Robson *et al.*, 2017; Sommerville *et al.*, 2019), rift basins are now perhaps too often regarded as dominantly fault-driven systems. Although they and the processes which govern them are frequently under-reported, there are many examples of buoyant and largely unfaulted basement highs within rift basin systems. The Dogger Block of the Mid North Sea High, offshore UK, is characterised by a negative Bouguer gravitational anomaly linked to the postulated Dogger Granite (Kimbell and Williamson, 2015; Donato, *pers. comm.*, 2019). Akin to the Cheviot Block within the case study area, in seismic reflection profiles it appears largely unbound by major (>100 m) vertically displacing normal faults. Yet it is frequently represented as being bounded by such fault systems to justify the presence of adjacent

depocentres (e.g., Milton-Worsell *et al.*, 2010; Monaghan *et al.*, 2017; Brackenridge *et al.*, 2020). The Utsira High, situated *c.* 150 km off the southern coast of Norway in the northern North Sea, constitutes another granite-cored and fault-bound basement high like the Alston Block within the northern Pennine Basin (Zervos *et al.*, 1987; Lundmark *et al.*, 2014). Like the Alston Block, it is bound by major vertically displacing fault systems, to the east, south and west (Osagiede *et al.*, 2020). However, its northern boundary is poorly defined by the shallow northerly dip of the basement, on to which a variably thick Jurassic syn-kinematic rift succession onlaps unconformably (Phillips *et al.*, 2019). The pre-salt Santos and Campos basins, offshore Brazil, which have gained economic significance due to their recently realised hydrocarbon potential, are characterised by sporadically uplifted intra-basin basement highs that have given rise to syn-rift carbonate ramps and platforms (Buckley *et al.*, 2015). Although the basement that underpins these deposits offshore is buried deeply and any gravitational signature of the basement is, therefore, highly attenuated, onshore the exposed basement does reveal an extensive network of potentially corresponding sporadically distributed low-density Proterozoic felsic intrusions (Marshak *et al.*, 1992). Based on such similarities, it is suggested that further studies, following the themes presented in this part of the thesis, could yet help unravel some important uncertainties surrounding the evolution of numerous worldwide rift basin systems and the sediments that accommodate within them.

5.11 Conclusions

After conducting a more model driven investigation of the early Carboniferous (Mississippian) northern Pennine 'block and basin' style rift basin in the preceding chapter of this thesis, a sedimentological and sedimentary provenance-based study is presented in this chapter. Based on some key findings, it is suggested that aspects of the (Visean) Fell Sandstone Formation, and stratigraphically equivalent deposits in the northern Pennine Basin, match classically depicted models for 'block and basin' style rift basin systems, within which blocks are bound by major (>100 m) vertically displacing normal faults. These include the overall basinward increase in deeper water and delta-dominant facies in the Northumberland-Solway Basin, the dominant basinward palaeocurrent direction in the Northumberland-Solway Basin, and the derivation of sediment from

comparatively uplifted 'blocks'. However, other trends and aspects, such as the up-system decrease in net sand content north-east of the Cheviot Block, the south-eastwards deflection in palaeocurrent in the Tweed Basin, and the contemporaneous uplift and shedding of sediment on central parts of the Alston Block and accumulation of kilometre-thick sediment along the eastern margin of the Alston Block, may not.

Highlighted divergences from pre-existing depositional models for 'block and basin' rift basin systems relate to occurrences of granite-cored and largely unfaulted pre-Carboniferous basement highs and monoclines. These highs are replicated, in the previous chapter of this thesis, using 2D lithosphere scale structural and geodynamic numerical modelling scenarios, in which the effects of lithospheric extension, the buoyancy of granite intrusions and flexural isostasy are accounted for. In 3D, they form regional domes, on to which the Carboniferous succession onlaps unconformably. All unfaulted basement highs in the northern Pennine Basin coincide with low-density granite intrusions. It is suggested that one such basement high, the Cheviot Block, confined and deflected the Fell Sandstone fluvio-deltaic system from the west, causing localised elevations in net sand content, due to reworking, and variations in palaeocurrent. Central parts of the Alston Block were comparatively uplifted with respect to its eastern margin because of flexural isostatic responses to buoyant basement rock. The findings thus presented are not just at variance with classically depicted depositional models for the 'block and basin' style northern Pennine rift basin, but also with more modern depictions of dominantly normal fault driven rift basins.

Part III

The late Carboniferous 'broken' Variscan foreland

A review of the theories surrounding late Carboniferous basin evolution in northern England and Scotland

6.1 Introduction

In the next part of this thesis, a series of investigations, focussing on the structural and sedimentological characteristics of the late Carboniferous (Namurian-Stephanian) basin fill of northern England and Scotland, are presented. These sediments were deposited following the culmination of early Carboniferous rifting and, due to late Carboniferous-early Permian basin inversion and more recent uplift, are now largely eroded, partially exposed or only shallowly buried. Parts of the late Carboniferous succession, the Westphalian (Scottish and Pennine) Coal Measures Groups, are perhaps amongst the most intensely studied stratigraphic intervals in the world. However, following the decline of the UK's coal industry, research on these strata has stagnated somewhat and, consequently, many of the concepts and seminal theories regarding the basins that accommodated these sediments have rarely been revisited. Where current scientific debate is lacking, ample subsurface data on these strata is now publicly available. These data are to be repurposed to shed new light on characteristics of the late Carboniferous successions of northern England and Scotland. An attempt is made to place these strata within the contexts of a more accurate, or at least more useful, tectonic and geodynamic framework.

In this chapter, a review of pre-existing concepts and theories surrounding late Carboniferous basin evolution in northern England and Scotland is presented. Basin evolution is discussed within the contexts of post-rift thermal subsidence, a model adopted by multiple authors for the late Carboniferous basins of northern England during the 1980s and 1990s (e.g., Leeder, 1982; Kimbell *et al.*, 1989; Fraser and Gawthorpe, 1990), following the release of McKenzie's classic (1978) paper on extensional basins. Late Carboniferous regional dextral transpression, accommodated by pre-existing (Caledonian) faults, is also discussed within the contexts of the preserved structure and sediments within the basins of northern England and Scotland (e.g.,

Coward, 1993; Ritchie *et al.*, 2003; De Paola *et al.*, 2005; Underhill *et al.*, 2008). Finally, some of the broad concepts and ideas surrounding the evolution of regional foreland basin systems, within which subsidence is controlled by adjacent collision zones and/or subduction zones, are discussed (DeCelles and Giles, 1996; Strecker *et al.*, 2011; Cataneanu, 2019). Numerous authors suggest that the Variscan Mountains, in the south (Fig. 2.4), had an important role in determining the evolution of late Carboniferous basins in southern Wales, central England, the Netherlands and northern Germany (Peace and Besly, 1997; Littke *et al.*, 2000; Burgess and Gayer, 2000; Kombrink *et al.*, 2008), further to the south.

6.2 The role of post-rift thermal subsidence on the late Carboniferous evolution of the Pennine Basin

Dan McKenzie, in 1978, first suggested a transient thermal influence on the subsidence of sedimentary basins following rifting or lithospheric extension. During extension, the lithosphere thins in a vertical direction and, consequently, the lithosphere-asthenosphere boundary, which is defined by the 1333 °C isotherm or the temperature beyond which mantle rock behaves plastically, becomes shallower (Fig. 6.1a) (*cf.* Egan and Meredith, 2007). Extended lithosphere is typically hotter than adjacent un-extended lithosphere, therefore, and despite being largely associated with subsidence due to crustal thinning and normal faulting, an element of uplift associated with thermal expansion of the lithosphere is also prompted by lithospheric extension (Wernicke, 1985). As the lithosphere's temperature field re-equilibrates following extension, heat is transferred from hotter regions of extended lithosphere to adjacent regions of cooler crust and mantle rock or is lost from the surface. Where heat is lost, the lithosphere-asthenosphere boundary subsides and the lithosphere contracts, prompting further topographic subsidence. The rate at which heat is lost from extended lithosphere is greatest immediately following extension and decreases exponentially through time, up to approximately 200 My after a rift 'event'. Therefore, subsidence rates associated with post-rift thermal subsidence also decrease exponentially through time.
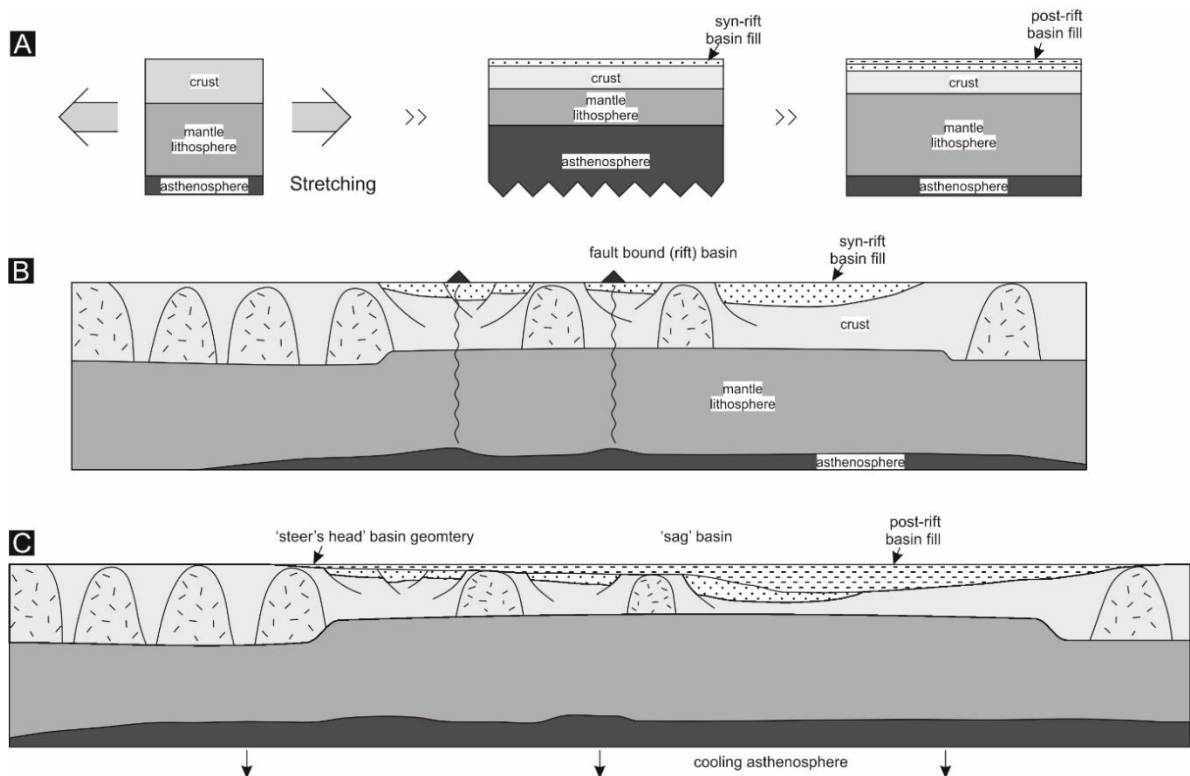
Figure 6.1a: The rift-sag lithosphere extension model (McKenzie 1978). 6.1b: The rift-sag lithosphere extension model applied to the early Carboniferous evolution of the Pennine Basin. Lithosphere extension causes tensional stress, listric faulting, high heat flow, volcanism and rift basin development in areas between granite plutons (after Leeder, 1982). 6.1c: The rift-sag lithosphere extension model applied to the late Carboniferous evolution of the Pennine Basin. The asthenosphere cools down exponentially and causes (post-rift) thermally induced, sag-type subsidence over the former rift province (after Leeder, 1982).

Partly because lithosphere mantle rock is typically extended over a broader region than the crust, many rift basins are characterised by 'steer's head' basin geometries, whereby basin margins are progressively incorporated within the basin during thermally influenced post-rift subsidence (White and McKenzie, 1988). Similar geometries along the northern and southern margins of the Pennine basin of northern England prompted Leeder (1982) to hypothesize a post-rift influence on the deposition of late Carboniferous (Namurian-Westphalian) sediments within the basin. Following localised subsidence during (back-arc) extension due to the subduction of the Rheic Ocean beneath northern France (Fig. 6.1b), he argued that intra-basin highs and basin margins in northern and central England subsided because of the thermal sagging of the NW European lithosphere as it re-equilibrated (Fig. 6.1c). An increasingly stabilized basin topography during late Carboniferous times was believed to have partly bought about the deposition of finer grained, dominantly deltaic,

lithofacies and inter-bedded coal seams (Collier, 1989). Regional basin inversion, in response to Variscan continental collision, is widely believed to have occurred after sedimentation had ceased in northern England and Scotland (e.g., Chadwick *et al.*, 1995).

6.3 Influences of dextral transpression caused by Uralian collision on basin evolution in central Scotland

Leeder's rift-sag concept represents one of the earliest attempts to place the late Carboniferous succession of northern Britain within a broader geodynamic setting, for which he should be commended. Many aspects of his model continue to be widely accepted (Chadwick *et al.*, 1995); however, despite their general acceptance, there has been growing recognition that depictions of late Carboniferous sedimentation within the contexts of post-rift thermal subsidence are over-simplifications (Leeder and McMahon, 1988; Coward, 1993; Besly, 2019). One frequently cited concern with Leeder's (1982) rift-sag (and subsequent basin inversion) model centres around frequent evidence of syn-depositional deformation preserved within late Carboniferous sediments of northern England and Scotland (Cameron and Stephenson, 1985). Alleged post-rift 'megasequences' (e.g., Fraser and Gawthorpe, 2003) are typically deposited during extended periods of comparative tectonic quiescence. By contrast, late Carboniferous sediments in northern England and Scotland are regularly characterised intra-formational unconformities, hiatuses and syn-depositional folding, particularly within the Midland Valley of Scotland (MVS) basin (Lumsden, 1967; Read, 1988; Picken, 1988; Ritchie *et al.*, 2003). The structures associated with these syn-depositional features are typically NNE-trending compressional-transpressional folds, such as the Leven, Midlothian, Clackmannan and Solway synclines, and, therefore, oblique with respect to any approximately N-S principal stress regime associated with Variscan Orogeny (Fig. 2.4).

Coward (1993) suggested that regional stresses associated with this style of deformation may have been associated with the continental 're-insertion' of NW Europe due to the approximately contemporaneous Uralian Orogeny, along the eastern margin of Baltica. Re-insertion was believed to have been accommodated by oblique (dextral) reactivation of dominantly NE-trending pre-existing (Caledonian) lineaments in northern Britain, such as the Highland Boundary

and Southern Upland fault zones (Fig. 6.2) (*cf.* Dewey, 1982). Coward (1993) stated that these stresses prevailed throughout late Carboniferous and early Permian times, by the end of which period, the emplacement of mafic dykes, volcanic vents and metalliferous ore bodies was partly accommodated by dominantly E-W tensile fractures and normal faults associated with this stress regime (Dunham *et al.*, 1990; Monaghan and Parrish, 2006; Dempsey, 2016). Because of the poor fit of Variscan (~N-S) compressional deformation within Coward's (1993) depicted regional oblique (dextral) stress regime (e.g., Copley and Woodcock, 2016), some authors have argued that Variscan Orogeny may have had negligible effects on basin inversion in northern England and Scotland (De Paola *et al.*, 2005).
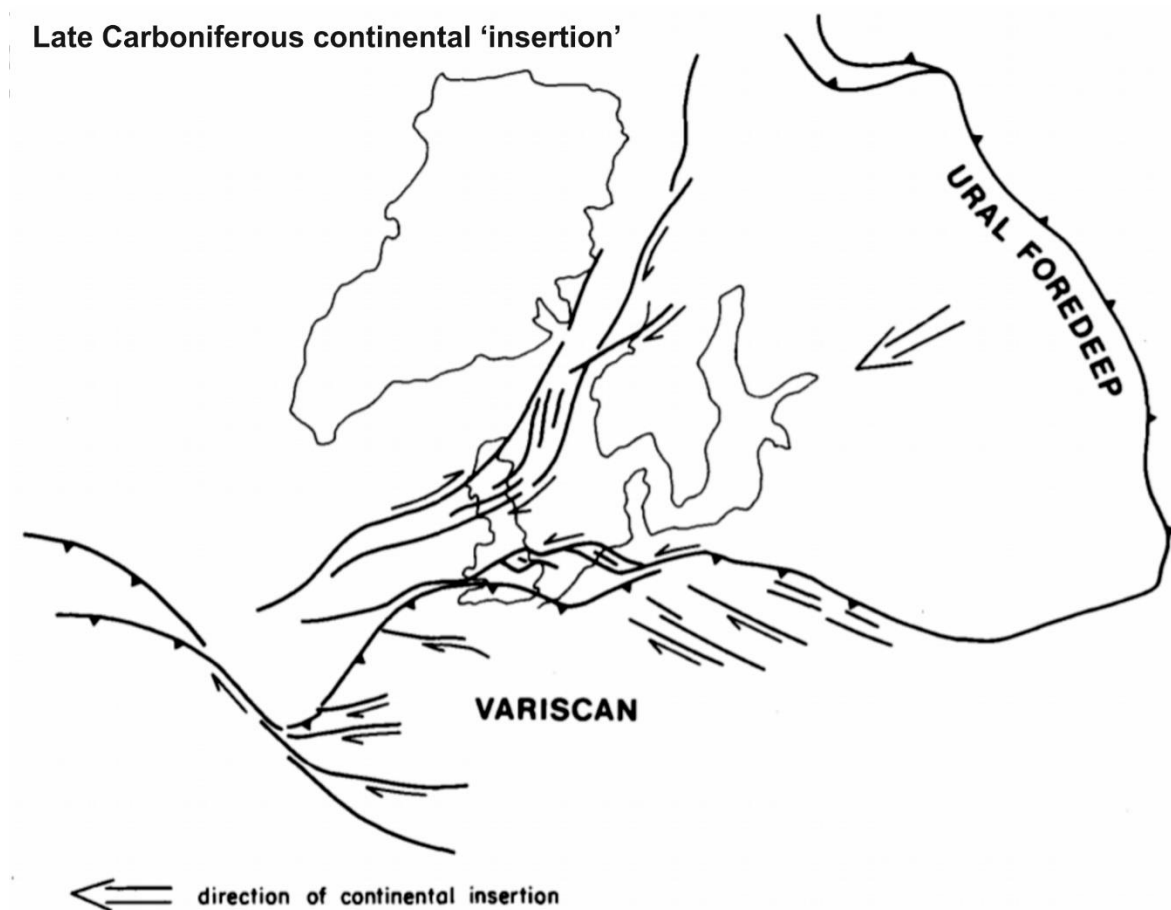
Figure 6.2: Simplified tectonic map of NW Europe during late Carboniferous and early Permian times, incorporating Uralian collision and accommodating dextral transpression along NE-trending structures in central Scotland and northern England (after Coward, 1993).

119

6.4 Syn-orogenic influences from the Variscan Mountains on basin evolution and foreland basin systems

Despite De Paola and other's (2005) suggestions, northern England and Scotland were situated in what could be considered the distal part of a foreland basin system, with respect to the Variscan Mountains in the south, during late Carboniferous times (Corfield *et al.*, 1996). Traditional models for foreland basin systems were first described by DeCelles and Giles in 1996. These systems are typically depicted in two-dimensions and compartmentalized into three, proximal foredeep, medial forebulge and distal backbulge, depozones. Accommodation is greatest in the proximal foredeep depozone and is determined by flexural isostatic responses of the lithosphere to adjacent orogens or collision zones, which behave as supra-lithospheric loads (Beaumont, 1981; Karner and Watts, 1983). In retro-arc foreland basin systems, adjacent to which an oceanic plate subducts along the opposite side of a collision zone from the foreland basin, so-called 'dynamic' subsidence due to the subduction of this oceanic plate comprises an additional accommodation mechanism (Painter and Carrapa, 2013). Subsidence due to this type of sub-lithospheric loading occurs over a wider region, greater than hundreds of kilometres, than that associated with flexure induced subsidence (Cataneanu, 2019). In more recently depicted 'broken' foreland basin systems, for which the modern-day Northern Patagonian foreland adjacent to the South American Andes is the archetypal example, reactivated basement structures may help define the margins of complex networks of intra-basin depocentres (Strecker *et al.*, 2011; Bilmes *et al.*, 2013). Intra-basin structures may be reactivated obliquely, invoking wrench influenced depocentres (Gianni *et al.* 2015), or reversely, invoking further intra-basin supra-lithospheric loading and associated subsidence (Lopez *et al.*, 2019). The reactivation of intra-basin structure is a consequence of a dissipating stress regime derived from the adjacent collision zone (Copley *et al.*, 2011).

Numerous studies in more proximal regions of the supposed Variscan foreland basin have highlighted important syn-orogenic influences on late Carboniferous sedimentation. Stresses originating from the Variscan Orogeny are widely considered responsible for basin inversion in the British Isles (Corfield *et al.*, 1996). In central England, some other controls include climate and

sediment supply (e.g., Peace and Besly, 1997). In the English Midlands, Besly and others (1988, 1993) associate the occurrence of red-bed sediments, contemporaneous expansion of arid continental sediments and basin inversion with shortening, erosion and a rain shadow effect due to uplift in the Variscan Mountains. Although they are sparsely preserved, late Carboniferous red-beds are documented widely across northern England and Scotland (Powell *et al.*, 1999; Jones and Holliday, 2006; Jones *et al.*, 2011). Asturian (Westphalian D) sediments sourced from the Variscan Mountains are proven in the Canonbie Coalfield, SW Scotland (Morton *et al.*, 2010). Based on their proximity to Variscan thrust-belts and exponentially increasing rates of subsidence during late Carboniferous times in southern Wales, the Netherlands and northern Germany, numerous authors have suggested an element of flexure induced accommodation associated with this orogeny (Littke *et al.*, 1994; Burgess and Gayer, 2000; Kombrink *et al.*, 2008). Comparatively milder, but nonetheless exponentially increasing, rates of late Carboniferous subsidence are also highlighted in northern England (Leeder and McMahon, 1988; Besly, 2019).

6.5 Summary

In both modern and ancient sedimentary basins, syn-kinematic sequences can indirectly reveal the nature of the various tectonic episodes that influenced the basin and its regional setting. Across northern England and Scotland, much of the youngest Carboniferous sequence is absent due to uplift and denudation. In contrast, near complete records of late Carboniferous sedimentation are locally preserved at the Canonbie Coalfield (Chadwick *et al.*, 1995; Jones *et al.*, 2011) and in the eastern part of the MVS (Ritchie *et al.*, 2003).

In Chapter 7, a structural mapping-based study is presented that uses subsurface (seismic and borehole) data from the Canonbie Coalfield in SW Scotland (see Fig. 1.1 for location). Multiple phases of accelerated intra-basin deformation are identified, which are accommodated by local basin inversion here. Some of the dominant controls on inversion style are discussed. In Chapter 8, a similar structural mapping-based study is presented in the eastern part of the MVS. Subsurface mapping here is augmented by more detailed descriptions and outcrop and borehole-based sedimentary logging on the local late Carboniferous succession. Stratigraphically similar phases of

deformation are identified and local controls on the late Carboniferous evolution of the MVS and sedimentation are discussed in Chapter 9. Based on these findings, a unique structural and geodynamic framework is discussed for deposition in the late Carboniferous basins of northern England and Scotland.

Seismic and borehole-based mapping of the late Carboniferous succession in the Canonbie Coalfield, SW Scotland

This chapter is based on a publication of a similar name:

Howell, L., Besly, B., Sooriyathasan, S., Egan, S., and Leslie, G. 2020. Seismic and borehole-based mapping of the late Carboniferous succession in the Canonbie Coalfield, SW Scotland: evidence for a 'broken' Variscan foreland? *Scottish Journal of Geology*, 57(1) https://doi.org/10.1144/sjg2020-007

7.1 Introduction

In this chapter, a structural mapping-based study using subsurface (seismic and borehole) data from the Canonbie Coalfield in SW Scotland is presented (see Fig. 1.1 for location). These coal-bearing strata were deposited in the northern part of the Solway Basin (Fig. 7.1), the complex characteristics of which have been discussed for decades (Leeder, 1982; Coward, 1993; Chadwick *et al.*, 1995; Jones *et al.*, 2011). Thanks to a series of recent works centred on the Canonbie Coalfield, there is exceptionally detailed constraint on sedimentological characteristics of the late Carboniferous basin fill in this part of the UK (Jones and Holliday, 2006; Morton *et al.*, 2010; Jones *et al.*, 2011). In both modern and ancient sedimentary basins, syn-kinematic sequences can indirectly reveal the nature of the various tectonic episodes that influenced the basin and its regional setting. In many ancient sedimentary basins, these sequences are often absent due to later uplift and denudation. In contrast, a near complete record of the late Carboniferous syn-kinematic megasequence (e.g., Besly *et al.*, 1993; Peace and Besly, 1997) is locally preserved at the Canonbie Coalfield (Chadwick *et al.*, 1995; Waters *et al.*, 2011; Jones *et al.*, 2011).
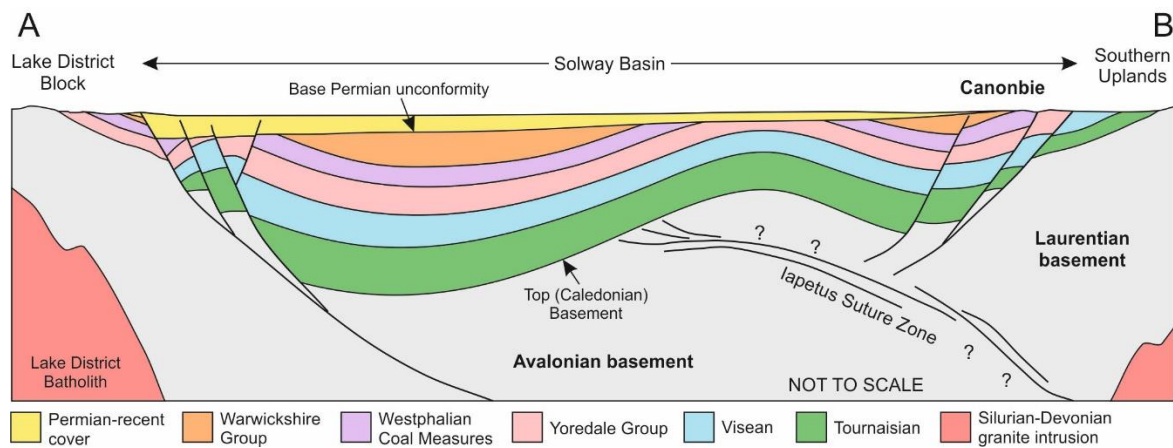
Figure 7.1: A schematic N-S cross-section through the Solway Basin, northern England, showing the location of the Canonbie Coalfield in relation to the rest of the basin and the adjacent pre-Carboniferous basement highs to the north and south. Section is subparallel to the axis of the Solway Syncline. For cross-section location, refer to Figure 1.1.

7.2 Seismo-stratigraphic analysis of the Canonbie Coalfield

7.2.1 Data

Several datasets have been utilised in the study of the late Carboniferous succession at Canonbie (Fig. 7.2). These include 12 UK Oil and Gas Authority and 7 UK Coal Authority onshore digital 2D seismic reflection profiles, originally acquired by Edinburgh Oil & Gas Ltd. and by the British Coal Corporation, respectively. Seismic surveys for coal exploration are typically shot at higher frequencies (<125 Hz) and with lower depths of penetration than surveys for oil and gas exploration (20-80 Hz; Gochioco, 1990). Therefore, seismic reflection profiles shot for coal exploration enable detailed mapping of onlapping and truncated seismic reflection geometries within sedimentary units at shallow depths, helping to constrain the timing of various deformation events. Note that the seismic reference datum from which the seismic reflection profiles are plotted for British Coal exploration surveys often varies from the sea level datum typically used for oil and gas surveys. Where the coal exploration datum was flat but shot above sea level, the reflection profile was shifted vertically in two-way travel time, assuming a constant near surface velocity of 2400 ms^{-1}. Where the reference datum was sloping, the reflection profile was not used for mapping in this study. These data are supported by 19 borehole penetrations, all of which provide stratigraphic constraints and some of which are associated with petrophysical (mainly gamma ray and acoustic)
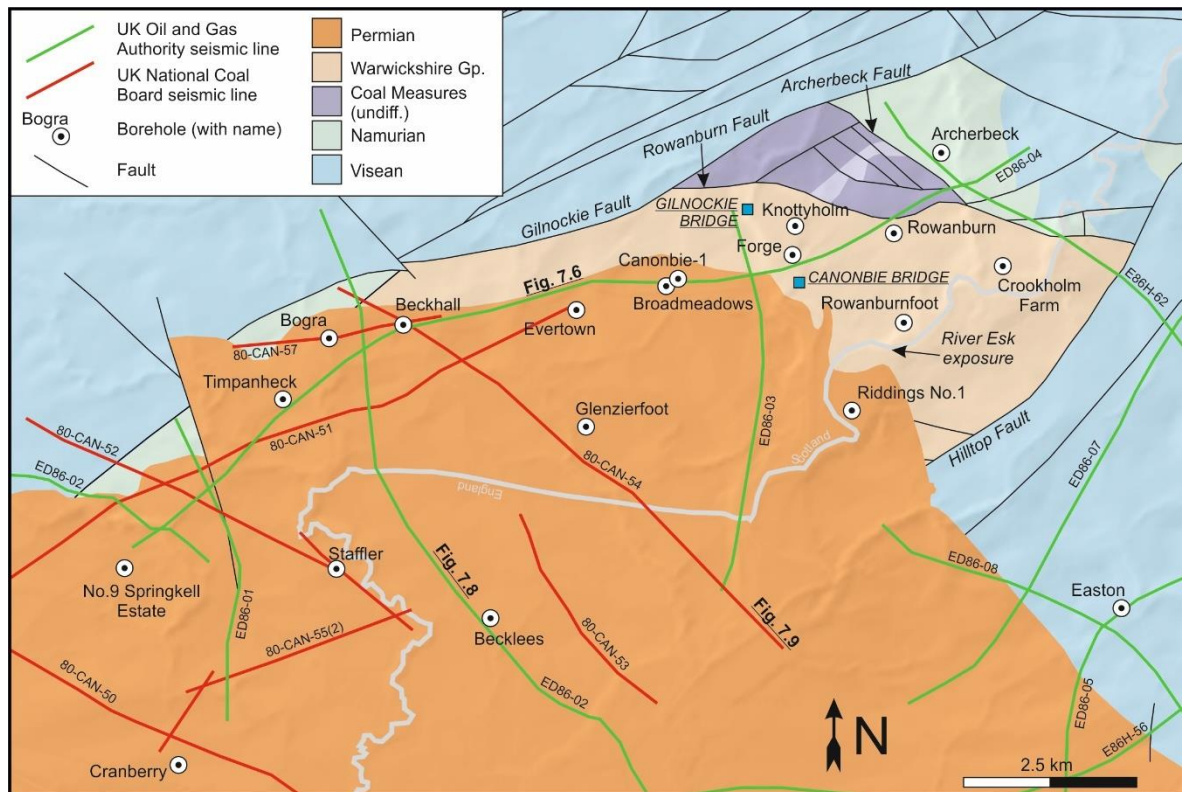
Figure 7.2: A summary of the seismic and borehole data from the Canonbie Coalfield used in this study. All seismic data was accessed through UKOGL (UK Onshore Geophysical Library). Borehole data was accessed through the UK OGA (Oil and Gas Authority), IHS Markit and the BGS's (British Geological Survey) archives at Keyworth. Contains BGS DiGmapGB-250 Scale data © UKRI (British Geological Survey, 2008).

data and time-depth calibration data. These boreholes were drilled between 1854 and 2008 for coal, oil and gas and coalbed methane exploration purposes (Picken, 1988; Creedy, 1991; Chadwick *et al.*, 1995). The quality of data associated with each borehole varies accordingly. Readers are encouraged to follow web links to uninterpreted versions of the seismic lines provided in this chapter, which can be found in the figure captions.

7.2.2 Stratigraphy

The Canonbie Coalfield is one of few places in the UK that preserves a near complete Westphalian stratigraphic record (Fig. 7.3). The stratigraphy at Canonbie consists of <300 m of Langsettian-Duckmantian (Westphalian) Pennine Lower and Middle Coal Measures Formations (herein: PLCM and PMCM). Ordinarily, in north-western Europe, the base of this succession is
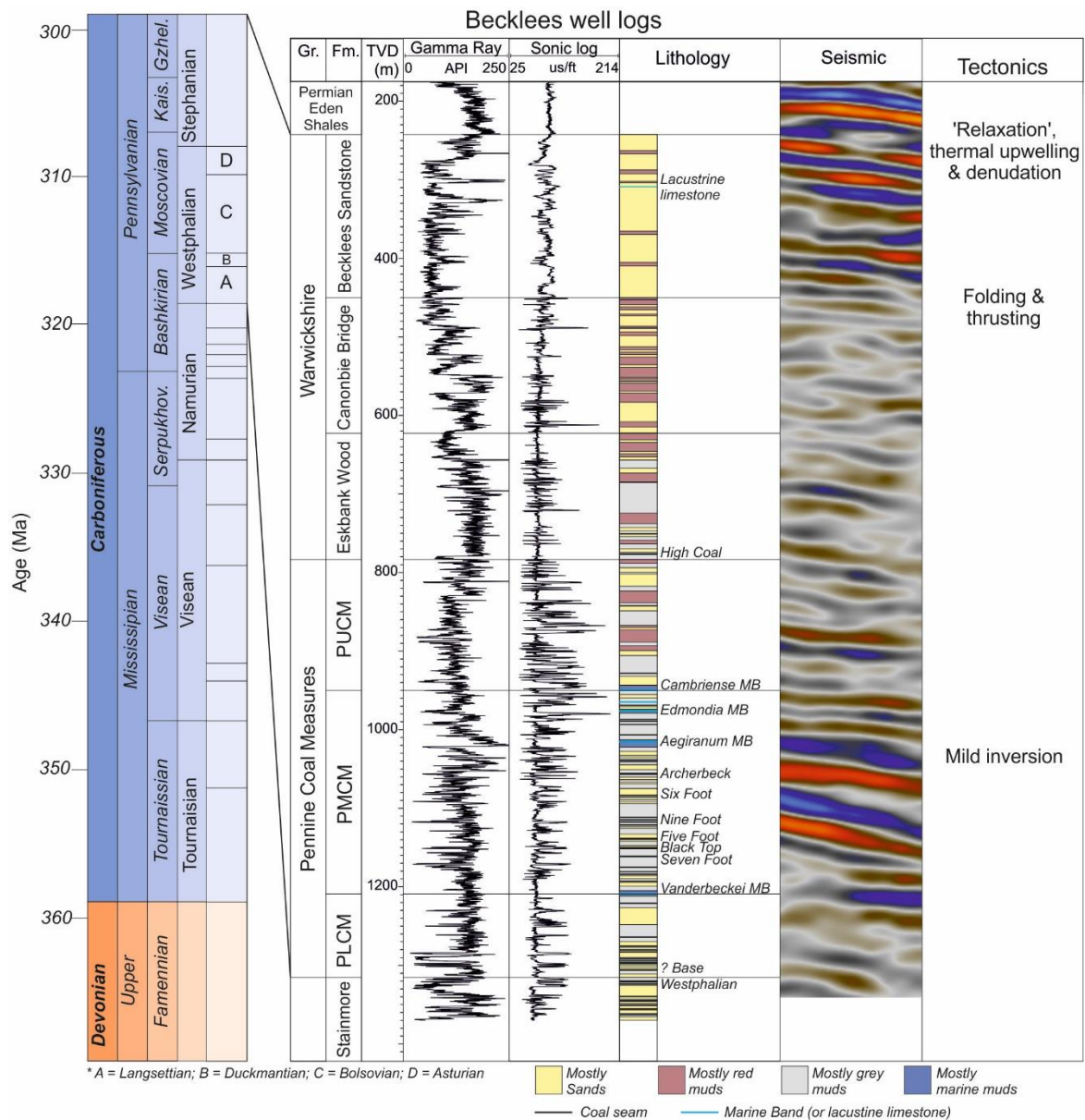
Figure 7.3: (left) Stratigraphic columns showing international and regional Stage units. (right) A seismic well tie for the Becklees borehole. Gamma ray, density, sonic and lithological logs (based on Jones and Holliday, 2006; Jones *et al.*, 2011) are shown along with synthetic and observed seismic traces. A = Langsettian; B = Duckmantian; C = Bolsovian; D = Asturian; Gr. = Group; Fm. = Formation; TVD = True Vertical Depth.

defined by the Subcrenatum Marine Band (Waters *et al.*, 2011) (Fig. 2.4). This unit is absent at Canonbie, and across the Scotland. The Pennine Coal Measures (PCM) Group is correlative across both the coalfield and NW Europe based on frequent stratigraphically defined coal seams and marine bands. The Pennine Upper Coal Measures Formation (PUCM) is poorly documented in historical accounts of the Canonbie Coalfield and contains only limited amounts of coal-bearing strata that provide stratigraphic control. Similarly- aged stratigraphy can be recognised further

afield in southern Scotland and in Cumbria, courtesy of inter-bedded Spirorbis-bearing limestone beds (Mykura, 1967) (also see Fig. 2.2).

Overall upwards-coarsening and primarily 'red-bed' Warwickshire Group strata, conformably overlie PCM strata at Canonbie (Fig. 7.3) (Jones *et al.*, 2011). Given the poor likeness of the Warwickshire Group strata at Canonbie with the Warwickshire Group Whitehaven Sandstone Formation of West Cumbria, and the paucity of stratigraphically correlative strata from both locations, three locally defined formations are used to describe the succession at Canonbie (Jones and Holliday, 2006). These are the Eskbank Wood, Canonbie Bridge Sandstone and Becklees Sandstone formations. Only strata of the Tenuis Chronozone (lower Westphalian D) have been proved within the lowermost mudstone dominated Eskbank Wood Formation (Jones *et al.* 2006). No biostratigraphically defined age constraints are given for the remainder of the Warwickshire Group. However, the Canonbie Bridge Formation shares petrographic characteristics with the Halesowen Formation of the English Midlands and is believed to be of predominantly Asturian (Westphalian D) age also (Jones *et al.*, 2011; Morton *et al.*, 2010). A chronostratigraphic correlation of the late Carboniferous succession preserved at Canonbie across Scotland, northern England and central England is discussed in Chapter 9.

7.2.3 Seismic horizons and time-depth conversion

Several latest Devonian to Permian-aged seismo-stratigraphic horizons were mapped in two-way travel time. The most consistent mappable surface is the base Permian angular unconformity against which Carboniferous reflectors truncate upwards (Fig. 7.4). The Westphalian-Stephanian succession is characterised by strong, semi-continuous seismic reflectors due to the presence of thick inter-bedded channel sands (Jones *et al.*, 2011) and low-density coals (Picken, 1988). Based on similar studies within the region (Kimbell *et al.*, 1989; Chadwick *et al.*, 1995), a single strong, positive, continuous reflector is believed to mark the Great Limestone Member (Alston Formation, Yoredale Group) at the base of the Namurian succession beneath the Canonbie Coalfield. Below this unit, similar inter-bedded limestone-derived reflectors characterise the Visean succession of the Tyne Limestone Formation (also Yoredale Group). The pre-Carboniferous basement horizon is interpreted as being represented by a series of strong positive continuous
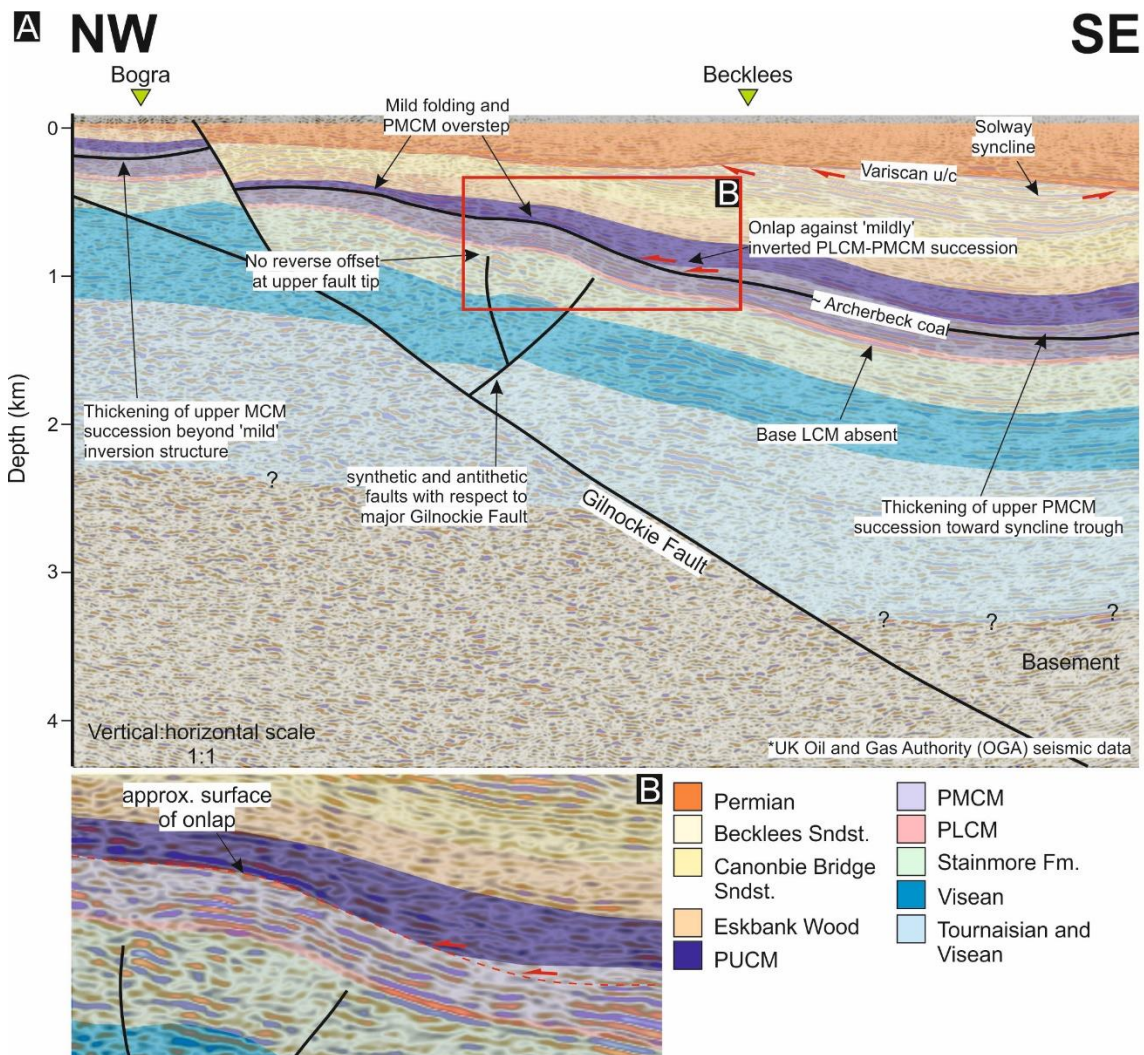
Figure 7.4: An interpreted NW-SE seismic profile (Seismic line ED86-02) depicting folding of the Solway Syncline, mild inversion along antithetic and synthetic normal faults of the Gilnockie Fault, onlapping Pennine Middle Coal Measures (PMCM) against mild inversion folds and normal offset along the Gilnockie Fault. For section location, see Figure 7.2. Uninterpreted profiles for all the seismic sections included in this study can be previewed at ukogl.org.uk.

reflectors, which are believed to represent subsurface equivalents of the Birrenswark Volcanic Formation (Inverclyde Group) (*cf.* Kimbell *et al.*, 1989).

Bulk sonic velocities for the Permian succession (2900 ms^{-1}), the Westphalian-Stephanian succession (3600 ms^{-1}) and the latest Devonian-Namurian succession (4500 ms^{-1}) were used to construct a simple velocity model. These values were derived from sonic velocity log data for the Easton, Timpanheck and Becklees boreholes. A seismic velocity of 5000 ms^{-1} was used for the basement (*cf.* Evans, 1994). The velocity model was used to convert the seismic surveys from time to depth domain. Although uncertainty surrounding the time-depth conversion process is

acknowledged, the velocity model is deemed adequate for the purposes of the structural interpretation reported in this study. Stratigraphic data derived from borehole reports was used to better constrain structural interpretations of the depth converted seismic survey.

7.3 Structure of the Canonbie Coalfield

To understand the late Carboniferous kinematic evolution of the Canonbie Coalfield better, an integrated interpretation of the depth-converted seismic dataset, borehole data and outcropping geology is presented. Several key structures have been identified as a result of that analysis (Fig. 7.5a). These include: 1) the NE-SW trending Bewcastle anticline and Hilltop Fault; 2) the NNE-SSW trending Solway syncline; 3) the NE-SW trending Gilnockie Fault; 4) ENE-WSW and E-W trending normal faults such as the Archerbeck, Rowanburn, Woodhouselees and Glenzierfoot Faults, and; 5) (N)NW-(S)SE trending strike-slip faults such as those exposed at surface laterally offsetting the coalfield's Permian cover. The Westphalian-Stephanian succession is described through a series of time-slices, focussing upon how this succession was influenced by the combined effects of these key structures during its deposition.

7.3.1 Namurian and Pennine Lower Coal Measures (PLCM)

Based on isochore thickness maps, and unlike the general case across the Midland Valley of Scotland (Ritchie *et al.*, 2003; Underhill *et al.*, 2008), Namurian and PLCM stratigraphy at Canonbie shows little evidence of varying significantly in thickness across the coalfield (Fig. 7.5b); although, this is in contrast with the southern part of the Solway Basin where Chadwick *et al.* (1995) observed mild thickening within the southern trough of the Solway Syncline and Akhurst *et al.* (1997) records a localised late Namurian angular unconformity. The local PCM subcrop is bound to the northwest by the Gilnockie Fault and to the southwest by the Hilltop Fault that both dip towards the southeast and display net normal and reverse displacement, respectively. From seismic data, Picken (1988) interpreted a known local basal Westphalian break in deposition (represented by the absence of the Subcrenatum marine band) as a low-angle overstepping unconformity that resulted from syn-depositional anticlinal growth along a *c.* N-S compressional axis (e.g., Fig. 10 in Picken, 1988). The originally observed outcropping example of this unconformity was argued to represent low-
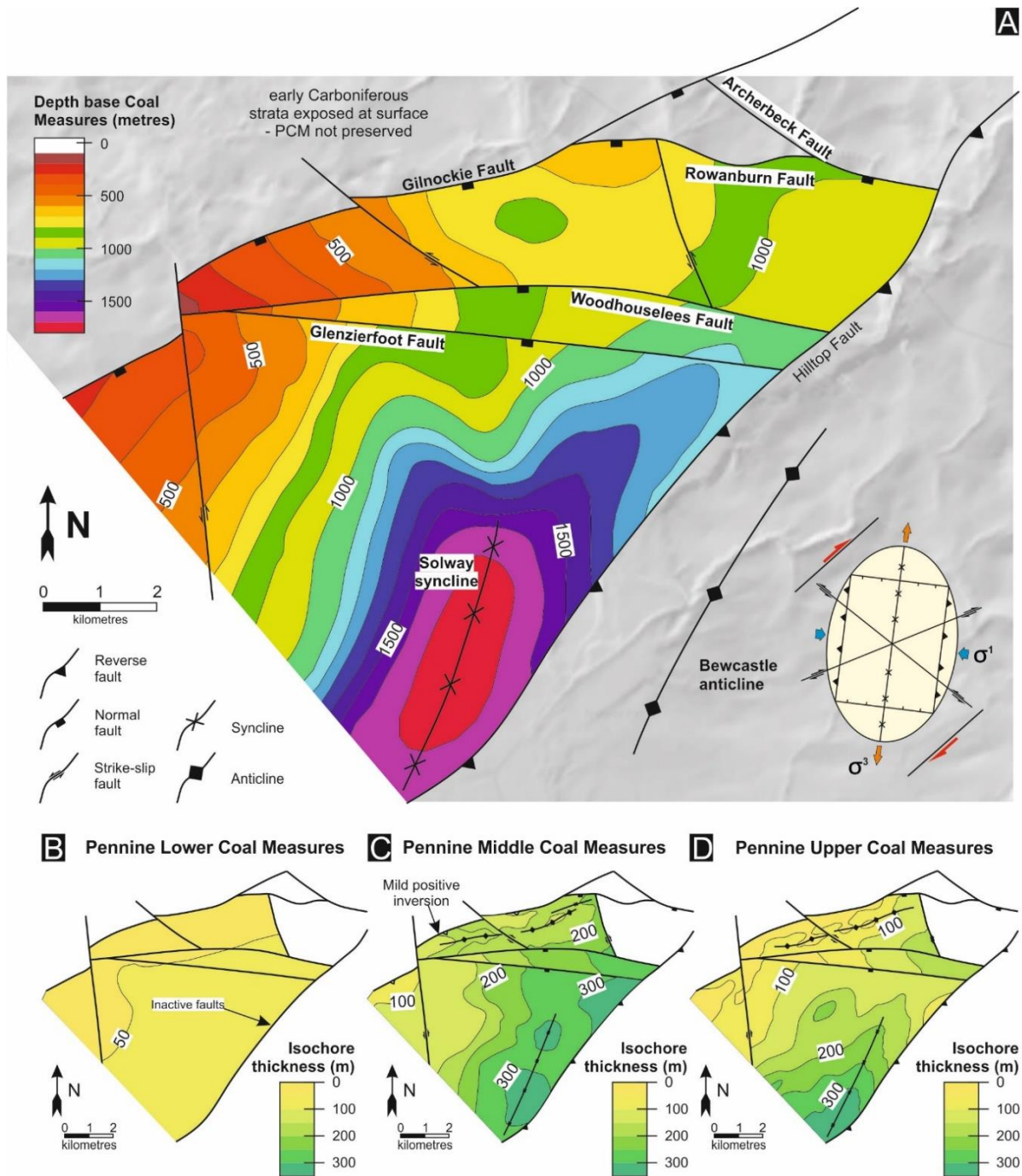
Figure 7.5: Depth map to base Pennine Coal Measures Formation in metres in the Canonbie coalfield. The dominant structural trends interpreted in the Canonbie Coalfield can be accounted for by dextral wrenching along NE-SW orientated faults (inset top-left; 2D strain ellipse illustrating predicted discontinuity trends after dextral wrench on NE-SW orientated faults). 7.5b, c and d: Isochore thickness maps for the Pennine Lower, Middle and Upper Coal Measures Formations respectively, based on the seismic interpretations of this study. Thickening during deposition of the Pennine Middle and Upper Measures Formations is controlled dominantly by growth within the Solway Syncline structure.

angle unconformable onlap and overstep (Lumsden *et al.*, 1967) but has recently been reinterpreted as, instead, representing a localized sedimentary feature, resulting from multiple phases of river channel-bank collapse (Jones and Holliday, 2016). After careful re-examination of this seismic dataset, the PLCM onlap surface of Picken (1988) is re-interprted as actually representing the Gilnockie Fault, along a 2D seismic profile parallel to the fault, which offsets late Carboniferous strata as well as the strata below it (Fig. 7.6). The absence of basal Westphalian stratigraphy within the Canonbie Coalfield is believed to represent a parallel disconformity.

7.3.2 Pennine Middle and Upper Coal Measures (PMCM and PUCM)

Variations in the thickness of PMCM and PUCM stratigraphy (Figs. 7.5c, d) suggest that the NNE-SSW trending Solway Syncline acted as a significant depocentre for Duckmantian and younger Westphalian stratigraphy (also see Fig. 7.7). Throughout the coalfield, these units also thicken gradually towards the Hilltop Fault, within the fault's footwall, but are at their thickest (<700 m) within the axis of the Solway Syncline. This structure forms a broad, slightly asymmetrical syncline in the south-eastern part of the coalfield (Fig. 7.5a). To the immediate south, a 'minor early Carboniferous high' (Picken, 1988) or local strike-parallel northwards plunge of the Solway syncline marks the southern margin of the Canonbie Coalfield. The Solway Syncline continues to the south beyond this 'high' (Fig. 7.1), where it meets the northern margin of the early Carboniferous Lake District Block (Chadwick *et al.*, 1995). Whilst the syncline's eastern limb is cross-cut by the Hilltop Fault, its western limb shallows progressively towards the north and west. In the north-western part of the coalfield, a series of bright reflectors within the PMCM can be seen gently onlapping against similarly bright reflectors along the syncline's western limb (Fig. 7.4, and inset Fig. 7.4b). Based on borehole stratigraphy, the reflector that most closely resembles the surface of onlap is thought to represent the approximately late Duckmantian (Westphalian B) Archerbeck coal seam (also PMCM) (Fig. 7.3).

Synthetic and antithetic faults that merge with the Gilnockie Fault at 1-2 km depth, spatially correlate with the upper limit of the Solway Syncline's western limb (Fig. 7.4), onto which the Upper Coal Measures and younger Westphalian stratigraphy thin (Fig. 7.5c, d). The Aegiranum
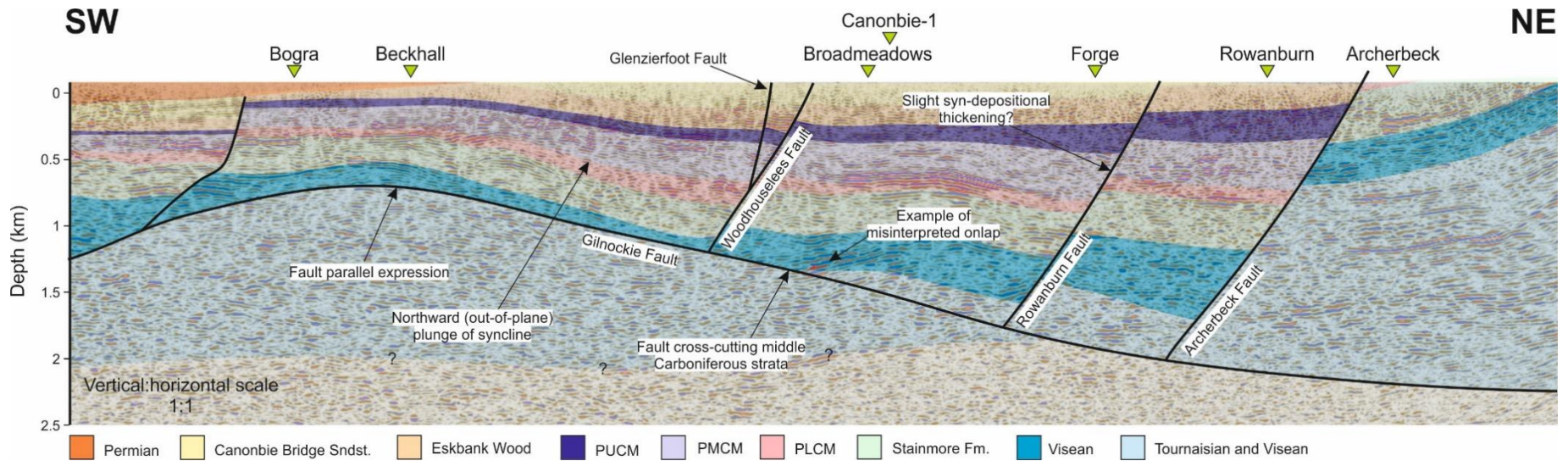
Figure 7.6: An interpreted SW–NE orientated seismic profile from the Canonbie Coalfield (Seismic line ED86-04), depicting normal faulting and strike-parallel plunge of the Solway Syncline. For section location, see Figure 7.2. Uninterpreted profiles for all the seismic sections included in this study can be previewed at ukogl.org.uk.

Marine Band (locally referred to as the Skelton Marine Band), which marks the base of the PUCM succession, is locally absent in borehole penetrations along the north-western margin of the Canonbie Coalfield (Timpanheck, Bogra and Beckhall; Fig. 7.2). The underlying stratigraphic units form a series of mild, together <2 km wide, parallel trending anticlines, which are overstepped by younger Westphalian stratigraphy (Fig. 7.4). These mild folds are together tilted south-eastwards by the coalfield wide Solway syncline. As with the Hilltop Fault, along the south-eastern margin of the coalfield, latest Devonian-Visean units (Inverclyde and Border Groups) within the hangingwall of the Gilnockie Fault thicken gently towards the fault, indicating normal movement at the time of latest Devonian-Visean deposition.

Evidence from borehole stratigraphy suggests that minor thickness increases in PMCM and PUCM units towards the ENE-WSW to E-W trending Archerbeck, Rowanburn, Woodhouselees and Glenzierfoot Faults within their hanging walls may be tentatively interpreted based on seismic reflection profiles, although growth of the Solway Syncline appears to have had a greater influence on thickness distribution of Westphalian stratigraphy. These structures all appear to dip steeply towards the south, displacing Carboniferous stratigraphy in a normal sense (Fig. 7.6). Latest Devonian to early Carboniferous-aged units (Inverclyde and Border Groups) are offset normally by and may be tentatively interpreted as gently thickening towards the Archerbeck, Rowanburn, Woodhouselees and Glenzierfoot Faults within their hanging walls, as they do towards the major parallel fault systems that bound the Solway Basin to the south (Chadwick *et al.*, 1995).

7.3.3 Warwickshire Group

Although much of the subcropping Warwickshire Group succession has been partly eroded prior to Permian deposition, thus limiting further use of isochore thickness maps, reflector geometries observed within the Canonbie Bridge and Becklees Sandstone Formations in the Solway syncline trough suggest that the nature of this depocentre was altered during deposition of the Becklees Sandstone Formation. In higher resolution coal exploration seismic reflection profiles, a thick succession (<200 m) of Becklees Sandstone Formation can be observed showing angular onlap against the Canonbie Bridge Sandstone Formation stratigraphy within the Solway syncline's western limb (Fig. 7.9). In addition, reflectors belonging to the Canonbie Bridge Sandstone
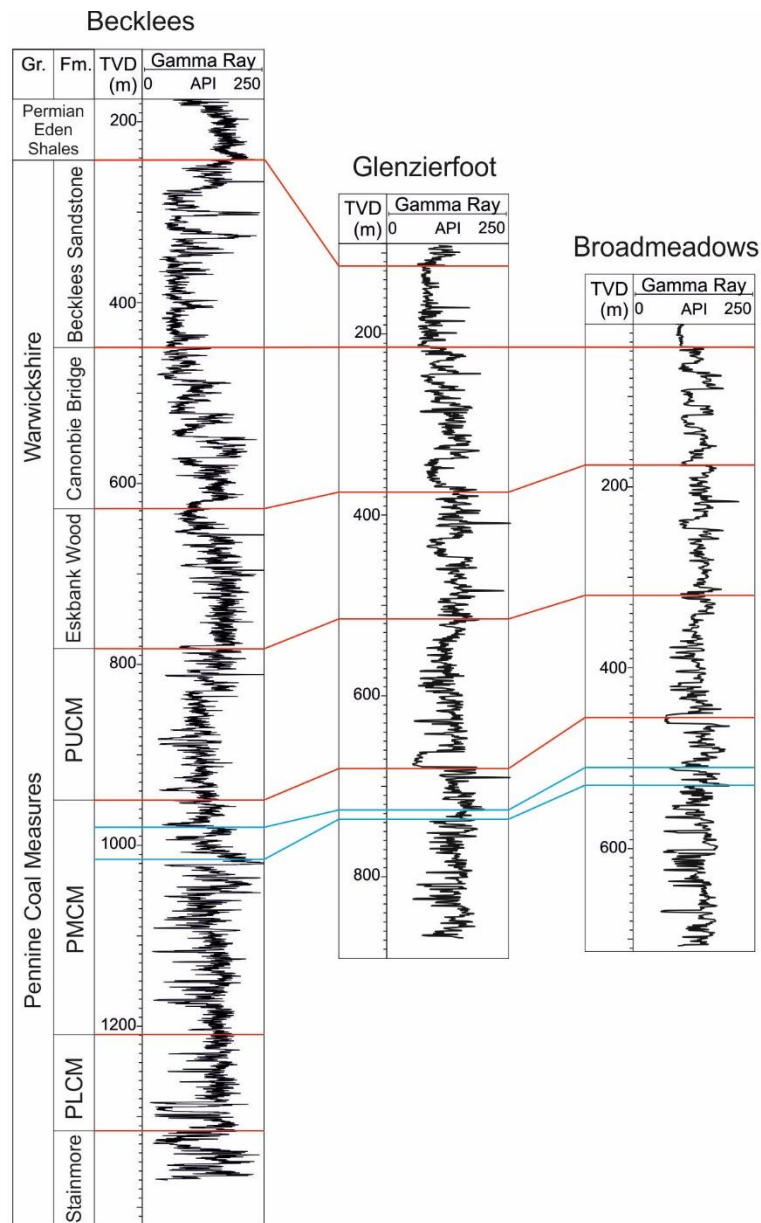
Figure 7.7: A wireline (gamma ray) correlation panel for the late Carboniferous successions of the Becklees, Glenzierfoot and Broadmeadows boreholes in the Canonbie Coalfield. Gamma ray curves for the Glenzierfoot and Broadmeadows boreholes are derived from Jones *et al.* (2011). Gr. = Group; Fm. = Formation; TVD = total vertical depth. For borehole locations, see Figure 7.2.

Formation within the syncline's western limb are slightly truncated against the surface of onlap (marked u/c 3; Fig. 7.9b). This surface of onlap is interpreted as an angular, partially erosional, unconformity. An additional unconformable horizon can be observed from the seismic data and down cuts into younger Becklees Sandstone stratigraphy within the Solway syncline, truncating underlying reflectors (u/c 4; Fig. 7.9b). Given that the Becklees Sandstone Formation has been interpreted as having been deposited in a fluvial environment (Jones *et al.*, 2011) and given the broad

U-shape geometry of the unconformity, this feature is interpreted as representing an erosive and, most likely, confined fluvial channel set (*cf.* Ramos *et al.*, 2002). Above angular unconformity u/c 3 (Fig. 7.9b), the axis of the Solway syncline appears to have migrated south-eastwards towards the Hilltop Fault. Given the discordance between reflectors within the Canonbie Bridge and Becklees Sandstone Formations in the syncline's western limb (Fig. 7.9a), this eastwards migration of the Solway syncline depocentre is perhaps associated with a steepening of this western limb. In addition, and along the syncline's north-western limb, the entirety of the Carboniferous succession forms a high amplitude (<1 km) anticline with a shorter and shallowly dipping north-western limb (Fig. 7.9a). This anticline correlates spatially with the Gilnockie Fault, which dips more shallowly, at least locally, within the uppermost 800 m of the subsurface. The onlapping reflector geometries described here within the Warwickshire Group of the Solway syncline (Fig. 7.9a), constrain the timing of the formation of this anticline to the earliest deposition of the Becklees Sandstone Formation (Jones *et al.*, 2011).

The NNE-trending Bewcastle anticline occurs within the hanging wall block of the parallel Hilltop Fault. Unlike the comparatively minor anticlines along the north-western margin of the coalfield, there are no timing constraints for the formation of this anticline, but it is assumed that they formed at similar times. The Hilltop Fault tips out within the Solway Basin around the southern margin of the coalfield (Chadwick *et al.*, 1995).

7.3.4 Stephanian-early Permian

Latest Carboniferous to early Permian deposits are absent from the Canonbie Coalfield, as is generally the case in the rest of north-western Europe (see Besly and Cleal, 2021). Both Permian strata and older Carboniferous strata are offset normally by one of the steeper synthetic faults to the Gilnockie Fault (Fig. 7.4) and ENE- to east-trending faults (Fig. 7.6). Older Westphalian strata are offset by a greater magnitude along this structure than Permian strata, suggesting that an episode of normal faulting preceded Permian deposition. At least two (N)NW-(S)SE trending faults cut, with apparent dextral offset, the Gilnockie Fault as well as the Permian-aged cover by <500 m along the western margin of the coalfield; this pattern is consistent all across the Northumberland-Solway

Basin (de Paola *et al.*, 2005). This group of structures is difficult to identify within seismic reflection profiles, suggesting that their vertical displacement is minimal. A strong degree of uncertainty surrounding the timing of these structures is acknowledged.
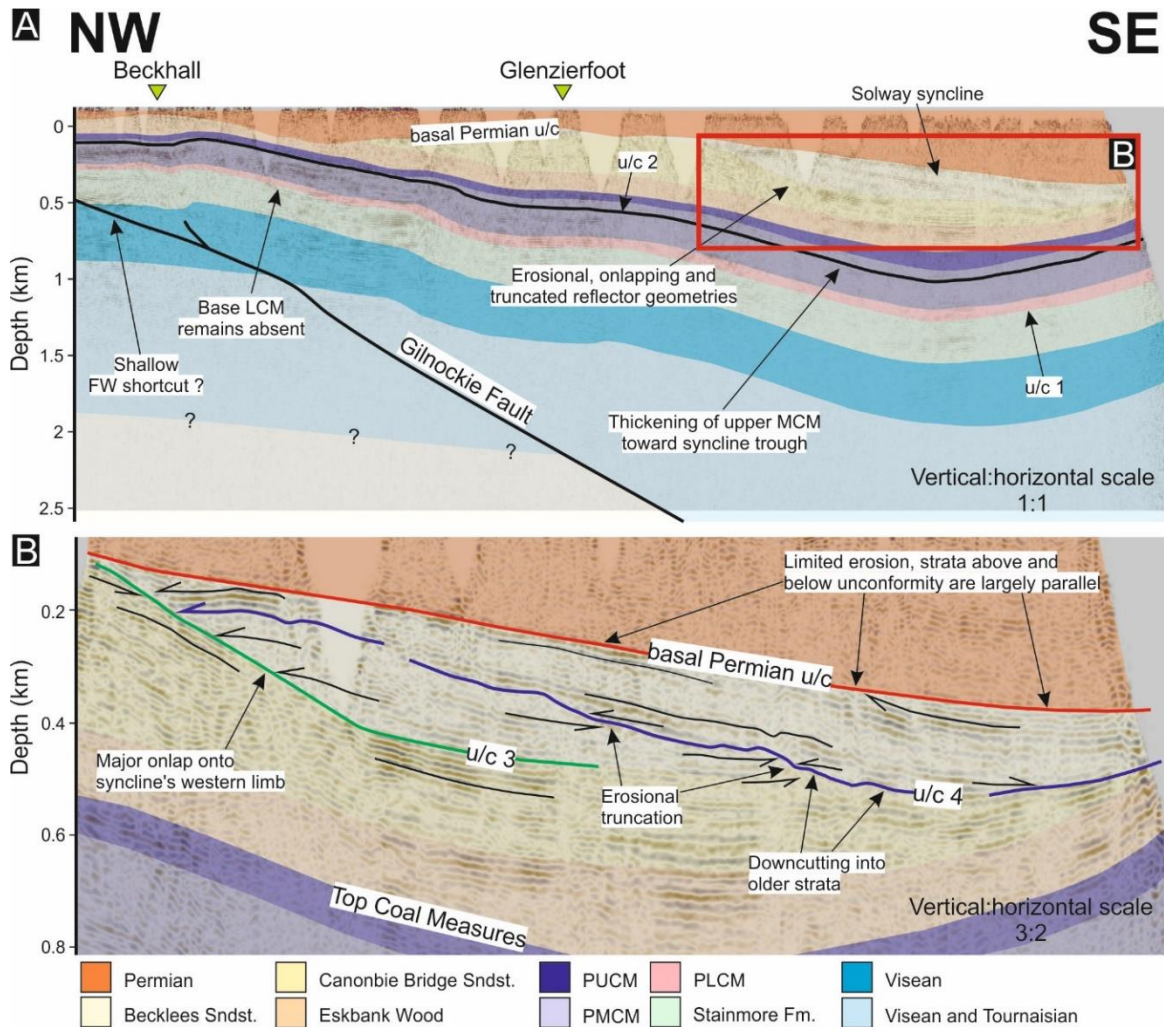
Figure 7.9a: An interpreted NW–SE orientated seismic profile depicting folding of the Solway Syncline (Seismic line 80-CAN-54). 7.9b: A closer look at the reflector geometries belonging to the Becklees Sandstone Formation (Warwickshire Group) within the axis of the Solway Syncline. A series of reflectors are shown onlapping against the western limb of the Solway Syncline. Erosional truncation of reflectors occurs within the axis of the Solway Syncline and is interpreted as representing down cutting, fluvial strata. For section location, see Figure 7.2. Uninterpreted profiles for all the seismic sections included in this study can be previewed at ukogl.org.uk.

7.4 Tectonic controls on the late Carboniferous evolution of the Canonbie Coalfield

Based on this structural mapping exercise, it is suggested that the fragmented late Carboniferous kinematic evolution of the Canonbie Coalfield can be constrained by at least three episodes of deformation (Fig. 7.10). These three episodes of deformation can be represented by unconformities described in the PMCM and the Warwickshire Group respectively (Figs. 7.4 and 7.9) and later normal fault movement prior to deposition of the basal Permian succession at Canonbie (Fig. 7.6).

7.4.1 Pennine Coal Measures (PCM) unconformity

Based on isochore thickness distributions for PMCM and PUCM and asymmetric, low amplitude folding correlating spatially with the Gilnockie Fault, the local PMCM unconformity is interpreted to indicate significant syn-depositional tectonism. Although folding of the entire Carboniferous succession beneath the base Permian unconformity has ultimately distorted the nature of the PMCM unconformity, 2D palinspastic cross-section restoration of a NE-SW section through the Canonbie Coalfield and Gilnockie Fault reveals that low amplitude folding occurred at the same time as this unconformity (Fig. 7.10c), resulting in 1.4 % along length shortening. Along strike, the steeper sided limbs of asymmetric, low-amplitude folds correlate laterally with the steeply dipping synthetic and antithetic normal faults of the Gilnockie Fault (Fig. 7.4), although there is interference between adjacent folds. Previous studies of inverted basins suggest that similar asymmetric, low-amplitude folding can be indicative of 'mild' positive fault inversion (sensu Song, 1997) - where the 'null point' or the point along an inverted fault's length at which there is zero net displacement (sensu Williams *et al.*, 1989) remains at the fault's upmost tip (Fig. 7.11a) (*cf.* Butler, 1998; Jackson *et al.*, 2013). Mild inversion structures are strongly dominated by folding due to partial reverse reactivation of a fault along its length, where thrusting does not accommodate a significant amount of shortening (Jackson *et al.*, 2013). Compressional stress at the time of folding is insufficient to prompt full reverse reactivation of these faults. The asymmetrical nature of the local PMCM and PUCM depocentre in the Canonbie Coalfield can be explained by these asymmetric and
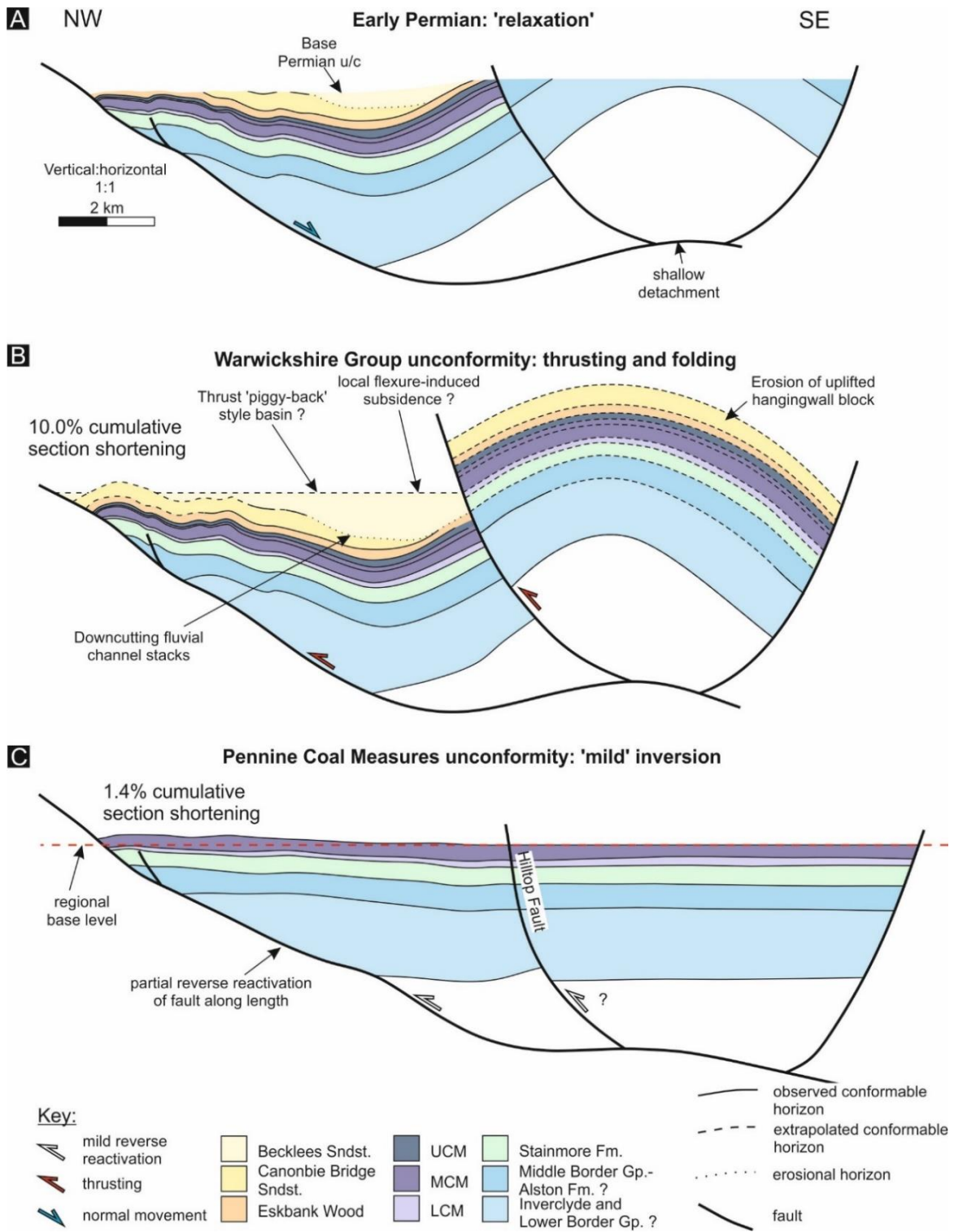
Figure 7.10: Two-dimensional palinspastic cross-section restorations for the NW–SE orientated section presented in Figure 7.9, and the adjacent footwall block. Timings of deformation events are constrained by onlapping reflector geometries. The cross-section can be restored by incorporating a sub-horizontal detachment at around 6-7 km depth. Restorations are performed using the unfolding, move-on-fault and decompaction modules in MOVE (Petroleum Experts) structural model building software.

mild inversion structures (e.g., Fig. 7.4). Oblique-slip (dextral) movement along similar NE-SW trending structures, such as the Gilnockie and Hilltop Faults, may have contributed to the slightly oblique NNE-SSW trending growth of the Solway syncline with respect to these faults.

7.4.2 Warwickshire Group unconformity

The Warwickshire Group unconformity appears to represent a more significant rearrangement of the local sedimentary basin (Fig. 7.10b). Two-dimensional palinspastic restoration of the NW-SE striking cross-section illustrated in Figure 7.9 suggests that the Warwickshire Group unconformity, seen in seismic data along the buried axis of the Solway syncline (Fig. 7.9), formed because of anticlinal folding due to shallowly dipping basement-involved thrusting along the Gilnockie Fault. This second basin reorganisation episode resulted in at least 10 % shortening (Fig. 7.10b). Unlike prior inversion that occurred during the deposition of the PMCM, shortening occurring during deposition of the younger Warwickshire Group succession appears to have been partly accommodated by the most shallow, comparatively shallowly-dipping part of the Gilnockie Fault (*cf.* Fig. 7.9a). As this part of the fault does not appear to have accommodated significant extension or shortening prior to this later episode of basin inversion, this part of the fault may have originated as a footwall short-cut (*cf.* Hayward and Graham, 1989).

The Warwickshire Group unconformity represents a significant rearrangement in the nature of the local Solway Syncline depocentre (Fig. 7.9a). Folding and thrusting appears to have caused a steepening of the syncline's north-western limb, and perhaps in doing so, confined the local longitudinal fluvial system causing it to become more erosive (Fig. 7.10b) (*cf.* Ramos *et al.*, 2002; Suriano *et al.*, 2015). Major reverse movement along the Hilltop Fault at this time and the resulting uplift of the hanging wall may have constituted a minor lithospheric load along the coalfield's south-western margin (*cf.* Karner and Watts, 1983). This would have perhaps prompted additional localised flexure-induced accommodation and restricted uplift of the Solway syncline's eastern limb and supplied the coalfield with an additional source of local clastic detritus (*cf.* Jones *et al.*, 2011). The minor Carboniferous high, that marks the southern limit of the coalfield (Picken, 1988; Chadwick *et al.*, 1995), may be attributed to the Hilltop Fault pinching out laterally at a similar
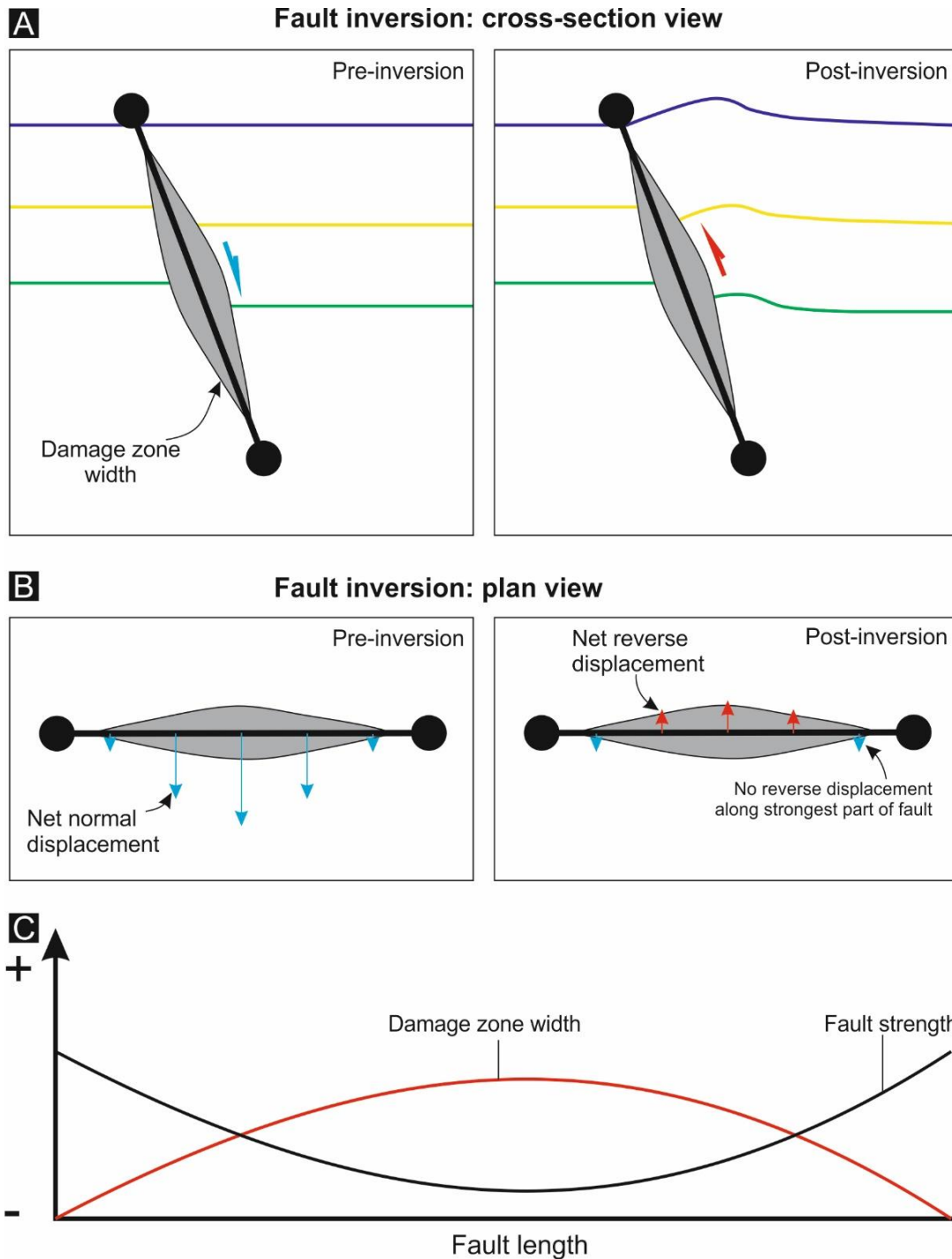
Figure 7.11: Schematic illustrations of the influences of variable fault strength along length on the style of positive normal fault inversion (based on Jackson *et al.*, 2013). 7.11a: Influence of variable fault strength along length on 'mild' (e.g., Song, 1997) positive normal fault inversion in cross-section view. 7.11b: Influence of variable fault strength along length on positive normal fault inversion in plan view. Note the change along strike from net normal displacement, closer to the fault tips, towards net reverse displacement, closer to the fault centre. 7.11c: Qualitative fault strength vs. damage zone width and fault strength relationships.

latitude if the depocentre immediately to the north (the coalfield) were partly attributed to local flexure-induced subsidence.

7.4.3 Basal Permian unconformity and latest Westphalian-early Permian relaxation

The post-Westphalian kinematic evolution of the coalfield, prior to deposition of the Permian succession appears to be represented by a 'relaxation' in compressional stresses (Fig. 7.10a) (*cf.* Dempsey, 2016). Normal offset occurs primarily along pre-existing E-W orientated faults, perhaps indicating dextral transtension (*cf.* Coward, 1993; Monaghan and Pringle, 2004; De Paola *et al.*, 2005; Pharaoh *et al.*, 2019) but also along the Gilnockie Fault (Fig. 7.4). The basal Permian angular unconformity cuts stratigraphy below it, perhaps suggesting further uplift prior to Permian deposition following the late Westphalian-Stephanian (*cf.* Underhill and Brodie, 1993), although this uplift event appears not to have been accommodated by fault movement.

7.6 Discussion

The implications of the findings presented in the previous sections are discussed in Chapter 9 where the Canonbie Coalfield and the eastern part of the Midland Valley of Scotland are set within the contexts of the distal part of a 'broken' Variscan foreland (*cf.* Strecker *et al.*, 1989).

7.6.1 Strain localisation along obliquely orientated structures

Given the important role that faulting, folding and positive inversion appears to have played in determining the characteristics of late Carboniferous depocentres in the Canonbie Coalfield, the localisation of strain along depocentre defining structures is considered. In northern Britain, the localisation of strain along obliquely orientated structural trends with respect to the apparent, approximately N-S (Variscan) compressional stress orientation requires fault damage zones significantly weaker (>30 %) than intact bedrock (Copley and Woodcock, 2016). Having possibly undergone reverse (dextral) reactivation during Namurian times and reverse reactivation during deposition of the PMCM, albeit only partial reactivation along fault length (e.g., Fig. 7.11a), NE-SW

trending faults such as the Gilnockie Fault are likely to have remained susceptible to further reverse reactivation, even in a contrasting lateral sense, during deposition of the Warwickshire Group. There is limited evidence to suggest that approximately E-W trending structures that were roughly perpendicular to the orientation of maximum compressional stress, at Canonbie or in the immediately surrounding region, accommodated significant basin shortening during this period (Fig. 7.6) (De Paola et al., 2005). Three-dimensional sandbox models and modern-day analogues for inverted basins suggest that steep faults orientated perpendicular to the orientation of maximum compressive stress are unlikely to accommodate significant shortening in low-strain settings (Keller and McClay, 1995; Di Domenica et al., 2014). E-W structures that were perpendicular with respect to compressional stress, may have remained 'frozen' during this period, leaving more oblique, recently active and, therefore, mechanically weaker structures to accommodate preferential shortening.

7.6.2 Strain location within rheologically weaker crustal rock

Line-length restoration suggests that at least 10 % cumulative shortening occurred along a NW-SE axis throughout the prolonged late Carboniferous inversion phase (Fig. 7.10). In reality, basin shortening is likely to have been larger due to both sub-seismic scale shortening and out-of-plane deformation. This shortening occurred in a region widely regarded as having occupied a low strain setting within the Carboniferous foreland (Corfield et al., 1996; De Paola et al., 2005). In the Midland Valley of Scotland, steeply dipping faults such as the Highland Boundary and Southern Upland fault systems are believed to have exerted a strong control on the magnitude of shortening (Ritchie et al., 2003; Underhill et al., 2008). A dissipating stress field derived from these faults may have contributed towards the localised stress field in the Canonbie Coalfield. However, despite their shared proximities to these fault systems, as well their similarly orientated structural fabrics, based on regional studies subsurface studies and accounts of outcropping geology (cf. Chadwick et al., 1995; Lumsden et al., 1967), there is a large disparity between the high magnitude of basin shortening observed at Canonbie compared with the Scottish Southern Uplands or the Lake District (Fig. 7.1). The Solway Basin and the Canonbie Coalfield is underpinned by relatively weak upper crustal rock, composed predominantly of thick Carboniferous sediment and weakly metamorphosed Ordovician-

Silurian slate and phyllite (Rickards and Woodcock, 2005; Stone *et al.*, 2012). This contrasts with the thinner Carboniferous successions preserved immediately to the south and north of the coalfield, which are underpinned by mechanically strong granitoid basement rock in the Lake District and partially granitic, greywacke dominant basement rock in the Southern Uplands of Scotland (Bott *et al.*, 1967; Allsop *et al.*, 1987; Howell *et al.*, 2019). Consequently, the Solway Basin may have also accommodated shortening for a wider region, including those mechanically stronger regions that were less able to accommodate basin shortening, just as the Solway Basin likely accommodated early Carboniferous extension for a wider region.

High magnitude seismic-scale folding and thrusting is often accommodated by a shallow to mid-level crustal detachment (Coward *et al.*, 1999). The northwards dipping Iapetus suture zone that, prior to Caledonian collision of Avalonia and Laurentia, separated present day Scotland from northern England (*cf.* Freeman *et al.*, 1988; Soper *et al.*, 1992) constitutes such a detachment. This detachment is undoubtedly at a relatively shallow depth beneath the Canonbie Coalfield and Solway Basin, regardless of the contrasting interpolations of the onshore Iapetus suture zone (Fig. 7.1) (Chadwick *et al.*, 1995; De Paola *et al.*, 2005). Furthermore, cross-section restorations of the Solway Syncline through the Canonbie Coalfield suggest a detachment at 6 to 7 km depth below surface (Fig. 7.9), which may reflect this suture. Along with the locally mechanically weak crustal rock underpinning the region, the favourable (slightly oblique) structural fabric orientation and the weak (following dextral reactivation) accommodating NE-trending faults, this detachment may therefore have also been able to aid the accommodation of greater localised basin shortening with respect to adjacent areas.

7.7 Conclusions

Local seismic and borehole-based mapping of the late Carboniferous succession in the Canonbie Coalfield (SW Scotland) provides evidence of repeated episodes of positive inversion, syn-depositional folding and unconformities within the Westphalian to Stephanian Pennine Coal Measures and Warwickshire Group successions. Positive inversion and syn-depositional folding dictated Westphalian-Stephanian depocentres within the Canonbie Coalfield. The basin history thus

revealed is at variance with generally accepted models in northern Britain that state these basins subsided due to post-rift thermal subsidence during the late Carboniferous (e.g., Leeder, 1982; Fraser and Gawthorpe, 1990). Local variations in crustal rheology, inherited fault strengths and their variation over time, fault orientation with respect to the evolving dominant stress field and mid-crustal detachments are suggested to play important roles in strain localisation and ultimately the nature of Westphalian-Stephanian depocentres at the Canonbie Coalfield. These findings, along with those presented in the succeeding chapter of this thesis, provide a rare opportunity to re-assess the structural and geodynamic controls on sedimentation in northern Britain and the remainder of the British Isles during the late Carboniferous Period.

Late Carboniferous tectono-stratigraphy of the (eastern) Midland Valley of Scotland: insights from seismic and borehole-based mapping, and coastal exposure

8.1 Introduction

Understanding the effects of adjacent collision zones on some of the world's ancient sedimentary basin systems is often limited by the fragmented preservation of these basins and complex intra-basin structure. Many studies find that understanding these relationships is typically important when considering both local and regional subsidence trends, palaeodrainage systems, sediment routing and changes to climate (Besly, 1988; Horton and DeCelles, 2001; Cataneanu, 2019; Lopez *et al.*, 2019; McKellar and Hartley, 2020). The Midland Valley of Scotland (MVS), which is situated in what could be considered the distal part of a late Carboniferous Variscan foreland basin (Fig. 2.1), appears to be no exception. Whereas several notable works based on the geology of NW Europe have long recognised the effects of the southerly Variscan Mountains on the regional late Carboniferous basin system (e.g., Besly, 1988; Corfield *et al.*, 1996; Peace and Besly, 1997; Littke *et al.*, 2000; Burgess and Gayer, 2000; Kombrink *et al.*, 2008), an oblique and largely pre-existing transpressional growth fabric appears to obstruct any indication of a Variscan phase of deformation or Variscan-influenced sedimentation in Scotland (Dewey, 1982; Read, 1988; Read and Forsyth, 1989; Richie *et al.*, 2003; Underhill *et al.*, 2008). What little remains of the local late Carboniferous sequence is poorly constrained stratigraphically and largely buried unconformably beneath younger Permian or Quaternary sediments (Cameron and Stephenson, 1985).

In this chapter, the results of a tectono-stratigraphic study on the late Carboniferous succession of the eastern part of the MVS are presented (see Fig. 1.1 for location). Based on the interpretation of high resolution (<125 Hz) coal board subsurface seismic reflection profiles archived by the UK Onshore Geophysical Library (UKOGL), frequent borehole constraint archived by the British Geological Survey (BGS), and the logging of coastal outcrop exposure, complex late

Carboniferous structure and stratigraphy has been unravelled. Evidence for three discrete phases of accelerated intra-basin deformation is identified within this sequence. The local late Carboniferous succession is characterised by changes in rates of sediment supply, accommodation, and depositional environment. This chapter forms the second data chapter of a four-chapter part of this thesis, during which the late Carboniferous stratigraphy of northern England and Scotland is explored within the contexts of a conceptual 'broken' Variscan foreland.

8.2 Late Carboniferous stratigraphy of the MVS

Some of the youngest Carboniferous sediments encountered in the MVS are preserved along the axes of the approximately NE- to NNE-trending Leven and Midlothian synclines in the eastern part of the MVS (Fig. 8.1) (also see Fig. 2.2). Most of these sediments are unconformably overlain by variably thick Quaternary-aged deposits in the Firth of Forth but outcrop exposure can be found immediately to the north and south of the firth and further inland, in the Fife and Lothian regions. In Fife, comparatively red, overall coarser-grained, and mostly barren (with respect to coal) late Carboniferous sediments belonging to the Scottish Upper Coal Measures Formation are encountered, which contrast with the greyer, finer-grained and coal-bearing sediments belonging to the underlying Lower and Middle Scottish Coal Measures formations (Binney and Kirkby, 1882). In central Scotland, the colour of similarly aged 'red-bed' sediments is largely attributed to post-depositional alteration during a regional early Permian depositional hiatus (Mykura, 1960). However, extensively more researched contemporaneous red-bed deposits in central England are considered mostly primary because of deposition in more arid continental conditions, which are attributed to denudation and rain shadow effects from the southerly Variscan Mountains (Fig. 2.1) (e.g., Besly and Cleal, 1997). Isotope ages for cross-cutting sub-volcanic vents and unconformably overlaying volcanic rock belonging to the Early Permian Mauchline Volcanic Formation (289 $\pm$ 5 Ma; Monaghan, 2010) provide upper age limits for the youngest and most poorly defined part of the late Carboniferous succession in central Scotland (Stephenson *et al.*, 2003). Frequent inter-bedded limestone beds, lingula or marine bands and named coal seams provide higher resolution chronostratigraphic constraints for the mostly deltaic sediments belonging to the Lower and Middle

Scottish Coal Measures formations and the underlying Clackmannan Group (e.g., Ramsbottom, 1979). Basin fill is imaged by multiple grids of 2D seismic reflection profiles, which were acquired because of coal and oil exploration during the late 20th century.
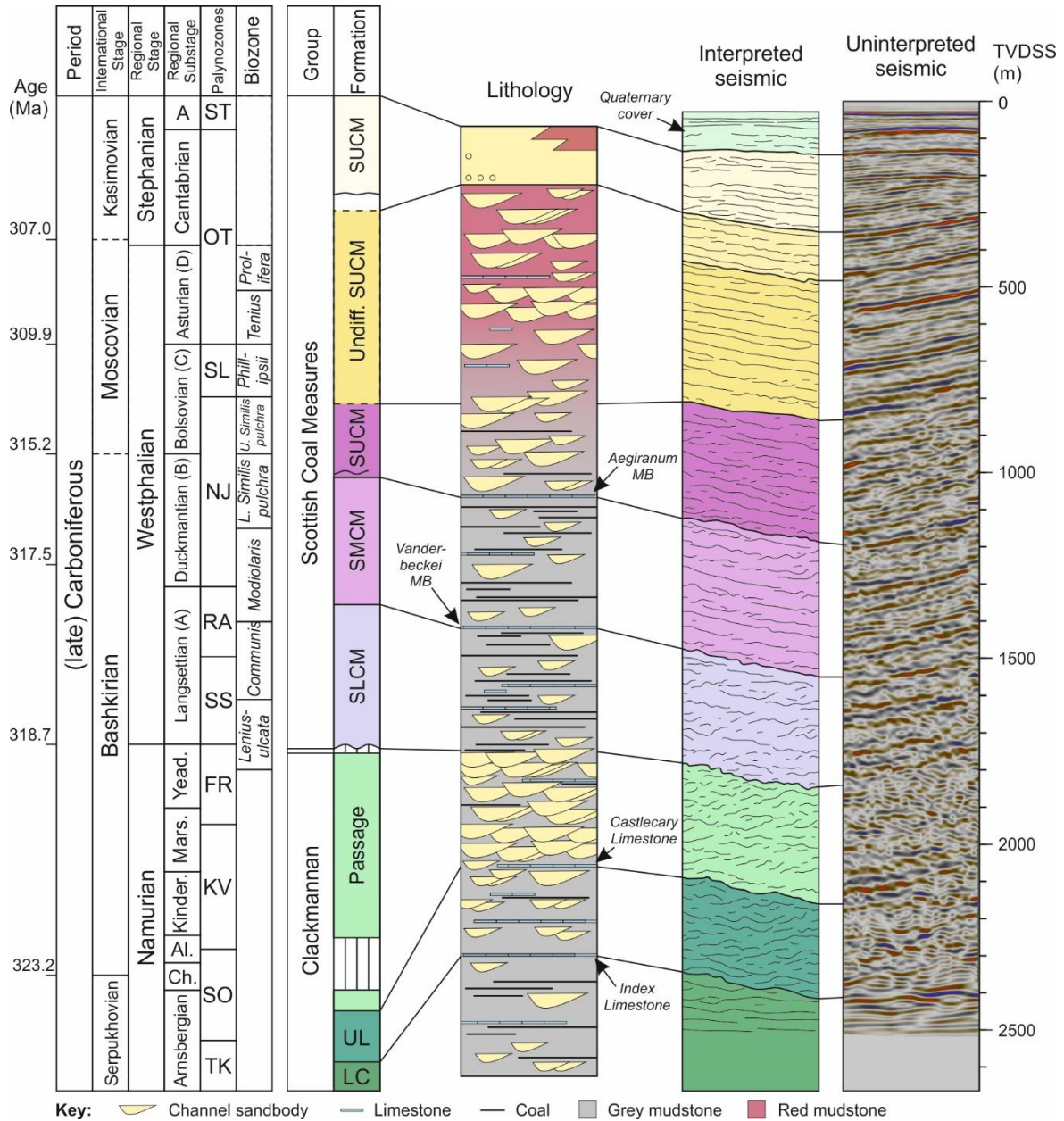
Figure 8.1: General vertical sections for the late Carboniferous succession of the Fife–Midlothian Coalfields and the Firth of Forth. Lithological and seismo-stratigraphic interpretations are based on the work done as part of this study.

8.3 Data and methods

Location maps for the data acquired as part of this study are presented in Figures 8.2 and 8.3. A 2D UK Coal Authority seismic survey acquired between 1979 and 1988 over the Firth of Forth is interpreted. The seismic data used as part of this study are curated by the UK Onshore Geophysical Library (UKOGL) and can be viewed uninterpreted and for free via their website (ukogl.org.uk). Like the seismic data described from the Canonbie Coalfield, Coal Authority seismic data from the Firth of Forth was acquired at a higher frequency. Seismic responses to the shallowest Carboniferous succession are higher resolution with respect to Oil and Gas Authority data, therefore. Strong simple and peg-leg seabed and sea surface multiples destructively interfere with shallow, <100 ms, bedrock seismic responses. To determine localised areas of uplift and accelerated subsidence, a series of isochron thickness maps for the study area have been constructed. To prove the validity of the seismic interpretations provided in this chapter, a series of sequential 2D cross-section restorations were performed using Petroleum Expert's MOVE structural modelling software.

Several outcrop exposures along the northern and southern coastlines of the Firth of Forth were logged using traditional sedimentary logging techniques (Fig. 8.3). Palaeocurrent dip direction measurements were taken to augment sedimentary logging. Outcrop data were recorded at Port Seton and Prestonpans and provide localised constraints on the characteristics of mid-late Namurian and early Westphalian sedimentary basin fill. Together, these localities provide virtually uninterrupted transects through stratigraphy, vertically, over 500 m. More detailed descriptions of these localities are given by Whitbread *et al.* (2015). Due to the overall limited exposure of youngest Carboniferous basin fill, outcrop data are augmented further by recording descriptions from various offshore borehole reports and illustrating these descriptions in sedimentary log format. Borehole data were also used to help constrain interpretations of offshore 2D seismic reflection profiles and are curated online by the British Geological Survey (BGS) or are available in a limited number of past publications (e.g., Ewing and Francis, 1960; Underhill *et al.*, 2008) (also see Table 8.1).
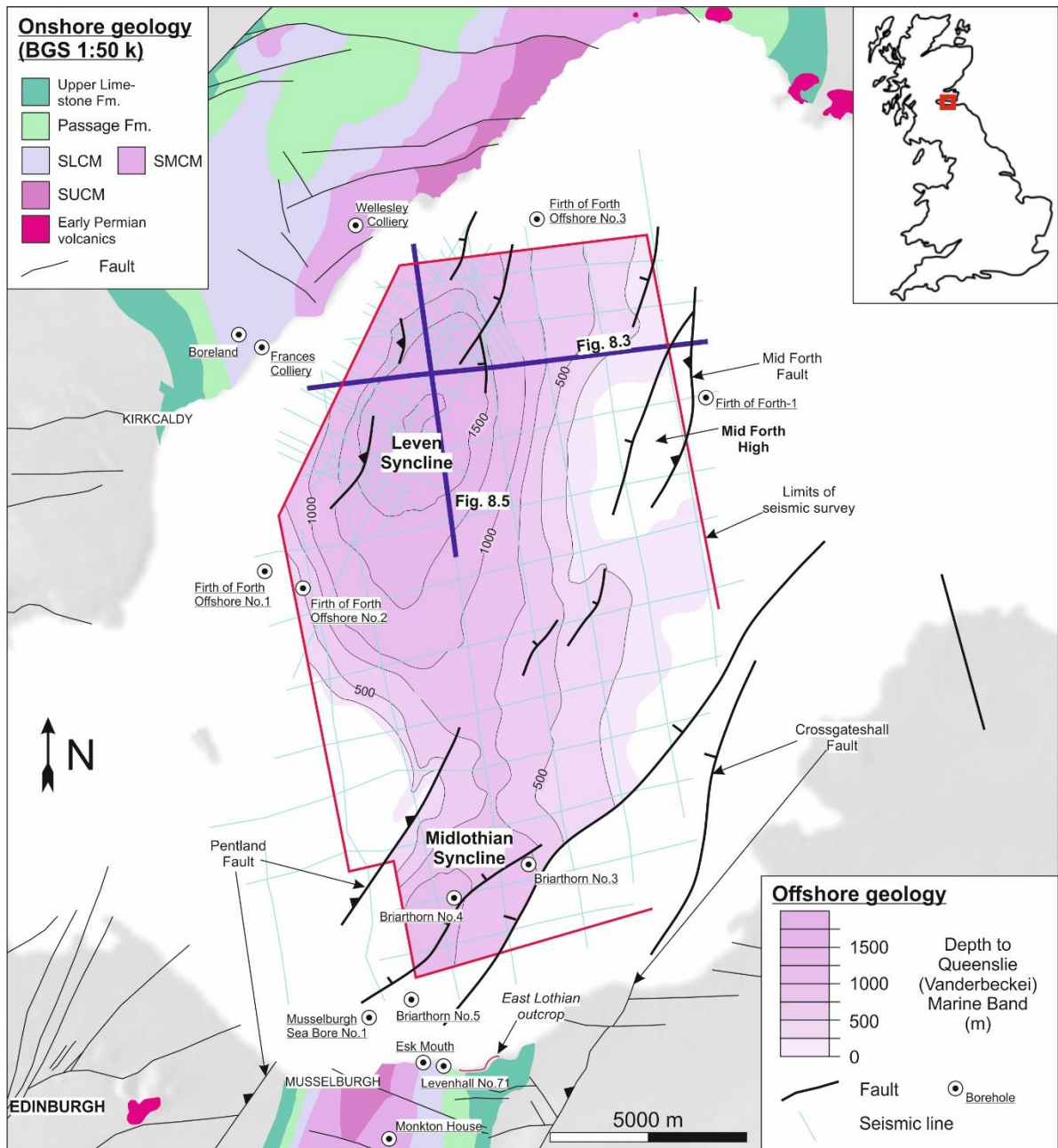
Figure 8.2: A location map for the study area described in this chapter. Borehole, outcrop, and seismic line locations are annotated along with key structures, such as the Leven and Midlothian synclines. Late Carboniferous successions at the Frances and Wellesley collieries are based on multiple boreholes at these locations (*cf.* Ewing and Francis, 1960). Contains BGS DiGmapGB-250 Scale data © UKRI (British Geological Survey, 2008). Terrane image modified after maps-for-free.com/.
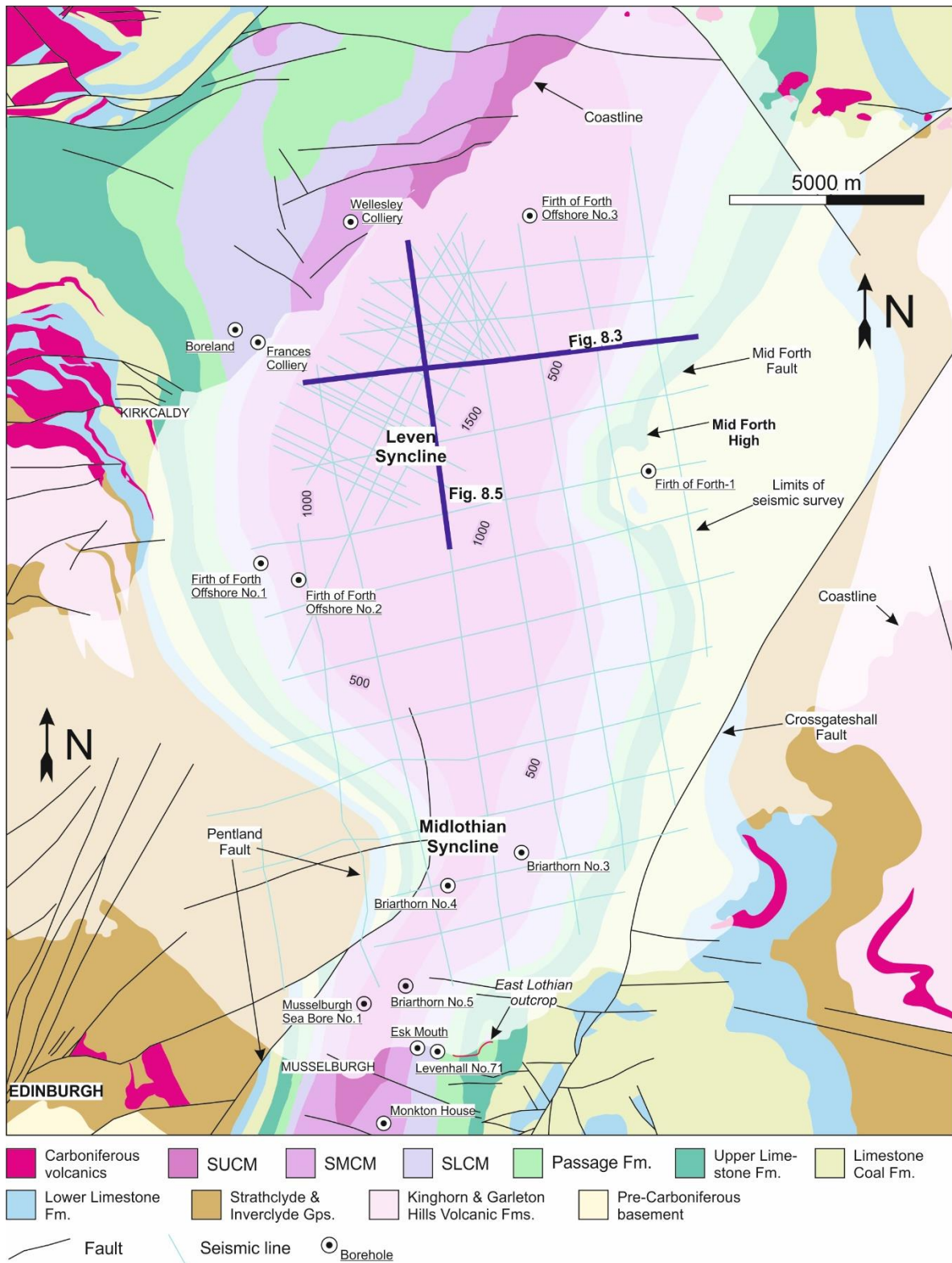
Figure 8.3: Combined onshore geological map and Quaternary subcrop map for the study area. Contains BGS DiGmapGB-250 Scale data © UKRI (British Geological Survey, 2008). Also see Underhill *et al.* (2008).

Borehole name	BGS reference	Easting (BNG)	Northing (BNG)	Year drilled	Derivation (web link)
Boreland	NT39SW44	330394	694222	1939	scans.bgs.ac.uk/ Ewing and Francis (1960)
Briarthorn No.2	NT37NE47	335870	676801	1975	scans.bgs.ac.uk/ Unpublished Coal Authority report
Briarthorn No.3	NT37NE48	337403	678448	1975	scans.bgs.ac.uk/ Unpublished Coal Authority report
Briarthorn No.4	NT37NE49	335700	678210	1975	scans.bgs.ac.uk/ Unpublished Coal Authority report
Briarthorn No.5	NT37NE50	335060	676483	1975	scans.bgs.ac.uk/ Unpublished Coal Authority report
Esk Mouth	NT37SW31	334530	673320	1956	scans.bgs.ac.uk/ Unpublished Coal Authority report
Firth of Forth-1	NT49SW1	342978	692116	1990	ukogl.org.uk/ Underhill *et al.* (2008)
Firth of Forth Offshore No.1	NT38NW1	330024	687894	1955	scans.bgs.ac.uk/ Ewing and Francis (1960)
Firth of Forth Offshore No.2	NT38NW2	331563	687394	1956	scans.bgs.ac.uk/ Ewing and Francis (1960)
Firth of Forth Offshore No.3	NT39NE43	339617	698271	1957	scans.bgs.ac.uk/ Ewing and Francis (1960)
Frances Colliery	-	-	-	-	Ewing and Francis (1960)
Levenhall No.71	-	-	-	-	Unpublished Coal Authority report
Monkton House	-	-	-	-	Unpublished Coal Authority report
Musselburgh Sea Bore No.1	NT37NW2	334054	676058	1958	scans.bgs.ac.uk/ Unpublished Coal Authority report
Shiells	NT26SE157	327890	660920	1982	scans.bgs.ac.uk/

					Unpublished Coal Authority report
Wellesley Colliery	-	-	-	-	Ewing and Francis (1960)

Table 8.1: Borehole data with derivation and web links.

8.4 Seismo-stratigraphic interpretation and depth conversion

The high amplitude seabed and rockhead reflectors, the upper and lower boundary of the Quaternary-aged deposits in the Forth Estuary, represent the two simplest mappable seismic horizons of the seismic survey (Fig. 8.1). Reflectors representing the underlying Carboniferous stratigraphy are typically truncated beneath these shallowest reflectors. The seismic response of the Scottish Coal Measures Group varies widely, perhaps reflecting the thickness and lateral persistency of inter-bedded sandstones or coal seams. Compared with the Central Coalfield, in the central part of the MVS, the late Carboniferous succession here is not so segmented by post-Carboniferous normal-oblique faulting (*cf.* Rippon *et al.*, 1996). Therefore, key intra-Carboniferous seismic horizons may be traced largely uninterruptedly across much of the study area. A network of (mostly) early Permian igneous intrusions locally disturb the seismic responses of the Carboniferous sequence. The mixed volcaniclastic-sedimentary early Carboniferous sequence is comparatively chaotic in seismic and obscures any responses of the local Devonian succession or the Caledonian basement.

Bulk sonic velocities of 1500 m s^{-1} and 2500 m s^{-1} were used for the water column and Quaternary-aged deposits, respectively, based on geophysical data from the Firth of Forth-1 oil exploration borehole drilled by Conoco in 1990. Checkshot data from this borehole also helps to constrain initial (twtt) interpretations of the early and middle Carboniferous succession. This study does not benefit from geophysical logs penetrating the youngest late Carboniferous sediments of the Forth Estuary. Bulk sonic velocities of 3650 m s^{-1} for these sediments were used for the time-depth conversion process, based on predicted seismic velocities for the late Carboniferous stratigraphy of the MVS presented by Conway *et al.* (1987) and Dentith and Hall (1990) (*cf.* Ritchie *et al.*, 2003). Although uncertainty surrounding the time-depth conversion process is acknowledged, the velocity model is deemed adequate for the purposes of the structural interpretation reported in this chapter.
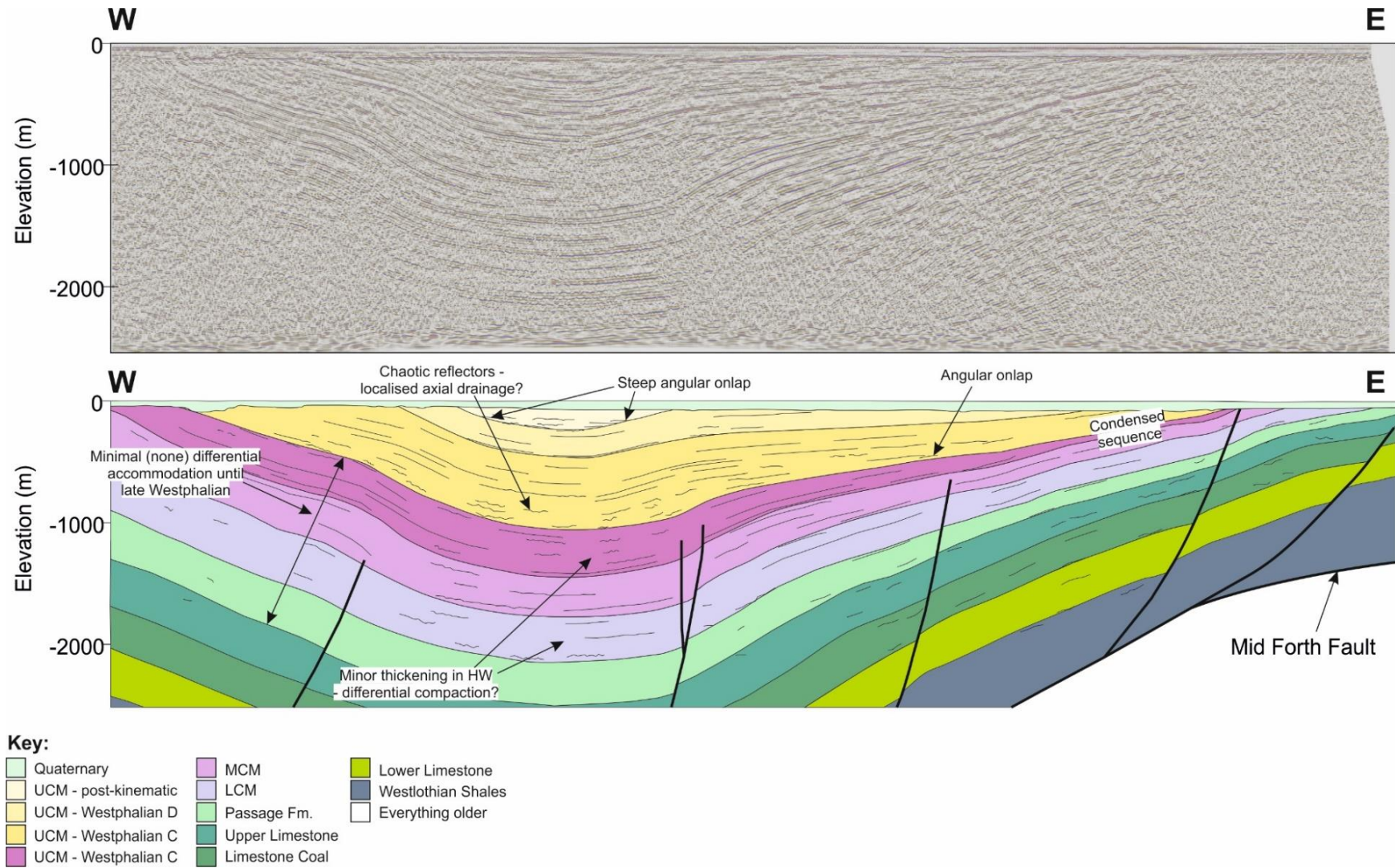
Figure 8.4: Uninterpreted and interpreted E-W seismic reflection profiles through the Leven Syncline. For 2D seismic line location, refer to Figure 8.2.

Stratigraphic data derived from borehole reports was used to better constrain structural interpretations of the depth converted seismic survey.

8.5 Subsurface structure of the MVS

The Leven and Midlothian synclines form two broad and approximately NNE-trending elongate troughs that merge in the centre of the Firth of Forth, approximately 2 km NE of Edinburgh (Fig. 8.2). Whereas in the central part of the MVS and around the areas of Glasgow and the Kincardine sub-basin, an en-échelon set of ENE- and ESE-trending, steeply dipping and normally displacing faults dominate the local structural fabric, in this study area, evidence of these fault trends is largely restricted to onshore Fife and within few stratigraphically interrupted borehole successions. In the Firth of Forth, the dominant north-easterly trend of more shallowly (>45 °) westwards dipping faults is partially obscured beneath Quaternary-aged deposits and a thick (>1 km-thick in places) sedimentary succession belonging to the Scottish Coal Measures Group (Fig. 8.4). Some of these faults crop out to the SW in West Lothian and Midlothian and merge with the SUFZ further to the south-west. Together, these faults rotate anticlockwise by approximately 5-10 ° along strike towards the north-east. In both the onshore and offshore areas, many of these faults vary between reverse and normally displacing along strike. The Pentland Fault, for example, juxtaposes Silurian-Early Devonian-aged basement rock in its hangingwall against Namurian-aged strata in its footwall at outcrop and to the south-west of Edinburgh. In the Firth of Forth, this same fault appears less prominent and displaces middle-late Carboniferous strata in a normal sense before it pinches out in the middle of the firth and overlaps with the locally reverse-displacing Mid Forth Fault.

8.6 Late Carboniferous seismo-stratigraphic analysis

Based on shared sedimentological characteristics, approximately intervening phases of syn-depositional deformation, and regionally correlative upper- and lower-unit boundaries, the late Carboniferous succession of the eastern MVS is described as discrete tectonostratigraphic units. These units comprise the (middle-late) Namurian Upper Limestone and Passage formations, the

Langsettian to Duckmantian (Westphalian A-B) SLCM and SMCM formations, a Bolsovian to Asturian (Westphalian C-D) unit that belongs to the (lower) SUCM Formation, and a latest Asturian to Stephanian (?) unit that belongs to the (uppermost) SUCM Formation.

The base of the Upper Limestone Formation is defined by the base of the Index Limestone (Waters *et al.*, 2007), while the base of the SCM Group and SLCM Formation is imperfectly defined by the first appearance of marine fauna beneath the coal-bearing strata of the SCM Group (MacGregor, 1960). The base of the SUCM Formation is defined more clearly by the fossiliferous Vanderbeckei Marine Band (Ramsbottom, 1979). Unfortunately, the base of the youngest late Carboniferous (uppermost) SUCM Formation tectonostratigraphic unit in this study area appears not to crop out onshore anywhere within the study area. Instead, the base of this unit is defined by a marked angular and probably erosive unconformity interpreted from seismic reflection profiles within the trough of the Leven Syncline.

8.6.1 Middle to late Namurian

The Upper Limestone and Passage formations in the Firth of Forth displays broad overall eastwards thinning (Fig. 8.4). Thickness variations associated with the Midlothian Syncline are more extreme than those associated with the Leven Syncline. Along the eastern limb of the Midlothian Syncline, the Passage Formation is less than 150 m thick. Along the western limit of the study area and along the Leven Syncline's western limb, this same unit is approximately 500 m thick (Fig. 8.5). Some other minor thickness variations are observed within the hangingwalls of steeply dipping and mostly deeply buried (>2 km) normal faults. Minor downcutting reflector geometries are observed in both the typically more mixed clastic-carbonate succession of the Upper Limestone Formation and the dominantly fluvial Passage Formation; this geometry is observed more so along the more shallowly buried successions preserved within the eastern limbs of the Midlothian and Leven synclines.
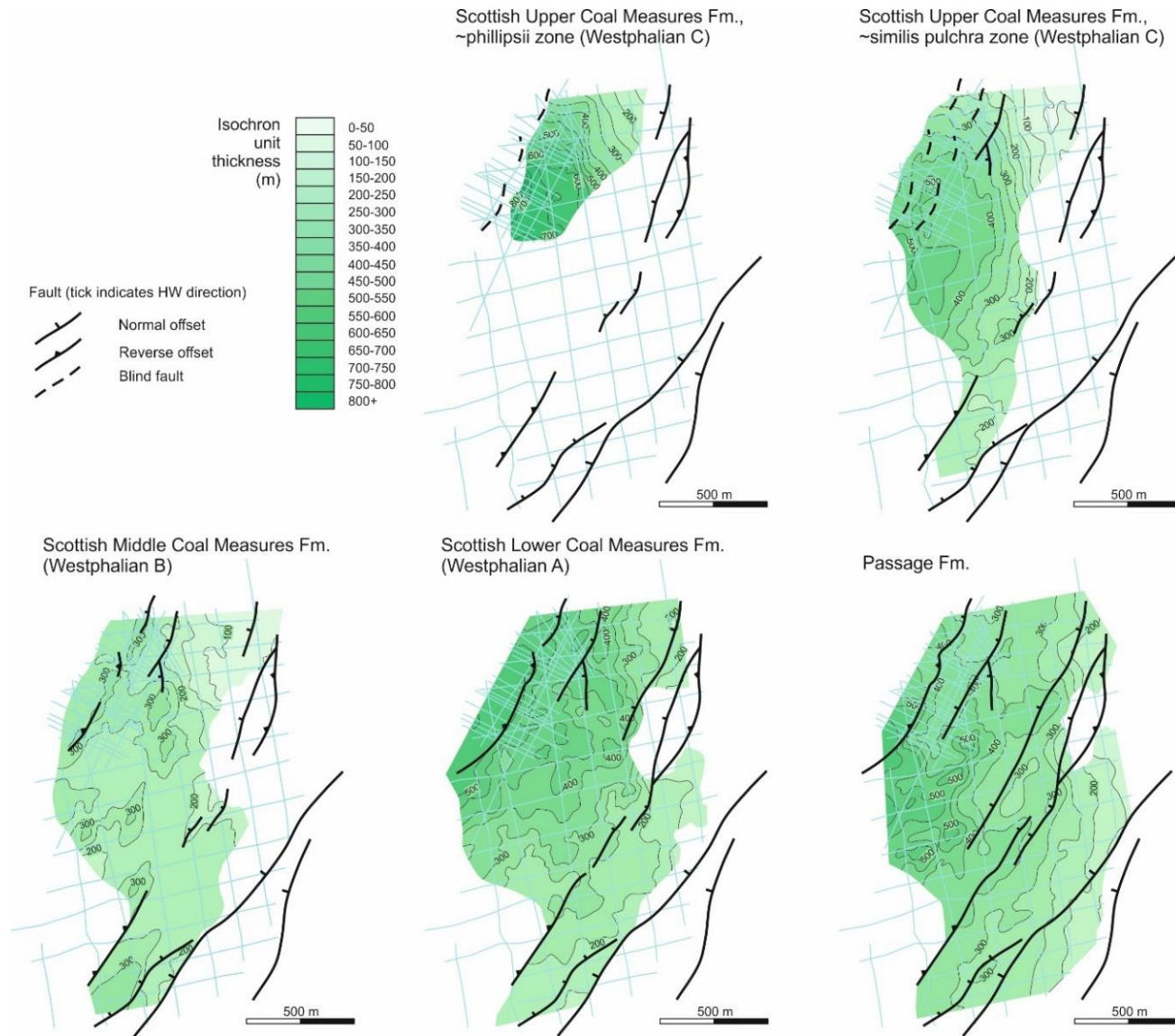
Figure 8.5: Depth-thickness (isochron) maps for the late Carboniferous succession of the MVS, based on the interpretation of 2D seismic data within the Firth of Forth.

156

8.6.2 Langsettian to Duckmantian

Deposition of the uppermost Passage Formation appears to have occurred more evenly across this eastern part of the MVS, relative to the immediately underlying succession. Similarly, seismic interpretations indicate more evenly distributed thicknesses for the Langsettian SLCM Formation. Towards the top of the Duckmantian SMCM Formation here, some of the continuous and more widely spaced reflectors that help define this unit in seismic profile merge, interfere and eventually becoming unresolvable progressively further up the eastern limb of the Leven Syncline (Fig. 8.4). A thickness map for the SMCM Formation shows a comparatively condensed succession to the NNE and along strike from the Mid Forth High Anticline – less than 50 m thick compared with over 300 m within the trough of the Leven Syncline (Fig. 8.5). A stratigraphically equivalent succession to the south of the Leven Syncline and beyond the trough of the Midlothian Syncline is absent due to erosion.

8.7.3 Duckmantian to Asturian

Overall thickness trends associated with the upper part of the SMCM Formation appear to represent more subdued forms of thickness trends associated with immediately overlying sediments belonging to the lower part of the SUCM Formation. The (lower) Bolsovian part of the SUCM Formation, which is characterised by non-marine bivalves belonging to the (upper) *similis pulchra* biozone, is largely absent above the condensed upper part of the SMCM Formation along the flanks of the Mid Forth High Anticline and the eastern part of East Fife (*cf.* Calver in Ewing and Francis, 1960). The thickness map for this interval indicates an equivalent succession that is over 500 m thick along the trough of the Leven Syncline (Fig. 8.5). A pronounced surface of onlap is observed in seismic along the eastern limb of the Leven Syncline, several tens of metres above the lower boundary of the *phillipsii* biozone (Fig. 8.4). Here, sets of semi-continuous and bright reflectors onlap against and overstep more continuous yet similarly bright reflectors. The bright and semi-continuous reflectors along the flanks of the Leven Syncline become characteristically chaotic within the trough of the same structure. A completely preserved late Bolsovian succession is present only within the trough of the Leven Syncline. The onlapping nature of reflectors representing these

strata suggests that at least for the lower part of this succession, thickness trends may have been like those associated with the lower Bolsovian succession prior to later denudation. Where they remain preserved, the immediately overlying sediments, which also belong to the SUCM Formation and contain fauna belonging to the uppermost (late Bolsovian) *phillipsii* biozone, appear to have been deposited more evenly again. The bright, continuous, and mostly evenly spaced Asturian reflectors suggest that these sediments too were deposited relatively evenly across the study area.

8.7.4 Latest Asturian to Stephanian

In seismic, approximately 250 m above the base of the Asturian and within the innermost trough of the Leven Syncline, a major onlapping discontinuity is observed separating reflectors that (presumably) represent part of the Asturian succession from the immediately overlying reflectors (Fig. 8.6). The subcrop of this discontinuity beneath Quaternary-aged sediments may be mapped around the innermost trough of the Leven Syncline but does not crop out onshore at any point. In the Firth of Forth, the onlapping and uppermost reflectors are mostly flat-lying and could be mistaken for seabed or sea surface multiples as a result. However, these onlapping reflectors that represent concealed late Carboniferous strata are comparatively hummocky and sometimes chaotic. Whereas the earlier seismic discontinuities described are largely restricted to the eastern limbs of the Midlothian-Leven synclines, this shallowest discontinuity is observed clearly along the western limb of the Leven Syncline also, and around the entirety of the Leven Syncline trough. At least one further onlapping discontinuity is observed within this latest Carboniferous seismic volume.

8.9 Facies, architectural elements, and facies associations

Based on traditional sedimentary logging, the late Carboniferous successions of the eastern part of the MVS is divided into distinct lithofacies, architectural elements and broad facies associations. For lithofacies and architectural element descriptions, the reader should refer to Tables 8.1 and 8.2, and Figure 8.7. Where sedimentary logs have been drawn from archived borehole descriptions and local mining terminologies were used to describe sedimentary facies; these terminologies are included in the lithofacies table (Table 8.2). Here four broad facies associations are described and interpreted.
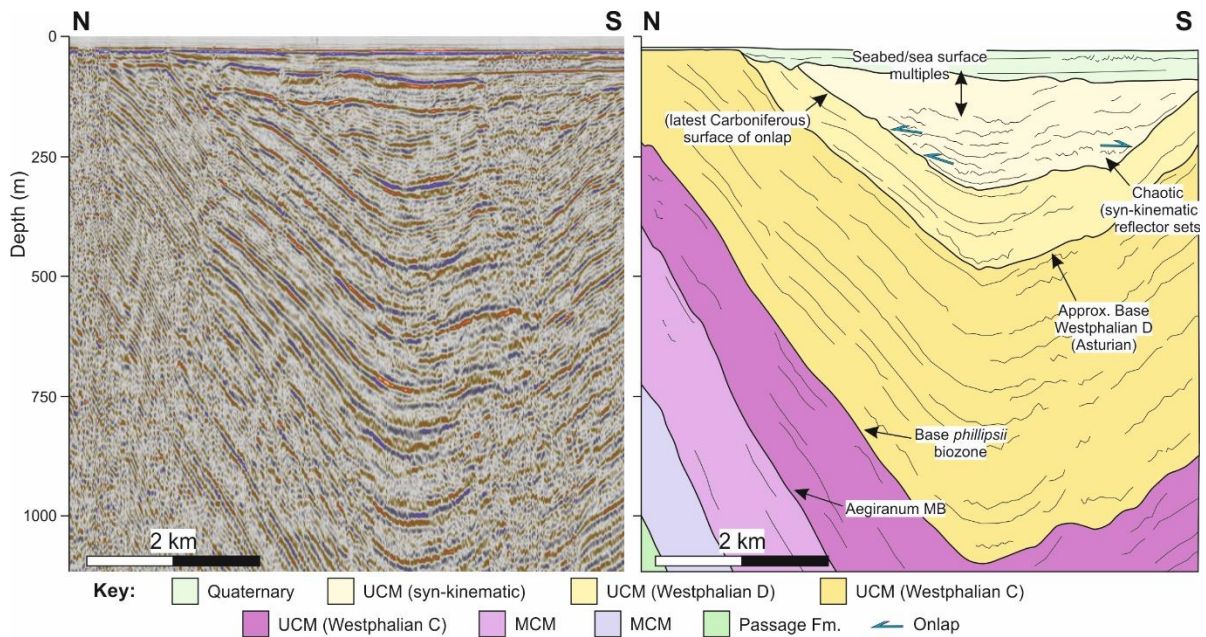
Figure 8.6: A N-S seismic reflection profile approximately parallel with the Leven Syncline, depicting a remarkable intra-formational (SUCM) Stephanian (?) angular unconformity. For seismic reflection profile location, refer to Figure 8.2.

8.9.1 Terrestrial floodplain deposits (FA 1)

Description

Terrestrial floodplain deposits (FA 1) comprise two architectural elements: floodplain (FP) and palaeosol (P). Floodplain facies are frequently buried beneath Quaternary beach sediments along coastal exposures and are rarely exposed inland. These deposits are observed most clearly when capping thick and mechanically resistive fluvial bar and channel deposits and deltaic deposits. Here, floodplain elements are dominated by parallel- to ripple-laminated very fine-grained sandstones, siltstones and mudstones, typically referred to as fakes in borehole reports. These are often heavily bioturbated and typically contain pedogenic lithofacies, plant debris and minor coal fragments. Palaeosols vary from dark grey to black in situ coals to nodular (sideritic) siltstones, and well-defined, variably calcified, structureless and entirely sideritic banded siltstones. Red-deep purple 'mottled' floodplain sediments dominate progressively upwards within the succession, according to infrequent borehole reports.

Inter-bedded siltstone to fine-grained sandstone floodplain elements are interpreted as having been deposited in waning stage flow environments (Miall, 1988). The thickest mudstone beds are believed to represent the settling of fines in near stationary bodies of water or perennial lakes (Porter and Gallois, 2008). Development of pedogenesis contemporary with deposition is governed by local behaviour of the water table (Besly and Fielding, 1989). Coaliferous pedogenic facies within the floodplain provide evidence of cohesive, vegetated overbank material with permanently waterlogged soils and overall humid conditions (Kraus *et al.*, 1999). Reddening may signify oxidisation shortly following deposition due to a deeper water table and subaerial exposure within a well-drained floodplain (Besly *et al.*, 1993). The occurrence of sideritic nodules could represent freshwater conditions (Besly and Turner, 1983), whereas locally deeper water tables may be a response to differential subsidence or a more arid climate (Besly and Fielding, 1989). More persistent (deeper) reddening and calcification may represent more prolonged subaerial exposure, perhaps due to uplift (Mykura, 1967).

8.9.2 Fluvial bar and channel deposits (FA 2)

Description

Fluvial bar and channel deposits (FA 2) comprise three architectural elements: fluvial channels (FC), sheets (S), and fluvial accretionary bar forms (FB). Locally, fluvial channels are stacked and amalgamated with minor conglomerates throughout and generally show a progressive fining upwards fill. Most channels are dominated by planar or trough cross-bedded sandstones. Few fluvial channel sands are structureless and most are capped by heterolithics containing terrestrial plant debris. Sheet-like elements make up a very small proportion of the association and are dominated by structureless to parallel-laminated sandstone. Fluvial accretionary bar forms have lensoidal geometries with internal second and third order bounding surfaces.

Code	Lithology & texture	Structure & other features	Interpretation	Scottish coal mining term
Fb	Grey to dark grey, carbonaceous siltstone.	Structureless to crudely parallel-laminated frequent bioturbation and sporadic wood/plant fragments/coal.	Suspension fall out from stationary waters. Stabilization for vegetation to develop and pedogenesis removing any of the lamination.	Blaes, Cashy blaes
Fm	Dark grey, carbonaceous mudstone to siltstone.	Structureless with frequent plant debris.	Suspension fall out from stationary waters. Stabilization for vegetation to develop and pedogensis removing any of the lamination.	Blaes, Dirt?
Fpl	Grey to dark grey siltstone.	Parallel-laminated.	Suspension fall out from stationary waters.	Blaes
Gm	Grey, granule to pebble sized, poorly sorted, sub-rounded to sub-angular, clast supported conglomerate.	Structureless.	Sub-aqueous, high energy Newtonian flow under high sediment load conditions, with suppressed bedform development.	Channel
Gt	Grey, granule to pebble sized, poorly sorted, sub-angular to angular, clast supported conglomerate.	Trough cross-bedded.	Sub-aqueous lower flow regime conditions with high sediment load, intermittent development and migration of dune-forms.	Channel
Lc	Light grey, sparitic limestone.	Structureless.	Sub-aqueous precipitation and crystallisation of carbonate.	Limestone
Lm	Grey to dark grey, carbonate mudstone to wackestone.	Fossiliferous laminations with frequent Ostracods, shell and Crinoid fragments.	Sub-aqueous reworking of allochthonous carbonate	Limestone, Lime craig

Pc	Black, bituminous to anthracitic coal.	Thinly laminated or massive. Disseminated pyrite nodules.	Organic (plant and tree) growth and development of organic hydromorphic soils, upon completely water-saturated floodplain or in swamps and shallow pools.	Coal
Ph	Grey to dark grey siltstone with large (<50 cm) rusty brown nodules.	Structureless to crudely laminated with occasional siderite or other carbonate nodules, plant debris and root traces.	Suspension fall out from near stationary waters. Stabilization for vegetation and reduced ('true') hydromorphic soils to develop.	Blaes and balls, Doggar
Pd	Rusty brown-red, sideritic or hematized siltstone.	Structureless to faintly laminated or banded. Horizontal zonation with upper brown/ochre mottled unit.	Suspension fall out from near stationary waters. Stabilization for vegetation and partially to well-drained soils to develop. Weathering and complete alteration of siltstone above water table.	Ironstone
Sf	Grey siltstone to fine-grained, poorly sorted, sub-rounded sandstone.	Flaser laminations with sporadic roots and variable bioturbation.	Alternation between oscillatory and unidirectional currents with periods of slack water.	Fakes
Sgt	Grey, medium to coarse-grained, poorly sorted, sub-angular sandstone with gravel grade clasts.	Gravel lined planar cross-bedding.	Sub-aqueous lower flow regime conditions with high sediment load, intermittent development and migration of dune-forms.	Sandstone (flaggy), Ragstone, Rock
Sh	Light grey to dark grey mudstone to fine-grained, sub-rounded sandstone with bimodal sorting.	Heterolithic bedding with occasional soft sediment deformation.	Oscillatory and unidirectional currents with rapidly fluctuating energy conditions.	Fakes
Sl	Light grey to grey, siltstone to fine-grained, sub-rounded	Lenticular lamination.	Alternation between oscillatory and	Fakes

	sandstone, with bimodal sorting.		unidirectional currents with periods of slack water.	
Sla	Light grey, very fine to fine-grained, moderate to well sorted, sub-rounded sandstone.	Parallel-laminated.	Sub-aqueous aggrading upper flow regime flat beds.	Sandstone (flaggy)
Sm	Light grey to grey, medium to coarse-grained, moderate to well sorted, sub-rounded sandstone.	Structureless.	Rapid deposition in high sediment load suppressing bedform development.	Freestone
Sp	Light grey to grey, very fine to medium-grained, moderately sorted, sub-rounded sandstone.	Planar cross-bedded.	Migration of straight-crested dune-scale bedforms and dune trains sub-aqueously under lower flow regime conditions.	Sandstone (flaggy), Rock
Sr	Light grey to grey, very fine to fine-grained, moderately sorted, sub-rounded sandstone.	Asymmetrical ripple-laminated.	Migration of ripple-scale bedforms in lower flow regime.	Sandstone (flaggy)
St	Light grey, fine to coarse-grained, moderately sorted, sub-rounded sandstone.	Trough cross-bedded with sporadic slumping.	Migration of sinuous-crested dune-scale bedforms and dune trains sub-aqueously under lower flow regime conditions.	Sandstone (flaggy), Rock

Table 8.2: Lithofacies scheme for late Carboniferous stratigraphy of the MVS. Scotch mining lithofacies names taken from Barrowman (1886).

Interpretation

This association represents the development and build-up of a fluvial channel belt in a bedload dominant fluvial system (*cf.* McAdams *et al.*, 1985). The progressively fining upward fill of the channels is interpreted as the gradual abandonment of channels with a steady rate of flow (Bromley, 1991), with the basal conglomeratic units representing channel lag deposits formed from bedload transport within high-energy flows (Bridge 1993; Fielding *et al.*, 2018). The heterolithic

channel elements represent channel abandonment (Martin & Turner, 1998). Accretionary bar form elements can be interpreted as bank-attached point bars/macroforms deposited on the inside of the channel bend (Miall, 1988), or as the deposits of mid-channel bars within the channel belt (Miall, 1985; Ashworth *et al.*, 2000).

8.9.3 Deltaic deposits (FA 3)

Description

Deltaic deposits (FA 3) comprise five architectural elements: delta top distributary channel (DC), delta front bar (DB), delta slope (DS) and inter-distributary bay (IB). Coarsening upwards successions of pro-delta sediments through to delta top distributary channels dominate this association. Delta slope elements coarsen upwards and are dominantly composed of parallel-laminated siltstone with minor sandstone lenses that increase in abundance upwards through the association. The delta front bars have lensoidal geometries and are dominantly composed of coarsening upwards successions of planar cross-bedded sandstones with flaser to lenticular sandstones and siltstones, which are sporadically bioturbated. The delta top distributary channels typically have erosional basal bounding surfaces and progressively fining upwards fills. The channels are dominated by planar and trough cross-bedded sandstones with minor conglomeratic foresets. Inter-distributary bay facies are typically darker grey and more heavily bioturbated siltstones that separate coarser-grained delta top distributary channels and delta bar forms.

Interpretation

This dominantly coarsening upwards association represents the progradation of deltaic deposits into a marginal marine environment (Mount, 1984). Siltstones are likely to have been deposited through suspension settling away from the sediment source (Stow and Shanmugam, 1980), whilst inter-bedded parallel and ripple-laminated sandstones are likely to have been transported from up-dip deltaic systems (Blair and McPherson, 2008). The presence of lenticular and flaser bedding suggests a somewhat oscillating current during deposition (Reineck and Wunderlich, 1968). Cross-bedded sandstones indicate the deposition of channel fill material, as

dune-scale bedform trains fill distributary channels (Bristow *et al.*, 1993). Inter-distributary bay sedimentation is dominated by flood-generated incursions from adjacent distributaries (Elliot, 1976).

8.9.4 Pro-delta deposits (FA 4)

Description

Pro-delta deposits (FA 4) consist of pro-delta floor (PD) facies and carbonate-dominated delta front (L) facies. Carbonate-dominated delta front facies typically overlay a thin (<3 cm) mudstone, which overlays shallower water associations. Variably fossiliferous carbonate-dominated delta front wackestones and micritic limestones are typically laterally persistent and thickest at the base of the succession, before they incorporate increasing amounts of inter-bedded calcareous mudstones and siltstones upwards within the succession. Locally, fossiliferous assemblages comprise both *Lingula*, and *Naiadites* and *Curvirimula*. Infrequent borehole penetrations report inter-bedded *Spirorbis* limestones within the youngest and mostly concealed parts of the succession. Pro-delta mudstones and siltstones are typically interbedded with sporadic carbonate lenses and nodules, and with thin sandstone lenses that increase in frequency upwards. The siltstones are typically weakly bioturbated by mostly vertical burrows.

Interpretation

Variably thick and well-formed limestones and carbonate lenses within the parallel-laminated siltstones suggest periods of temporarily low clastic supply accommodating the production of carbonate in shallow water (Mount, 1984). Given the presence of these beds immediately above much shallower water associations, their occurrence is suggested to partly indicate contemporaneous high amplitude eustatic sea level transgressions (e.g Saunders and Ramsbottom, 1986). The presence of *Lingula* and type of bioturbation suggests deposition in dominantly shallow marine conditions, whereas closely inter-bedded *Naiadites* and *Curvirimula* assemblages suggest regular fluctuations in salinity and marine restriction (Read and Forsyth, 1989). *Spirorbis* limestone is believed to signify more freshwater lacustrine conditions during deposition (Jones and Holliday, 2006).

Element	Code	Facies	Description	Facies tract
Fluvial Channel	FC	Gm, Gt, Sgt, St, Sp, Sm, Sh, Sr	'U' shaped, fining upwards association with an erosional basal bounding surface. The association is dominated by planar (Sp) and trough (St) cross-bedded, well-sorted sandstones with minor basal conglomerates.	Fluvial deposits
Sheet	S	Sm, Sla	Tabular, sheet-like, fining upwards association with an erosional basal bounding surface. The association is dominated by structureless (Sm) to parallel-laminated (Sla) sandstones.	Fluvial deposits
Fluvial accretionary barform	FB	Gt, Gm, Sgt, St, Sp, Sr	Lensoidal, fining upwards association dominantly composed of cross-bedded sandstone (St & Sp) with palaeocurrents of accretionary surfaces varying < 120° compared with local palaeoflow.	Fluvial deposits
Palaeosol	P	Pc, Ph, Pd	Typically, stratigraphically thin (> 20 cm) but with well-defined beds of coal (Pc) or pedogenic facies (Ph & Pd).	Fluvial, Terrestrial floodplain and Deltaic deposits
Floodplain	FP	Fpl, C, Fb, Fm, Pg, Pn	Tabular association of structureless (Fm) to parallel-laminated (Fpl) siltstone with minor coal (C) and pedogenic facies (Ps & Pn).	Terrestrial floodplain
Delta Top Distributary Channel	DC	Sgt, Sh, St, Sp, Sr	'U' shaped, fining upwards association with an erosional basal bounding surface. The association is dominated by planar (Sp) and trough (St) cross-bedded sandstones.	Deltaic deposits
Inter-distributary bay	IB	Fb, Fm, Fpl, Sh, Sl, Sr	Typically comprising a collection of small (<2 m) coarsening upwards sequences of parallel- and ripple-laminated siltstones to sandstones (Fpl & Sr).	Deltaic deposits
Delta Front Bar	DB	Sp, Sr, Sl, Sf	Lensoidal, coarsening upwards association dominantly composed of planar cross-bedded sandstones (Sp) with flaser (Sf) to lenticular (Sl) sandstones and siltstones.	Deltaic deposits

Delta Slope	DS	Fpl, Fm, Fb	Lensoidal, coarsening upwards association dominantly composed of parallel-laminated siltstone (Fpl) with minor sandstone lenses.	Deltaic deposits
Pro-delta floor	PD	Fpl, Lc, Lm	Tabular, coarsening upwards association dominantly composed of parallel-laminated siltstone (Fpl) with minor carbonate lenses.	Pro-delta deposits
Carbonate-dominated delta front	L	Lc, Lm	Succession of thin (>1 cm) carbonaceous mudstone (Lm) overlain by tabular and well-defined limestone (Lc) with further inter-bedded carbonaceous mudstones.	Pro-delta deposits

Table 8.3: Architectural elements for late Carboniferous stratigraphy of the MVS.

8.10 Late Carboniferous sedimentology

8.10.1 Middle to late Namurian

At low tide, the East Lothian coastline exposes a near complete, approximately 500 m, succession of Upper Limestone Formation and Passage formation strata (Figs. 8.8 and 8.9). The base of the Upper Limestone Formation is marked clearly by the approximately 1.7 m thick Index Limestone at Prestonpans. Locally, the Index Limestone appears to rest immediately above a low angle but distinctly angular and truncating unconformity (Fig. 8.10a). The underlying and truncated delta slope deposits (DS) yield a distinctly marine fossiliferous assemblage, are heavily bioturbated and, where unaltered, comprise mostly flaser or lenticular ripple-laminated siltstone and fine-grained sandstone. Above its base, the Upper Limestone Formation is characterised by numerous shallowing up sequences of which pro-delta associations appear to comprise approximately 25 % across East Lothian, although finer-grained deposits are more likely to be obscured beneath beach sediment. Downcutting (<1 m) and typically conglomeratic delta top distributary channel (DC) sandstones erode most of the sparsely preserved delta front bar (DB) and delta slope (DS) siltstones and sandstones. Few of the named inter-bedded limestone beds of the region are present at Prestonpans. However, the Orchard and Calmy limestones appear at Port Seton. Numerous thickly stacked (<20 m) amalgamated delta top distributary channel (DC), fluvial channel (FC) and accretionary bar form (FB) sandstones together comprise approximately 50 % of

the Upper Limestone Formation across the two outcrop localities in East Lothian, along the eastern limb of the regional Midlothian syncline. Palaeosols are typically nodular, sideritic and heavily rooted, although there are several remaining unmined inter-bedded coal beds (<50 cm) exposed along the East Lothian coastline.

Figure 8.7: Representative field photographs portraying: a) a partially-drained, banded and sideritic palaeosol (Pd) (*cf.* Besly and Fielding, 1988); b) a 'true' hydromorphic palaeosol (Ph) (*cf.* Besly ad Fielding, 1988) with siderite nodules; c) a coal seam (Pc) overlain by a trough-cross-bedded sandstone (St); d) well-defined and sideritic roots; e) amalgamated trough-cross-bedded sandstones (St); f) Planar and gravelly cross-bedded sandstones (Sgt); g) large (<10 cm) plant debris; h) heavily bioturbated siltstone (Sf); i) a coarsening upwards delta bar (DB) succession; j) asymmetric ripple-laminated sandstone (Sr); k) parallel-laminated siltstone (Fpl) and; l) a fossiliferous limestone (Lm).

The Passage Formation is distinctly more fluvial (Fig. 8.9). Along the East Lothian coastline, stacked and variably conglomeratic fluvial channel (FC) and accretionary bar form (AB) sandstones comprise <75 % of the formation. Inter-bedded pro-delta and deltaic deposits are observed immediately above or below shallowly dipping fluvial channel stacks but are mostly inferred to be buried beneath beach sediments. The stratigraphically correlative No. 5 and No. 6 Marine bands are inferred <100 m to the east of the port at Port Seton and <20 m vertically below the base of the SLCM Formation, where metres of the typically uninterrupted Passage Formation are buried. Moderate bioturbation is not uncommon in some of the finer-grained sediments. However, fossiliferous assemblages are rare. Palaeosols are altogether more oxidised or 'redder' – along the coastline there are several examples of <50 cm-thick, calcified, and banded siderite palaeosol beds (Fig. 8.10d). Heavily rooted horizons and preserved terrestrial plant debris are common here, although plant debris is largely not intact. The style of palaeosols observed in East Lothian contrast markedly from the dominant contemporaneous palaeosol types documented in borehole reports to the north in East Fife, mostly surrounding the trough of the Leven syncline. Here, the overall thicker (<500 m) Passage Formation is inter-bedded sporadically with numerous well-defined and named coal seams (Fig. 8.11).

Based on palaeocurrent measurements, coarser-grained sediments within the Upper Limestone Formation appear to be sourced primarily from northerly and easterly directions (Fig. 8.9). Sandstones sourced from these areas within this formation are typically subarkosic, muscovitic, contain abundant lithic detritus and have distinctively red-brown weathered surfaces consequently. These assemblages differ compared to the overall more quartzitic compositions of less frequent, but typically just as thick (<20 m), sandstone channel stacks sourced from the south and south-west within the Upper Limestone Formation. Similar trends are apparent within the underlying Limestone Coal Formation at Prestonpans. Here, several thick channel stacks display distinctive soft sediment deformation that are interpreted as 'seismites' (e.g., Montenat *et al.*, 2007), due to earthquake-induced ground shaking shortly following deposition (Fig. 8.8). Within the Passage Formation, northerly and north-easterly sourced sediments dominate more so. The distinctive mineralogical assemblages remain. By and large, palaeocurrent features within these strata ranges

from well to poorly dispersed between beds and channel stacks. These data do not appear to align with the dominant NNE structural trend in this part of the MVS. Poor 3D exposure limits additional palaeocurrent measurements and further analysis of these data.
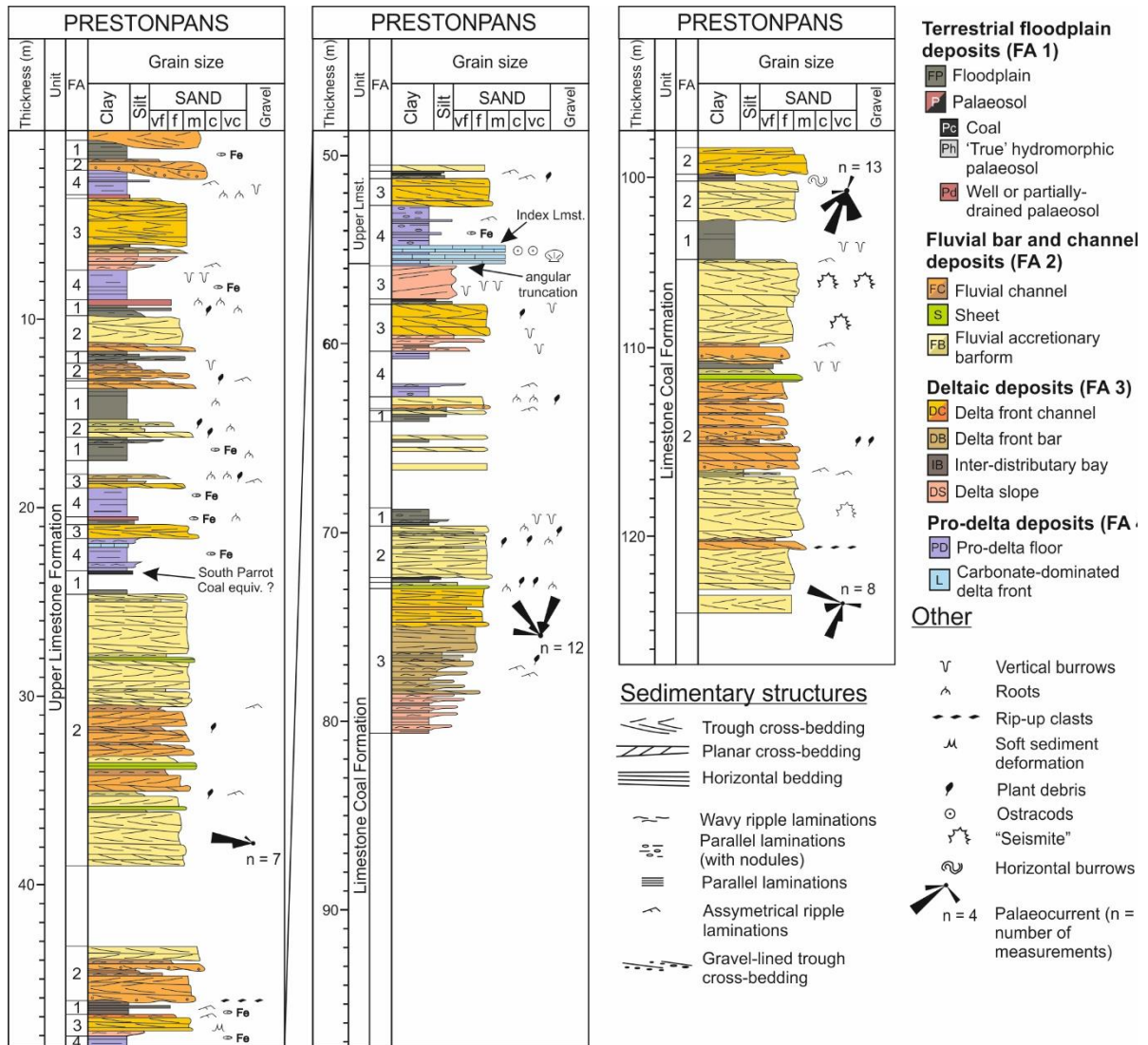
Figure 8.8: A sedimentary log for the Limestone Coal and Upper Limestone formations exposed along the Prestonpans coastline, East Lothian. FA = Facies Association. British National Grid reference: 338063, 674308. For further descriptions of the outcrop locality, the reader may refer to Whitbread *et al.* (2015).
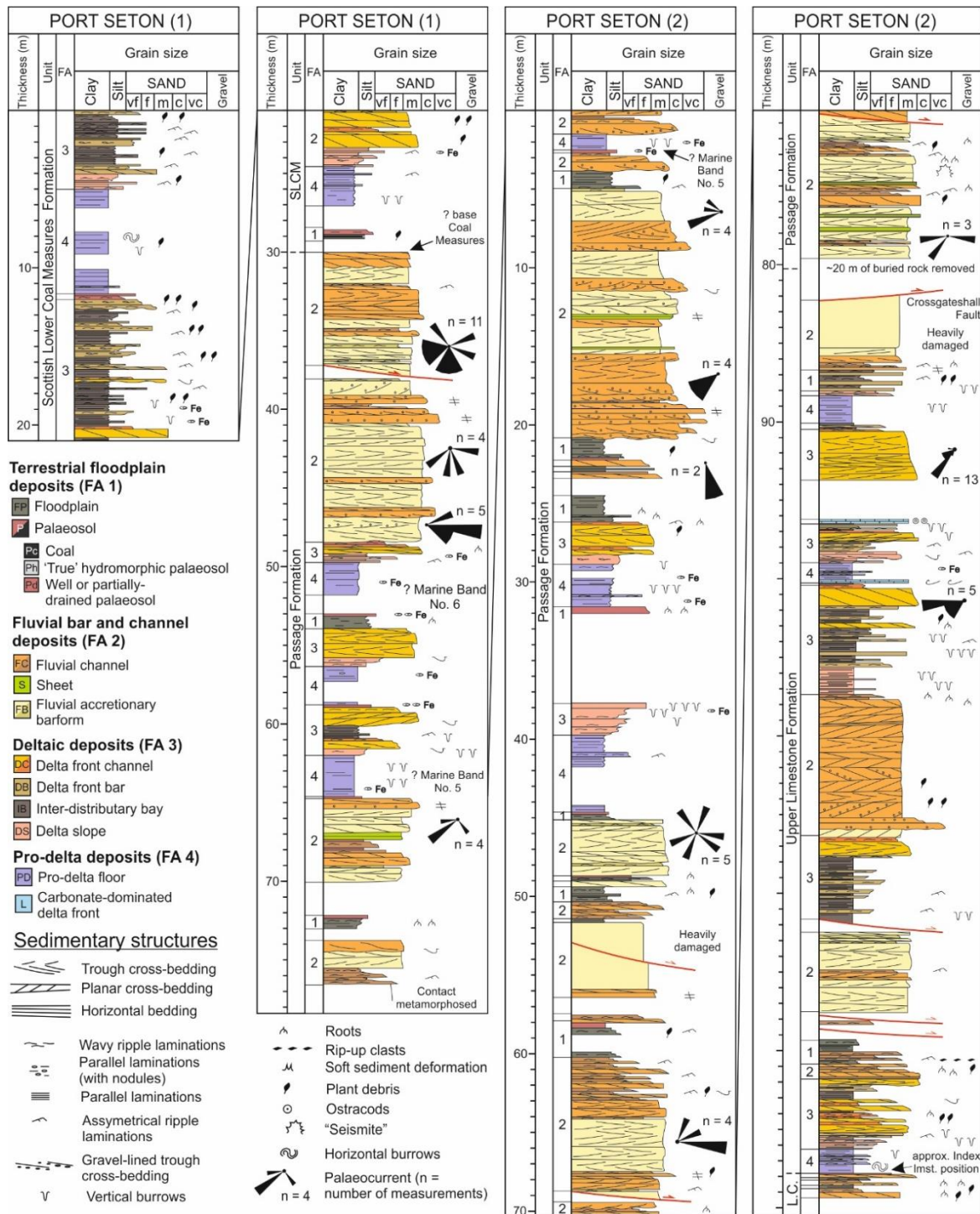
Figure 8.9: A sedimentary log for the Upper Limestone, Passage and Scottish Lower Coal Measures (SLCM) formations exposed along the Port Seton coastline, East Lothian. FA = Facies Association. For further descriptions of the outcrop location, the reader may refer to Whitbread *et al.* (2015). British National Grid reference: 341269, 675948. For further descriptions of the outcrop locality, the reader may refer to Whitbread *et al.* (2015).

Figure 8.10a: Photograph portraying the unconformable contact between the top of the Limestone Coal Formation and the base of the Index Limestone at Prestonpans. 8.10b: A delta top distributary channel (DC) deposit incising into delta slope (DS) deposits within the Upper Limestone Formation, Prestonpans. 8.10c: 'Reddened' and amalgamated fluvial channel (FC) deposits belonging to the Scottish Upper Coal Measures Formation, East Wemsyss. Taken from a Google Street View Image and courtesy of Lee Jackson. 8.10d: Preferential bleaching of more permeable fluvial channel (FC) deposits above a contact with a heavily oxidised sideritic palaeosol (Ps) deposit within the Passage Formation, Port Seton. 8.9e: Soft-sediment deformation features interpreted as 'seismites' within the Limestone Coal Formation, Prestonpans. 8.9f: Overall coarsening upwards delta slope (DS) and delta bar (DB) deposits within the Upper Limestone Formation, Prestonpans.
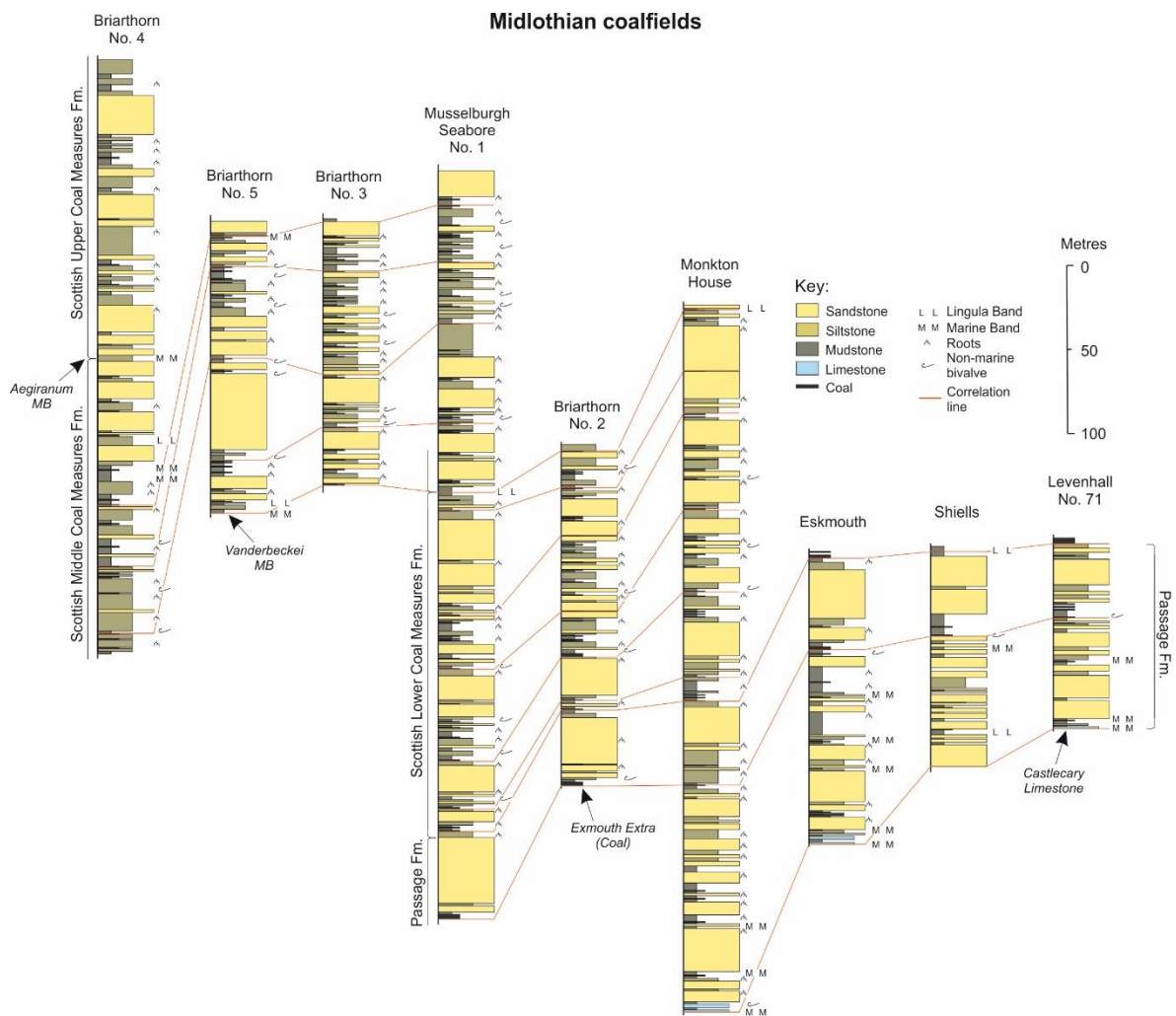
Figure 8.11: A borehole correlation panel for the Midlothian coalfields, within the southern part of the immediate study area. MB = Marine Band. Based on an unpublished British Geological Survey technical report for the 32E (Edinburgh) mapping sheet. For borehole locations, refer to Figure 8.2 or 8.3.

8.10.2 Langsettian to Duckmantian

The base of the SLCM Formation is marked by clear facies changes from dominantly fluvial, overall coarser-grained and redder, to dominantly deltaic, overall finer-grained and dark grey (Fig. 8.9). Few localities expose unmined and extensive (tens of metres) sections of the SLCM or SMCM formations. However, approximately 30 m of mostly uninterrupted lowermost SLCM Formation is observed within the port of Port Seton. The formation here consists mostly of alternating beds of parallel- to ripple-laminated and ripple-laminated siltstone and sandstone inter-distributary bay (IB) facies. These are typically moderately bioturbated, with both vertical and horizontal burrows, and

173

contain abundant and large, approximately 5 cm, intact plant debris. Delta top distributary (DC) and fluvial channel (FC) elements comprise a comparatively small proportion, approximately 15 %, of the formation. These are typically finer grained and less conglomeratic than their equivalents in the underlying Passage Formation. They appear to be similarly sourced from northerly and southerly directions, with similar distinctive mineralogical assemblages and have a similarly red weathered surface, indicating their dominantly subarkosic compositions. At outcrop, several thin, approximately 20 cm, but well-defined beds of sideritic pedogenic (Ps) facies are observed.

Numerous borehole records indicate a marked increase in inter-bedded coal seams, or organic hydromorpic palaeosols (Pc), from the base of the SLCM Formation and throughout the Langsettian and Duckmantian successions (Figs. 8.11 and 8.12). Coarser-grained sandstones (DB and DC ?) appear to comprise a similarly small proportion (15 to 20 %) of contemporaneous borehole successions in the Fife and Midlothian coalfields. Inter-bedded fossiliferous marine bands composed dominantly of mudstones and siltstones (PD ?) or stratigraphically thin (< 50 cm) limestone beds (L ?) occur sporadically and are mostly laterally persistent throughout the successions encountered in the Fife and Midlothian coalfields. Few boreholes, one being the Firth of Forth Offshore No. 3 borehole, encounter basalts and tuffs preserved within the Langsettian and Duckmantian successions (*cf.* Ewing and Francis, 1960). No stratigraphic equivalent to these subsurface volcaniclastic deposits was encountered at outcrop.

8.10.3 Bolsovian to Asturian

Within the Briarthorn No. 4 borehole succession, the first occurrence of parallel-laminated 'ocherous' mudstone (FP or P?) is 172 m above the base of the SUCM Formation, and approximately 30 m below the base Quaternary unconformity, although grey beds remain dominant here (Fig. 8.11). Plant debris is common within the SUCM Formation here, although inter-bedded coal seams are increasingly scarce and thin (<20 cm) upwards within the succession. Satellite imagery and photographs of coastal exposure along the Fife coastline (Fig. 8.10c) suggest a comparatively monotonous succession, along the axis of the Leven Syncline, consisting mostly of partially reddened and highly amalgamated fluvial channel (FC) and fluvial bar form (FB) deposits. These

coarser elements appear to comprise similarly elevated proportions, between 40 and 50 %, of the

entire SUCM succession across the two boreholes that penetrate this interval, the Briarthorn No. 4

and Firth of Forth Offshore No. 3 boreholes (Fig. 8.12), which are also situated approximately along

the axes of the Leven or Midlothian synclines (Fig. 8.3).
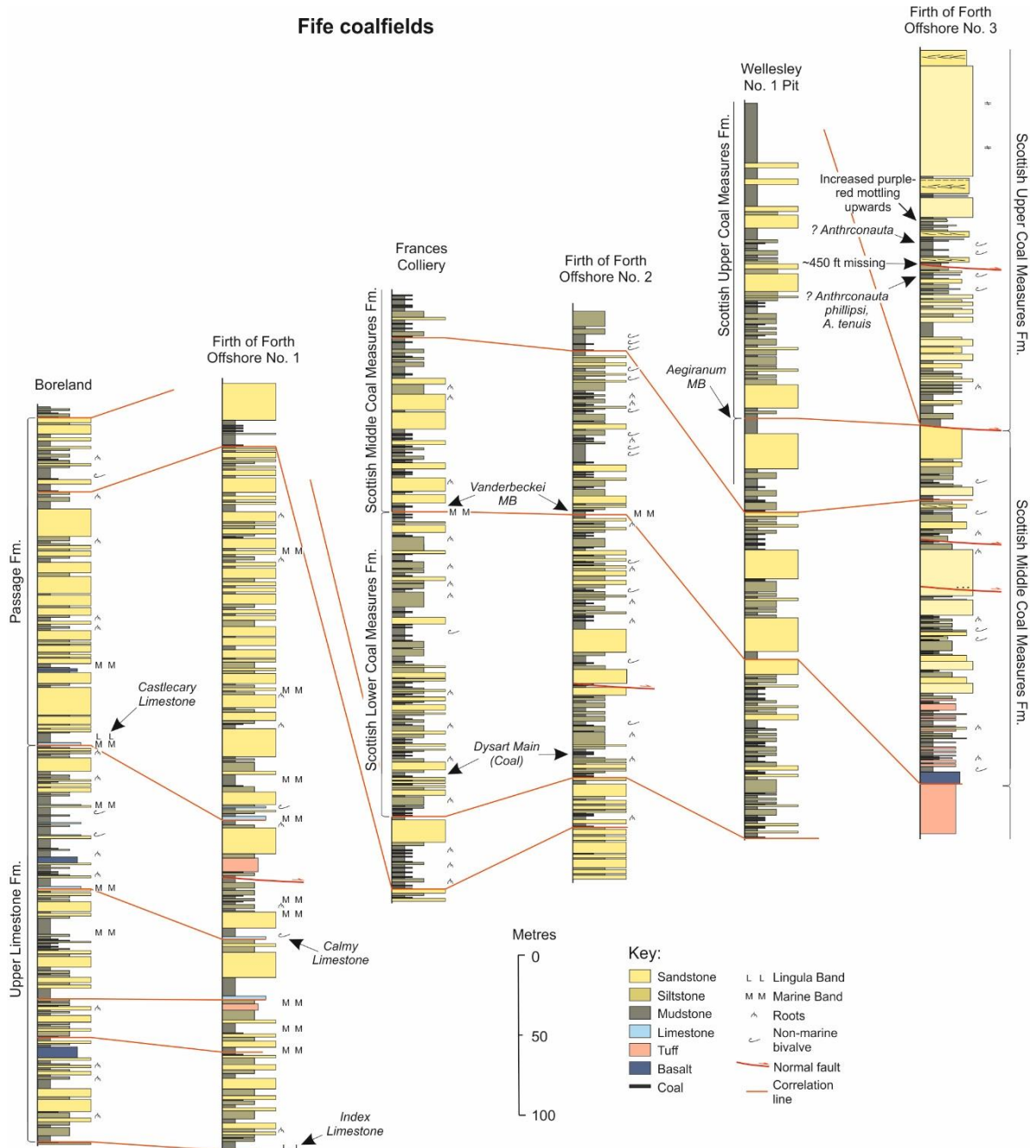
Figure 8.12: A borehole correlation panel for the Fife coalfields, within the northern part of the immediate study area. MB = Marine Band. Based on vertical sections presented by Ewing and Francis (1960) and lithological information derived from borehole scans curated by the British Geological Survey (https://mapapps2.bgs.ac.uk/geoindex/home.html). For borehole locations, refer to Figure 8.2.

Calver (in Ewing and Francis, 1960) reports faunal assemblages characteristic of the *tenius* biozone at 182.3 m TVDSS in the Firth of Forth Tower Borehole No.3 (Fig. 8.12), which would make these sediments Asturian (Westphalian D) in age. The faulted base of the SUCM Formation within this borehole is penetrated at 301.0 m TVDSS, making this the most complete direct recording of some of the youngest Carboniferous sediments in the (eastern) MVS. Finer-grained, mudstone-siltstone (dominantly FP?) comprise approximately 45 % of the succession here. These are interrupted sporadically by thick (<5 m), rooted and mostly fine- to medium-grained sandstone beds (FB or FC?), of which some are reportedly planar-bedded (S?) or structureless (FC?). Finer- and coarse-grained deposits alike are reportedly increasingly mottled purple, yellow or red progressively upwards within the succession here. Within the uppermost part of the SUCM Formation here, down to approximately 160 m TVDSS, no grey beds remain. A few thin fossiliferous, ostracods and non-marine lamellibranch, mudstone and limestones beds reportedly persist up to depths of approximately 195 m TVDSS.

8.10.4 Latest Asturian to Stephanian

It is unclear whether any boreholes have penetrated these youngest, seismically defined, late Carboniferous strata. This is perhaps due to the great depths to the so-called productive coal measures along the trough of the Leven Syncline, and the absence of any potential hydrocarbon trapping structure, where this unit is exclusively preserved in the (eastern) MVS. In the Firth of Forth Tower No. 3 borehole succession and approximately 50 m above a palynologically constrained Asturian interval, a "hard and limy" band is reported at 146.5 m TVDSS (Fig. 8.12). The depth to this "limy" band, which may bare some similarities with partially or well-drained palaeosol (Pd) lithofacies observed at crop, correlates approximately in this part of the Firth of Forth with depth to the seismically defined onlapping unconformity at the base of this latest late Carboniferous tectono-stratigraphic unit. In the Firth of Forth Tower No. 3 borehole and above this band, the (presumably) late Carboniferous succession is composed of approximately 90 % medium-grained and typically structureless sandstone. A few medium-grained or trough-cross-bedded sandstones and inter-bedded mudstones interrupt this succession beneath the base Quaternary unconformity.

8.11 (Local) tectonic controls on basin evolution

8.11.1 Middle-late Namurian deformation

The spatial correlation of the eastern limbs of the Midlothian and Leven synclines with the thinnest unit thicknesses of the middle-late Namurian Upper Limestone and Passage formations suggests localised syn-depositional folding (Fig. 8.4). Nowhere within the MVS study area, are obvious localised breaks in the middle to late Namurian stratigraphic record encountered, perhaps suggesting that this phase of deformation was characteristically mild here because subsidence kept pace with sedimentation. The absence of the Alportian and Chokerian Substages from the stratigraphy of the MVS occurs regionally across parts of North America and northern England and may be attributed to eustasy (Read, 1981), as opposed to tectonically induced uplift. Minor thickness variations associated with the hangingwalls of deeply buried (>2 km) and steeply dipping normal faults may be associated with differential compaction rates of the varyingly thick early Carboniferous syn-rift succession of the MVS (Fig. 8.4) (*cf.* Collier, 1989). The overall more uniform thicknesses of the uppermost part of the Passage Formation, the Langsettian SLCM Formation and most of the SMCM Formation (Fig. 8.5) suggests relative tectonic quiescence following this phase of deformation. Unit thickness variations associated with NE-trending synclines and anticlines are observed in the older early Namurian (Pendleian) Limestone Coal Formation in the western part of the MVS (e.g., Cameron and Stephenson, 1985 and references therein). However, these thickness variations are not so apparent in the Limestone Coal Formation of this eastern part of the MVS.

8.11.2 (Late) Duckmantian-Bolsovian deformation

The onlapping and overstepping discontinuity observed in seismic within reflector sets belonging to the SUCM Formation along the eastern limb of the Midlothian Syncline and most clearly along the eastern limb of the Leven Syncline (Fig. 8.4) is interpreted as representing an angular unconformity due to syn-depositional folding. The long-lived depositional hiatus towards the Mid Forth High Anticline represented by the local absence of most of the (upper) *similis pulchra* biozone (Calver in Ewing and Francis, 1960) suggests folding of greater magnitude than that associated with middle to late Namurian deformation because, in this instance, subsidence did not

keep pace with sedimentation. Although the local angular unconformity near the base of the SUCM Formation, whose interpretation is based on seismic data, most likely represents a short-lived pulse of compression, the thinning of the uppermost SMCM Formation and part of the lower SUCM Formation towards the Mid Forth High Anticline suggests that syn-depositional folding may have been drawn out over an extended period (Fig. 8.5). Before this proposed pulse of higher magnitude deformation, folding appears to have been comparatively milder. This is indicated in part by the uninterrupted presence of the Aegiranum Marine Band that marks the base of the Bolsovian SUCM Formation within the late Carboniferous succession. The overall more uniform thickness of the later Bolsovian units in the region suggests another period of comparative tectonic quiescence following this discrete phase of late Duckmantian to early Bolsovian deformation.

8.11.3 Latest Asturian-Stephanian deformation

The remarkable angular and onlapping discontinuity observed in seismic along the trough of the Leven Syncline (Fig. 8.6) represents a major angular unconformity. The typically flat nature of the reflectors belonging to the uppermost seismic volume suggests that this unit was deposited after folding of the syncline had largely ceased and that, therefore, this unconformity represents a major phase of basin shortening preserved within the late Carboniferous succession. Although the unconformable contact appears to be sharp in seismic, the observation of multiple onlapping discontinuities within this uppermost seismic volume suggests that deformation may have occurred over a protracted period. Whilst folding throughout the suceeding late Carboniferous times in the Leven Syncline appears to have been accommodated solely by the eastern limb of the syncline, the presence of onlapping reflector geometries against the western limb and to the south of the syncline trough suggests that basin shortening was also accommodating by folding of the syncline's western limb and perhaps combined with an element of N-S shortening.

8.11.4 Deep structural controls on late Carboniferous deformation

Traditionally, the Mid Forth Fault has been interpreted structurally as a set of near-vertical faults or a flower structure, the middle-late Carboniferous oblique-reverse reactivation of which is believed to have prompted the approximately NNE-trending Mid Forth High Anticline, the main

hydrocarbon trapping structure of the MVS (Ritchie *et al.*, 2003; Underhill *et al.*, 2008). However, this interpretation leaves a significant space problem associated with the Leven and Midlothian synclines, with nothing to accommodate this folding. Instead, it is suggested that both the Mid Forth High Anticline and the westwards dip of the Leven Syncline's eastern limb are accommodated by a shallow westerly dipping detachment fault, buried <6 km beneath the trough of the Leven Syncline and associated with the parallel Mid Forth Fault (Fig. 8.13). In three dimensions and around the Mid Forth High, the Mid Forth Fault and other NNE-trending splays associated with this deeper detachment fault may resemble a less steeply dipping and perhaps less traditional quasi-flower structure (Fig. 8.2). It is suggested that the Crossgateshall and Pentland faults may also be associated with this detachment fault to the south and that, similarly, these approximately NNE-trending faults accommodated folding of the Midlothian Syncline. Despite the interpretation of present-day normal displacement on most of the approximately NNE-trending faults in this part of the MVS, particularly in the northern part of the immediate study area, to accommodate this folding during late Carboniferous times displacement would have needed to have been reverse or oblique-reverse. The overall thinning of late Carboniferous strata upon the eastern limb of the Leven Syncline compared with the consistent thickness of these same strata upon the syncline's western limb suggests some sort of discordance (Fig. 8.5). It is suggested that the overall steeper and more consistent dip of the Leven Syncline's western limb may instead be accommodated by the reverse or oblique-reverse reactivation of a more steeply dipping and buried fault (Fig. 8.13). This and similar more steeply dipping fault zones may have been less susceptible to reverse reactivation throughout periods of overall lower deviatoric compressional stress during phases of middle to late Namurian and late Duckmantian to early Bolsovian deformation, due to their steeper dips, thus remaining unreactivated or 'frozen' during these times. The geometry of this fold in the western part of the study area can be replicated using the trishear fault-propagation algorithm (e.g., Allmendinger, 1998), when incorporating a large, between 2 and 3 km, reverse offset, and an upper fault tip at approximately 10 km depth.
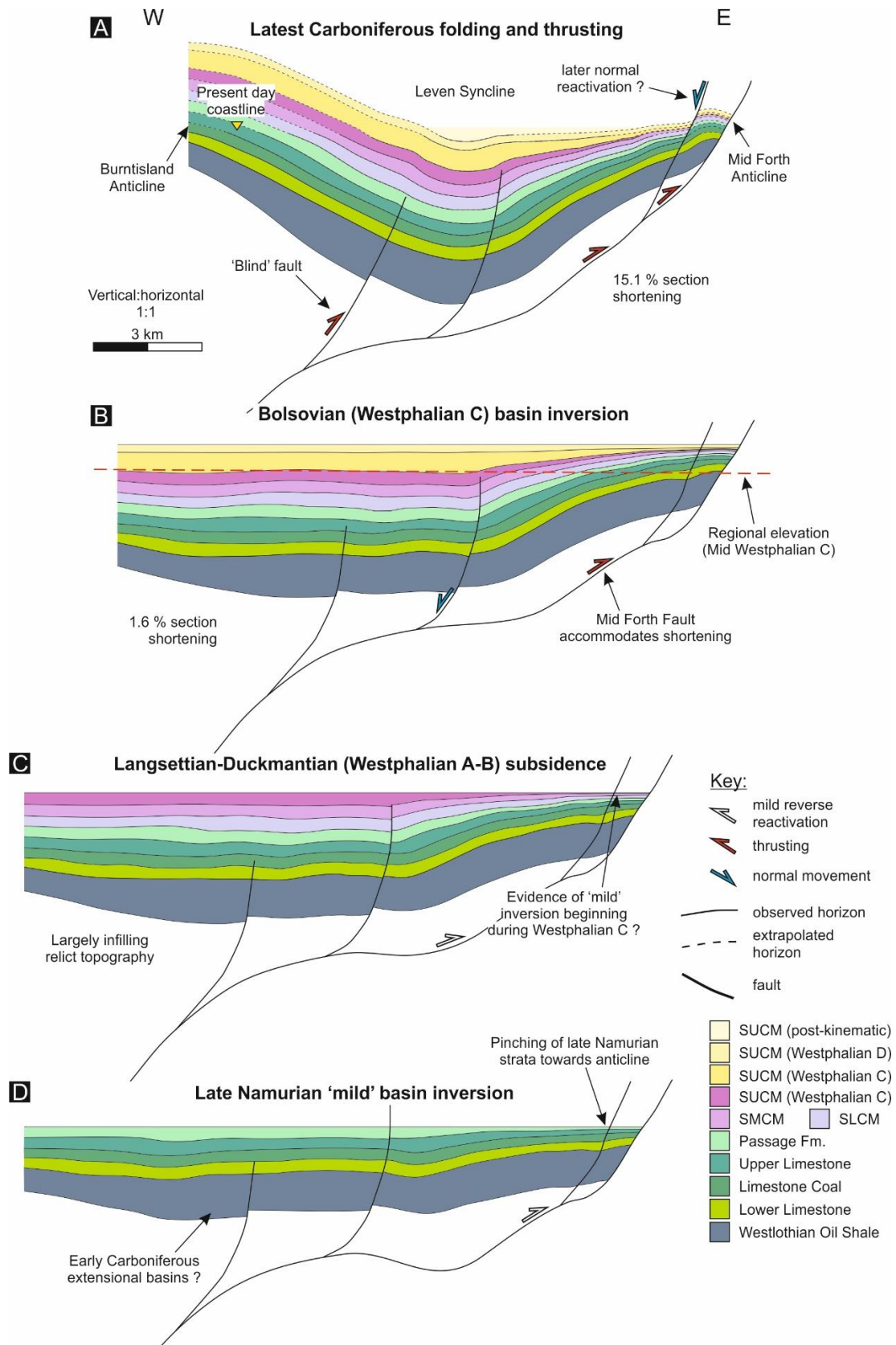
Figure 8.13: Cross-section restorations for the E-W section through the Leven Syncline presented in Figure 8.4. Geology of the Burntisland Anticline is based on outcropping bedrock geology (British Geological Survey, 2008). Fault restorations were performed using the simple shear (Egan *et al.*, 1999) and trishear (Allmendinger, 1998) algorithms and supported by MOVE structural modelling software.

Thickening of late Carboniferous units towards the syncline troughs, parallel axial drainage trends and localised unconformities along the fold limbs (Fig. 8.5) suggests that the Leven and Midlothian synclines were important late Carboniferous depocentres. Along strike variation of these depocentres may also be accounted for by the characteristics and behaviour of deeper accommodating faults. For example, where the Mid Forth Fault displaces strata greatest in a reverse sense along strike, along the western flank of the Mid Forth High Anticline, the magnitude of folding is also greatest (Fig. 8.2). In contrast, to the SW along strike and where the Mid Forth Fault displaces strata in a net normal sense, the magnitude of folding is far less. Along strike reverse to normal displacement variations in faults are an under-reported, yet not uncommon, feature of sedimentary basins characterised by polyphase tectonic histories or transpressional tectonism (Betts, 2001).

In this study area, the greater reverse displacement of the Mid Forth Fault and associated fault splays may be partly associated with the anticlockwise rotation of this fault trend (Fig. 8.2) towards the NE along strike to a more perpendicular orientation with respect to NE-SW dextral transpression (Fig. 6.2) (e.g., Coward, 1993). The greater overall reverse displacement of the Pentland Fault along strike to the SW may be explained by the progressively closer proximity of the fault along strike to the SW to one of the major basin-defining structures, the SUFZ (Fig. 1.1). Along strike fault offset variations may also be explained when considering the early Carboniferous (syn-rift) kinematic histories of these faults and their pre-inversion strength variations along strike. Vertical fault strength variations are discussed already in literature within the contexts of fault inversion (Fig. 7.11) (e.g., Jackson *et al.*, 2013). The central part of a normal fault, in a vertical sense, is considered the weakest part of the structure as this part has typically accommodated greatest displacement (Fig. 7.11c). As a result, the central part is therefore typically more susceptible to reverse reactivation during subsequent changes in stress regime whereas the stronger fault tips may remain 'frozen' during inversion (Fig. 7.11a) (Jackson *et al.*, 2013). This same reasoning could also be applied in a lateral sense (Fig. 7.11b). The central part of a fault such as the Pentland Fault, in a lateral sense, is likely to have been weaker prior to basin inversion and undergone greatest reverse reactivation consequently during inversion. The stronger fault tips appear not to be net reverse

reactivated and, in contrast, appear net normally displaced following early Carboniferous rifting or have been normally reactivated during the approximately 300 My following Carboniferous times.

Other possible interpretations of the Leven and Midlothian synclines may suggest that this folding was due to local and fault parallel down warping due to propagating normal faults (e.g., Gawthorpe *et al.*, 1997). Cross-section restorations do not definitely prove interpretations, they merely validate their feasibility. For such an alternative 'propagating normal fault' interpretation to be considered seriously, a set of major, vertically displacing and approximately E-W trending normal faults, which were actively extending during late Carboniferous times, are required. No such accommodating normal fault sets are apparent (see Fig. 8.5). Although the Crossgateshall, Pentland and Mid Forth are all at least partially buried in the Firth of Forth, numerous studies suggest that these faults clearly demonstrate an extensive history of frequent reactivation (Floyd, 1994) and that, therefore, these structures would have been capable of accommodating significant basin shortening.

8.12 (Local) controls on sedimentation

Palaeodrainage and fluvial systems in general are particularly sensitive to changes in topography, syn-depositional folding, and fault growth (Gawthorpe and Leeder, 2000; Delcaillau *et al.*, 2006; Hartley and Evenstar, 2018). In this sense and given the attention mid-late Namurian syn-depositional folding in central Scotland has received (Underhill *et al.*, 2008), the small influence of this earlier phase of deformation on local depositional trends, such as palaeocurrent, is perhaps surprising. Whereas axial palaeodrainage is typically anticipated along key growth trends during phases of accelerated deformation, in the (eastern) MVS, measured palaeocurrent is often oblique or approximately perpendicular with respect to syn-depositional structural trends, and widely dispersed (Figs. 8.8 and 8.9). Borehole penetrations and seismic reflection profiles reveal the thickest mid-late Namurian accumulations preserved within the cores of active synclines (Fig. 8.5). However, mid-late Namurian fluvial deposits are laterally consistent across the region. Finer-grained elements appear to comprise a greater overall proportion of the thickest Passage Formation accumulations (Figs. 8.11 and 8.12).

Based on the findings of this study and numerous curated borehole reports, the distribution of pedogenic facies appears to correlate with syn-depositional folding during mid-late Namurian deformation (Fig. 8.14a). In East Lothian, along the eastern limb of the Midlothian Syncline and within the Passage Formation, the overwhelming pedogenic lithofacies types are partially to well-drained and sideritic palaeosols (Pd). These facies contrast markedly with the contemporaneous thick coal seams and organic hydromorphic palaeosols (Pc) observed in boreholes across the remainder of the Midlothian and Fife coalfields (Figs. 8.11 and 8.12). Development of pedogenesis facies contemporary with deposition is governed by local behaviour of the water table (Besly and Fielding, 1989). A locally deeper water table during mid-late Namurian in East Lothian, leading to development of more sideritic and oxidised palaeogenic facies, may have been a response to syn-depositional folding and consequential localised uplift. Alternatively, some pedogenic lithofacies along this comparatively uplifted fold limb may have been responses to periods of extended non-deposition following uplift. Contemporaneous coal beds elsewhere within the region suggest that a locally deeper water table elsewhere within the region is unlikely to have been a response to a temporarily arid climate. Instead, a deeper water table here may have been one response to mid-late Namurian deformation and localised syn-depositional subsidence. Periods of comparative tectonic stability may have provided more favourable conditions for the development of more uniform and widespread floodplain, susceptible to peat accumulation (Fig. 8.14b).

Based on seismic attributes and isochore thickness maps (Fig. 8.5), the later and greater magnitude phases of basin shortening, during the mid-Westphalian and latest Westphalian-Stephanian, appeared to have influenced sedimentation more strongly in the (eastern) MVS (Fig. 8.14c). A clear switch from continuous and parallel reflectors to chaotic and hummocky reflectors, from the flanks of the Leven Syncline towards the axis of the syncline, may indicate contemporaneous lateral facies changes (Fig. 8.4). Thick fluvial channel stacks are typically represented by hummocky and comparatively chaotic reflector sets, like those described, and are typically concentrated within lowland areas due to the influences of topography on drainage. The chaotic nature of SUCM Formation reflectors within the uppermost defined late Carboniferous tectono-stratigraphic unit (Fig. 8.6), combined with the typically coarse and structureless nature of
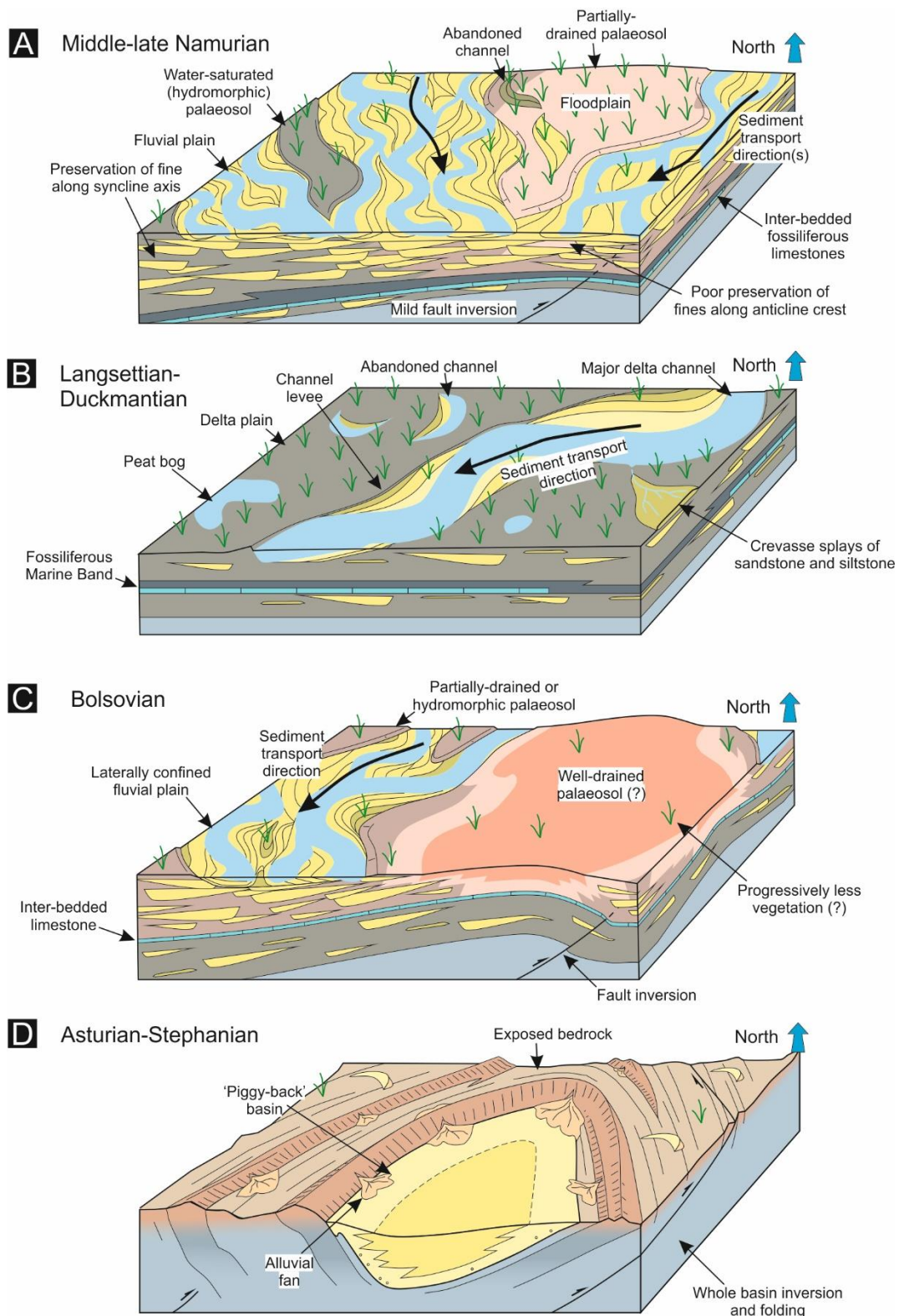
Figure 8.14: Structural and sedimentological interpretations for the late Carboniferous succession of the MVS, based on findings presented in this chapter. 8.14a: Middle-late Namurian (Passage Formation. 8.13b: Langsettian-Duckmantian (Westphalian A-B or SLCM and SMCM Formations). 8.14c: Bolsovian (Westphalian C or SUCM Formation). 8.14d: Asturian (Westphalian D)-Stephanian (SUCM Formation).

the sediments that correlate with these reflectors (Fig. 8.12), may be indicative of laterally discontinuous alluvial fan and debris flow deposits (Fig. 8.14d). Examples of these seismic responses preserved within sedimentary sequences are most common in rift basins; particularly, around the flanks of comparatively uplifted intra-basin highs (e.g., Elliot *et al.*, 2014). However, such deposits are also common in intra-foreland settings or in fold and thrust belts, adjacent to folded or thrusted bedrock units (*cf.* 'piggy-back' basins) (Nichols, 1987). Similarly, it is suggested that these reflectors represent syn-kinematic alluvial fan deposits.

The Namurian and early Westphalian successions of the MVS have traditionally been depicted within the contexts of high amplitude sea level fluctuations (e.g., Crowley and Baum, 1991). Within dominantly 'layer-cake' stratigraphic frameworks, coarser-grained, clastic, and fluvio-deltaic sediments expanded into the basin during cyclical periods of sea level lowstand (Read and Forsyth, 1989; Ellen *et al.*, 2019). Thus, the occurrence of these coarser-grained lithofaces is believed to be a direct consequence of eustasy and accommodation. These depictions are not contested, given the cyclical occurrence of inter-bedded marine and lacustrine facies within the dominantly deltaic and fluvial successions of the Upper Limestone and Passage Formations and the Scottish Coal Measures Group (e.g., Figs. 8.8 and 8.9). However, it is suggested that controls on late Carboniferous sedimentation in the MVS were more complex.

Based on the investigations presented in this chapter, it is suggested that expansion of mineralogically distinctive fluvial and deltaic sediments occurred from both the north-east and the south (Figs. 8.8 and 8.9). The north-easterly sediment supply, with respect to the MVS basin, is likely to have been sourced from the Norwegian or (eastern) Greenlandic Caledonides – these hinterlands represented persistent sources of clastic sediment for northern Britain throughout the Devonian and Carboniferous periods (Hallsworth and Chisholm, 2008). Comparatively more minor quantities of coarse clastic sediment from the north are likely to have been sourced from the (Scottish) Grampian Highlands (Hallsworth *et al.*, 2000), whereas clastic sediment from the south is perhaps most likely derived from the (Scottish) Southern Uplands during Namurian times. Further geochemical analyses would be required to constrain sedimentary provenance in the MVS more

precisely. The timings of major influxes of coarse clastic sediment coincide approximately with periods of accelerated intra-basin deformation. Expansion of coarse-grained, dominantly bedload, fluvial deposits belonging to the Passage Formation temporally aligns with my proposed phase of middle-late Namurian intra-basin deformation and contemporaneous observations of higher magnitude phases of basin shortening closer to the margins of the MVS (Lumsden, 1967), which may more strongly reflect behaviour of potential hinterlands (e.g., Zhang *et al.*, 2020). The overall bathymetric deepening of lithofacies following deposition of the Passage Formation may indicate a reduction in sediment supply, because of decelerated deformation in the basin's adjacent hinterlands. Similarly, the thicker inter-bedded fluvial sandstones of the SUCM Formation (Figs. 8.11 and 8.12) closely succeed one further, and more dramatic, phase of observed intra-basin deformation. These relationships are explored in greater detail in the next chapter of this thesis.

8.13 Conclusions

Detailed seismic- and borehole-based mapping, and sedimentary logging of the late Carboniferous succession in the eastern part of the MVS has revealed complex structure and sedimentological assemblages. The Midlothian and Leven synclines host laterally and temporally varying (mostly) fluvial and deltaic successions. Three phases of localised accelerated intra-basin deformation are identified: during the middle-late Namurian, the (latest) Duckmantian-Bolsovian, and (latest) Asturian-Stephanian times. The nature of these deformation phases and how they appear to influence local depocenter characteristics is controlled by local basin inversion and the pre-Carboniferous structure of this part of the MVS. These findings, along with those presented in the preceding chapter of this thesis based on the Canonbie Coalfield, provide a rare opportunity to re-assess the structural and geodynamic controls on sedimentation in northern England and Scotland, and across the remainder of the British Isles during the late Carboniferous Period.

Similar and possibly younger pre-Permian stratigraphy is recognised elsewhere within the MVS, namely in south-west Ayrshire and the Mauchline Basin (Mykura, 1967). However, this area does not benefit from the same density of subsurface (seismic and borehole) data that the eastern part of the MVS does. Because of the absence of seismic data specifically, investigations in Ayrshire

would have had to have been primarily based on the sedimentary record. Due to the coronavirus pandemic, travel was prohibited during the later stages of this study and desk-based investigations were preferred.

Variscan-influenced sedimentation in northern England and Scotland: a case for a 'broken' Variscan foreland?

9.1 Introduction

Local seismic and borehole-based mapping of the late Carboniferous succession in the Canonbie Coalfield (SW Scotland) provides evidence of repeated episodes of positive inversion, syn-depositional folding, and unconformities within the Westphalian to Stephanian Pennine Coal Measures and Warwickshire Group successions. Evidence for stratigraphically equivalent unconformities and phases of accelerated syn-depositional deformation is identified within the Clackmannan and Scottish Coal Measures groups in the eastern part of the Midland Valley of Scotland (MVS). The basin histories thus revealed are at variance with some generally accepted models for northern England and central Scotland, which state these basins subsided due to post-rift thermal subsidence during late Carboniferous times (Fig. 6.1) (e.g., Leeder, 1982).

In this chapter, the significance of the findings presented in Part 3 of this thesis are discussed. One-dimensional regional subsidence history plots are constructed for northern England and Scotland, and elsewhere in NW Europe using stratigraphic constraint from borehole data and some of the structural based mapping exercise presented in this thesis. Phases of accelerated intra-Carboniferous deformation are correlated between the Canonbie Coalfield, the eastern part of the MVS and elsewhere within the British Isles and NW Europe. This correlation represents an original tectono-stratigraphic framework for the late Carboniferous succession of northern Britain, based on which some of the other key structural and geodynamic controls on sedimentation are discussed. The influences of phases of accelerated deformation on fluctuations in sediment supply and local subsidence are discussed, as well as the effects of geodynamic setting on basin accommodation. Comparisons are made between northern England and Scotland and analogous basins; in particular, foreland systems (e.g., Cataneanu, 2019) and 'broken' foreland systems within which sedimentation

is controlled by localised reactivation of comparatively weak pre-existing basement structures (e.g., Strecker *et al.*, 1989; Bilmes *et al.*, 2013; Lopez *et al.*, 2019).

9.2 Late Carboniferous regional burial history

One-dimensional burial history plots can be used to help indicate contemporaneous tectonic activity. To determine regional and temporal variations in subsidence rate, decompacted 1D burial history curves are constructed in the basin modelling software Genesis (Zetaware) for boreholes and pseudo-boreholes across this study area and elsewhere within the British Isles (*cf.* Mitten *et al.*, 2020). Calculation of the decompacted rock unit thickness was performed in Genesis and is lithology specific (Perrier and Quiblier, 1974). The results from the seismo-stratigraphic analysis of the MVS and the Canonbie Coalfield, presented in the previous chapters of this thesis, are used to determine depths to unit tops and unit thicknesses for pseudo-boreholes. These are augmented by constraint from actual boreholes within the region, from where lithological constraints have also been derived (Table 9.1). The biostratigraphic zonation scheme of Waters *et al.* (2011) and chronostratigraphic scheme of Davydov (2004) have been used for numerical age constraints (Fig. 2.1). The estimations of Ridd *et al.* (1970) and Underhill *et al.* (2008) provide constraints for eroded overburden thicknesses. Deposition is assumed to have occurred at or close to sea level, so the effects of bathymetry are unaccounted for.

Namurian and early Westphalian deposits in central-southern Scotland and northern England are widely considered to have accumulated during a period of exponentially decaying rates of post-rift thermal subsidence (e.g., McKenzie, 1978), following accelerated subsidence during early Carboniferous rifting (Fig. 6.1) (Leeder, 1982; Kimbell *et al.*, 1989; Fraser and Gawthorpe, 1990). However, across northern Britain, including within the MVS, subsidence rates increase progressively throughout mid-late Namurian and early Westphalian times (Fig. 9.1a). Rates of subsidence vary slightly across northern Britain. Areas of greatest late Carboniferous subsidence spatially align with deeper early Carboniferous depocentres. Nonetheless, comparatively more rapid subsidence rates during these times are consistent across the region. Subsidence rates appear to decrease somewhat during later Westphalian times (Bolsovian-Asturian); although how well these

subsidence rates correlate regionally (over hundreds of kilometres) is less certain for this more poorly preserved part of the late Carboniferous stratigraphy. Latest Westphalian-Stephanian rates of burial are more difficult to determine due to poor chrono-stratigraphic constraints.
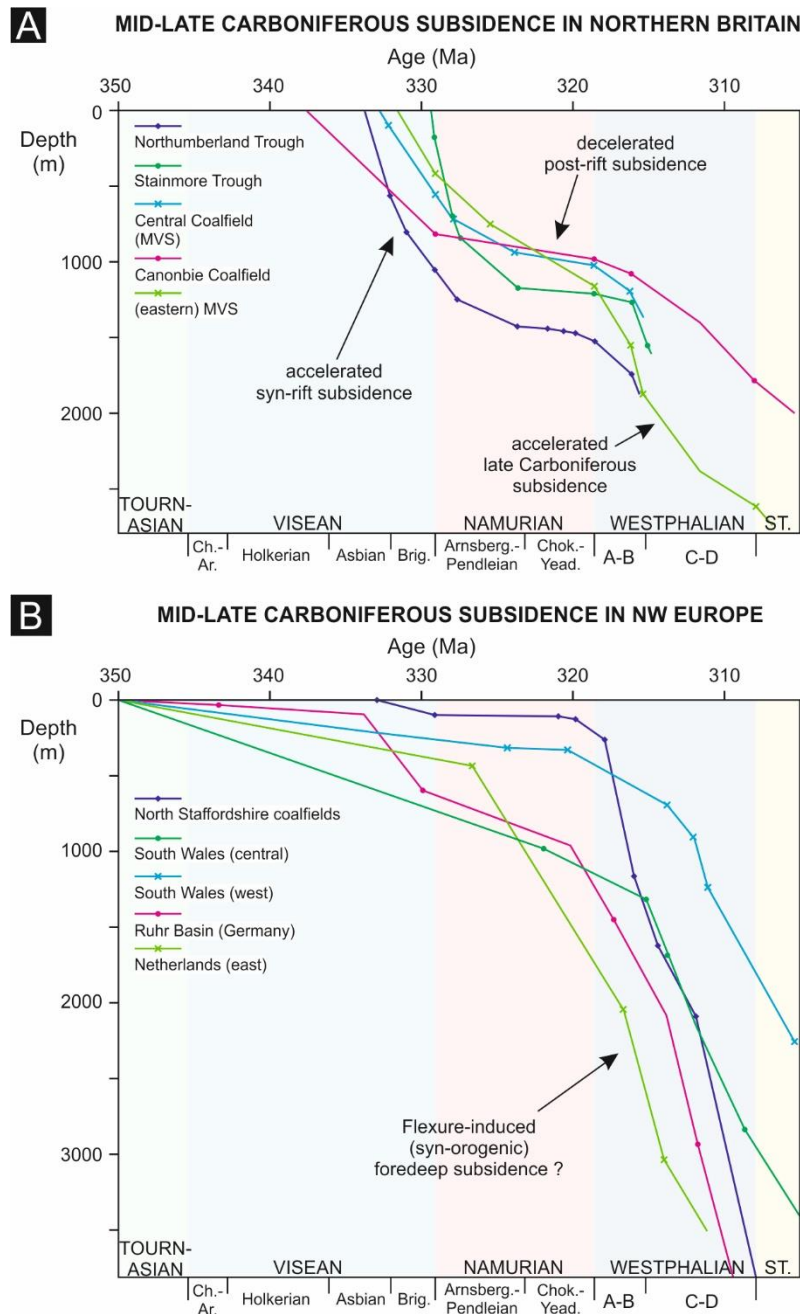
Figure 9.1a: Middle-late Carboniferous burial history plots for borehole and pseudo-borehole locations across northern England and central Scotland. Stratigraphic data taken from Ridd *et al.* (1970), Monaghan (2014), UKOGL and seismic interpretations presented in this thesis (Figs. 7.8 and 8.3). Figure 9.1b: Contemporaneous middle-late Carboniferous burial history plots for the central England, South Wales, northern Germany and the Netherlands (Besly, 2019). Stratigraphic data taken from Waters *et al.* (2011), Burgess and Gayer (2000), Littke *et al.* (2000) and Kombrink (2008).

Basin	Borehole name	BGS reference	Easting (BNG)	Northing (BNG)	Derivation (web link)
Northumberland Trough	Harton Dome	NZ36NE80	439660	565620	Ridd *et al.* (1970)
Stainmore Trough	Brafferton-1	NZ22SE105	428432	521493	ukogl.org.uk/
Central Coalfield (MVS)	Bargeddie-1	NS66SE415	269318	664649	ukogl.org.uk/

Table 9.1: Borehole data and derivation for mid-late Carboniferous subsidence plots in northern Britain (Fig. 9.1a). Plots for the Canonbie Coalfield and the (eastern) MVS are based on seismic interpretations presented in Chapter 7 and 8, respectively.

9.3 Regional tectonic implications

In the preceding chapter of this thesis, three distinct phases of late Carboniferous compressive or transpressive deformation preserved within the late Carboniferous succession of the eastern part of the MVS have been interpreted, based on unit thickness trends, subsurface seismic discontinuities interpreted as angular unconformities and sedimentological characteristics. These occurred during: 1) the middle to late Namurian; 2) late Duckmantian to early Bolsovian times and; 3) latest Asturian to Stephanian. The latest two of these phases corelate with the two intra-Carboniferous unconformities observed in the Canonbie Coalfield (Chapter 7), but also with similarly timed deformation in the English Midlands (e.g., Peace and Besly, 1997) and elsewhere in NW Europe and North America (Poole, 1988). These correlations are explored within this next section. The recognition of these regional phases of deformation provides an important tectonic framework, within which the controls on late Carboniferous sedimentation in northern England and Scotland can be more accurately discussed.

9.3.1 Middle-late Namurian deformation

Evidence of middle to late Namurian syn-depositional compressive or transpressive deformation can be found across the MVS and in parts of northern England in seismic and borehole data (Fig. 9.2) (Lumsden, 1967; Read, 1988; Chadwick *et al.*, 1995; Akhurst *et al.*, 1997; Ritchie *et al.*, 2003; Underhill *et al.*, 2008). This deformation is typically accommodated by NNE- to NE-trending structures such as the Solway Syncline, and the Midlothian and Leven synclines. Attributing late

Late Carboniferous chronostratigraphic correlation
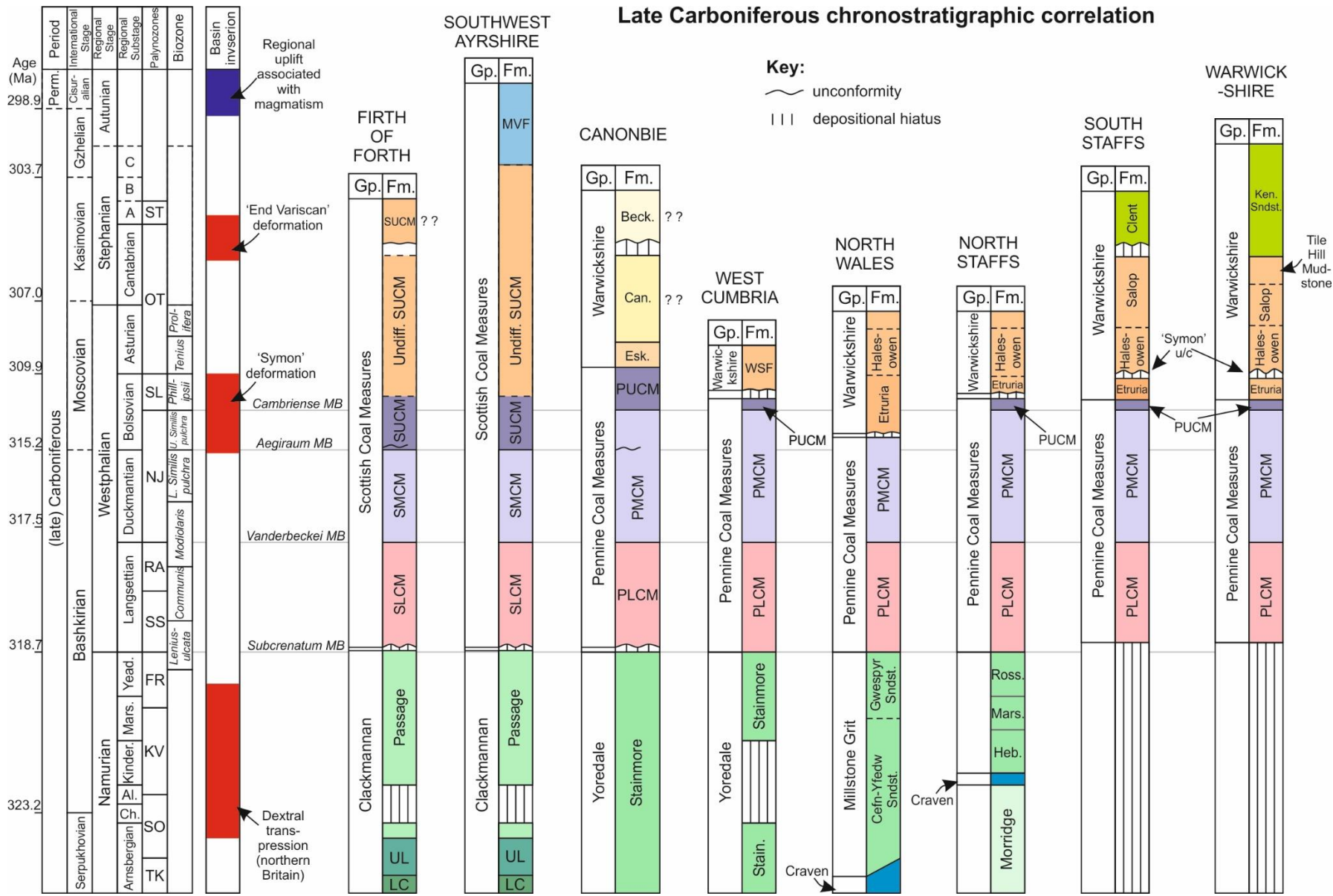
Figure 9.2: (left) Stratigraphic columns showing international and regional Stage units of the late Carboniferous. (middle) Phases of accelerated intra-basin deformation or basin inversion, based on results presented in this thesis and approximately stratigraphically equivalent unconformities elsewhere in the British Isles. (right) Chronostratigraphic correlation of the Pennine and Scottish Coal Measures, and Warwickshire Group based on Jones *et al.* (2006; 2011), Powell *et al.* (1999) and Waters *et al.* (2011, and references therein), and augmented by the seismic and regional interpretations of this thesis. Davydov's (2004) chronostratigraphic correlation for the Carboniferous Period is adopted, along with the palynozone subdivisions of Waters *et al.* (2011). Timing of regional uplift associated with magmatism based on isotope ages for early Permian igneous intrusions (e.g., Monaghan and Pringle, 2004). SLCM = Scottish Lower Coal Measures (Fm.); SMCM = Scottish Middle Coal Measures; SUCM = Scottish Upper Coal Measures; PLCM = Pennine Lower Coal Measures; PUCM = Pennine Upper Coal Measures; Esk. = Eskbank Wood; Can. = Canonbie Bridge Sandstone; Beck. = Becklees Sandstone; WSF = Whitehaven Sandstone; WSM = Whitehaven Sandstone Member; MBM = Millyeat Beds Member. For locations, see inset of Figure 7.1.

Carboniferous growth of the NNE-SSW trending syncline to either (Variscan) SE or SSW shortening axes, creates a series of geometric problems, particularly in a lower strain setting (*cf.* Copley and Woodcock, 2016). Many authors have therefore attributed late Carboniferous deformation in the MVS to E-W compression (Dewey, 1982), or dextral wrenching along key basin-defining and NW-SE orientated structures such as the Highland Boundary and Southern Upland fault zones and associated E-W compression (Fig. 9.3a) (Read, 1988; Coward, 1993). Contemporaneous influxes of clastic material, presumably from associated hinterlands, and expansion of dominantly fluvial deposits into Carboniferous basins (Chapter 8) (Waters *et al.*, 2020), would appear to support this hypothesis. The approximately 5-10 ° anticlockwise rotation in the trends of key intra-basin structures such as the NE-SW trending Pentland, Mid Forth and Crossgateshall faults along strike to the NW in the MVS (Fig. 8.2) may have caused these faults to have acted as restraining bends during dextral transpression (Fig. 9.3a).

The cause of Namurian basin shortening in northern England and Scotland is unclear. Multiple authors have argued that dextral transpression along key NE-SW basin bounding faults accommodated Uralian shortening along the eastern margin of the Baltic plate (e.g., Coward, 1993) (Fig. 6.2). However, earliest stratigraphic ages for sediments accumulated in basins associated with Uralian collision invariably post-date Namurian deformation in northern England and Scotland, by approximately 15 My according to Brown *et al.* (2006). In Coward's paper in 1993, it is worth remembering that he suggested that Uralian collision was responsible only for much later Stephanian to early Permian fault reactivation (*cf.* De Paola *et al.*, 2005; Pharoah *et al.*, 2020). Following the NE to SW-trending Highland Boundary and Southern Upland fault zones loosely along strike (Fig. 2.1), Namurian basin shortening in northern England and Scotland coincides approximately with phases of accelerated basin subsidence or fault-accommodated rifting in Nova Scotia, western Ireland, the North Sea, the southern Pennines, and Svalbard and the western Barents Sea. In the Carboniferous intermontane basin of Nova Scotia, eastern Canada, 'middle' Carboniferous sediments indicate transitions from purely extensional to briefly transpressions regimes before the establishment of transtensional conditions (Calder, 1998). In southern and central parts of the North Sea, like the depositional history of northern County Clare in western

Ireland and the southern Pennines, accelerated subsidence in the early Namurian created narrow, deep and anoxic basins within which organic rich mudstones and turbiditic sediments accumulated (Leeder and Hardman, 1990; Wignall and Best, 2000; Newport *et al.*, 2017). These phases of deformation coincide further with a phase of fault-controlled subsidence in Svalbard and the western Barents Sea (Johannessen and Steel, 1992; Gudlaugsson *et al.*, 1998). Rifting here is suggested to have been a response to "intensified" plate divergence and lithospheric extension between Norway and Greenland at this time, which began towards the end of the Devonian Period (Johannessen and Steel, 1992; Nøttvedt *et al.*, 1993). Any correlation of this sort is inevitably contestable. However, the timing and overall mild characteristics of shortening revealed by this study in northern England, Scotland and further to the south and south-west are sufficient to at least tentatively suggest that deformation may have been associated with distant lithospheric extension in the Arctic, rather than seemingly later Uralian collision.

9.3.2 (Late) Duckmantian-Bolsovian deformation

Several authors who have more recently studied the late Carboniferous succession of the northern England and Scotland have assumed a constant (NE-SW dextral) stress regime throughout this period (Fig. 6.2) (e.g., Underhill *et al.*, 2008). Such a hypothesis might have been supported by the continued accommodation of shortening by dominantly NE-trending structures during this later (late) Duckmantian to early Bolsovian phase of deformation revealed in both the Canonbie Coalfield and the (eastern) MVS. However, based on an alleged period of comparative tectonic quiescence separating this mid-Westphalian phase of deformation and the preceding phase of deformation in the MVS (Fig. 9.3b), and observations of contemporaneous phases of deformation elsewhere in NW Europe, it is suggested that this next (late) Duckmantian-Bolsovian phase of deformation instead represents the beginning of Variscan-influenced sedimentation in northern Britain.

The late Duckmantian to early Bolsovian timing of this next phase of deformation correlates strongly with angular unconformities throughout the British Isles and in northern Germany (Fig. 9.2) (Clarke, 1901; Poole, 1988; Peace and Besly, 1997; Smith, 1999). The most widely publicised of
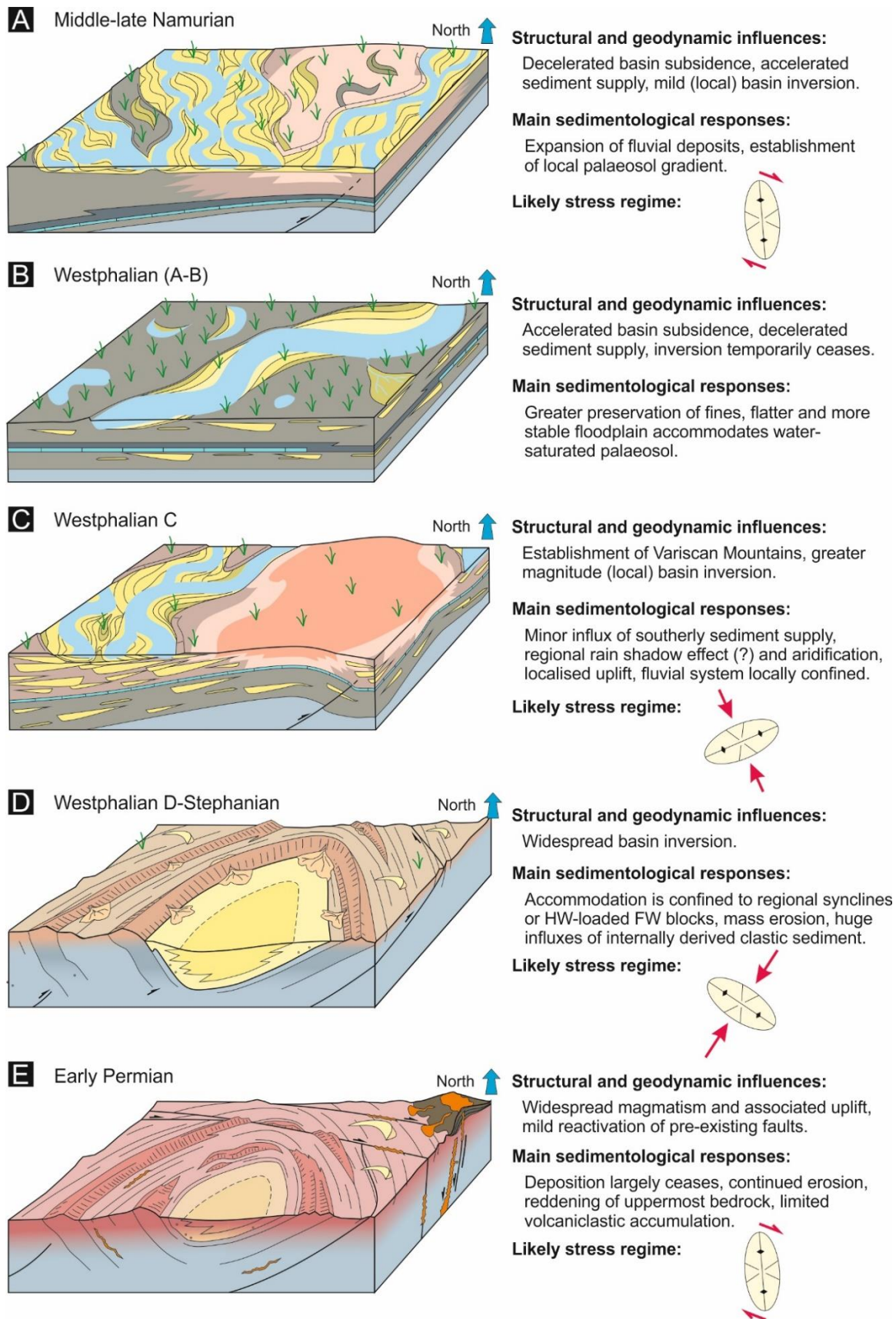
Figure 9.3: Illustrated evolution of the late Carboniferous basins of northern England and Scotland. Interpretations based on findings and discussion presented within this thesis. For more detailed sedimentological descriptions, the reader may refer to Figure 8.13.

these is the 'Symon' unconformity, a compound or diachronous unconformity that locally separates the Etruria Formation from the underlying Pennine Coal Measures Group in the coalfields of Shropshire, South Staffordshire and Warwickshire in the English Midlands. This unconformity has been attributed to Variscan compression from the south to south-east (Corfield *et al.*, 1996; Peace and Besly, 1997). Following the beginning of so-called 'Symon deformation', fluvial red-bed material derived predominantly from the south and south-east began expanding into the basins of the English Midlands (Besly, 1988). Similarly timed phases of deformation could be implied by an angular and erosive unconformity at the base of the Whitehaven Sandstone Formation in West Cumbria (Akhurst *et al.*, 1997) (Fig. 9.2).

9.3.3 Latest Asturian-Stephanian deformation

The Warwickshire Group unconformity of the Canonbie Coalfield, which is observed in seismic (Fig. 7.9), crops out along the River Esk, within the study area, and was recognised by Jones *et al.* (2011) who observed polygonal cracks penetrating the underlying Canonbie Bridge Sandstone filled by markedly more poorly sorted and quartz-rich arenitic Becklees Sandstone Formation, suggesting a prolonged depositional hiatus. The shallowest intra-Carboniferous unconformity observed in seismic within the SUCM Formation in the Leven Syncline (Fig. 8.6) shows striking similarities with its (likely) stratigraphic equivalent at the Canonbie Coalfield. Given the greater magnitude of shortening accommodated by this phase of deformation (Fig. 7.10), and the general absence of pre-Permian compressional deformation accommodated by the Becklees Sandstone Formation in the Canonbie Coalfield or the shallowest part of the SUCM Formation in the MVS, it is suggested that this unconformity could represent the final major pulse of Variscan basin inversion in the British Isles (Fig. 9.2) (e.g., Peace and Besly, 1997).

Latest Carboniferous basin shortening is typically associated with the climax of the Variscan Orogeny during approximately latest Asturian to Stephanian times (Corfield *et al.*, 1996; Peace and Besly, 1997). Although, the timing of this phase of deformation correlates approximately with the formation of the Cantabrian and Iberian oroclines, several hundred kilometres to the south and SSW of the study area (Fig. 2.1) (Murphy *et al.*, 2016), the effects of this event are still widely referred to

as 'Variscan' in the British Isles (Woodcock and Strachan, 2009). It is widely assumed that in northern Britain, this deformation occurred after the deposition of the late Carboniferous succession (Underhill *et al.*, 2008). Partly due to the uplift and denudation associated with this phase of deformation and the deposition of younger strata over these rocks, nowhere before in northern Britain has this phase of deformation been observed so clearly preserved in seismic reflection profiles within the late Carboniferous succession.

Tectono-stratigraphically equivalent (post-inversion) units in the British Isles may therefore be represented by the Clent Formation of the English Midlands, which unconformably rests on top of the Enville Member (Salop Formation) in South Staffordshire, or the Kennilworth Sandstone Formation, which locally rests unconformably on top of the Tile Hill Mudstone and Salop formations in Oxfordshire (approximately 40 km SE) and conformably upon the Tile Hill Mudstone Formation in Warwickshire (Besly and Cleal, 1997; Peace and Besly, 1997) (Fig. 9.2). This may suggest a younger age (Autunian or Gzhelian-Asselian) for the Becklees Sandstone Formation and (uppermost) SUCM Formation in the eastern MVS than anticipated prior to this study (*cf.* Besly and Cleal, 2021). The polygonal cracks observed by Jones *et al.* (2011) at the base of the Beckless Sandstone Formation either represent a time-gap of up to 8 My or, likelier, that the Canonbie Bridge Sandstone Formation represents a condensed (200 m thick) time-equivalent unit relative to the far thicker Warwickshire Group successions of central England (>1 km thick) (Fig. 9.4). The "hard and limy band" described within the Firth of Forth Tower No. 3 borehole succession, offshore in the Firth of Forth (MVS), could be tentatively interpreted as representing a similar depositional hiatus (Fig. 8.12). Because this latest episode of deformation correlates approximately with the *c.* 310-295 Ma (Murphy *et al.*, 2016) formation of the Iberian and Cantabrian oroclines, an alternative more SSW-orientated compressional stress direction could be implied (Fig. 9.3). On inspection of further UKOGL 2D seismic reflection profiles in northern England, similar onlapping and truncating relationships are easily identified within the southern part of the Solway Basin (Fig. 9.5). This profile perhaps represents the strongest indication of the preservation of this latest phase of 'Variscan' basin inversion in the northern part of the British Isles.
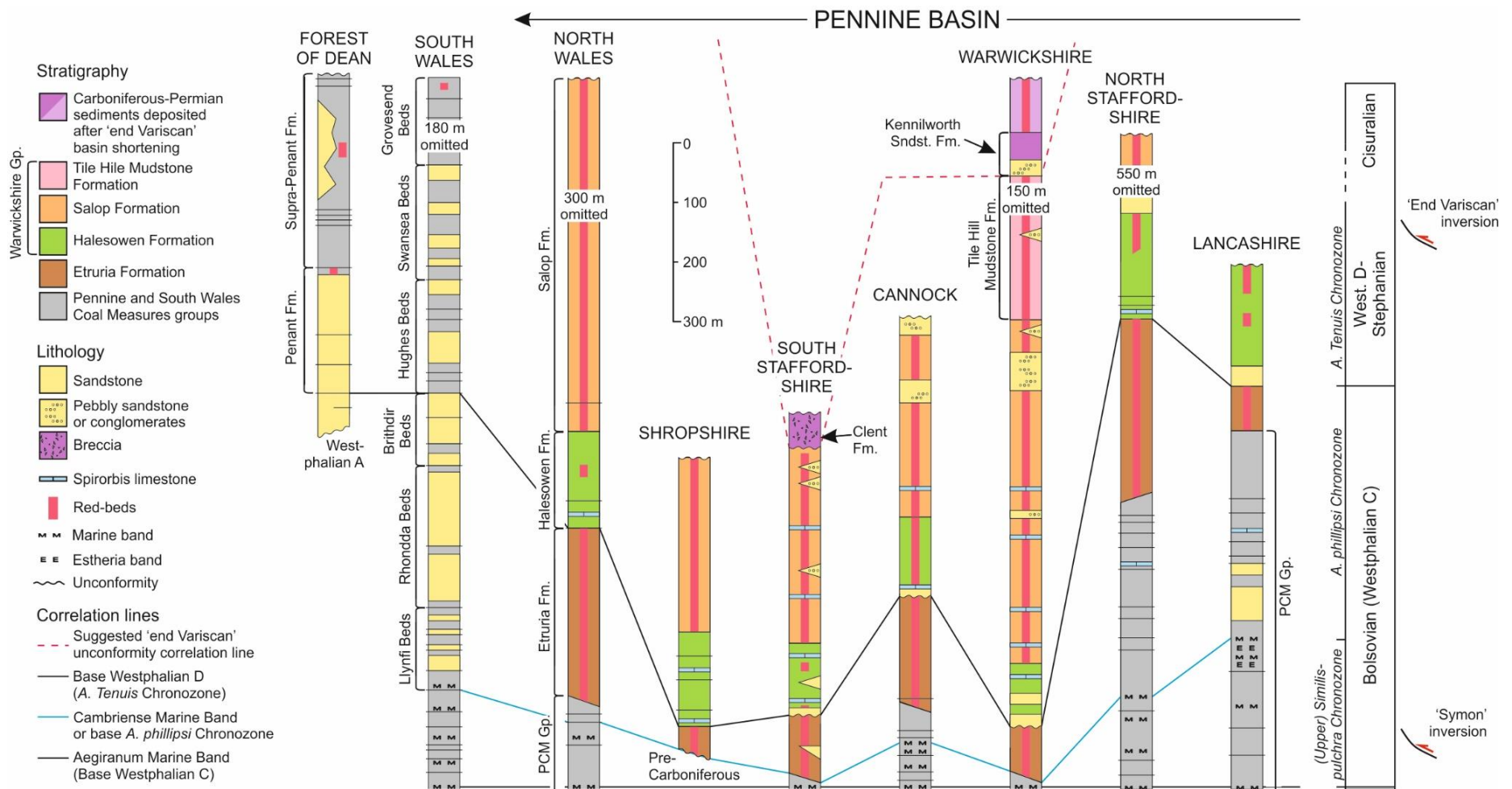
Figure 9.4 (left): Depth correlation for the Bolsovian-Duckmantian (Westphalian C-D), Stephanian and lowermost (Cisuralian) Permian sequences of the British Isles. Based on Ramsbottom (1970) and Powell *et al.* (1999), with additions based on Lumsden and Calver (1958), Calver in Ewing and Francis (1960), Davies (1970), McMillan and Brand (1995), Jones *et al.* (2006), and results presented in this thesis. Continued onto next page.
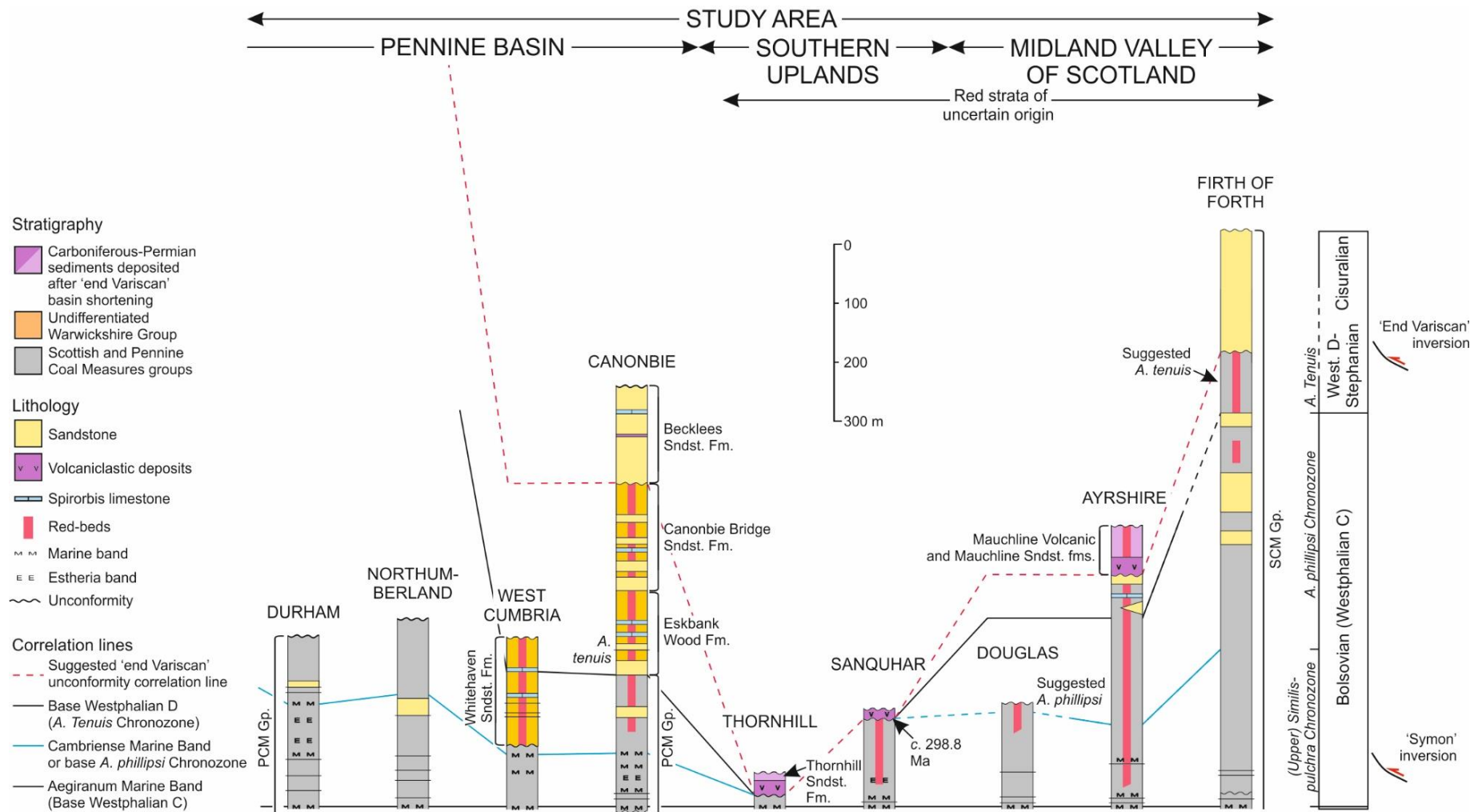
Figure 9.4 (right): Depth correlation for the Bolsovian–Duckmantian (Westphalian C-D), Stephanian and lowermost (Cisuralian) Permian sequences of the British Isles. Continued from previous page.

9.3.4 Early Permian

The regional stress framework represented by a mid-late Namurian NE-orientated dextral strain ellipse also accommodates preferential intrusion of Early Permian igneous material along tensile and approximately ENE- and WNW-orientated faults and pre-Permian normal activation of these faults (Fig. 9.3) (e.g., De Paola *et al.*, 2005). These regional stress fields may have been caused by dextral reactivation of basement involved faults such as the Gilnockie, Mid Forth or Castlegate faults within the immediate study area, or by reactivation along major thick-skinned faults such as the Southern Upland and Highland Boundary fault systems. If so, these Namurian and Early Permian phases of movement may represent responses to a longer-lived stress regime, associated with perhaps both Arctic rifting, during Namurian times, and perhaps Uralian Orogeny, during Early Permian times (Fig. 6.2) (*cf.* Coward, 1993), both of which were interrupted sporadically throughout late Carboniferous times by phases of more southerly Variscan deformation.

9.3.5 The potentially problematic orientation of NE-trending accommodating fault lineaments, relative to (southerly) Variscan compression

Corfield *et al.* (1996) attribute late Carboniferous deformation to a south or south-easterly (Variscan) derived compressional stress field in the English Midlands (Fig. 9.3c). Several authors argue that the obliquity of the dominant NE-SW trending accommodating structures during late Carboniferous deformation, relative to the orientation of Variscan (southerly) compressive stress (Fig. 2.1), represents something of a geometric problem (Coward, 1993; De Paola *et al.*, 2005; Copley and Woodcock, 2016). To reactivate pre-existing faults, a small degree of obliquity relative to maximum compressive stress (approximately 15 °) is preferential (Sibley and McCay, 1995). However, to reactivate highly oblique faults, these faults need to be significantly weaker than the accommodating bedrock to avoid the nucleation of new discontinuities. Based on numerical modelling experiments, Copley and Woodcock (2016) suggest that for southerly (Variscan) derived compressive stresses to reverse reactivated some of the NNE-SSW trending lineaments of northern England and Scotland, which were active during late Carboniferous times, these faults had to be at least 30 % weaker than the accommodating bedrock.

Perhaps the preceding middle to late Namurian phase of deformation, although mild, provides some important context for this mid-Westphalian and Variscan phase of deformation. By middle to late Namurian times and at shallower intervals, abundant organic material had already been deposited as inter-bedded coal seams. Middle to late Namurian deformation likely contributed to the smearing of this organic material within the shallow parts of these fault zones, thus rendering them more susceptible to future reactivation (Andrews, 2020). Both the Solway and Leven synclines, of the Canonbie Coalfield and the Firth of Forth respectively, were restored by incorporating NE-trending faults that dipped shallowly or were near horizontal beneath the folds (Figs. 7.10 and 8.13). Shallowly dipping faults are more susceptible to reverse reactivation than steeper faults (Sibley and McClay, 1995), although, it is unclear how steeply some of the more E-W trending fault systems dipped. Furthermore, in central Scotland, Namurian basin shortening, and early Carboniferous basin (oblique) extension, are believed to have been accommodated largely by the same NE-SW trending lineaments that accommodated latest Carboniferous basin shortening (Underhill *et al.*, 2008; Young and Caldwell, 2019). These phases of earlier deformation are likely to have weakened these lineaments further, particularly at deeper intervals. Whether this deformation or any of the other factors suggested here were sufficient to weaken the fault rock over 30 % more than the accommodating bedrock (or other pre-existing fault trends) (e.g., Copley and Woodcock, 2019) remains unclear and possibly still problematic without further substantial investigation. However, it is the view of the author that the timing of this late Duckmantian to Bolsovian phase of deformation, in relation to similar phases of deformation in the British Isles (Fig. 9.2) (Peace and Besly, 1997) and NW Europe (Poole, 1988), strongly suggests Variscan compression from the south. If alternative stress regimes were to be suggested, a feasible cause for these stresses is required.

9.3.6 An alternative (eustatic) interpretation of the unconformities

If any of these supposedly regionally correlative unconformities were truly synchronous, there is a valid counterargument that they may be a result of eustatic sea level fall (e.g., Read and Forsyth, 1989). However, based on the evidence collected in this thesis, namely the angular onlapping nature of these unconformities, the local absence of stratigraphy along anticline crests, and contemporaneous syn-depositional folding, there is high confidence that the latest of the two

Carboniferous synclines described at Canonbie and in the eastern part of the MVS are due to folding and tectonic forces. Previous authors (e.g., Lumsden *et al.*, 1967; Picken, 1988) suggested that a further, base Westphalian, unconformity at the Canonbie Coalfield was also due to tectonic forces. However, this older unconformity, which is largely restricted to Scotland, is argued to be more likely associated with sea level fall because of the parallel nature of these strata and the absence of any syn-depositional folding (see Section 7.3.1). Palaeocurrent trends suggest a dominantly NE-derived sediment supply at approximately the interval of this unconformity. Therefore, it may be inferred that sediment supply was greater progressively towards the north-east, and that unconformities due to regression may have been more frequent in this part of the basin because here, sediment supply more frequently outpaced subsidence (*cf.* Christie-Blick, 1991). Whereas suggestions of folding induced unconformities at Canonbie, in the Firth of Forth, and at the Oxfordshire Coalfield based on Peace and Besly's (1997) work there (also see Smith, 1999), can be made confidently due to seismic data available and the criteria outlined, suggestions of folding, and tectonic, induced unconformities elsewhere (e.g., Fig. 9.2) are far less certain, thus highlighting the need for further research in these other areas.

9.4 Regional structural and geodynamic controls

Constraints on regional late Carboniferous tectonism and subsidence in northern Britain are notoriously poor, and particularly so during the latest (Westphalian-Stephanian) part of the Carboniferous Period. The findings presented in this thesis represent major revisions of our current understanding. Thus, an opportunity to re-evaluate the role of late Carboniferous tectonism and subsidence in determining the regional sedimentary basin system, and ultimately more effectively characterise the broader geodynamic system, is provided.

9.4.1 Tectonic controls on late Carboniferous sediment supply

The strong temporal correlation between the expansion of coarse-grained, dominantly bedload, fluvial sediments into the MVS basin and an observed phase of accelerated middle to late Namurian deformation were discussed in Section 8.12. Throughout the British Isles, including northern England and Scotland, all phases of late Carboniferous deformation (Fig. 9.2) can be
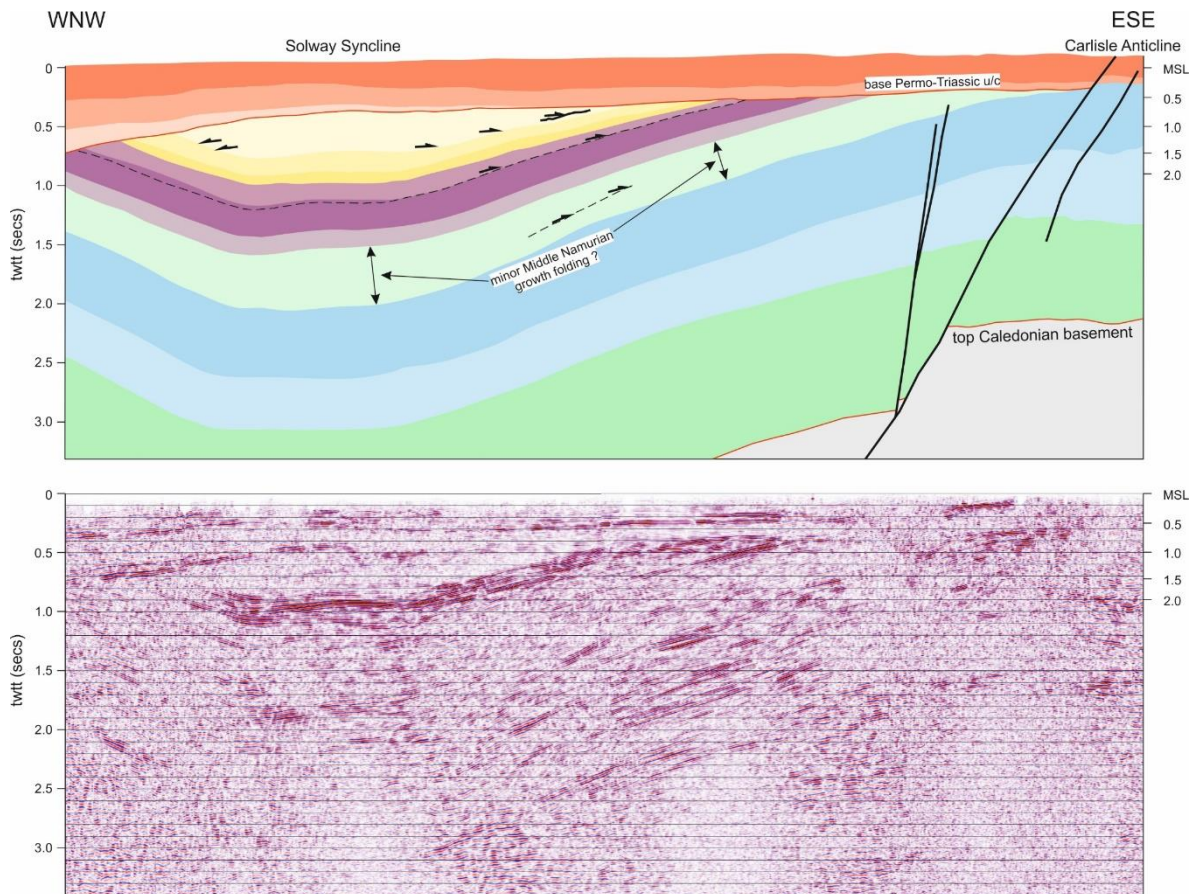
Figure 9.5: Interpreted and uninterpreted seismic reflection profiles through the southern part of the Solway Basin, northern England. The reader may visit the following web link for a further uninterprted version of this seismic profile: ukogl.org.uk/. For profile location, see Figure 1.1.

associated with influxes in clastic sediment supply (Fig. 9.6). In the Northumberland and Solway basins, middle to late Namurian (Kinderscoutian) basin fill is characterised by an abrupt transition from typical 'Yoredale' deposits, characterized by marine limestones in a dominantly siliciclastic succession, to a largely northerly-derived sandstone-dominated fluvial succession recognizable as the Millstone Grit Group, not unlike the stratigraphically equivalent Passage Formation of the MVS (Fig. 9.3a) (Waters *et al.*, 2014). Besly and others (1988, 1993) describe the largely Bolsovian expansion of arid continental sediments derived from the Variscan Mountains into the late Carboniferous basins of the English Midlands (Fig. 9.3c). These sediments have been found as far north as the Canonbie Coalfield (Morton *et al.*, 2010), and the timing of this expansion occurred shortly after the correlated phase of accelerated (late) Duckmantian-Bolsovian deformation described in this thesis (Fig. 9.2). Fraser and Gawthorpe (1990) identify a, perhaps less widely felt, phase of early Namurian (Pendleian) basin inversion in the East Midlands that may also be
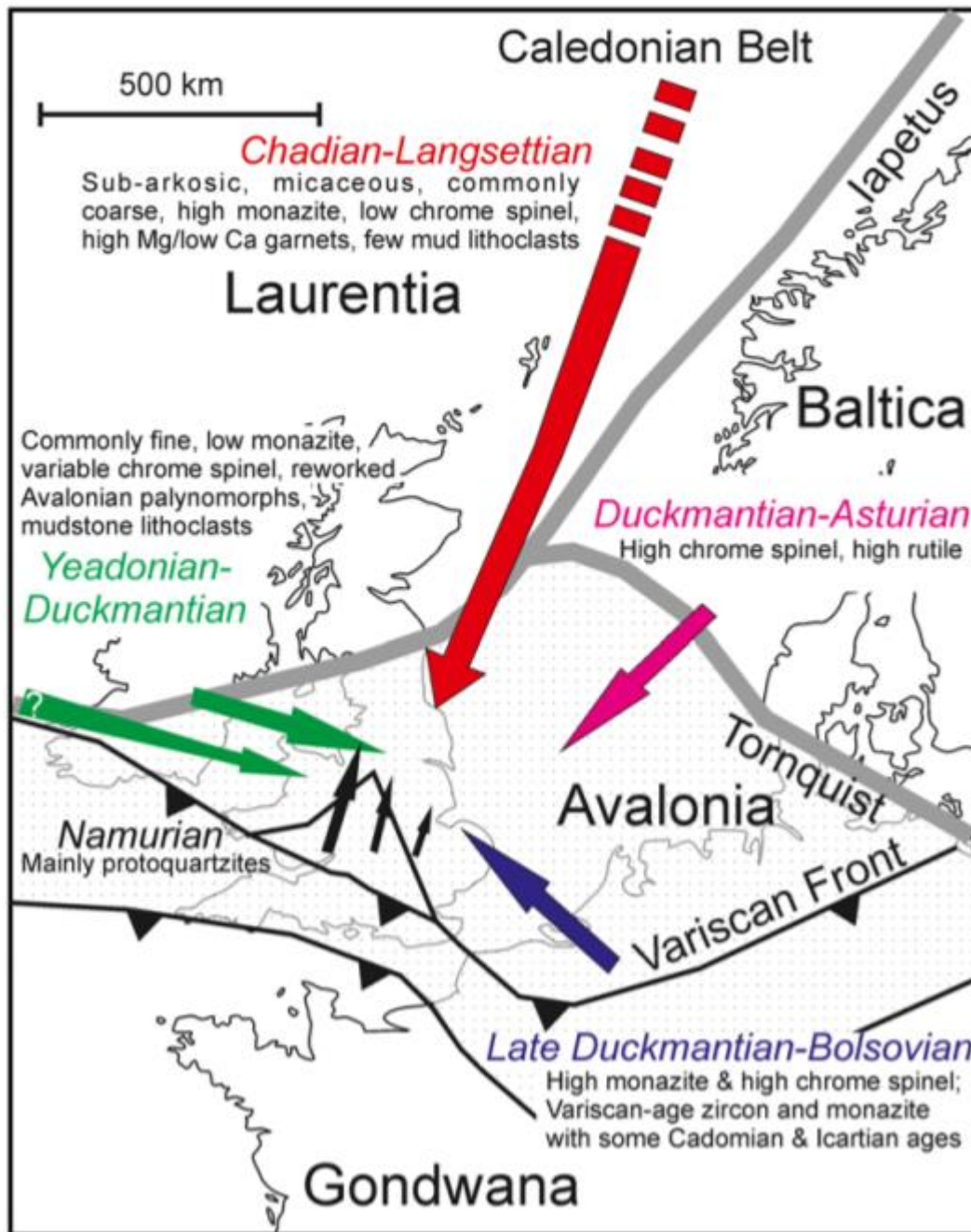
Figure 9.6: A plate tectonic reconstruction showing classically interpreted sediment source areas and flow directions for the late Carboniferous basins of northern Britain (after Waters *et al.* 2020). Interpretations based on Chisholm *et al.* (1996), McLean and Chisholm (1996), Hallsworth & Chisholm (2000, 2017), Hallsworth *et al.* (2000), Morton and Witham (2002), Chisholm and Hallsworth (2005) and Morton *et al.* (2005, 2014).

associated with the contemporaneous and more restricted expansion of southerly-derived 'Millstone Grit' and siliciclastic turbidite deposits (e.g., the Morridge Formation) into the southern Pennine Basin (Trewin and Holdsworth, 1973).

For some of the examples of accelerated clastic sediment supply discussed, deformation within collision zones is likely to have prompted uplift and erosion in these sediment source areas. A dissipating stress regime is likely to have prompted reactivation, uplift and erosion within other sediment source areas, so that sediment supply, following phases of accelerated deformation, need not have necessarily been solely derived from the focal point of deformation. One example for this is following latest Asturian-Stephanian deformation, after which influxes of coarse clastic sediment were likely derived from within the basin because of widespread basin inversion (Fig. 9.3d) (*cf.* Jones *et al.*, 2011). The tectono-stratigraphic framework presented here (Fig. 9.2) may provide a platform from which some hotly contested ideas surrounding late Carboniferous sedimentary provenance could be re-appraised (Fig. 9.6) (Waters *et al.*, 2020). The late Carboniferous succession of the Pennine Basin has been the subject of many previous geochemical provenance studies (e.g., Lancaster *et al.*, 2017). However, central Scotland has received comparatively little attention.

9.4.2 Controls on basin subsidence and sediment accommodation

How basin inversion has an increasing influence on the nature of mostly localised late Carboniferous depocentres in northern England and Scotland has already been discussed in Section 8.11. In this section, discussion is focussed on more regional influences on accommodation.

The role of regional subsidence in determining deposition trends is rarely plain. Partly, this is because system-scale depositional processes, such as transgression and regression, are broadly governed by both subsidence and sediment supply. Nonetheless, some of the prolonged periods of accelerated subsidence identified by burial history plots from northern Britain (Fig. 9.1a) are associated with deposition of progressively deeper water sedimentary facies (transgression), whereas decelerated subsidence rates are associated with shallower facies (regression) (Fig. 9.3a). Despite the superimposed high amplitude sea level fluctuations and the inferred variations in sediment supply throughout the Namurian and (early) Westphalian stages, similar associations can be made of the Upper Limestone and Passage formations and the SCM Group in the MVS. Regionally, subsidence rates were less during deposition of the (Arnsbergian-Langsettian) Passage Formation compared with those during deposition of the (Pendleian-Arsnbergian) Upper Limestone Formation. Overall

higher proportions of shallower water fluvial deposits are observed within the Passage Formation, compared with the Upper Limestone Formation, perhaps because of these changes in accommodation. The overall sparser preservation of finer-grained sediments within the Passage Formation may also be attributed to greater re-working of these sediments due to decelerated rates of accommodation space creation. Accelerated subsidence rates during (early) Westphalian are contemporaneous with the overall increased proportions of deeper water deltaic sediments observed within the SLCM and SMCM formations (Fig. 9.3b).

9.4.2.1 Subsidence mechanisms in foreland systems

In traditional flexure-induced foreland basins, accelerated subsidence rates and sediment accommodation are typically attributed to supra-lithopsheric (orogenic) loading due to an adjacent collision zone, and flexural isostasy (e.g., Karner and Watts, 1983) (Fig. 9.7a). Similarly timed, yet overall greater accelerated subsidence trends compared with those documented here in northern England and Scotland have been formally recognised in the coalfields of South Wales (Kelling, 1988; Burgess and Gayer, 2000), the Netherlands and the adjacent offshore area (Kombrink *et al.*, 2008), and the Ruhr Basin of northern Germany (Littke *et al.*, 2000) (Fig. 9.1b and left part of Fig. 9.4). In these regions, subsidence trends are attributed to supra-lithospheric (orogenic) loading because of the Variscan Mountains (Fig. 2.1). However, for subsidence trends in northern England and Scotland to also be attributed to these forces, an unrealistically high value for lithospheric rigidity or effective elastic thickness (T_e) would most likely be required. Besly (2019) tentatively suggested that accelerated rates of late Carboniferous subsidence in northern Britain and parts of the southern North Sea could be attributed to various phases of intra-Carboniferous deformation. However, in this study the timing of widespread phases of compressional and transpressional deformation have been constrained in northern Britain (Fig. 9.2) and limited syn-depositional deformation during one of the periods of most clearly accelerated subsidence, during Langsettian to (early) Duckmantian times, has been found (Fig. 9.1).

In retro-arc foreland settings, subsidence may be modified as a response to both supra-lithospheric (orogenic) loading (Fig. 9.7a) but also to sub-lithospheric (dynamic) loading due to the
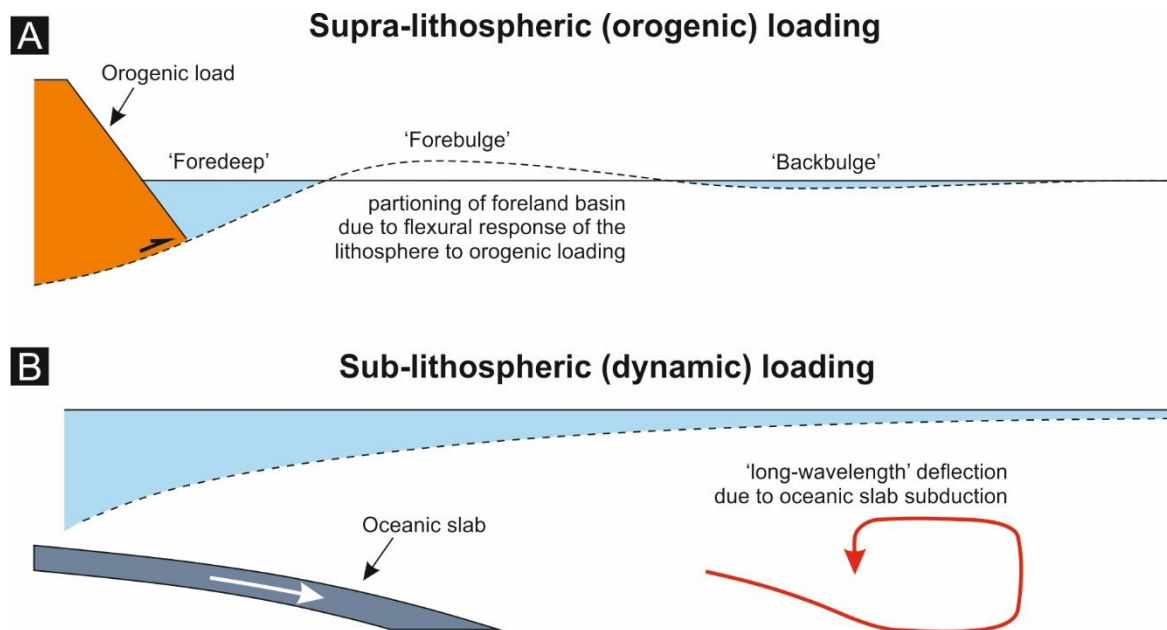
Figure 9.7: Schematic illustrations of regional (geodynamic) subsidence mechanisms in retro-arc foreland basins (adapted from Cataneanu, 2019). 9.7a: Supra-lithospheric (orogenic) loading. 9.7b: Sub-lithospheric (dynamic) loading.

subduction of an oceanic plate (Fig. 9.7b) (Painter and Carrapa, 2013). The 'foredeep' depocentre, which is caused by supra-lithospheric loading and should not be confused with the combined foreland basin system, can be defined as the area of greatest accommodation immediately adjacent to the orogenic load (DeCelles and Giles, 1996) (Fig. 9.7c). Accommodation in the 'foredeep' is proportional to the rheology and thickness of the underlying lithosphere, and the magnitude of the orogenic load (Watts, 1992; Beaumont *et al.* 1993). Examples of 'foredeep' depocentres developed on more flexurally rigid lithosphere are generally much wider, such as in the Western Canada Basin (<400 km; Cataneanu *et al.*, 1997), and the main Karoo Basin in South Africa (<500 km; Cataneanu *et al.*, 1998). Where the foreland basin system is developed on lithosphere with much less flexural rigidity or highly deformed lithosphere, 'foredeeps' are generally much narrower. Examples include the Alpine "molasse" basins of Europe (<150 km; Homewood *et al.*, 1986; Crampton and Allen, 1995), and foreland systems developed on younger, and therefore less rigid, lithosphere (e.g., Cataneanu *et al.*, 2001).

Cataneanu (2019) describes foreland modification due to sub-lithospheric or 'dynamic' loading, as being of greater *wavelength* than modification due to orogenic loading as the effects are felt more widely, at 'continental' scales (*cf.* Mitrovica *et al.*, 1989; Waschbusch *et al.*, 1996; Cataneanu *et al.*, 1999).. The effects of 'dynamic' subsidence are considered independent from supra-lithospheric loading. The width of modification to the foreland due to 'dynamic' subsidence is a function of the age of the subsiding oceanic lithosphere. Younger oceanic lithosphere is hotter and more buoyant, and therefore subsides at a shallower angle, effecting a wider area of the overlying foreland basin, progressively further away from the convergent plate boundary (Beaumont *et al.*, 1993). Based on isochronous thickness maps, Painter and Carrapa (2013) suggest that the area of foreland influenced by dynamic subsidence of magnitude >300 m over 5 My in the North American Cordillera foreland basin well exceeded 700 km, perpendicular to the subsided oceanic slab. Based on numerical modelling experiments that are applied to the Andean foreland basin in South America, Gianni *et al.* (2018) predict a region of approximately 500 km wide, perpendicular to the oceanic slab, where subsidence due to 'flat-slab subduction' exceeds 1 km, which is centred approximately 750 km away from the convergent plate boundary. Conversely, far milder subsidence, <500 km, centred along the plate boundary is predicted when assuming a normal angle, 30 °, of subduction (Gianni *et al.*, 2018).

9.4.2.2 Potential foreland regional subsidence mechanisms

Recent age constraints from studies on the late Palaeozoic Variscan Mountains suggest an approximately Asturian or early Stephanian (*c.* 310-315 Ma; Murphy *et al.*, 2016) age for the formation of the Iberian and Cantabrian oroclines in present-day Spain and Portugal. Prior to this event, it is likely that a Palaeo-Tethyan oceanic slab subsided along the southern margin of Iberia to the north beneath central and NW Europe (Fig. 9.7c), as it was ultimately the final collision of Gondwana to the south of Iberia that prompted the formation of these oroclines (Fig. 2.1). At present day, this convergence zone is approximately 2000 km from central Scotland. Although, opening of the Bay of Biscay during Cretaceous times is likely to have increased this distance by several hundred kilometres (García-Mondéjar, 1996). Even during periods of comparative tectonic quiescence and limited intra-foreland deformation, sub-lithospheric (dynamic) loading could have contributed to accelerated late Carboniferous subsidence rates during late Namurian and early to

middle Westphalian times in northern England and Scotland (*cf.* Kombrink, 2008), if comparable 'flat-slab' oceanic subduction were to be assumed (e.g., the Andean foreland basin in South America; Gianni *et al.*, 2018). If 'flat-slab' oceanic subduction were considered unlikely, then the regional accommodation of hundreds of kilometres of sediment in northern England and Scotland due to 'dynamic' subsidence would perhaps be doubtful. Any alternative subsidence mechanism is unlikely to have incorporated the reactivation of faults, given that the periods of greatest accommodation rates occur during phases of relative tectonic quiescence (compared Figs. 9.1 and 9.2) and that accelerated late Carboniferous subsidence was so widespread (Fig. 9.1). These regional subsidence trends, throughout the English Midlands, northern England and Scotland, remain an area of key uncertainty.

The influences of supra-lithospheric (orogenic) loading from so-called External Variscan thrust nappes that crop out in South Wales, approximately 450 km from central Scotland, could more simply help explain marked thicknesses for latest Carboniferous (Westphalian D) sediments across the British Isles (Fig. 9.4). South Wales and parts of the English Midlands could be described as having occupied the more proximal 'foredeep' part of the Variscan foreland system during Asturian times (Fig. 9.7a), having accumulated <1 km of sediment in parts during these times (Fig. 9.4). Conversely, central Scotland and parts of northern England could be considered part of the more distal 'forebulge' or 'backbulge' part of the Variscan foreland system (Fig. 9.7a), having accumulated only tens of metres or no sediment at all (Fig. 9.4).

Regional interpretations based on subsidence trends are made with a significant caveat. Structural mapping-based investigations described in this thesis reveal marked lateral accommodation variations (Figs. 7.5 and 8.4), which may mask regional subsidence trends related to geodynamic processes. Bolsovian (Westphalian C) sediment thicknesses are more difficult to make sense of regionally (Fig. 9.4), perhaps because the deposition of these sediments succeeded one regional phase of intra-basin deformation and folding (Fig. 9.2). Further investigations using these data should be mindful of this pitfall (*cf.* Leeder and McMahon, 1988).

9.4.3 Structural and geodynamic controls on late Carboniferous red-beds

Borehole penetrations of the late Carboniferous succession in the MVS encounter a progressively reddened sequence upwards through the SUCM Formation (Fig. 8.1). Similarly, Jones and others (1993, 2006, 2011) describe progressively redder Warwickshire Group strata, upwards in the Canonbie Coalfield and in West Cumbria (Fig. 7.3). Two contrasting theories have been developed to explain the origin of late Carboniferous red beds (Besly *et al.*, 1993). Studies on the red bed sequences of the English Midlands have shown that for much of these strata, reddening or oxidisation occurred at, or soon after, deposition partly because of an arid or semi-arid climate (Besly and Turner, 1983; Besly, 1988). Syn-depositionally formed red beds of this type typically contain iron oxide and/or caliche type within well-drained palaeosols. Red-bed heterogeneity may result from changes in the degree of drainage, redox conditions or pattern of pedogenesis immediately following deposition (Besly *et al.*, 1993). An alternative view is that red beds within the uppermost Carboniferous succession were formed because of penetrative early Permian weathering following basin inversion (Mykura, 1960). In this scenario, all organic material is destroyed, and siderite concretions and cements are replaced by haematite (Glennie, 1970). For the late Carboniferous red-beds of Scotland, the latter view is preferred (Mykura, 1967). Red beds formed in this way may reach thicknesses up to several hundred metres beneath weathering surfaces, depending on the depth of penetration of oxidizing conditions. However, this mechanism may not provide a satisfactory explanation for the occurrence of thick, inter-bedded and reddened mudstones, which are comparatively impermeable and less susceptible to this type of penetrative weathering, several hundred metres beneath any regional unconformity in the MVS (Figs. 8.12 and 8.13) (*cf.* Jones *et al.*, 2011).

Besly (1988) suggests an orogenic influence on syn-depositionally formed late Carboniferous red-bed sequences in central England, a view that is shared by Jones and others (2011) about contemporaneous red-beds in the Canonbie Coalfield (Fig. 9.3c). It is suggested that the Variscan Mountains prompted a rain shadow effect and aridification in the Carboniferous basins to the north (Fig. 2.1). The beginning of early Bolsovian aridification correlates strongly with one phase of accelerated basin wide deformation suggested in this thesis (Fig. 9.2). It is unclear how widely felt

such a rain shadow effect may have been felt, or what, if any, sort of a delay to this sudden climate change in northern England and Scotland in comparison with central England could be anticipated. The overall northward drift of NW Europe during late Carboniferous and early Permian times, and the closure of Palaeothethys oceanic circulation, is likely to have prompted additional and perhaps less dramatic aridification during these times as well. In the absence of palaeosol samples belonging to the late Carboniferous succession of Scotland, these questions highlight the benefits of preserving subsurface core samples. Following the decline of the UK's coal industry, limited core samples penetrating the concealed late Carboniferous succession in the eastern part of the MVS remain. Few of these limited samples are taken within the comparatively 'barren' SUCM Formation, given the formation's largely poor fossiliferous content or economic importance. Therefore, it is difficult to determine whether these red-beds are primary or secondary in origin, and difficult to determine possible syn-orogenic influences on these deposits. Nevertheless, changes to late Carboniferous climate could be considered one additional and important geodynamic influence on late Carboniferous sedimentation in northern England and Scotland.

9.5 Comparisons with analogous basins

Based on the findings presented in this part of the thesis, it is suggested that syn-depositional basin inversion, accelerated subsidence rates and changes in sediment supply associated with basin inversion strongly influenced late Carboniferous sedimentation in northern England and Scotland. These findings provide evidence that suggests that the late Carboniferous basins of northern Britain did not perfectly conform with a rift-sag tectonostratigraphic framework, comparable with the Aegean or Tyrrhenian seas for example (*cf.* Leeder, 1982) (Fig. 6.1). Similarly, it is suggested that depicting northern England and Scotland as having resided within a widespread NE-SW wrench zone (e.g., Read and Forsyth, 1989) (Fig. 6.2) is still too simplistic to begin explaining some of the transient and complex structural and geodynamic influences on sedimentation in this part of the British Isles. However, northern England and Scotland, which were situated in what could be described as the distal part of Variscan foreland system, display some similarities with 'broken' forelands (e.g., Bilmes *et al.*, 2013) (Fig. 9.8).

Whereas, traditionally, foreland basins have been described simply as narrow (several hundreds of kilometres) and uninterrupted depocentres that are controlled by supra-lithospheric loading and flexural isostasy (Beaumont, 1981), foreland *systems*, as described by Cataneanu (2019), integrate continental-scale controls on intra-basin deformation, sediment supply, 'dynamic' subsidence, and climate. These controls are exerted well beyond the downwarped area of basin immediately adjacent to a collision zone or 'foredeep'. In 'broken' foreland systems, palaeodrainage, sediment routing and subsidence trends are frequently disrupted by uplifted intra-basin blocks due to deformation relating to the adjacent orogen (e.g., Strecker *et al.*, 2011). The archetypal example of this type of basin is the modern 'broken' Northern Patagonian foreland in Argentina, which is adjacent to the Andean Mountains (Bilmes *et al.*, 2013; Gianni *et al.*, 2015; Lopez *et al.*, 2019; Bucher *et al.*, 2020) (Figs. 9.8a and c). A similar example can be found in the Laramide Province of the western USA (e.g., Bader, 2019). Like the late Carboniferous depocentres described at the Canonbie Coalfield and in the eastern part of the MVS, in South America, several narrow Quaternary-aged depocentres that have been prompted by reverse reactivation of inherited basement structures exist oblique to the predominant collision zone, and some up to 1000 km away from the convergent plate boundary (Gianni *et al.*, 2015). These depocentres are defined by comparatively uplifted intra-basin blocks that have been reactivated contemporaneously with Andean collision, after having initially formed as earlier Mesozoic rift basins (Bilmes *et al.*, 2013) (Fig. 9.8c). Chronostratigraphic correlations for Westphalian and Stephanian unconformities across the British Isles strongly suggest that syn-depositional deformation, at these times, were responses to Variscan collision (Fig. 9.2). As with reactivation in northern England and Scotland, the style of deformation and depocentres are strongly controlled by inherited basement fabric and fault architecture (Bilmes *et al.*, 2013). The (Neogene) syn-kinematic sedimentary sequence of the South American foreland is characterised by stratigraphically frequent angular unconformities, and evidence of complex sediment routing and palaeodrainage systems (Lopez *et al.*, 2019).

Late Carboniferous subsidence rates and sediment thickness variations for the Asturian (Westphalian D) succession in South Wales and the English Midlands strongly suggest foreland-type (supra-lithospheric) geodynamic influences on subsidence, in response to the Variscan Orogeny

(*cf.* Burgess and Gayer, 2000) (Figs. 9.8b and d). At this time, northern England and central Scotland are likely to have occupied the distal part of the (Variscan) foreland system (*cf.* DeCelles and Giles, 1996), and, consequently, accommodated comparatively little sediment. The contrasting styles of local basin inversion reported in Chapters 7 and 8 provide additional context on less regionally consistent deposition. Some of the puzzling Bolsovian (Westphalian C) thickness trends in the English Midlands (Fig. 9.4) may yet be partly accounted for by inconsistencies in local basin inversion style, as they have been in this thesis for the Canonbie Coalfield and the (eastern) MVS. Without further research, the potential influences of 'dynamic' subsidence from the subduction of the Palaeotethyian plate, along the southern margin of Iberia, are highly uncertain. Numerical modelling and evidence-based investigations suggest that 'flat-slab' style oceanic subduction is more likely to favour 'dynamic' subsidence at scales sufficient to accommodate sediments comparable with the Scottish and Pennine Coal Measure groups in northern England and Scotland, and up to 1000 km away from the convergent plate boundary (Painter and Carrapa, 2013; Gianni *et al.*, 2018). At present, central Scotland is approximately 2000 km from the southern margin of Iberia, although the Cretaceous opening of the Bay of Biscay and other phases of lithosphere extension are likely to have increased this distance since late Carboniferous times (García-Mondéjar, 1996). Even so, 'flat-slab' subduction typically requires younger, and therefore hotter and more buoyant, oceanic lithosphere. The Nazca plate, which is subsiding beneath South America, is relatively young at <50 My old (Sánchez *et al.*, 2019). Not enough is known about the nature of the Palaeotethyian plate as it subsided beneath southern and central Europe during late Carboniferous times to consider this possible control on regional subsidence likely.

Classically interpreted foreland basins are typically depicted as being dominated by a sediment supply derived almost exclusively from an adjacent collision zone (Homewood *et al.*, 1986). Basin geometry in the so-called 'forebulge' depozone may, therefore, determine sediment supply to the distal part of the basin (e.g., Cataneanu, 2019). By contrast, sediment supply in northern England and Scotland is unquestionably dominated by a north-easterly hinterland. This hinterland may be considered independent from Variscan influences, in the south, although the role of a

dissipating stress field derived from the Variscan Mountains in determining uplift and erosion rates here may remain significant.

The pre-Westphalian history of syn-depositional deformation in the northern Pennine Basin and Scotland appears not to correlate with Variscan deformation. Despite accelerated rates of late Carboniferous subsidence in northern England and Scotland, subsidence prior to this does appear to fit within an exponentially decaying 'McKenzian' (1978) post-rift trend (Fig. 9.1). Some of the local variations in early Westphalian accommodation respond to varying thicknesses and compaction rates of early Carboniferous (rift) basin fill (*cf.* Collier, 1989). As discussed in Section 9.4.3, the role of a collision zone in determining late Westphalian climate fits within a foreland basin-type model (*cf.* Besly, 1988). More research is required in central Scotland, to determine the origin and palaeogeographic implications of the late Carboniferous 'red-beds' here (Jones *et al.*, 2011). However, the effects of orogens on climate are rarely discussed within the contexts of ancient foreland systems (*cf.* Cataneanu, 2019). Perhaps this additional case study could help challenge some more generic depictions of foreland systems.

Whilst no regional depositional model is flawless, this should not detract from their value. Leeder's (1982) initial depiction of the Pennine Basin as a rift-sag basin provided some much-needed regional context to the Carboniferous succession of the British Isles and allowed many to re-interpret this system. Many of the studies that leant heavily on Leeder's interpretation have since helped unlock significant economic potential within Carboniferous bedrock across northern England, Scotland and the remainder of NW Europe (e.g., Fraser and Gawthorpe, 1990, 2003; Andrews *et al.*, 2013; Busby, 2014). Likewise, a comparison between the late Carboniferous basins of the British Isles and some popular examples of foreland systems is not flawless, but it provides a fresh framework from which geologists can investigate and exploit Carboniferous strata. The work in the succeeding chapter of this thesis highlights the importance of understanding Carboniferous rocks on regional scales and will discuss some of the economic implications of the findings presented thus far in this thesis.
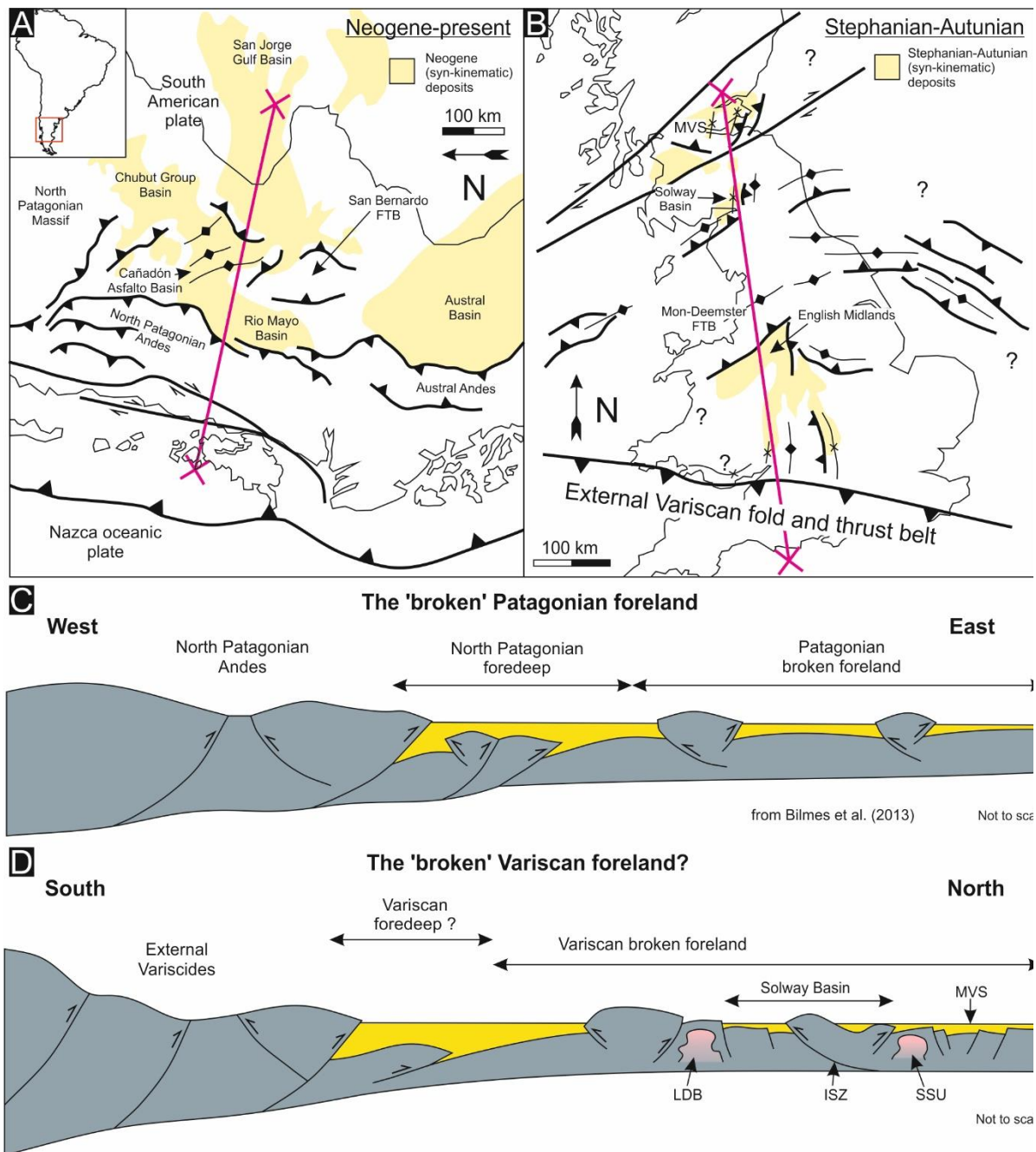
Figure 9.8a: A plate tectonic setting map for the North Patagonian Andes and the North Patagonian broken foreland (based on Gianni *et al.*, 2015). 9.8b: A Stephanian-early Permian (Cisuralian) palaeogeographic reconstruction of the Variscan foreland basin system of the British Isles, based partly on Peace and Besly (1997) and findings presented in this study. 9.8c: A schematic cross-section of the North Patagonian Andes, the North Patagonian fold and thrust belt (FTB), North Patagonian foredeep and the North Patagonian broken foreland (from Bilmes *et al.*, 2013). 9.8d: A schematic late Westphalian reconstruction of the Variscan collision zone, external Variscides, Variscan fordeep and the northern British broken foreland. LDB = Lake District Block; ISZ = Iapetus Suture Zone; SSU = Scottish Southern Uplands; MVS = Midland Valley of Scotland.

9.6 Conclusions

In contrast with classically depicted exponentially decaying rates of post-rift, Carboniferous subsidence in northern England and Scotland accelerates from middle-late Namurian times and throughout the Westphalian. Three phases of accelerated late Carboniferous syn-depositional deformation are correlated across northern England and Scotland, the last two of which coincide with regional deformation across the British Isles that is associated with the Variscan Orogeny. All phases of deformation are succeeded by temporarily increased amounts of clastic sediment supply to the basins of northern England and Scotland. The regional depositional trends discussed in this chapter, and the more local depositional and structural trends discussed in the preceding two chapters, help inform an original structural and geodynamic model for the late Carboniferous basins of the British Isles. It is suggested that northern England and Scotland formed part of an expansive 'broken' Variscan foreland *system* during late Carboniferous times. Like the 'broken' North Patagonian foreland in South America, late Carboniferous sedimentation in northern England and Scotland was partially determined by both (regional) isostatic responses to the Variscan Orogeny, and localised basin inversion, although key areas of uncertainty still remain.

Part IV

Deep geothermal energy in northern England and

thesis synthesis

Deep geothermal energy in northern England: insights from 3D finite difference temperature modelling

This chapter is based on a publication of the same name:

Source code availability

Matlab-based source code for the work presented in this chapter can be downloaded for free at https://github.com/lphowell/Geothermal-Modelling/tree/master/Geothermal_NEngland

10.1 Introduction

Over the past century, coal, including that sourced from the Canonbie, Fife and Midlothian coalfields, fuelled the bulk of the UK's power and heating. Due to both the increased availability of domestic natural gas and the UK's recent effort to decarbonise its energy supply, this is no longer the case. On the contrary, the use of coal is widely condemned by western media as coal is now regarded as the 'dirtiest' fossil fuel because of the associated CO_2 and other pollutant emissions. However, UK coal mining has left a legacy of abandoned infrastructure that has the potential to be repurposed as the UK seeks to further decarbonise its energy supply (Andrews *et al.*, 2020). At the time of writing, the British Geological Survey are constructing and operating a research site in Glasgow to further understand the potential of water from abandoned coalmines for geothermal energy (Watson *et al.*, 2019). Coupled CO_2 sequestration and enhanced coal bed methane recovery offers a further, if riskier, low carbon subsurface energy prospect for northern England and southern Scotland (Jones *et al.*, 2004). This technology remains in its infancy, although the Canonbie Coalfield

itself was investigated as recently as 2015 for coal bed methane purposes. Development plans were abandoned due to, amongst other factors, the 'structural complexity' of the coalfield.

In the next part of this thesis (Part IV), some of the key findings presented within the preceding chapters of this thesis are discussed along with their importance in terms of some of the economic and societal challenges we face during the 21st century. Given that one of today's most significant challenges concerns our collective fight against the increasing effects of climate change, part of this discussion will also focus on one possible way of exploiting Carboniferous bedrock more sustainably to meet energy demands, through deep geothermal energy.

10.2 An introduction to deep geothermal energy and predictive subsurface temperature modelling

Deep (>1 km) geothermal may provide one alternative energy resource as part of a worldwide effort to reduce our reliance on fossil fuels and combat climate change (Zhang *et al.*, 2019). Nonetheless, the UK lags behind its neighboring north-western European counterparts with regards to harnessing its deep geothermal potential. This is reflected by the fewer number of geothermal boreholes drilled (Gluyas *et al.*, 2018), the smaller contribution of geothermal towards the combined energy mix (BP Energy Outlook, 2019), smaller research output, as well as the now somewhat outdated subsurface temperature and heat flow maps for the UK (e.g., Downing and Gray, 1986a, 1986b; Lee *et al.*, 1987; Busby, 2010, 2014; Busby *et al.* 2011) (Fig. 10.1). These maps are commonly constructed by contouring around sparsely distributed and sometimes unreliable data points (Rollin, 1995), rendering them often irresolute and inaccurate. Despite increasing interest in UK geothermal, as several recent and ongoing projects testify to (Younger *et al.*, 2016; Adams *et al.*, 2019; Monaghan *et al.*, 2019; Paulillo *et al.*, 2020), the reliance on these quasi-resource maps remains a cause for concern.

Where data is either sparse or unreliable, predictive modelling may comprise a useful tool (Pérez-Zárate *et al.*, 2019). Numerically based 3D regional subsurface temperature models help communicate regional geothermal potential (e.g., Cacace *et al.*, 2010; Calcagno *et al.*, 2014; Fuchs and
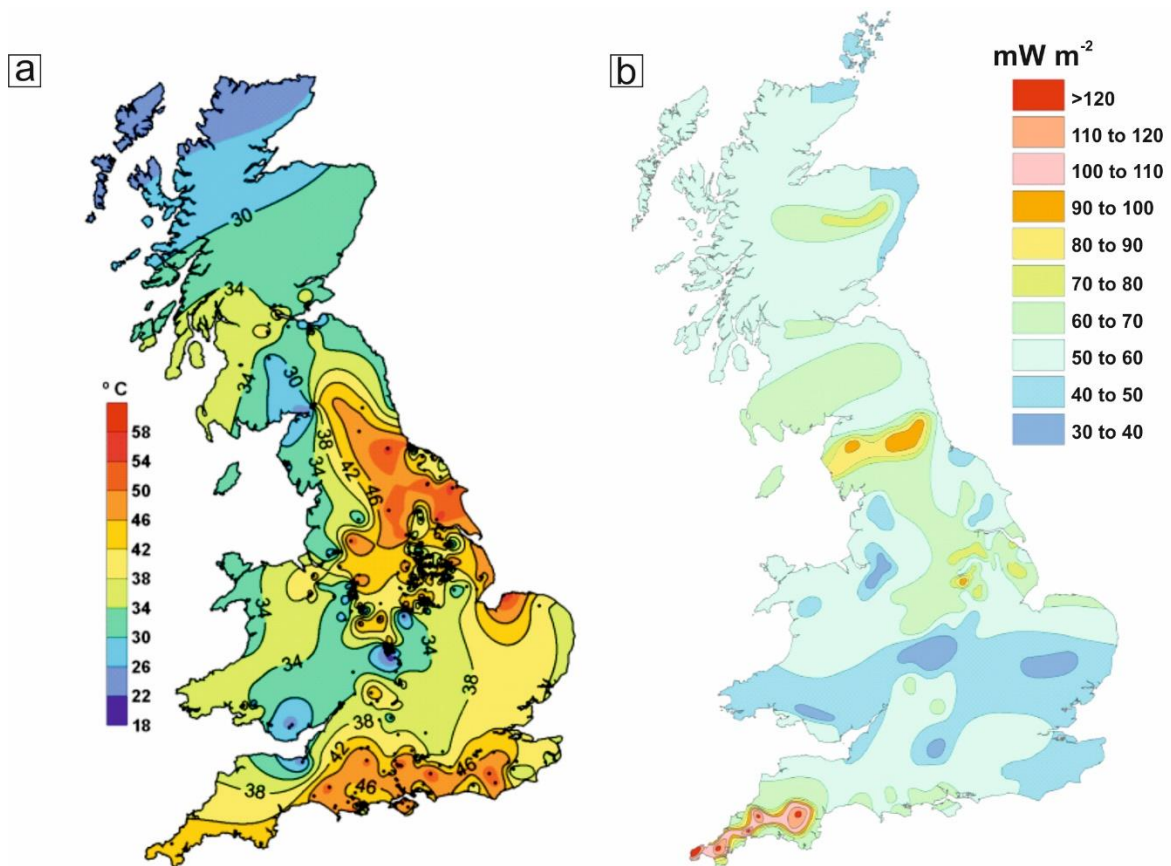
Figure 10.1a: UK subsurface temperature maps for 1 km depth (from Busby *et al.*, 2011). 10.1b: UK heat flow maps (after Downing and Gray, 1986a).

Balling, 2016). Such models typically implement elaborate, but often complex and, consequently, less reproducible finite element techniques (e.g., Cacace and Jacquey, 2017). Finite difference analyses offer less computationally intensive alternatives to these methods. Although the resolution and accuracy of finite difference models are limited by the typically rectangular nodal arrangements of finite difference grids, for smaller problems, such as for the (<1 km) area around a geothermal well head, a finite difference grid can be sufficiently scaled to compromise between both model accuracy and rapid model convergence (e.g., Croucher *et al.*, 2020; Keller *et al.*, 2020). Finite difference techniques are also adopted for subsurface temperature problems where the geological uncertainty is greater than the model resolution, such as for the deep lithosphere and mantle (e.g., Fullea *et al.*, 2009). However, for intermediate scale problems, such as for subsurface temperature and heat flow density mapping (Fig. 10.1), a combination of the, often, inflexible finite difference temperature grids, and the coarse model resolutions required to reduce run times, can render such methods too inaccurate (*cf.* Gibson *et al.*, 2008).

In this chapter, an innovative 3D finite difference thermal modelling method is presented and used to predict deep subsurface temperature and heat flow density in northern England. Due to the averaging techniques described for thermal conductivity and radiogenic heat production, the resolution of the adopted geological model is effectively far greater than the temperature model's coarse nodal spacing. Consequently, the accuracy of the model is not compromised to reduce computational intensity. Formulae for 3D steady-state conductive heat transfer is documented and MATLAB script and data files can be accessed via the web link provided at the beginning of this chapter. Comparisons are made between results from the simulations presented in this chapter and measured borehole temperatures and heat flow densities. This technique replicates some key influences of complex geological structure on subsurface temperature distribution. Its main strengths are its robustness, simplicity and reproducibility relative to more elaborate finite element techniques. Compared to other finite difference techniques, the methodology presented offers higher resolution and geologically more realistic solutions. The UK's first deep 3D temperature model and associated geothermal resource maps are presented.

10.3 A history of geothermal exploration in northern England

The study area for these temperature simulations is in northern England and comprises the northern part of the Lake District, the north-east of England and the Scottish borders (Fig. 10.2). The primary energy demand for this region is roughly along the north-east coast and includes Newcastle-upon-Tyne, South Shields and Sunderland. Besides Carlisle, the remainder of the study area is amongst the most sparsely populated areas of England. Ideally for the purposes of this study, this is an area that has had widely documented but ultimately unsuccessful geothermal exploration.

In the mid-2000s, drilling of the Eastgate boreholes, County Durham (Fig. 10.2), sought to exploit one of the major deep geothermal plays of the region, the ancient Caledonian 'hot dry rock' granite (Manning *et al.*, 2007). Drilled to a depth of 995 m, the middle to deep part of the first Eastgate borehole encountered remarkably high permeability, up to 4 Darcy, and naturally fractured granite. An appraisal well, Eastgate-2, confirmed the source of these naturally occurring fractures belonged fault zones associated with adjacent Carboniferous basins (Hirst, 2012). The 1821 m
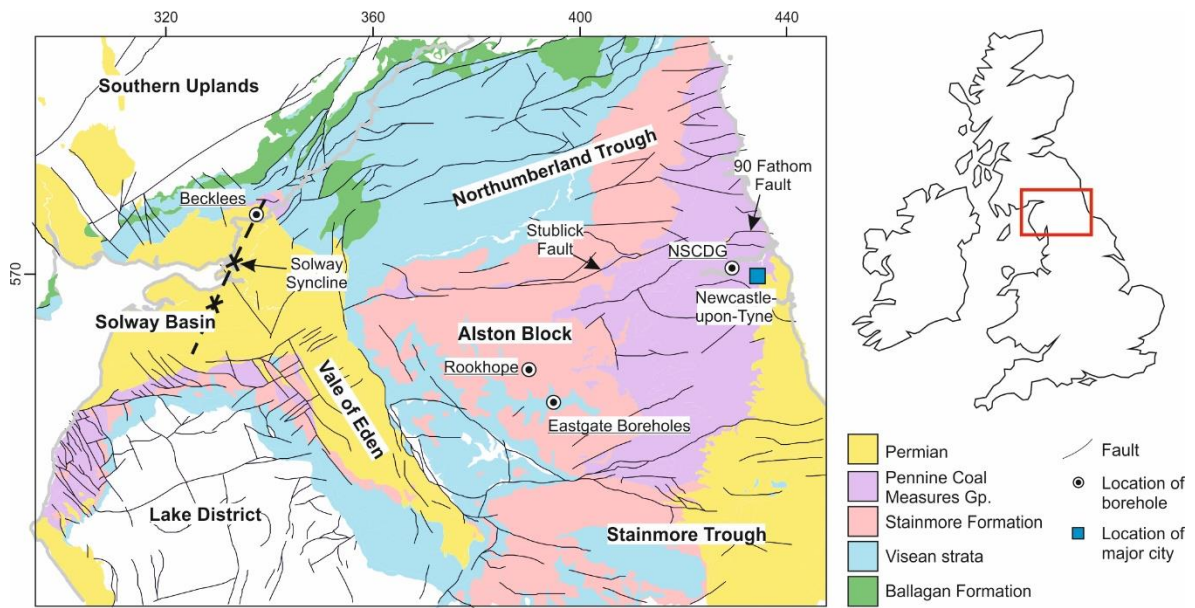
Figure 10.2: A geological map for the area of investigation of this chapter with annotated structural features and borehole locations. Contains BGS DiGmapGB-250 Scale data © UKRI (British Geological Survey, 2008).

Newcastle Science Central Deep Geothermal Borehole (NSCDG on Fig 10.2). sought to exploit porous Carboniferous sedimentary bedrock belonging to the Fell Sandstone Formation, and permeable fault rock associated with the regional Ninety Fathom and Stublick faults (Younger *et al.*, 2016). To the west of Newcastle-upon-Tyne, where the borehole was drilled, temperatures were encountered at depth above the average UK geothermal gradient, but with overall low hydraulic conductivities. Prior to the drilling of these three wells, the Rookhope Borehole, County Durham, was never intentionally drilled for geothermal purposes during 1960-61. Importantly, however, it was amongst the first boreholes to convince the scientific community in the UK that the earth beneath them held significant 'geothermal' potential (Bott *et al.*, 1972), confirming what many local underground coal workers and mineral explorers had suspected previously (Gluyas *et al.*, 2018).

Despite the magnitude of these recent aforementioned investments (Proctor, 2014), what was known about deep subsurface temperature and heat flow in the UK then and what we continue to know now is based upon somewhat outdated quasi-resource maps (e.g., Downing and Gray, 1986a; Busby *et al.*, 2011) (Fig. 10.1). In this study area, for example, maps depicting temperature at 1 km depth are based on contours around just six clusters of temperature data points (Fig. 10.3). These data are situated predominantly within the Carboniferous basins of the region and only two of

these appear to be based on equilibrium measurements (Burley *et al.*, 1984). On further inspection of these maps and the UK Geothermal Catalogue (Burley *et al.*, 1984), heat flow maps for this region are based on contours around just 9 data points (Fig. 10.1b). Based on the type of conductivity and temperature measurement, amongst other factors, Rollin (1995) graded the reliability of these data with quality functions from 0 to 1, with 1 being good and 0 being poor. The highest grade awarded for a data point in the study area was 0.65. Just five data points surpassed 0.25.
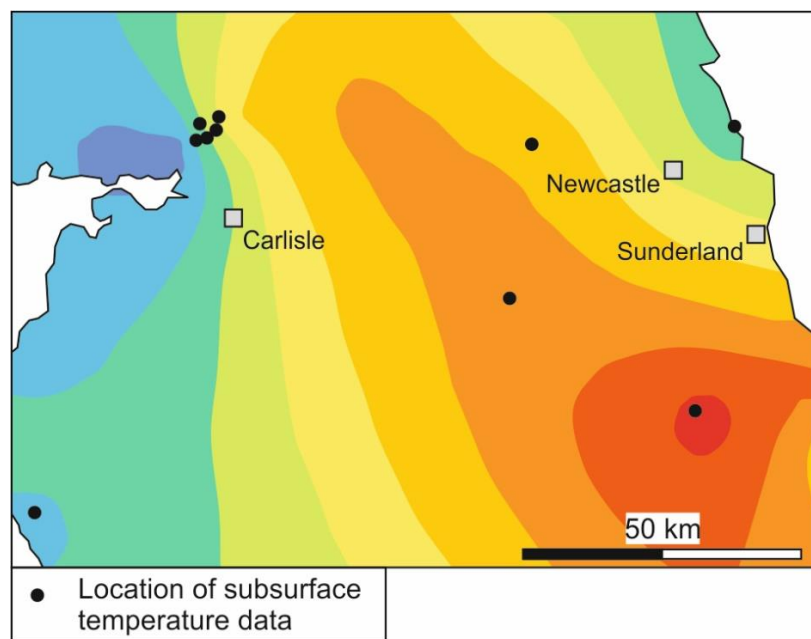
Figure 10.3: Subsurface temperature contours (from Fig. 10.1a) and locations of data points (*cf.* Burley *et al.*, 1984). The spatial extent of the conductivity maps presented here is identical to the spatial extent of the geological map presented in Figure 10.2.

10.4 Geological modelling constraints

A series of surface elevation grids comprise the primary dataset of this study (Fig. 10.4). A structural model of the Carboniferous-Permian basins of the study area is based on the seismic interpretations of Chadwick *et al.* (1995) (*cf.* Terrington and Thorpe, 2013). The structure of pre-Carboniferous basement bound Caledonian granites is based upon the gravity interpretations of Kimbell *et al.* (2010). The bases of these granite intrusions are assumed flat at 9 km depth (*cf.* Kimbell *et al.*, 2010) (Fig. 10.4). The geological model does not include the Cheviot granites or other granites along the Southern Uplands, which are located beyond the northern margin of the study

area. Likewise, the geological model neglects all fault zones within the study area. Surface elevation grids are extrapolated to fill a 110 km by 150 km (wide) volume. The coordinates at which elevation values are given each correspond to separate nodes within the temperature grid and are uniformly spaced at 500 m.
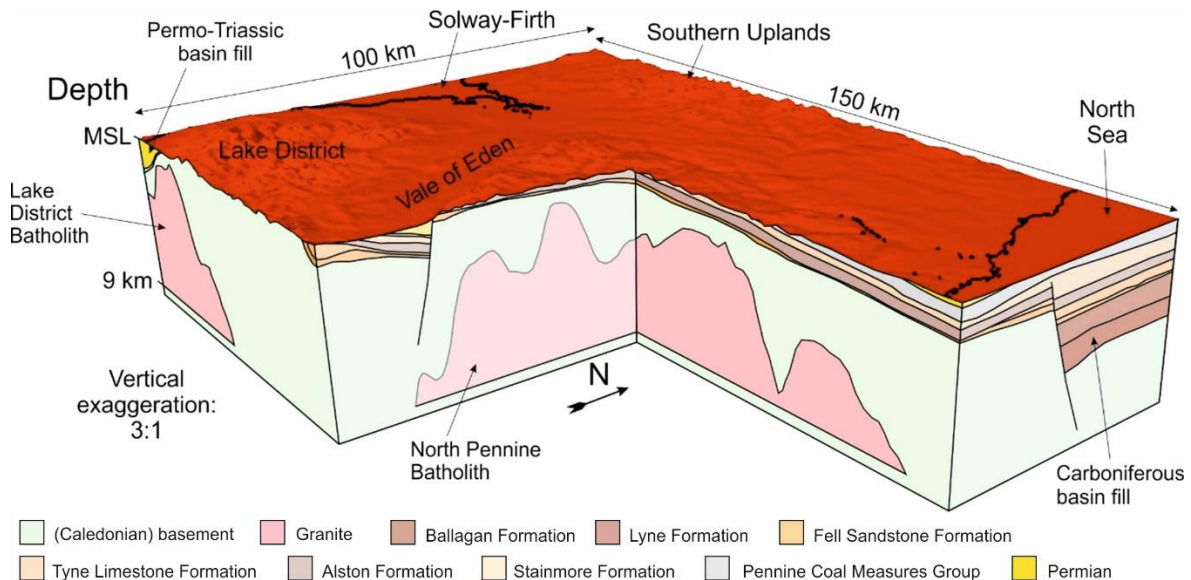
Figure 10.4: A schematic illustration of the 3D geological model. Carboniferous basin structure after Chadwick *et al.* (1995) and Caledonian granite thicknesses after Kimbell *et al.* (2010). As with Kimbell *et al.* (2010), the model assumes flat bases to the batholiths at 9 km depth. This is a simplification of uncertain geology. MSL = mean sea level. The depicted 3D model was produced using Petrel (Schlumberger) software.

Surface elevation grids separate geological units that are assigned distinct thermal properties within my temperature model (Table 10.1). Thermal conductivity of the crust is a function of temperature and pressure, as well as composition (Norden *et al.*, 2020); therefore, conductivity of the middle to lower crust decreases linearly with depth, from 3.1 W m^{-1} K^{-1} at 9 km depth, to 2.2 W m^{-1} K^{-1} at 30 km depth (*cf.* Vilá *et al.*, 2010). Thermal properties for basement rock and basin fill are based on numerous literary sources (Table 10.1). Borehole temperatures for comparison with the modelled subsurface temperature grid are derived from the UK Geothermal Catalogue (Burley *et al.*, 1984) and published literature (e.g., Younger *et al.*, 2016). Typically, finite difference techniques dictate that the thermal property matrices within temperature models are divided into a series of variably sized cuboids, the volume of which are defined by the nodal spacing of the temperature grid (e.g., Fullea *et al.*, 2009). However, in Section 10.5.3, techniques for deriving

more geologically realistic thermal property matrices from geological model are described, whilst still implementing a less computationally intensive finite difference methodology and coarse nodal spacing.

Geological unit	Thermal conductivity (W m⁻¹ K⁻¹)	RHP (µW m⁻³)	Reference
Lower Permian	2.5	1.0	Norden and Förster (2006)
Pennine Coal Measures Group	1.9	0.92	Downing and Gray (1986)
Stainmore Formation	2.38	0.88	Younger *et al.* (2016)
Alston Formation	2.5	0.88	Younger *et al.* (2016)
Tyne Limestone Formation	2.7	0.85	Younger *et al.* (2016)
Fell Sandstone Formation	2.6	0.85	Younger *et al.* (2016)
Lyne Formation	2.7	0.85	Younger *et al.* (2016)
Ballagan Formation	2.92	0.85	Downing and Gray (1986b)
Pre-Carboniferous (Caledonian) basement	2.87	1.49	Downing and Gray (1986b)
Granite Batholiths	3.1	4.1	Downing and Gray (1986b); Manning *et al.* (2007)
Middle-Lower crust	3.1-2.2	1.5	Norden *et al.* (2008); Vila *et al.* (2010)
Mantle	4.1	0.1	Vila *et al.* (2010)

Table 10.1: Regional thermal parameters for temperature simulation. RHP = radiogenic heat production.

10.5 Numerical modelling method

A summary of the adopted modelling approach is illustrated in Figure 10.5. These methods may be amended depending on the characteristics of geological models or the specifications of subsurface temperature models, although the crux of this technique will remain unchanged. It is recommended that the meshing process is treated separately from temperature simulation, to reduce memory drainage and ultimately reduce temperature convergence times.
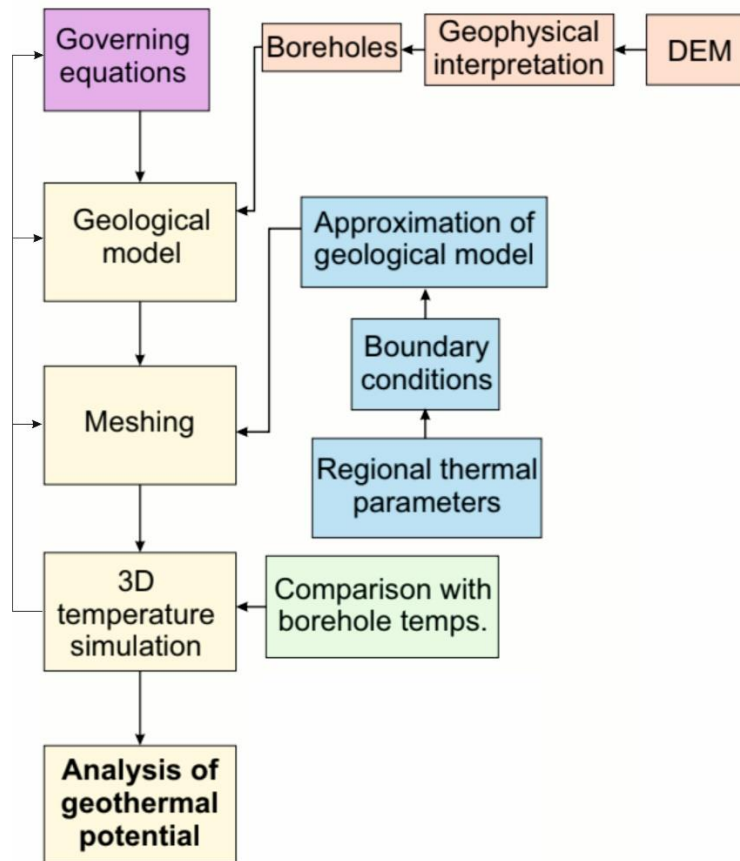
Figure 10.5: An illustrated summary of the numerical modelling approach presented in this chapter. DEM = (surface) digital elevation model.

10.5.1 Governing equations

To calculate subsurface temperature, a steady-state conductive heat equation, or diffusion equation is solved according to Fourier's law. The diffusion equation operates on the basis of energy conservation and relates heat flow (q) to temperature gradients (∇T). In its differential form, it can be given as:

$$q = -k \, \nabla T$$

(Eq. 10.1)

where k is the bulk rock thermal conductivity tensor. Temperature change experienced by each node within the temperature grid is equal to the heat conducted into or out of a node, plus

radiogenic heat production (Q). Thus, the following relationship between change in heat flow (∇q) and time (t) can be determined:

$$(\rho\, c)\frac{\partial T}{\partial t} = -\nabla q + Q$$

(Eq. 10.2)

where ρ is the bulk rock density and c is the bulk specific heat capacity. When Equation 10.1 is substituted into Equation 10.2, the equation for transient diffusion is given:

$$(\rho\, c)\frac{\partial T}{\partial t} = \nabla(k\,\nabla T) + Q$$

(Eq. 10.3)

Under steady-state conditions, any transient effect is neglected. Therefore, the equation can be rearranged further as thus:

$$\nabla(k\,\nabla T) = -Q$$

(Eq. 10.4)

This equation is solved for the temperature using a 3D implementation of the finite difference methodology with algorithms developed using the MATLAB (Mathworks) numerical computing environment.

10.5.2 Boundary conditions and model validation

The solution to Equation 10.4 using the finite difference method requires definition of boundary conditions. For subsurface thermal modelling, an upper boundary (surface) temperature of 10 °C is adopted, in concurrence with UK annual mean average air temperature (Busby *et al.*, 2009). The lower boundary temperature at the base of the model represents a more irreconcilable problem. The base of the lithosphere is at a depth of approximately 125 km beneath much of north-western Europe and is represented by the 1333 °C isotherm (Sclater and Christie, 1980).
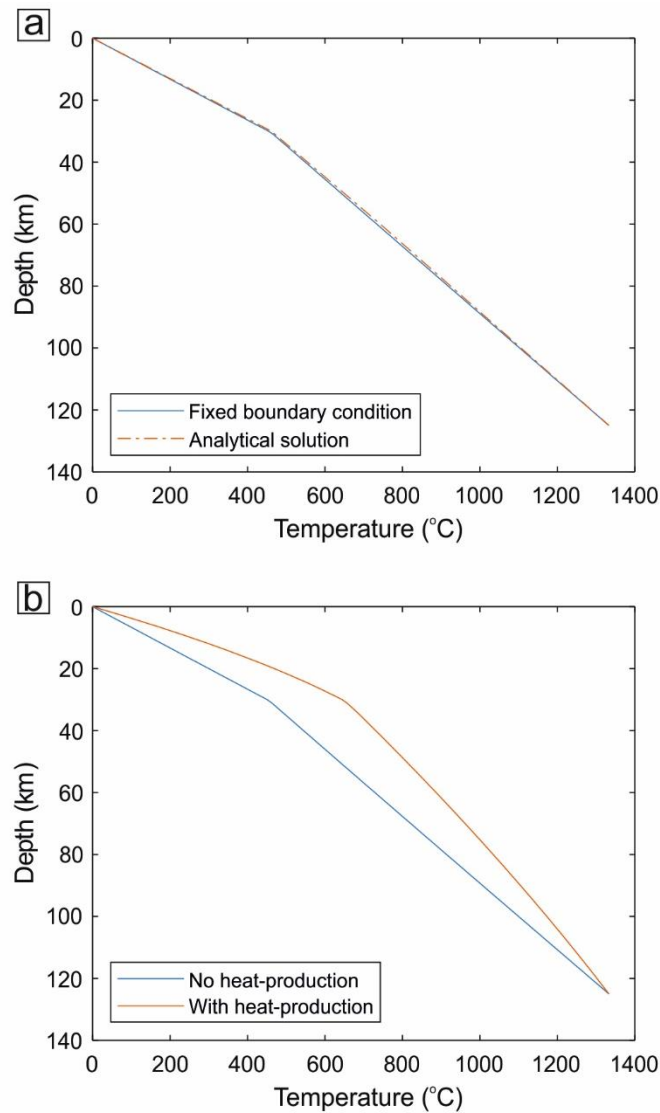
Figure 10.6a: A comparison between analytical and fixed boundary condition solutions for one-dimensional lithosphere-scale non-homogeneous conductive heat flow. See Table 10.1 for modelling parameters. 10.6b: A comparison between fixed boundary condition solutions for one-dimensional lithosphere-scale non-homogeneous conductive heat flow with no internal heat production (Q) and with internal heat production.

To validate the differential solution against an analytical solution in one-dimension and determine the likely lithosphere-scale geothermal structure of the case study area, the linear equation is reiterated until an asymptotic solution, the modelled geothermal gradient, is reached (Fig. 10.6). When adopting a uniform grid spacing of 1 km, the modelled geothermal gradient approaches its steady state solution after approximately 10,000 iterations. To reduce convergence time, the temperature matrix can be populated with a pre-defined temperature distribution (e.g., Bayer *et al.*, 1997) or be thermally conditioned using temperatures from previous model simulations. Besides boundary temperatures, thermal conductivity has a primary control on the geothermal

gradient. The decreased geothermal gradient with depth, after 30 km, reflects the increased thermal conductivity of mantle rock below the Moho boundary relative to crustal rock (e.g., Čermác and Rybach, 1982) (Table 10.1). With the addition of radiogenic heat production, the modelled geothermal gradient forms a convex upwards curve.

The lateral boundaries of the 3D model, in the x and y directions, are closed. Thus $\delta T/\delta x = 0$, and $\delta T/\delta y = 0$. This implies no heat is transferred beyond the lateral boundaries of the model and that these boundaries represent surfaces of symmetry. Neither of these assumptions fit reality but they provide approximations for complex geological structures. To reduce the potentially detrimental effects of these boundaries, a wide aspect model ratio is necessary. Increasing the dimensions of the temperature model to three decreases convergence time by the nodal widths of the model in both the x and y directions, by 150 km and 110 km respectively to fit the geological model of northern England (Fig. 10.3). To reduce computational intensity, therefore, a shallow lower boundary condition of 665.6 °C at 30 km depth is adopted, in concurrence with results from the one-dimensional lithosphere-scale model (Fig. 10.6), and the resolution of the model, in terms of node spacing within the temperature grid, is 500 m.

10.5.3 Approximation of geological model

The shortcomings of a finite difference model relate to its inflexibility. In implementing a finite difference methodology, the value for radiogenic heat production of a single node comprises heat production for the entire cubic rock volume for which that node represents. Likewise, for thermal conductivity, one value calculated between two adjacent nodes represents the combined conductivity for that transect of rock, which is 500 m long in this instance. Therefore, where the modelled rock volume is structurally complex or characteristically heterogeneous, thermal properties for individual temperature nodes may be misrepresentative, rendering the temperature model inaccurate. These issues are exacerbated when coarse model resolutions are necessary, as they are here. Thus, a technique for deriving more representative 3D thermal property matrices from structurally complex geological models is demonstrated.

Thermal properties for distinct points within the bounds of the 3D temperature model reflect the corresponding depths of those points at specific x and y coordinates relative to the depths of geological boundaries in a geological model. Depending on the preassigned distance between temperature nodes (∇i), the corresponding depth of a temperature node in a geological model is determined by:

$$depth = (z - 1)\,\nabla i$$

(Eq. 10.5)

Where z is a reference to the depth corresponding to the position of a given node within the temperature matrix.

Geological boundaries separate the numerous units of the geological model, which are assigned a series of distinct thermal properties (Table 10.1). To avoid removing any of the geological model that is situated above sea level, the depths of geological horizons are given relative to surface elevation.

10.5.3.1 Thermal conductivity matrices

By finding the harmonic mean of multiple thermal conductivity values at uniformly spaced points between the respective nodes (Hantschel and Kauerauf, 2009), resolution issues are overcome for thermal conductivity tensors between adjacent temperature nodes, i.e., $k_{i+1/2}$ and $k_{i-1/2}$. Depending on the interval spacing resolution (res) of sampled k points relative to temperature node spacing (∇i), the distance between these sampling points (ss) is determined as:

$$ss = \nabla i / res$$

(Eq. 10.6)

A resolution 50 times that of the temperature node spacing is adopted so that $ss = 10$ m.

For each node within the temperature matrix there are references to depths of geological boundaries at corresponding x and y coordinates of the geological model. The precision of these depth values is not fixed to the resolution of the temperature model. Therefore, determining thermal conductivity values for distinct points at x and y coordinates between vertically adjacent temperature nodes based on their corresponding depths within a geological model is uncomplicated. However, as inputted spatial data for geological boundaries are limited to the x and y coordinates of the temperature matrix, this exact method may not be applied to determine more representative thermal conductivity tensors laterally in between temperature nodes. To avoid inputting finer and more computationally intensive spatial data for geological boundaries, depths of geological boundaries are interpolated between laterally adjacent temperature nodes. These interpolated depths are used as a basis for determining k values in between laterally adjacent temperature nodes. The harmonic mean of these values may then be determined.

10.5.3.2 Radiogenic heat production matrices

Poor resolutions for Q value matrices are not as detrimental to the accuracy of predictive subsurface temperature models as k value matrices. Nonetheless, more representative matrices of Q values may be attained by adopting similar approaches to those just described for thermal conductivity. Q values are determined for multiple points up to half the temperature node spacing away from a given temperature node in the x, y and z directions, which is 250 m in this instance. This is managed by adopting the same technique for determining k values at points in between temperature nodes in the z direction, and the x and y directions, respectively. The arithmetic mean of these values is then determined (Hantschel and Kauerauf, 2009).

Figure 10.7 illustrates the benefit of deriving more accurate thermal property matrices from geological models in this way. Compared with finding the harmonic mean between just two conductivity values at points corresponding to adjacent temperature nodes (Fig. 10.7b), the more geologically representative thermal conductivity matrix generated by using these averaging techniques is smoother (Fig. 10.7a). Sharp lateral conductivity changes correspond only to steeply dipping beds or fault offsets in the more geologically representative scenario (Fig. 10.7a), rather

than also shallowly dipping beds or the variable dips of beds with vertical thicknesses less than the temperature node spacing (Fig. 10.7b).
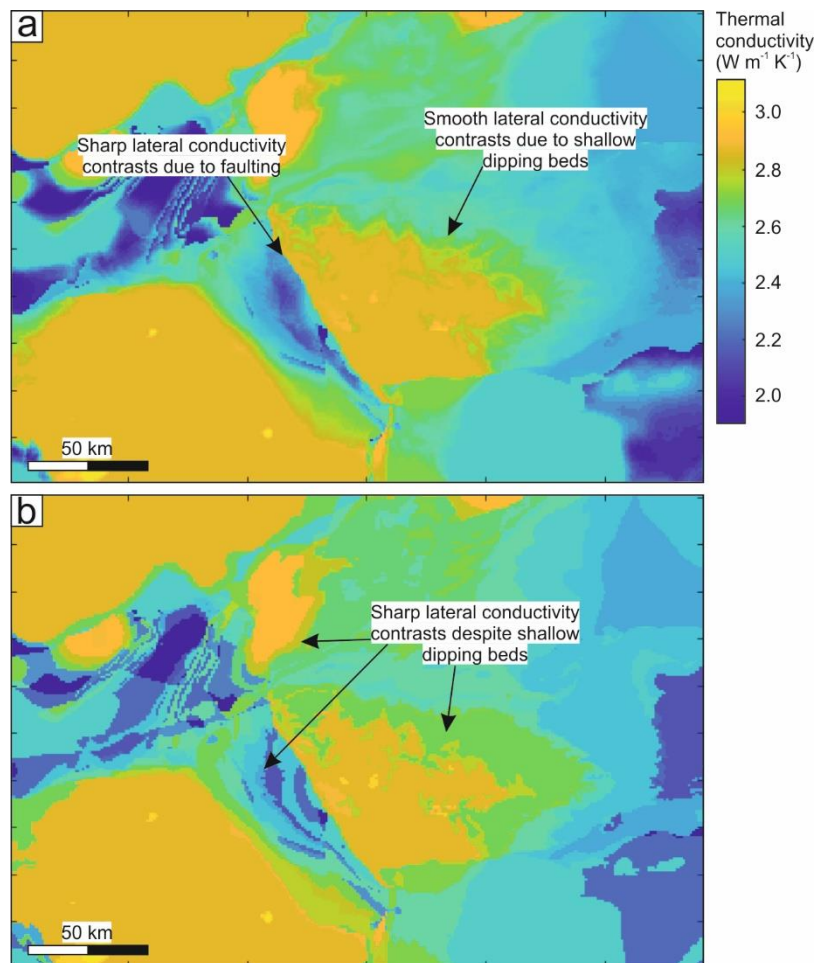
Figure 10.7a: Vertical thermal conductivity tensors between 500 m and 1000 m below surface determined by calculating the harmonic mean of multiple values between these two depths for northern England. 10.7b: Vertical thermal conductivity tensors between 500 m and 1000 m below surface determined by calculating the harmonic mean of just the two values at temperature nodes. For thermal conductivity values of rock units see Table 10.1. The spatial extent of the conductivity maps presented here is identical to the spatial extent of the geological map presented in Figure 10.2.

10.6 3D temperature simulation

The simulated 3D subsurface temperature model reflects the controls of geological structure on vertical and lateral heat transfer and heat production. Temperatures calculated at depths of less than approximately 5 km are influenced by a combination of sedimentary basin fill and heat producing granite intrusions within the basement (Fig. 10.8). At depths greater than 5 km, the basement has a predominant control on temperature distribution. Parts of the model that are less

than 10 km away from the lateral boundaries are ignored, which are more strongly influenced by boundary conditions.

10.6.1 Predicted shallow subsurface temperatures

The dominant 'hot spots' at 1 km depth are situated upon the central part of the Alston Block (Fig. 10.2a), the northern part of the Solway Syncline, the southern part of the Bewcastle Anticline, along the Vale of Eden and along the eastern margins of the Alston Block, and the Stainmore Trough (Fig. 10.8a). The modelled hot spot at 1 km depth on the central part of the Alston Block, where temperatures reach 46 °C, correlates strongly with the North Pennine Batholith (Fig. 10.2b). However, the absence of any such hot spot in the Lake District, which is underpinned by the Lake District Batholith, at 1 km depth suggests that other factors influence this particular hot spot. It is suggested that elevated temperatures on the Alston Block are influenced also by the local, variably thick, and comparatively insulating Carboniferous cover (*cf.* Bott *et al.*, 1972) (Fig. 10.4). This cover thickens towards the east and incorporates progressively younger and more insulating coal-bearing strata. These trends may account for the preservation of greater heat at 1 km depth towards the vertically adjacent eastern margin of the heat producing North Pennine Batholith, despite the eastwards thinning of this structure here (Kimbell *et al.*, 2010).

Owing to the comparatively thick and thermally insulating sedimentary fill preserved in the Vale of Eden Basin and lateral heat transfer from the radiothermal Lake District and North Pennine batholiths, the 3D subsurface temperature model predicts elevated temperatures at 1 km in this region, up to 43 °C (Fig. 10.8a). The parallel, NNE-SSW orientated Solway Syncline and Bewcastle Anticline provide more interesting thermal anomalies at 1 km depth. The northern part of the Solway Syncline is comparatively hot at 1 km depth, up to 43 °C. Towards the south where this structure plunges, modelled temperatures at 1 km decrease to less than 39 °C. Conversely, the northern part of the Bewcastle Anticline is coolest, less than 37 °C, where thermally conductive pre-Carboniferous basement rock is shallowest. Where this structure also plunges to the south and preserves progressively thicker and younger insulating Carboniferous strata, temperatures increase up to 43 °C. Some of these thermal trends may be explained by the non-uniform presence and
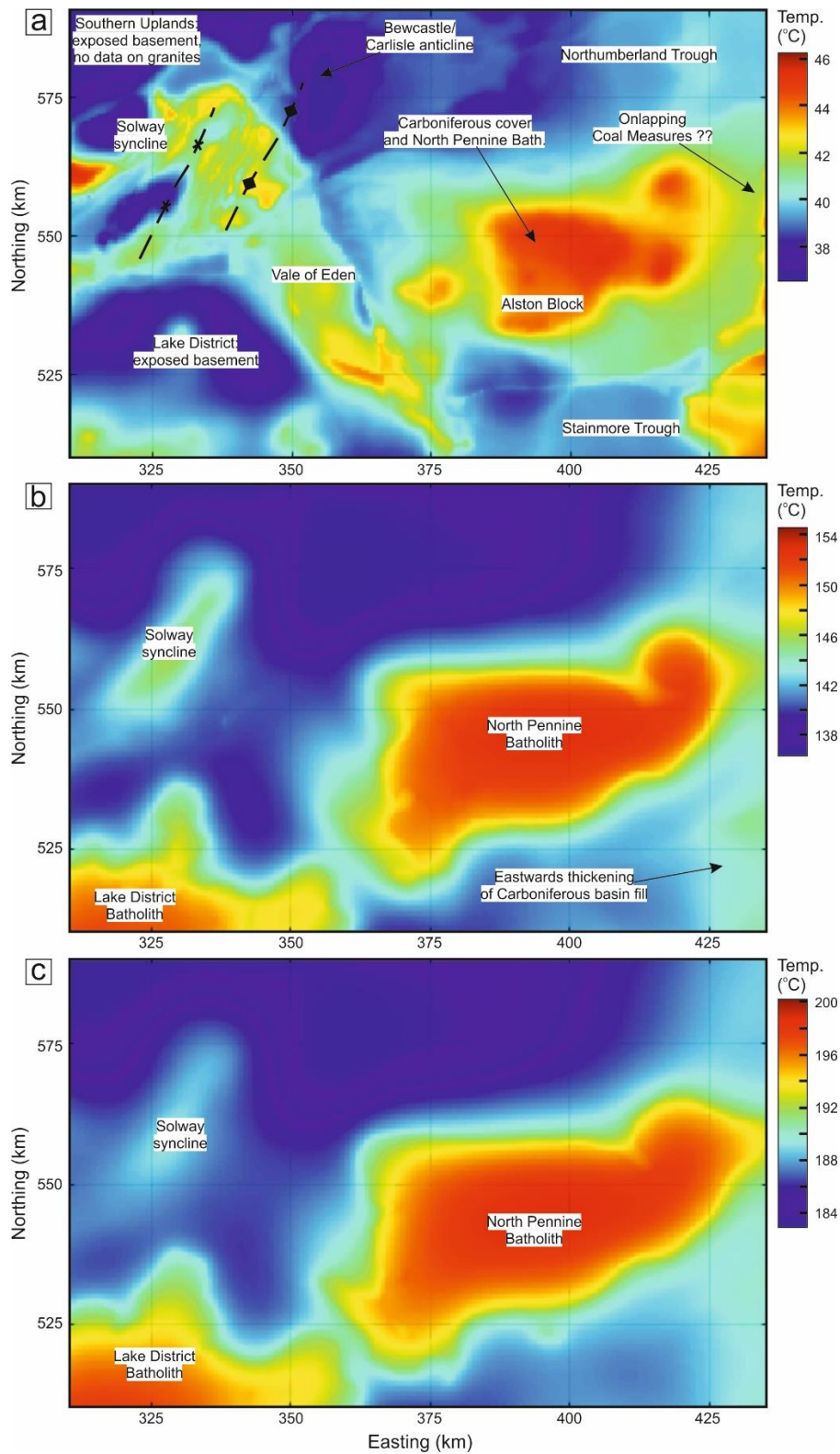
Figure 10.8a: Modelled temperature at 1 km depth. Compare with Fig. 10.1b (Busby *et al.*, 2011). 10.8b: Modelled temperature at 5 km depth. 10.8c: Modelled temperature at 7 km depth. To reduce the effects of boundary conditions on temperature maps, a 10 km width along each of the lateral margins of the temperature model are disregarded.

comparative thicknesses of coal-bearing and thermally insulating strata in this part of the Northumberland-Solway Basin. Some other thermal trends, however, may instead be explained by the vertical distributions of variably conductive rock units within the subsurface and the effects of these distributions on geothermal gradients at different depths. Transitioning from relatively insulating to conducting rock units with depth results in a decreased geothermal gradient with depth. The opposite arrangement results in an increased geothermal gradient with depth. Because the thermally insulating Pennine Coal Measures Group is at depths greater than 2 km to the south of the Solway Syncline, towards where the fold plunges, the geothermal gradient at these depths here is greater. Resulting temperatures at shallower depths, 1 km depth, are less. In contrast, in the northern part of the Solway Syncline, the thermally insulating Coal Measures are at depths between 0.5 and 2 km. As a result, the geothermal gradient is steepest at these depths and temperatures at 1 km are comparatively elevated.

10.6.2 Predicted deep subsurface temperatures

Maximum vertical sedimentary basin thickness in the study area is approximately 8 km. Around these depths, little is known about the characteristics of basin fill (*cf.* Chadwick *et al.*, 1995) so differentiating thermal properties is difficult. The two main hot spots for these depths are associated with the radiothermal Lake District and North Pennine batholiths, where temperatures reach up to 154 °C (Fig. 10.8c). Faintly elevated temperatures at 5 km depth (Fig. 10.8b) are associated with the Solway Syncline and the eastwards thickening of Carboniferous strata within the northern Pennine Basin. At 7 km depth, elevated temperatures associated with the Solway Syncline are diminished further, as the modelled geotherm equilibrates laterally as it approaches the lower boundary condition (Fig. 10.8c). Slight local temperature elevations may be associated with the greater thicknesses of Carboniferous strata towards the east of the study area, up to 190 °C. However, at these depths, any other sources of localized temperature anomalies are dwarfed by comparison with anomalies due to the Lake District and North Pennine batholiths.
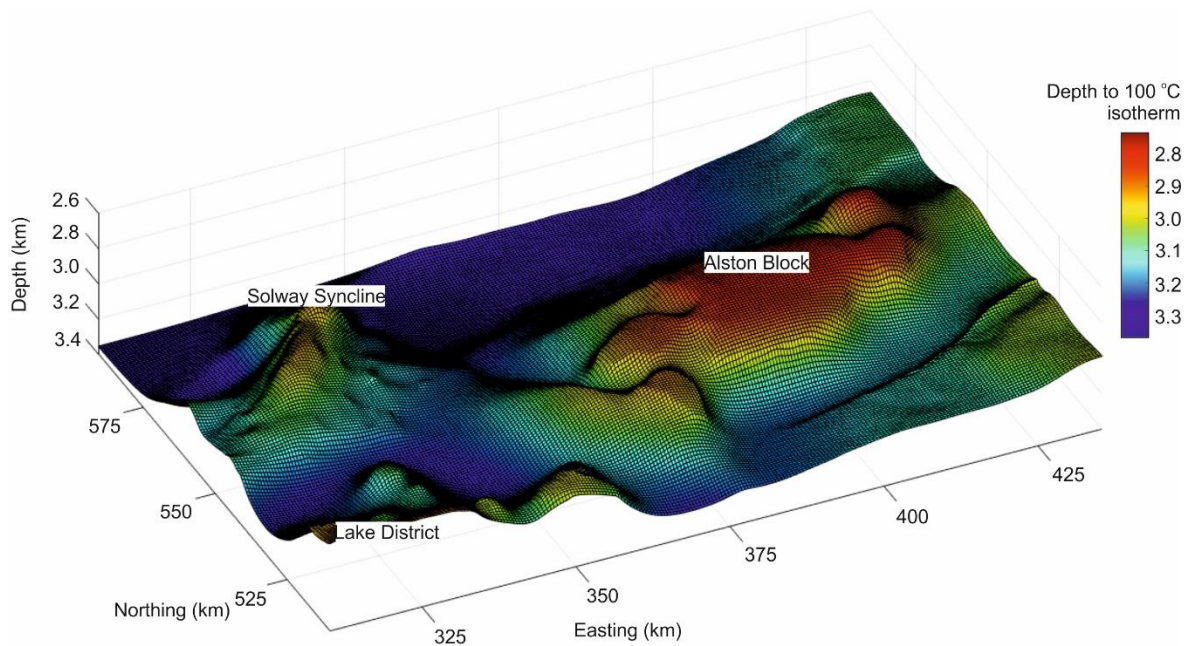
Figure 10.9: Modelled depth to the 100 °C isotherm. To reduce the effects of boundary conditions on the isotherm elevation map, a 10 km width along each of the lateral margins of the temperature model are disregarded.

10.6.3 Predicted isotherm depth

By cubically interpolating vertically between temperature nodes, the depth to the 100 °C isotherm is determined across the study area. The depth to this temperature boundary varies between approximately 2.87 km and 3.51 km below surface in the study area (Fig. 10.9). The modelled isotherm is shallowest in the south-western part of the Lake District, although boundary conditions may exaggerate these shallow depths. The isotherm is also shallower than 3 km in the Alston Block, in the centre of the study area and towards Newcastle-upon-Tyne, suggesting that the two radiothermal granite intrusions within the study area strongly influence these depths. Markedly shallower depths, between approximately 3 km and 3.2 km below surface, for the isotherm are also predicted for the Solway Basin, the Vale of Eden Basin and the eastern part of the study area. In these areas, comparatively thick Pennine Coal Measures Group successions are believed to be preserved. The greatest depths to the 100 °C isotherm are predicted in the western and central parts of the Northumberland Basin and in the Southern Uplands.
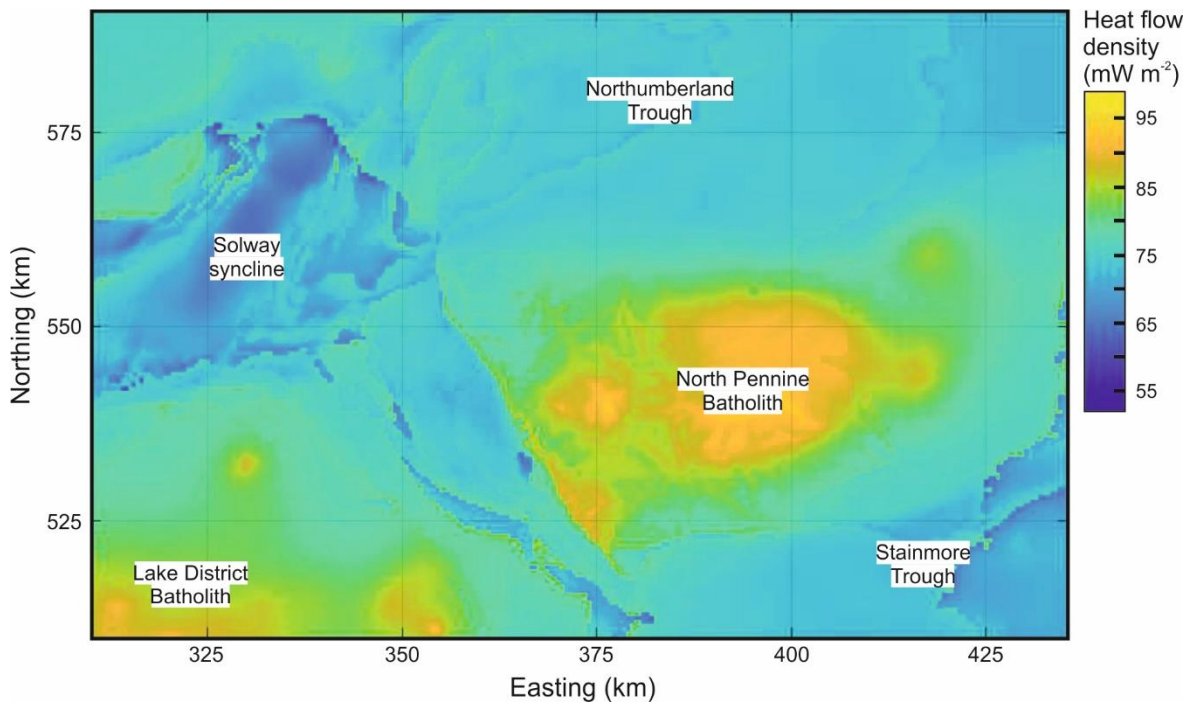
Figure 10.10: Modelled surface (from 500 m depth to the surface) heat flow density map for northern England based on predicted subsurface temperatures and vertical conductivity values. Compare with Fig. 10.1b (Downing and Gray, 1986a). To reduce the effects of boundary conditions on heat flow density map, a 10 km width along each of the lateral margins of the temperature model are disregarded.

10.6.4 Predicted heat flow

The heat flow equation (Eq. 10.1) is solved using the modelled temperature difference (∇T) and vertical thermal conductivity (k) (Fig. 10.7) between temperature nodes at surface and 500 m below surface to determine surface heat flow density (Fig. 10.10). Because the heat flow equation integrates thermal conductivity and temperature gradient, areas where predicted heat flow is comparatively elevated with respect to the remainder of the study area do not perfectly conform to subsurface temperature 'hot spots' (Fig. 10.8). Instead, areas with elevated surface heat flow density correspond to regions where shallow subsurface temperatures and bedrock conductivity are high, such as on the central and eastern parts of the Alston Block and the Lake District. In these areas, predicted surface heat flow exceeds 90 mW m^{-2}. Predicted heat flow in the case study area is more strictly aligned to depositional settings during early Carboniferous rifting (e.g., Howell *et al.*, 2019) than subsurface temperature. Comparatively uplifted pre-Carboniferous basement blocks have overall greater heat flow, whereas deeper basins, which were typically infilled by thermally insulating sedimentary rock, have overall lower heat flow.

10.7 Model verification

To demonstrate the accuracy of the subsurface temperature model, simulated temperatures are compared with further temperature data from previous studies, including resource maps based on contouring methods (Fig. 10.1), and measured equilibrium borehole temperatures from the case study area. Variations between results from these simulations and temperature measurements are also considered that may not be resolved by adopting these predictive modelling techniques.

10.7.1 Comparisons of modelled and measured subsurface temperature data

Overall, there is a wide dispersion of temperatures at 1 km depth in the study area (Fig. 10.11a). The mean modelled temperature at 1 km depth of 41.36 °C indicates an average shallow geothermal gradient of 31.36 °C km⁻¹, which is slightly greater than the UK average of 28 °C km⁻¹, although the study area is widely considered to be geothermally hotter than much of the rest of the UK (Busby *et al.*, 2011). There are broad similarities between the distributions of modelled hot and cold temperature anomalies (Fig. 10.8) and previously predicted anomalies based on contouring (Busby *et al.*, 2011) (Fig. 10.3).

Equilibrium borehole temperature measurements effectively remove drilling induced transient temperature effects (Oxburgh *et al.*, 1972). Analyzing these data, when possible, should be considered an integral part of verifying predictive temperature models. Predicted subsurface temperatures show strong similarities with measured temperatures from the Rookhope Borehole (Fig. 10.11d), which are described in detail by Bott *et al.* (1972). In particular, the decreased geothermal gradient after approximately 450 m depth below surface is well reproduced by the modelling methodology presented in this chapter. This depth corresponds to the top (Caledonian) basement unconformity, which locally separates overlying and comparatively thermally insulating Carboniferous sediments from the more conductive and radiogenic North Pennine Batholith.

There are stronger dissimilarities between predicted subsurface temperatures and measured equilibrium temperatures from the Newcastle Science Central Deep Geothermal Borehole (Younger *et al.*, 2016) (Fig. 10.11e). The implementation of this modelling methodology under-predicts the
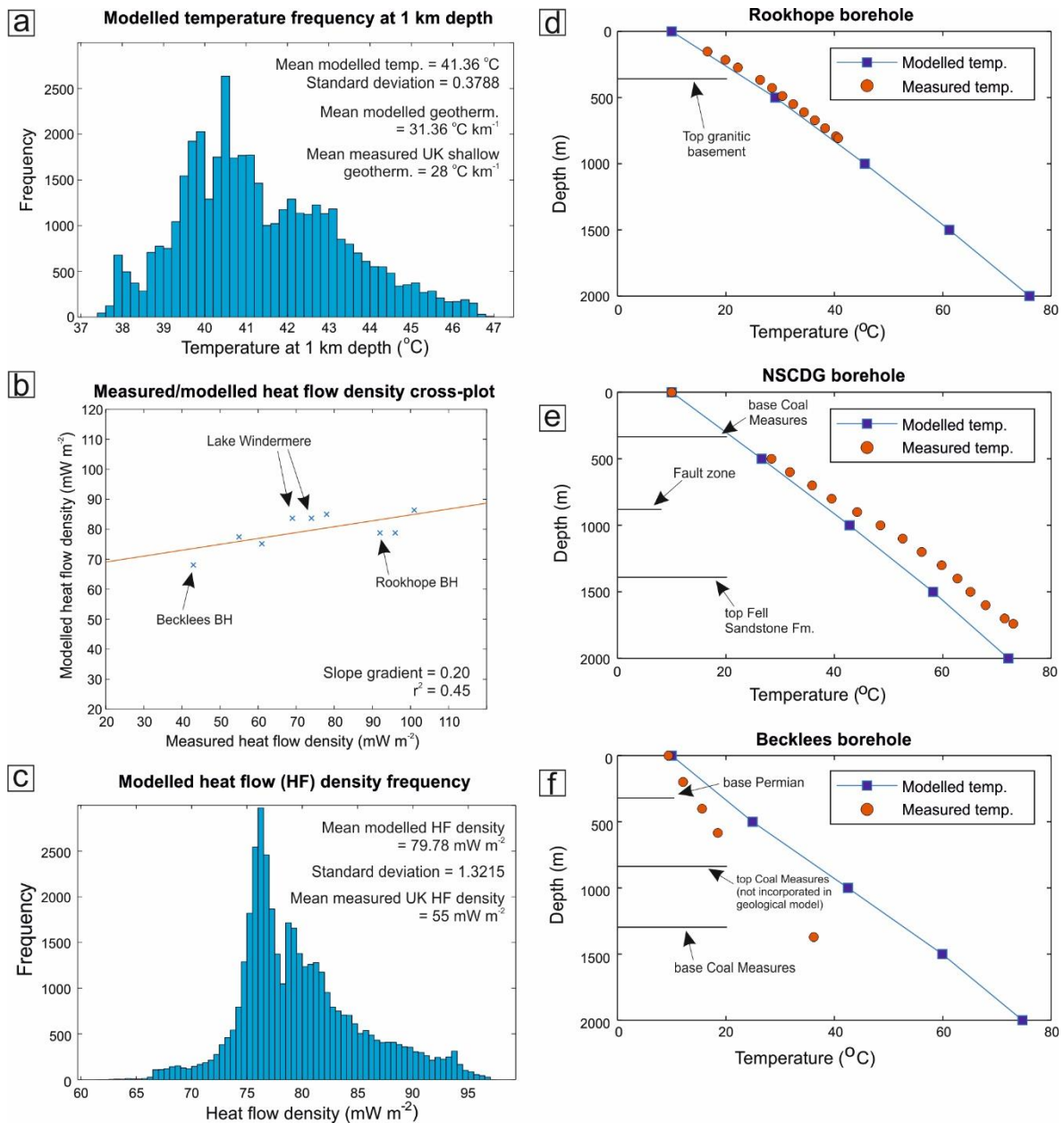
Figure 10.11a: A cross-plot between measured heat flow density data and modelled data in the study area. Modelled data are taken from approximately the equivalent location as measured data. 10.11b and c: Frequency charts for modelled temperature values at 1 km depth, and shallow (<500 m) heat flow density values, respectively. Mean measured UK shallow (<1 km) geothermal gradient and mean measured UK heat flow density taken from Busby *et al.* (2011) and Busby (2010). 10.11d, e and f: Comparisons between modelled subsurface temperatures and measured equilibrium borehole temperatures for the Rookhope Borehole, the Newcastle Science Central Deep Geothermal Borehole and the Becklees Borehole, respectively. For locations of boreholes, see Figure 10.3a. Measured equilibrium boreholes temperatures taken from Burley *et al.* (1984) and Younger *et al.* (2016).

temperature gradient with respect to measured temperatures in this region. This under-prediction could perceivably be attributed to the spatial variability of thermal properties (*cf.* Fuchs *et al.*, 2020),

or to the Ninety Fathom and Stublick fault system, which cuts across this region as well as geothermally hotter regions to the west (Fig. 10.2a). If these faults behave as non-sealing conduits, they may facilitate accelerated heat fluxes via fluid convection (*cf.* Calcagno *et al.*, 2014).

The greatest disconnect between predicted and measured equilibrium temperature is associated with the youngest and most scarcely preserved Carboniferous sediments of the study area that are encountered in the Becklees borehole (*cf.* Jones *et al.*, 2011) (Fig. 10.11f). Like temperatures in the Becklees borehole, predicted geothermal gradient steepens between 500 and 1000 m depth below surface. For predicted subsurface temperatures, this is due to the presence of thermally insulating Pennine Coal Measures Group stratigraphy within the geological model between these depths (Chadwick *et al.*, 1995) (Fig. 10.4). However, instead of encountering a thick succession solely of this insulating rock unit, the Becklees borehole encounters approximately 600 m of sandstone-rich and variably porous sedimentary rock belonging to the Warwickshire Group, overlaying an approximately 500 m thick succession of the Pennine Coal Measures Group (Jones *et al.*, 2011) (Fig. 7.4). These overlaying units are likely to be more conductive due to their compositions (e.g., Rybach, 1981) and may provide high permeability pathways for heat convection (Kaiser *et al.*, 2011; Scheck-Wenderoth *et al.*, 2014). Modelled subsurface temperatures may be over-predicted with respect to measured temperatures in the Becklees borehole as a result (Fig. 10.11f). However, as most of the remainder of Carboniferous sediments in northern England are typically tight (e.g., Younger *et al.*, 2016), these sources of inaccuracy are acknowledged, while this simplistic, yet more robust, modelling approach is still maintained.

10.7.2 Comparisons of modelled and measured heat flow density data

Contoured heat flow density maps provide more precise constraints for the temperature model, given the greater density of heat flow data in the case study area (Fig. 10.1b). The two bullseyes over the Lake District and Alston Block, where heat flow is locally greater than 90 mW m^{-2}, are broadly replicated, as are the lower heat flows in the Northumberland-Solway Basin and Stainmore Trough (Fig. 10.10). These temperature simulations offer greater resolution compared with these contoured resource maps. Figure 10.11b shows a cross-plot for measured heat flow data

and modelled data taken from equivalent locations. Overall, there is a positive correlation, suggesting that the modelling technique successfully replicates areas of greater heat flow density. However, the dispersion of modelled heat flow density data falls short of equivalent measured data (also see Fig. 10.11b). This is indicated by the shallow cross-plot gradient of 0.2 (Fig. 10.11b).

At these shallow (<500 m) depths, modelled heat flow inaccuracies could perceivably be attributed to the neglected influences of superficial deposits, given that in northern England, many heat flow measurements were recorded in the shallowest tens of metres of the subsurface (Burley *et al.*, 1984), and that superficial cover thicknesses locally exceed 60 m (McMillan, 2011). Whilst neglecting the influences of superficial cover has not had a noticeably detrimental effect on subsurface temperature predictions (e.g., Figs. 10.8, 10.11d, e and f), their admission appears to have more negatively impacted the dispersion of surface heat flow density data (Fig. 10.11c), because these data are more directly proportional to the thermal conductivity of the shallow subsurface (Eq. 10.1). In temperate regions of the world, including northern England, transient temperature effects relating to palaeoclimate are proven to also have detrimental effects on shallow heat flow density predictions (e.g., Slagstad *et al.*, 2009; Majorowicz *et al.*, 2012). A steady-state subsurface temperature model is, by definition, incapable of accounting for these effects; although a simplistic alteration to the temperature model's top boundary condition following temperature convergence, and repeated model iterations, would effectively replicate this transient effect. A surface heat flow over-estimation would be anticipated had the effects of transient climate adjustment had a detrimental effect on modelled heat flow data (Majorowicz *et al.*, 2012). Nonetheless, a comparison between modelled and measured heat flow density data suggests no consistent over-estimation (Fig. 10.11e).

10.8 Conclusions

Predictive subsurface temperature and heat flow density maps can be extracted from the finite difference models presented in this chapter (Figs. 10.8, 9 and 10) that are higher resolution and geologically realistic compared to maps constructed by contouring around sparsely distributed and often unreliable data points (Fig. 10.1). Due to the averaging technique presented, the resolution of

the geological model is scarcely compromised to reduce computational intensity. Its main strengths are its robustness, simplicity, and reproducibility relative to more elaborate finite element techniques (e.g., Cacace and Jacquey, 2017). Compared to other finite difference techniques (e.g., Fullea *et al.*, 2009; Keller *et al.*, 2020), this methodology offers higher resolution, geologically more realistic, and quicker solutions for regional scale (>10 km) problems such as subsurface temperature and heat flow density mapping. The main inaccuracies of the model in northern England relate to geological inputs, such as bedrock and superficial cover. Fuchs and Balling (2016) and Fuchs *et al.* (2020) discuss the importance of geological constraints and their regional variability for subsurface temperature models such as these. Other inaccuracies may relate to fluid convection. When deemed necessary and where data constraints are sufficient, the incorporation of fluid convection through rock units within temperature calculations may comprise a simple upgrade on these methods (e.g., Oxburgh *et al.*, 1972). However, to predict the influences of more complex structures, such as permeable fault zones, on subsurface temperature, more elaborate methods and finer resolution models may be necessary (*cf.* Calcagno *et al.*, 2014). The method presented here represents a useful tool for understanding controls on subsurface temperature distribution and geothermal potential. MATLAB scripts and program files for the northern England temperature model can be accessed via the web link at the beginning of this chapter.

Summary

11.1 Introduction

Throughout this thesis, key aspects of basin evolution in northern England and Scotland have been discussed, during early Carboniferous (Mississippian) and late Carboniferous (approximately Pennsylvanian) times, respectively. In this final chapter, a summary of the original work that this thesis contributes is given and the main aims and objectives, which are outlined in Chapter 1 and in Sections 3.6 and 6.5, are addressed.

11.2 'Block and basin' style rift basins

In the early Carboniferous northern Pennine Basin of northern England, the occurrence of granite within intra-basin basement highs, or 'blocks', is widely believed to relate to the relative 'rigidity' and 'buoyancy' of granite in relation to accommodating basement (Bott, 1967). It has been suggested that during periods of tectonic extension, normal faulting around the peripheral regions of granite batholiths permits granite-cored blocks to isostatically resist subsidence, thus forming stable areas during periods of widespread faulting-induced subsidence (Donato *et al.*, 1993). The so-called 'block and basin' tectono-stratigraphic framework for the northern Pennine Basin, within which buoyant granite intrusions underpin intra-rift basin blocks, had long held traction in some sectors of sedimentology (Johnson, 1967). However, many of the elements of such a model are based on primitive tectonic frameworks and, unsurprisingly, corresponding depositional models often reflect this (Grayson and Oldham, 1986). In Part II of this thesis, this tectonic framework was re-assessed and its influence on sedimentation during periods of basin extension was investigated.

In Chapter 4, the role of low-density, or buoyant, granite intrusions within intra-basin basement highs and the classically depicted 'block and basin' rift basin framework of the early Carboniferous northern Pennine Basin in northern England was investigated. One-dimensional modelling experiments indicate that comparatively less dense crust is incapable of 'isostatically resisting' subsidence during lithospheric extension in the way suggested by classic tectonic models

for the region (Fig. 4.2). Instead, when local isostasy is assumed, the occurrence of granite-cored, intra-basin basement highs relates to initial isostatic compensation following granite emplacement. An integrated two-dimensional lithospheric numerical modelling approach highlights the role of flexural rigidity in limiting the amplitude whilst increasing the wavelength of isostatic deflection. Considering these models, it was suggested that such a response leaves residual second-order stresses associated with the under-compensated buoyancy of the granite body and flexural tension (Fig. 4.9). The observed basin geometries of the early Carboniferous northern Pennine Basin can be replicated by incorporating a density deficiency within the crust, flexural rigidity, simple shear deformation within the shallower subsurface and pure shear deformation within the deeper subsurface (Fig. 4.8). It was proposed that the interaction of three factors dictate the tectonic framework within a partially granitic, brittle-ductile lithosphere and the occurrence of inter-basinal highs: 1) non-tectonic, 'second-order' stresses such as the flexural response of the lithosphere and residual, under-compensated buoyancy forces in relation to granite bodies; 2) extensional tectonic stress and importantly; 3) inherited basement fabric.

In Chapter 5 and using a combined sedimentological and sedimentary provenance approach, the syn-rift (Visean) fluvio-deltaic Fell Sandstone Formation and age-equivalent strata within the 'block and basin' style northern Pennine Basin was examined. It was suggested that some aspects of the basin fill matched classically depicted models for 'block and basin' style rift basin systems. These include the overall basinward increase in deeper water and delta-dominant facies in the Northumberland-Solway Basin, the dominant basinward palaeocurrent direction in the Northumberland-Solway Basin, and the derivation of sediment from comparatively uplifted "blocks" (e.g., Fig. 5.7). However, other aspects, such as the up-system decrease in net sand content north-east of the Cheviot Block, the south-eastwards deflection in palaeocurrent in the Tweed Basin, and the contemporaneous uplift and shedding of sediment on central parts of the Alston Block and accumulation of kilometre-thick sediment along the eastern margin of the Alston Block, did not (e.g., Fig. 5.8). Highlighted divergences from pre-existing 'block and basin' type models relate to occurrences of pre-Carboniferous basement domes or monoclines, which are unbound by major (>100 m) vertically displacing faults and on to which the Carboniferous succession onlaps

unconformably. Such structures in the northern Pennine Basin are all granite cored. This is because their origins as basement highs are associated with their buoyant compositions and flexural isostatic processes (Howell *et al.*, 2019). It was suggested that one such basement high, the Cheviot Block, confined and deflected the Fell Sandstone fluvio-deltaic system from the west, causing locally elevated net sand content and variations in dominant palaeodrainage direction (Fig. 5.11), and that central parts of the Alston Block were comparatively uplifted because of flexural isostatic responses to buoyant basement rock (Fig. 5.12). The findings thus presented were not just at variance with classically depicted depositional models for the 'block and basin' style northern Pennine rift basin (e.g., Johnson, 1967), but also with more modern depictions of dominantly normal fault driven rift basins (e.g., Gawthorpe and Leeder, 2000).

11.3 The late Carboniferous 'broken' Variscan foreland

Despite some of the sediments that accumulated in the late Carboniferous basins of northern England and Scotland representing perhaps some of the most widely researched stratigraphic units in the world, the Scottish and Pennine Coal Measures groups, the origin of these basins remains enigmatic (Dewey, 1982; Leeder, 1982; Leeder and McMahon, 1988; Besly, 1988, 2019; Underhill *et al.*, 2008). The alleged late Carboniferous evolution of basins in northern England and Scotland contrast markedly. Whereas the late Carboniferous basins of northern England are believed to have subsided because of post-rift or thermally induced sagging (e.g., Fraser and Gawthorpe, 1990), central Scotland is believed to have been incorporated within a regional wrench zone (Underhill *et al.*, 2008). In both modern and ancient sedimentary basins, syn-kinematic sequences can indirectly reveal the nature of the various tectonic episodes that influenced the basin and its regional setting. Across northern England and Scotland, much of the youngest Carboniferous sequence is absent due to uplift and denudation. However, near complete records of late Carboniferous sedimentation are locally preserved at the Canonbie Coalfield (Chadwick *et al.*, 1995; Jones *et al.*, 2011) and in the eastern part of the MVS (Ritchie *et al.*, 2003).

In Chapter 7, the first of two localised studies on the late Carboniferous evolution of basins in northern England and Scotland was presented. Local seismic and borehole-based mapping of the

Carboniferous Pennine Coal Measures and Warwickshire Group successions in the Canonbie Coalfield (SW Scotland) provides evidence of repeated episodes of positive inversion, syn-depositional folding and unconformities. An early Westphalian phase of comparatively minor basin inversion was recognised, based on onlapping seismic reflector geometries against NE-trending positive inversion structures (Fig. 7.10). A late Westphalian-Stephanian unconformity recognised within the Warwickshire Group succession signifies N-S, *c.* 10 % local basin shortening. Local inversion structures appear to have strongly influenced local Westphalian-Stephanian depocentres. Variations in crustal rheology, fault strength and orientation, and mid-crustal detachments are suggested to have played important roles in determining strain localisation and the nature of Westphalian-Stephanian depocentres in the Canonbie Coalfield.

In Chapter 8, detailed seismic- and borehole-based mapping, and sedimentary logging, of the late Carboniferous succession in the eastern part of the MVS revealed complex structure and sedimentological assemblages. Laterally and temporally varying (mostly) fluvial and deltaic successions were described within the approximately NNE-trending Midlothian and Leven synclines. Three phases of localised accelerated intra-basin deformation were identified: during the middle-late Namurian, the (latest) Duckmantian-Bolsovian, and (latest) Asturian-Stephanian times (Fig. 8.12). Like the Canonbie Coalfield, the nature of these deformation phases and how they appeared to influence local depocentres appeared to have been controlled by local basin inversion and the pre-Carboniferous structure preserved in this part of the MVS.

The findings presented in Chapters 7 and 8 provided a rare opportunity to re-assess the structural and geodynamic controls on late Carboniferous sedimentation in northern England and Scotland. In Chapter 9, a synthesis of data presented in these chapters and other regional data from across the British Isles was presented so that potential tectonic and geodynamic controls on late Carboniferous basin evolution could be considered. In contrast with classically depicted exponentially decaying rates of post-rift (e.g., McKenzie, 1978), burial history plots revealed that Carboniferous subsidence in northern England and Scotland accelerates from middle-late Namurian times and throughout the Westphalian (Fig. 9.1). Three phases of accelerated late Carboniferous syn-depositional deformation were correlated across northern England and Scotland, the last two of

which coincide with regional deformation across the British Isles that is associated with the Variscan Mountains (e.g., Corfield *et al.*, 1996; Peace and Besly, 1997) (Fig. 9.2). All phases of deformation are succeeded by temporarily increased amounts of clastic sediment supply to the basins of northern England and Scotland (*cf.* Waters *et al.*, 2020). The regional depositional trends discussed in Chapter 9, and the more local depositional and structural trends discussed in the preceding two chapters, help inform an original structural and geodynamic model for the late Carboniferous basins of the British Isles. It is suggested that northern England and Scotland formed part of an expansive 'broken' Variscan foreland system during late Carboniferous times. Like the 'broken' North Patagonian foreland in South America (Strecker *et al.*, 2011; Bilmes *et al.*, 2013), late Carboniferous sedimentation in northern England and Scotland was determined by both (regional) isostatic responses to the Variscan Mountains, and localised basin inversion (Fig. 9.8).

11.4 Deep geothermal energy in northern England

To place this thesis within the contexts of the 21st century, when efforts to combat climate change are becoming increasingly important and widely publicised, an investigation into the deep geothermal energy potential of northern England was presented in Chapter 10. Many of the most widely used deep geothermal resource maps for the UK are produced by contouring around sparsely distributed and often unreliable data points (e.g., Downing and Gray, 1986a; Busby *et al.*, 2011) (Fig. 10.1). A MATLAB-based 3D finite difference temperature modelling methodology was introduced, which provided a means for producing higher resolution and geologically realistic versions of these maps.

The adopted case study area in northern England represented a region where both sedimentary basins and radiothermal granite bodies comprise potential deep geothermal resources (Manning *et al.*, 2007; Younger *et al.*, 2016; Gluyas *et al.*, 2018) (Fig. 10.5). A 3D temperature model was divided into discrete geological units, which were then assigned separate thermal properties. Assuming conductive heat transfer and steady-state and fixed boundary conditions, this model simulated subsurface temperature in 3D. Due to the averaging technique adopted for thermal properties, the resolution of the geological model was scarcely compromised with respect to similar

finite element methods (e.g., Bayer *et al.*, 1997; Jacquey and Cacace, 2017). One predicted 'hot spot' at 1 km depth in the central part of the case study area corresponded with the granitic North Pennine Batholith (Fig. 10.8a). Other shallow hot spots corresponded with thermally insulating sedimentary rock units and the geological structures that incorporated these units. Predictive heat flow density maps highlighted areas with accelerated surface heat flow density associated with shallow conductive basement rock and heat producing granite bodies (Fig. 10.10). Predicted subsurface temperatures showed broad similarities with measured equilibrium borehole temperatures. Inaccuracies may have related to convective heat transfer involving fault systems, or input variables relating to the geological model (*cf.* Norden *et al.*, 2016). The produced predictive subsurface temperature and heat flow density maps were higher resolution and geologically realistic relative to pre-existing contoured maps. The method presented in this chapter represents a useful tool for understanding controls on subsurface temperature distribution and geothermal potential.

11.5 Synthesis

The Carboniferous basins of northern England initiated as a response to lithosphere extension. Relative subsidence and uplift were governed by normal faulting and preferential fault reactivation but also isostasy and flexure of the lithosphere. These fundamental factors dictated sediment routing, supply and palaeodrainage, and partly determined regional characteristics of early Carboniferous basin fill. The basins of northern England and Scotland transitioned towards becoming part of a regional foreland basin system during Namurian and Westphalian times with respect to the southerly Variscan Mountains, within which these areas occupied the distal part of the foreland. The basins of northern England and Scotland were impacted by an evolving stress regime that prompted sporadic local basin inversion and fold growth. Factors such as (post-rift) thermal subsidence partly determined regional accommodation trends during these times. By end Westphalian and Stephanian times, the so-called Variscan foreland system represented a fully-fledged 'broken' foreland, comparable with northern Patagonia (e.g., Bilmes *et al.*, 2013) and within which major depocentres were determined by folding and thrusting. The regional framework presented in this thesis provides a useful tool for better understanding the Carboniferous bedrock of

the British Isles. This framework could be used in combination with other tools, such as the regional subsurface temperature modelling methodology presented in Chapter 10 of this thesis, to aid deep geothermal exploration. Perhaps, more importantly, it may help reinvigorate research into these rocks. History has taught us that there are many advantages to having a thorough understanding of our subsurface.

11.6 Economic implications of key findings

Parts II and III of this thesis did not directly address any specific economic or societal issues. However, the findings presented do have numerous economic implications. Deep geothermal energy was discussed in the previous chapter. Amongst the problems highlighted with the subsurface temperature model presented in this chapter were inadequacies in geological inputs. The regional tectonic and depositional models presented throughout this thesis could provide a means of refining these inputs. Furthermore, in better understanding controls on the regional distribution of petrophysical properties, such as porosity and permeability, future investments in deep geothermal may be more informed. Some of these benefits could equally apply to the UK's fledgling unconventional hydrocarbon industry.

The greatest economic implications for most of the findings presented in this thesis perhaps apply to the offshore conventional hydrocarbon industry. Carboniferous plays in the central and southern North Sea have longed been considered difficult targets (*cf.* Besly, 2019), owing partly to sparse subsurface data and difficulties in imaging these intervals through seismic, beneath (Upper Permian) Zechstein salt (Grant *et al.*, 2020). Consequently, onshore Carboniferous strata provides an important analogue. The findings presented in Chapters 7,8 and 9 highlight the combined influences of local-scale basin inversion, regional-scale tectonism and geodynamics, and global eustasy on depositional processes during late Carboniferous times. This work could benefit exploration in equivalent basins elsewhere throughout the UK continental shelf and beyond (*cf.* Besly *et al.*, 1993). The work presented in Chapters 4 and 5 could help better constrain palaeogeographic reconstructions offshore for the early Carboniferous (syn-rift) succession (*cf.* Booth *et al.*, 2020). More generally speaking, rift basins host a significant proportion of the world's hydrocarbon

resources and appreciating further controls on deposition, such as basement density and flexural isostasy, could yet unlock further economic potential in these systems. Subsurface temperature or palaeotemperature is an important consideration when predicting hydrocarbon generation. Therefore, the work presented in Chapter 10 could also benefit the hydrocarbon industry.

11.7 Possibilities for future research

11.7.1 'Block and basin' style rift basins

In Part II of this thesis and in describing a rift basin system influenced by the combined effects of normal faulting, lithospheric extension, basement buoyancy effects and flexural isostasy, the depiction of the northern Pennine Basin presented in this thesis contrasts with both traditional 'block and basin' style rift basin frameworks (e.g., Johnson, 1967), but also with more modern and widely accepted depositional models for generic rift basins (e.g., Gawthorpe and Leeder, 2000). Towards the end of Chapter 5, some other rift basins that appear to have been, at least partly, governed by the some of the same controls that governed basin geometry and sedimentation during early Carboniferous times in the northern Pennine Basin were discussed. Further studies using regional seismic and borehole-based mapping and gravity back-stripping methods (e.g., Kimbell *et al.*, 2006; Kimbell and Williamson, 2015), to constrain density of the basement, could unravel some complications associated with these basins, including offshore equivalents of the northern Pennine Basin in the central North Sea and the Irish Sea (*cf.* Grant *et al.*, 2020). Some work linking the onshore exposures of early Carboniferous strata in northern England with the buried offshore rift basin, as others have done (e.g., Booth *et al.*, 2020), may help set these systems within a broader and more useful palaeogeographic context. The combined influences of eustatic sea level fluctuations and tectonism on facies variations still require more detailed consideration.

11.7.2 The late Carboniferous 'broken' Variscan foreland

Although preservation of latest Carboniferous sediments in northern England and Scotland is scarce, there is further preservation than that discussed in Chapter 7 and 8. The Mauchline Basin, in eastern Ayrshire (Fig. 1.1), accommodates the most complete record of late Carboniferous-early

Permian stratigraphy in northern England and Scotland (Wagner, 1983). Like the Canonbie Coalfield, the youngest Carboniferous sediments in this sequence are distinctly 'red' (Jones *et al.*, 2011). However, there are no seismic reflection profiles or recently published studies associated with these strata comparable with the wealth of information provided for the Canonbie Coalfield or the eastern part of the Midland Valley of Scotland (Ritchie *et al.*, 2003; Jones *et al.*, 2006, 2011; Underhill *et al.*, 2008; Morton *et al.*, 2015). As with all Carboniferous 'red beds' in the British Isles, these rocks have received comparatively little attention, due to their barrenness with respect to coal. However, understanding them and the potential regional controls that influenced their deposition could advance our palaeogeographical understanding of any alleged 'broken' Variscan foreland basin system, in Scotland, far beyond anything that has been suggested in this thesis. As with the Scottish and Pennine Coal Measures Groups, much of the remainder of the Coal Measures and Warwickshire groups of the onshore UK and equivalent strata on the offshore continental shelf have received little recent attention in recent years, particularly at basin scales. Perhaps by adopting a similar tectono-stratigraphic framework to that outlined in Chapter 9, more coherent stories and regional analyses could be made of these strata.

11.7.3 Deep geothermal energy in northern England and the UK

As alluded to at the beginning of Chapter 10, numerical modelling as a tool for quantifying geothermal resource is not an entirely new concept. Some of the more complicated modelling techniques described in Section 10.2 are already being used to predict regional subsurface temperatures in Germany (Bayer *et al.*, 1997; Noack *et al.*, 2010; Sippel *et al.*, 2013), France (Calcagno *et al.*, 2014; Sosio *et al.*, 2019), Denmark (Fuchs and Balling, 2016; Poulsen *et al.*, 2017; Fuchs *et al.*, 2020), Mexico (Calcagno *et al.*, 2018) and the Netherlands (Bonté *et al.*, 2012; Lipsey *et al.*, 2016). An attempt to do the same in the UK using any numerical method would represent a major advance in the understanding of its geothermal potential. This study has shown that there are sufficient subsurface data to constrain this sort of model. Such an endeavour represents just one way in which subsurface data, skills and a knowledge of the subsurface can be repurposed as we seek to source our energy more sustainably.

11.7.4 Areas of greatest research potential

Of the themes covered within this thesis, the theme with greatest remaining research potential is arguably the 'block and basin' rift basin theme. The work presented in this part of the thesis begins to challenge high-profile and universal depictions of rift basin systems (e.g., Gawthorpe and Leeder, 2000). Therefore, the scope of any future work exploring the influences of basement density and flexural isostasy on rift basins could impact the wider geological community. Whilst further examples of rift basin systems influenced by these forces are clearly required to fully explore this theme, the early Carboniferous sedimentary record in northern England still offers fresh encouragement. The models presented in this thesis assumed that basement highs, as well as the rigidity of the lithosphere, remained largely static during lithosphere extension. However, extending the lithosphere and, by virtue, heating the lithosphere is considered a largely dynamic process (e.g., Watts, 2001 and references therein). Some of the conglomeratic and alluvial fan sequences deposited approximately during the onset of rifting and found along the flanks of the Cheviot Block, the western Pennines and the Lake District Block suggest an accelerated "unroofing" of granite-cored highs at this time (Johnson and Marshall, 1971; Robson, 1977), which may not be solely explained by normal faulting induced footwall uplift (*cf.* Kusznir *et al.*, 1991). Further combinations of numerical modelling and sedimentological based studies in these basins could yet shed further light on the underappreciated influences of basement density and flexural isostasy on rift basin systems

11.8 Closing remarks

Fraser and Gawthorpe (2003) write in their atlas of Carboniferous basin evolution in northern England that "perhaps all we really know about the Carboniferous is no more than skimming the surface". Similarly, Besly (2019) in his review of the adjacent Carboniferous of southern North Sea states that an integrated basin-wide understanding of this system is "still in its infancy". Their sentiments are echoed. It is hoped that some of the work included within this thesis may inspire and guide future geologists so that they may reconsider the frequently researched, yet still poorly understood, Carboniferous geology of the British Isles. Most of the regional ideas outlined at the ends of Parts II and III of this thesis are designed to pique interest and be challenged.

Although we may be unaware of a lot of them, many of the challenges we are likely to face in the future will rely on a thorough understanding of the geology immediately beneath us.

References

Adams, C., Monaghan, A. and Gluyas, J., 2019. Mining for heat. *Geoscientist*, *29*(4), pp.10-15. http://nora.nerc.ac.uk/id/eprint/523186/

Aikin, A., 1811. VIII. Observations on the Wrekin, and on the great Coal-field of Shropshire. *Transactions of the Geological Society of London*, *1*(1), pp.191-212. https://doi.org/10.1144/transgsla.1.191

Airy, G.B., 1855. On the computation of the effect of the attraction of mountain-masses, as disturbing the apparent astronomical latitude of stations in geodetic surveys. *Philosophical Transactions of the Royal Society of London*, *145*, pp.101-104. https://doi.org/10.1098/rstl.1855.0003

Akhurst, M.C., Chadwick, R.A., Holliday, D.W., McCormac, M., McMillan, A.A., Millward, D., Young, B., Ambrose, K., Auton, C.A., Barclay, W.J., Barnes, R.P., Beddoc-Stephens, B., James, J.W.C., Johnson, H., Jones, N.S., Glover, B.W., Hawkins, M.P., Kimbell, G.S., MacPherson, K.A.T., Merritt, J.W., Milodowski, A.E., Riley, N.J., Robins, N.S., Stone, P. and Wingfield, R.T.R., 1997. The geology of the west Cumbria district. *Memoir of the British Geological Survey, Sheets 28,37 and 47* (England and Wales). http://pubs.bgs.ac.uk/publications.html?pubID=B01506

Al-Hafdh, N.M.S., 1985. *The alteration petrology of the Cheviot granite* (Doctoral dissertation, Newcastle University).

Allen, J.R.L., 1960. The Mam Tor sandstones, a" turbidite" facies of the Namurian deltas of Derbyshire, England. Journal of Sedimentary Research, 30(2), pp.193-208. https://doi.org/10.1306/74D709FC-2B21-11D7-8648000102C1865D

Allmendinger, R.W., 1998. Inverse and forward numerical modeling of trishear fault-propagation folds. *Tectonics*, *17*(4), pp.640-656. https://doi.org/10.1029/98TC01907

Allsop, J.M., 1987. Patterns of late Caledonian intrusive activity in eastern and northern England from geophysics, radiometric dating and basement geology. *Proceedings of the Yorkshire Geological Society*, *46*(4), pp.335-353. https://doi.org/10.1144/pygs.46.4.335

Anderson, I. and Underhill, J.R., 2020. Structural constraints on Lower Carboniferous shale gas exploration in the Craven Basin, NW England. *Petroleum Geoscience*, *26*(2), pp.303-324. https://doi.org/10.1144/petgeo2019-125

Andrews, B.J., Cumberpatch, Z.A., Shipton, Z.K. and Lord, R., 2020. Collapse processes in abandoned pillar and stall coal mines: implications for shallow mine geothermal energy. *Geothermics*, *88*, p.101904. https://doi.org/10.1016/j.geothermics.2020.101904

Andrews, I.J. 2013. The Carboniferous Bowland Shale gas study: geology and resource estimation. *British Geological Survey for Department of Energy and Climate Change*, London, UK. http://nora.nerc.ac.uk/id/eprint/503839/1/BGS_DECC_BowlandShaleGasReport_MAIN_REPORT.pdf

Armstrong, H.A. and Purnell, M.A., 1987. Dinantian conodont biostratigraphy of the Northumberland Trough. *Journal of Micropalaeontology, 6*(2), pp.97-112. https://doi.org/10.1144/jm.6.2.97

Arsenikos, S., Quinn, M., Kimbell, G., Williamson, P., Pharaoh, T., Leslie, G. and Monaghan, A., 2019. Structural development of the Devono-Carboniferous plays of the UK North Sea. Geological Society, London, Special Publications, 471(1), pp.65-90. https://doi.org/10.1144/SP471.3

Ashworth, P.J., Best, J.L., Roden, J.E., Bristow, C.S. and Klaassen, G.J., 2000. Morphological evolution and dynamics of a large, sand braid-bar, Jamuna River, Bangladesh. *Sedimentology, 47*(3), pp.533-555. https://doi.org/10.1046/j.1365-3091.2000.00305.x

Bader, J.W., 2019. Structural inheritance and the role of basement anisotropies in the Laramide structural and tectonic evolution of the North American Cordilleran foreland, Wyoming. *Lithosphere, 11*(1), pp.129-148. https://doi.org/10.1130/L1022.1

Barrett, B.J., Collier, R.E.L., Hodgson, D.M., Gawthorpe, R.L., Dorrell, R.M. and Cullen, T.M., 2019. Quantifying faulting and base level controls on syn-rift sedimentation using stratigraphic architectures of coeval, adjacent Early-Middle Pleistocene fan deltas in Lake Corinth, Greece. *Basin Research, 31*(6), pp.1040-1065. https://doi.org/10.1111/bre.12356

Barrett, P.A., 1988. Early Carboniferous of the Solway Basin: A tectonostratigraphic model and its bearing on hydrocarbon potential. *Marine and Petroleum Geology, 5*(3), pp.271-281. https://doi.org/10.1016/0264-8172(88)90006-2

Barrowman, J., 1886. A glossary of Scotch mining terms. *Transactions of the Mining Institute of Scotland, 19*.

Bayer, U., Scheck, M. and Köhler, M., 1997. Modeling of the 3D thermal field in the northeast German basin. *Geologische Rundschau, 86*(2), pp.241-251. https://doi.org/10.1007/s005310050137

Beaumont, C., 1981. Foreland basins. *Geophysical Journal International, 65*(2), pp.291-329. https://doi.org/10.1111/j.1365-246X.1981.tb02715.x

Beaumont, C., Quinlan, G.M., Stockmal, G.S., Caldwell, W.G.E. and Kauffman, E.G., 1993. The evolution of the Western Interior Basin: causes, consequences and unsolved problems. *Evolution of the Western Interior Basin: Geological Association of Canada Special Paper, 39*, pp.97-117.

Bell, F.G., 1978. Petrographical factors relating to porosity and permeability in the Fell Sandstone. *Quarterly Journal of Engineering Geology and Hydrogeology, 11*(2), pp.113-126. https://doi.org/10.1144/GSL.QJEG.1978.011.02.01

Bell, R.A., Darling, W.G., Ward, R.S., Basava-Reddi, L., Halwa, L., Manamsa, K. and Dochartaigh, B.Ó., 2017. A baseline survey of dissolved methane in aquifers of Great Britain. Science of

the Total Environment, 601, pp.1803-1813.
https://doi.org/10.1016/j.scitotenv.2017.05.191

Bell, R.E., McNeill, L.C., Bull, J.M., Henstock, T.J., Collier, R.L. and Leeder, M.R., 2009. Fault architecture, basin structure and evolution of the Gulf of Corinth Rift, central Greece. *Basin Research*, *21*(6), pp.824-855. https://doi.org/10.1111/j.1365-2117.2009.00401.x

Besly, B.M. and Turner, P., 1983. Origin of red beds in a moist tropical climate (Etruria Formation, Upper Carboniferous, UK). *Geological Society, London, Special Publications*, *11*(1), pp.131-147. https://doi.org/10.1144/GSL.SP.1983.011.01.14

Besly, B.M., 1988. Palaeogeographic implications of late Westphalian to early Permian red-beds, Central England. In: *Sedimentation in a synorogenic basin complex. The Upper Carboniferous of Northwest Europe* (pp. 200-221).

Besly, B.M. and Fielding, C.R., 1989. Palaeosols in Westphalian coal-bearing and red-bed sequences, central and northern England. *Palaeogeography, Palaeoclimatology, Palaeoecology*, *70*(4), pp.303-330. https://doi.org/10.1016/0031-0182(89)90110-7

Besly, B.M. and Cleal, C.J., 1997. Upper Carboniferous stratigraphy of the West Midlands (UK) revised in the light of borehole geophysical logs and detrital compositional suites. *Geological Journal*, *32*(2), pp.85-118. https://doi.org/10.1002/(SICI)1099-1034(199706)32:2<85::AID-GJ732>3.0.CO;2-O

Besly, B., 2019. Exploration and development in the Carboniferous of the Southern North Sea: a 30-year retrospective. *Geological Society, London, Special Publications*, *471*(1), pp.17-64. https://doi.org/10.1144/SP471.10

Besly, B.M. and Cleal, C.J., 2021. Absence of regional stratigraphic hiatus in the late Carboniferous (Asturian-Stephanian) in the northern Variscan foreland: a review of the bio-and lithostratigraphical evidence in central england. *Proceedings of the Geologists' Association*, *132*(1), pp. 50-65. https://doi.org/10.1016/j.pgeola.2020.09.004

Bilmes, A., D'Elia, L., Franzese, J.R., Veiga, G.D. and Hernández, M., 2013. Miocene block uplift and basin formation in the Patagonian foreland: the Gastre Basin, Argentina. *Tectonophysics*, *601*, pp.98-111. https://doi.org/10.1016/j.tecto.2013.05.001

Blair, T.C. and Mcpherson, J.G., 2008. Quaternary sedimentology of the Rose Creek fan delta, Walker Lake, Nevada, USA, and implications to fan-delta facies models. *Sedimentology*, *55*(3), pp.579-615. https://doi.org/10.1111/j.1365-3091.2007.00913.x

Bluck, B.J., 1978. Sedimentation in a late orogenic basin: the Old Red Sandstone of the Midland Valley of Scotland. In: Bowes, D.R. and Leake, B.E. (eds.). *Crustal evolution in northwestern Britain and adjacent regions*. Special Issue of the Geological Journal, No.10, pp. 249-278.

Binney, E.W. and Kirkby, J.W., 1882. On the upper beds of the Fifeshire Coal-measures. Quarterly Journal of the Geological Society, 38(1-4), pp.245-256. https://doi.org/10.1144/GSL.JGS.1882.038.01-04.28

Bonté, D., Van Wees, J.D. and Verweij, J.M., 2012. Subsurface temperature of the onshore Netherlands: new temperature dataset and modelling. *Netherlands Journal of Geosciences*, *91*(4), pp.491-515. https://doi.org/10.1017/S0016774600000354

Booth, M.G., Underhill, J.R., Gardiner, A. and McLean, D., 2020. Sedimentary and tectonic controls on Lower Carboniferous (Visean) mixed carbonate–siliciclastic deposition in NE England and the Southern North Sea: implications for reservoir architecture. *Petroleum Geoscience*, *26*(2), pp.204-231. https://doi.org/10.1144/petgeo2019-101

Bott, M.H.P. and Masson-Smith, D., 1957. The geological interpretation of a gravity survey of the Alston Block and the Durham Coalfield. *Quarterly Journal of the Geological Society*, *113*(1-4), pp.93-118. https://doi.org/10.1144/GSL.JGS.1957.113.01-04.05

Bott, M.H.P., 1962. A simple criterion for interpreting negative gravity anomalies. *Geophysics*, *27*(3), pp.376-381. https://doi.org/10.1190/1.1439026

Bott, M.H.P., 1967. Geophysical investigations of the northern Pennine basement rocks. *Proceedings of the Yorkshire Geological Society*, *36*(2), pp.139-168. https://doi.org/10.1144/pygs.36.2.139

Bott, M.P. and Smithson, S.B., 1967. Gravity investigations of subsurface shape and mass distributions of granite batholiths. *Geological Society of America Bulletin*, *78*(7), pp.859-878. https://doi.org/10.1130/0016-7606(1967)78[859:GIOSSA]2.0.CO;2

Bott, M.H.P., Johnson, G.A.L., Mansfield, J. and Wheilden, J., 1972. Terrestrial heat flow in north-east England. *Geophysical Journal International*, *27*(3), pp.277-288. https://doi.org/10.1111/j.1365-246X.1972.tb06093.x

Bott, M.H.P., Robinson, J. and Kohnstamm, M.A., 1978. Granite beneath Market Weighton, east Yorkshire. *Journal of the Geological Society*, *135*(5), pp.535-543. https://doi.org/10.1144/gsjgs.135.5.0535

Bouchez, J.L., 1997. Granite is never isotropic: an introduction to AMS studies of granitic rocks. In *Granite: from segregation of melt to emplacement fabrics* (pp. 95-112). Springer, Dordrecht. https://doi.org/10.1007/978-94-017-1717-5_6

BP, 2019. BP Energy Outlook 2019 edition. *London, United Kingdom.*

Brackenridge, R.E., Underhill, J.R., Jamieson, R. and Bell, A., 2020. Structural and stratigraphic evolution of the Mid North Sea High region of the UK Continental Shelf. *Petroleum Geoscience*, *26*(2), pp. 154-173. https://doi.org/10.1144/petgeo2019-076

Breward, N., 2004. Preliminary Report on the Regional Geochemistry of Strathmore. *British Geological Survey Internal Report*, IR/04/113. 22pp. http://nora.nerc.ac.uk/id/eprint/509356/1/IR04113.pdf

Brewer, J.A., Matthews, D.H., Warner, M.R., Hall, J., Smythe, D.K. and Whittington, R.J., 1983. BIRPS deep seismic reflection studies of the British Caledonides. *Nature*, *305*(5931), p.206. https://doi.org/10.1038/305206a0

Bridge, J.S., 1993. Description and interpretation of fluvial deposits: a critical perspective. *Sedimentology*, *40*(4), pp.801-810. https://doi.org/10.1111/j.1365-3091.1993.tb01361.x

Bristow, C.S., Best, J.L. and Roy, A.G., 1993. Morphology and facies models of channel confluences. *Alluvial Sedimentation*, pp.89-100. https://doi.org/10.1002/9781444303995.ch8

British Geological Survey, 1992. *Regional geochemistry of the Lake District and adjacent areas.* Keyworth, Nottingham: British Geological Survey.

British Geological Survey, 2008. *Digital Geological Map of Great Britain 1:625 000 scale (DiGMapGB-625), Bedrock data. Version 5.17.* Keyworth, Nottingham: British Geological Survey. Release date 11-2-2008.

Brodie, J. and White, N., 1994. Sedimentary basin inversion caused by igneous underplating: Northwest European continental shelf. *Geology, 22*(2), pp.147-150. https://doi.org/10.1130/0091-7613(1994)022<0147:SBICBI>2.3.CO;2

Bromley, M.H., 1991. Architectural features of the Kayenta Formation (Lower Jurassic), Colorado Plateau, USA: relationship to salt tectonics in the Paradox Basin. *Sedimentary Geology, 73*(1-2), pp.77-99. https://doi.org/10.1016/0037-0738(91)90024-8

Brown, D., Juhlin, C., Tryggvason, A., Friberg, M., Rybalka, A., Puchkov, V. and Petrov, G., 2006. Structural architecture of the southern and middle Urals foreland from reflection seismic profiles. *Tectonics, 25*(1). https://doi.org/10.1029/2005TC001834

Brown, G.C., 1979. Geochemical and geophysical constraints on the origin and evolution of Caledonian granites. *Geological Society, London, Special Publications, 8*(1), pp.643-651. https://doi.org/10.1144/GSL.SP.1979.008.01.78

Browne, M.A.E., Dean, M.T., Hall, I.H.S., McAdam, A.D., Monro, S.K. and Chisholm, J.I., 1999. A lithostratigraphical framework for the Carboniferous rocks of the Midland Valley of Scotland. *British Geological Survey Research Report*, RR/99/07. http://nora.nerc.ac.uk/id/eprint/3229/1/RR99007.pdf

Browne, M.A.E, Smith, R.A. and Aitken, A.M., 2002. Stratigraphical framework for the Devonian (Old Red Sandstone) rocks of Scotland south of a line from Fort William to Aberdeen. *British Geological Survey Research Report*, RR/01/04. http://nora.nerc.ac.uk/id/eprint/3231/1/Devonian[1].pdf

Bucher, J., Pérez, M.E., Ruiz, L.R.G., D'Elía, L. and Bilmes, A., 2020. New middle Miocene (Langhian-Serravallian) vertebrate localities in northwestern Patagonia, Argentina: A contribution to high latitude south american land mammal ages sequence. *Journal of South American Earth Sciences*, p.103024. https://doi.org/10.1016/j.jsames.2020.103024

Buckley, J.P., Bosence, D. and Elders, C., 2015. Tectonic setting and stratigraphic architecture of an Early Cretaceous lacustrine carbonate platform, Sugar Loaf High, Santos Basin, Brazil. *Geological Society, London, Special Publications, 418*(1), pp.175-191. https://doi.org/10.1144/SP418.13

Burgess, I.C. and Harrison, R.K., 1967. Carboniferous basement beds in the Roman Fell district, Westmorland. *Proceedings of the Yorkshire Geological Society, 36*(2), pp.203-225. https://doi.org/10.1144/pygs.36.2.203

Burgess, I C and Holliday, D W. 1979. Geology of the country around Brough-under-Stainmore. Memoir for 1:50 000 geological sheet 31 and parts of sheets 25 and 30. Geological Survey of Great Britain (England and Wales). London: HMSO. 131pp.

Burgess, P.M. and Gayer, R.A., 2000. Late Carboniferous tectonic subsidence in South Wales: implications for Variscan basin evolution and tectonic history in SW Britain. *Journal of the Geological Society, 157*(1), pp.93-104. https://doi.org/10.1144/jgs.157.1.93

Burov, E.B. and Diament, M., 1995. The effective elastic thickness (T e) of continental lithosphere: what does it really mean? *Journal of Geophysical Research: Solid Earth, 100*(B3), pp.3905-3927. https://doi.org/10.1029/94JB02770

Burley, A.J., Edmunds, W.M. and Gale, I.N., 1984. Investigation of the geothermal potential of the UK: catalogue of geothermal data for the land area of the United Kingdom. http://nora.nerc.ac.uk/id/eprint/512272/

Busby, J., Lewis, M., Reeves, H. and Lawley, R., 2009. Initial geological considerations before installing ground source heat pump systems. *Quarterly Journal of Engineering Geology and Hydrogeology, 42*(3), pp.295-306. https://doi.org/10.1144/1470-9236/08-092

Busby, J., 2010. Geothermal prospects in the United Kingdom. In: *Proceedings World Geothermal Congress 2010*, Bali, Indonesia, 25-29 April. http://nora.nerc.ac.uk/id/eprint/15965/1/GeothermalProspectsUK.pdf

Busby, J., Kingdon, A. and Williams, J., 2011. The measured shallow temperature field in Britain. *Quarterly Journal of Engineering Geology and Hydrogeology, 44*(3), pp.373-387. https://doi.org/10.1144/1470-9236/10-049

Busby, J., 2014. Geothermal energy in sedimentary basins in the UK. *Hydrogeology journal, 22*(1), pp.129-141. https://doi.org/10.1007/s10040-013-1054-4

Busby, L.P., 2019. Thermal conductivity and subsurface temperature data pertaining to the Glasgow Geothermal Energy Research Field Site (GGERFS). *British Geological Survey Open Report*, OR/19/015. 21pp. http://nora.nerc.ac.uk/id/eprint/523450/1/OR19015.pdf

Butler, M., 1998. The geological history of the southern Wessex Basin—a review of new information from oil exploration. *Geological Society, London, Special Publications, 133*(1), pp.67-86. https://doi.org/10.1144/GSL.SP.1998.133.01.04

Butler, M., 2019. Seismostratigraphic analysis of Paleozoic sequences of the Midlands Microcraton. *Geological Society, London, Special Publications, 471*(1), pp.317-332. https://doi.org/10.1144/SP471.6

Cacace, M., Kaiser, B.O., Lewerenz, B. and Scheck-Wenderoth, M., 2010. Geothermal energy in sedimentary basins: What we can learn from regional numerical models. *Geochemistry, 70*, pp.33-46. https://doi.org/10.1016/j.chemer.2010.05.017

Cacace, M. and Jacquey, A.B., 2017. Flexible parallel implicit modelling of coupled thermal–hydraulic–mechanical processes in fractured rocks. *Solid Earth, 8*, pp.921-941. https://doi.org/10.5194/se-8-921-2017

Calcagno, P., Baujard, C., Guillou-Frottier, L., Dagallier, A. and Genter, A., 2014. Estimation of the deep geothermal potential within the Tertiary Limagne basin (French Massif Central): An integrated 3D geological and thermal approach. *Geothermics, 51*, pp.496-508. https://doi.org/10.1016/j.geothermics.2014.02.002

Calcagno, P., Evanno, G., Trumpy, E., Gutiérrez-Negrín, L.C., Macías, J.L., Carrasco-Núñez, G. and Liotta, D., 2018. Preliminary 3-D geological models of los humeros and Acoculco geothermal fields (Mexico)–H2020 GEMex project. *Advances in Geosciences, 45*, pp.321-333. https://doi.org/10.5194/adgeo-45-321-2018

Calder, J.H., 1998. The carboniferous evolution of Nova Scotia. *Geological Society, London, Special Publications, 143*(1), pp.261-302. https://doi.org/10.1144/GSL.SP.1998.143.01.19

Caldwell, W.G.E. and Young, G.M., 2013. Structural controls in the western offshore Midland Valley of Scotland: implications for Late Palaeozoic regional tectonics. *Geological Magazine, 150*(4), pp.673-698. https://doi.org/10.1017/S0016756812000878

Cameron, I B, and Stephenson, D. 1985. *British regional geology: The Midland Valley of Scotland. Third edition.* Keyworth, Nottingham: British Geological Survey.

Cann, J.R. and Banks, D.A., 2001. Constraints on the genesis of the mineralization of the Alston Block, Northern Pennine Orefield, northern England. *Proceedings of the Yorkshire Geological Society, 53*(3), pp.187-196. https://doi.org/10.1144/pygs.53.3.187

Carney, J.N., Ambrose, K., Brandon, A., Cornwall, J.D., Hobbs, P.R.N., Lewis, M.A., Merriman, R.J., Ritchie, M.A. and Royles, C.P., 2001. Geology of the country between Loughborough, Burton and Derby. *Sheet description of the British Geological Survey, 1:50000 Series Sheet 141 Loughborough* (England and Wales). 92 pp. http://pubs.bgs.ac.uk/publications.html?pubID=B06078

Catuneanu, O., Beaumont, C. and Waschbusch, P., 1997. Interplay of static loads and subduction dynamics in foreland basins: Reciprocal stratigraphies and the "missing" peripheral bulge. *Geology, 25*(12), pp.1087-1090. https://doi.org/10.1130/0091-7613(1997)025<1087:IOSLAS>2.3.CO;2

Catuneanu, O., Hancox, P.J. and Rubidge, B.S., 1998. Reciprocal flexural behaviour and contrasting stratigraphies: a new basin development model for the Karoo retroarc foreland system, South Africa. *Basin research, 10*(4), pp.417-440. https://doi.org/10.1046/j.1365-2117.1998.00078.x

Catuneanu, O., Sweet, A.R. and Miall, A.D., 1999. Concept and styles of reciprocal stratigraphies: Western Canada foreland system. *Terra Nova-Oxford, 11*(1), pp.1-8.

Catuneanu, O., 2001. Flexural partitioning of the late Archaean Witwatersrand foreland system, South Africa. *Sedimentary Geology, 141*, pp.95-112. https://doi.org/10.1016/S0037-0738(01)00070-7

Catuneanu, O., 2019. First-order foreland cycles: Interplay of flexural tectonics, dynamic loading, and sedimentation. *Journal of Geodynamics, 129*, pp.290-298. https://doi.org/10.1016/j.jog.2018.03.001

Čermác, V. and Rybach, L., 1982. Thermal properties: Thermal conductivity and specific heat of minerals and rocks. *Landolt-Börnstein Zahlenwerte und Functionen aus Naturwissenschaften und Technik, Neue Serie, Physikalische Eigenschaften der Gesteine*, pp.305-343.

Chadwick, R.A. and Holliday, D.W., 1991. Deep crustal structure and Carboniferous basin development within the Iapetus convergence zone, northern England. *Journal of the Geological Society, 148*(1), pp.41-53. https://doi.org/10.1144/gsjgs.148.1.0041

Chadwick, B.A., Holliday, D.W., Holloway, S., Hulbert, A.G. and Lawrence, D.J.D., 1995. The structure and evolution of the Northumberland-Solway Basin and adjacent areas. Subsurface memoir of the British Geological Survey. London: HMSO.

Chisholm, J I, MacAdam, A D, Brand, P J. 1989. Lithostratigraphical classification of Upper Devonian and Lower Carboniferous rocks in the Lothians. *British Geological Survey Technical Report*, WA/89/26.

Chisholm, J.I., 1990. The upper Band-Better bed sequence (lower Coal Measures, Westphalian A) in the central and South Pennine area of England. *Geological Magazine, 127*(1), pp.55-74.

Chisholm, J.I., Waters, C.N., Hallsworth, C.R., Turner, N., Strong, G.E. and Jones, N.S. 1996. Provenance of Lower Coal Measures around Bradford, West Yorkshire. *Proceedings of the Yorkshire Geological Society, 51*, 153–166, https://doi.org/10.1144/pygs.51.2.153

Chisholm, J.I. and Hallsworth, C.R. 2005. Provenance of Upper Carboniferous sandstones in east Derbyshire: role of the Wales–Brabant High. *Proceedings of the Yorkshire Geological Society, 55*, 209–233, https://doi.org/10.1144/pygs.55.3.209

Christie-Blick, N., 1991. Onlap, offlap, and the origin of unconformity-bounded depositional sequences. *Marine Geology, 97*(1-2), pp.35-56. https://doi.org/10.1016/0025-3227(91)90018-Y

Chroston, P.N., Allsop, J.M. and Cornwell, J.D., 1987. New seismic refraction evidence on the origin of the Bouguer anomaly low near Hunstanton, Norfolk. *Proceedings of the Yorkshire Geological Society, 46*(4), pp.311-319. https://doi.org/10.1144/pygs.46.4.311

Clark, G. and Jacks, D., 2007. Coal and the industrial revolution, 1700–1869. *European Review of Economic History, 11*(1), pp.39-72. https://doi.org/10.1017/S1361491606001870

Clarke, W.J., 1901. The Unconformity in the Coal-Measures of the Shropshire Coalfields. Quarterly Journal of the Geological Society, 57(1-4), pp.86-95. https://doi.org/10.1144/GSL.JGS.1901.057.01-04.09

Clayton, G., Coquel, R., Doubinger, J., Gueinn, K.J., Loboziak, S., Owens, B. and Streel, M., 1977. Carboniferous miospores of Western Europe: illustration and zonation. *Mededelingen-Rijks Geologische Dienst, 29*, pp.1-71.

Clayton, G., Higgs, K., Keegan, J.B. and Sevastopulo, G.D., 1978. Correlation of the palynological zonation of the Dinantian of the British Isles. *Palinologia*, *1*(1), pp.137-147.

Clayton, G. and Loboziak, S., 1985. Early Carboniferous (early Viséan–Serpukhovian) palynomorphs. *Journal of Micropalaeontology*, *4*(1), pp.83-91.

Collier, R.L., 1989. Tectonic evolution of the Northumberland Basin; the effects of renewed extension upon an inverted extensional basin. *Journal of the Geological Society*, *146*(6), pp.981-989. https://doi.org/10.1144/gsjgs.146.6.0981

Collier, R.L., 1991. The Lower Carboniferous Stainmore Basin, N. England: extensional basin tectonics and sedimentation. *Journal of the Geological Society*, *148*(2), pp.379-390. https://doi.org/10.1144/gsjgs.148.2.0379

Contreras, J., Anders, M.H. and Scholz, C.H., 2000. Growth of a normal fault system: observations from the Lake Malawi basin of the east African rift. *Journal of Structural Geology*, *22*(2), pp.159-168. https://doi.org/10.1016/S0191-8141(99)00157-1

Conway, A., Dentith, M.C., Doody, J.J. and Hall, J., 1987. Preliminary interpretation of upper crustal structure across the Midland Valley of Scotland from two East–West seismic refraction profiles. *Journal of the Geological Society*, *144*(6), pp.865-870. https://doi.org/10.1144/gsjgs.144.6.0865

Cooley, J.W. and Tukey, J.W., 1965. An algorithm for the machine calculation of complex Fourier series. *Mathematics of computation*, *19*(90), pp.297-301. https://doi.org/10.2307/2003354

Corfield, S.M., Gawthorpe, R.L., Gage, M., Fraser, A.J. and Besly, B.M., 1996. Inversion tectonics of the Variscan foreland of the British Isles. *Journal of the Geological Society*, *153*(1), pp.17-32. https://doi.org/10.1144/gsjgs.153.1.0017

Copley, A. and Woodcock, N., 2016. Estimates of fault strength from the Variscan foreland of the northern UK. *Earth and Planetary Science Letters*, *451*, pp.108-113. https://doi.org/10.1016/j.epsl.2016.07.024

Coward, M.P., 1993. The effect of Late Caledonian and Variscan continental escape tectonics on basement structure, Paleozoic basin kinematics and subsequent Mesozoic basin development in NW Europe. In: *Geological Society, London, Petroleum Geology Conference Series* (Vol. 4, No. 1, pp. 1095-1108). Geological Society of London. https://doi.org/10.1144/0041095

Coward, M.P., De Donatis, M., Mazzoli, S., Paltrinieri, W. and Wezel, F.C., 1999. Frontal part of the northern Apennines fold and thrust belt in the Romagna-Marche area (Italy): Shallow and deep structural styles. *Tectonics*, *18*(3), pp.559-574. https://doi.org/10.1029/1999TC900003

Craig, G.Y. and Nairn, A.E.M., 1956. The lower Carboniferous outliers of the Colvend and Rerrick shores, Kirkcudbrightshire. *Geological Magazine*, *93*(3), pp.249-256.

Crampton, S.L. and Allen, P.A., 1995. Recognition of forebulge unconformities associated with early stage foreland basin development: example from the North Alpine Foreland Basin. *AAPG*

bulletin, 79(10), pp.1495-1514. https://doi.org/10.1306/7834DA1C-1721-11D7-8645000102C1865D

Creedy, D.P., 1991. An introduction to geological aspects of methane occurrence and control in British deep coal mines. *Quarterly Journal of Engineering Geology and Hydrogeology, 24*(2), pp.209-220. https://doi.org/10.1144/GSL.QJEG.1991.024.02.04

Croucher, A., O'Sullivan, M., O'Sullivan, J., Yeh, A., Burnell, J. and Kissling, W., 2020. Waiwera: A parallel open-source geothermal flow simulator. *Computers & Geosciences*, p.104529. https://doi.org/10.1016/j.cageo.2020.104529

Crowley, T.J. and Baum, S.K., 1991. Estimating Carboniferous sea-level fluctuations from Gondwanan ice extent. *Geology, 19*(10), pp.975-977. https://doi.org/10.1130/0091-7613(1991)019<0975:ECSLFF>2.3.CO;2

Cullen, T.M., Collier, R.E.L., Gawthorpe, R.L., Hodgson, D.M. and Barrett, B.J., 2020. Axial and transverse deep-water sediment supply to syn-rift fault terraces: Insights from the West Xylokastro Fault Block, Gulf of Corinth, Greece. *Basin Research, 32*(5), pp.1115-1149. https://doi.org/10.1111/bre.12416

Davies, J.R., Wilson, D. and Williamson, I.T., 2004. Geology of the country around Flint. Memoir of the British Geological Survey, Sheet 108 (England and Wales). http://pubs.bgs.ac.uk/publications.html?pubID=B06065

Davydov V., Wardlaw B.R., Gradstein F.M., 2004. *The Carboniferous Period*. In: Gradstein F.M., Ogg J.G., Smith A.G., (Eds.). A geologic time scale 2004. Cambridge: Cambridge University Press. pp. 222–248.

Day, J B W and others, 1970. Geology of the neighbourhood around Bewcastle. *Memoir of the British Geological Survey, Sheet 12.* (England and Wales).

Dean, M T, Browne, M A E, Waters, C N, and Powell, J H. 2011. A lithostratigraphical framework for the Carboniferous successions of northern Great Britain (Onshore). *British Geological Survey Research Report*, RR/10/07. 174pp. http://nora.nerc.ac.uk/id/eprint/13985/1/RR10007.pdf

de Castro, D.L., Bezerra, F.H. and Branco, R.M.C., 2008. Geophysical evidence of crustal-heterogeneity control of fault growth in the Neocomian Iguatu basin, NE Brazil. Journal of South American Earth Sciences, 26(3), pp.271-285. https://doi.org/10.1016/j.jsames.2008.07.002

DeCelles, P.G. and Giles, K.A., 1996. Foreland basin systems. *Basin research, 8*(2), pp.105-123. https://doi.org/10.1046/j.1365-2117.1996.01491.x

Deegan, C.E., 1973. Tectonic control of sedimentation at the margin of a Carboniferous depositional basin in Kirkcudbrightshire. Scottish Journal of Geology, 9(1), pp.1-28.

Delcaillau, B., Carozza, J.M. and Laville, E., 2006. Recent fold growth and drainage development: the Janauri and Chandigarh anticlines in the Siwalik foothills, northwest India. *Geomorphology, 76*(3-4), pp.241-256. https://doi.org/10.1016/j.geomorph.2005.11.005

Dentith, M.C. and Hall, J., 1990. MAVIS: geophysical constraints on the structure of the Carboniferous basin of West Lothian, Scotland. *Earth and Environmental Science Transactions of The Royal Society of Edinburgh*, *81*(2), pp.117-126. https://doi.org/10.1017/S0263593300005186

De Paola, N., Holdsworth, R.E., McCaffrey, K.J. and Barchi, M.R., 2005. Partitioned transtension: an alternative to basin inversion models. *Journal of Structural Geology*, *27*(4), pp.607-625. https://doi.org/10.1016/j.jsg.2005.01.006

de Saint-Blanquat, M., Law, R.D., Bouchez, J.L. and Morgan, S.S., 2001. Internal structure and emplacement of the Papoose Flat pluton: An integrated structural, petrographic, and magnetic susceptibility study. Geological Society of America Bulletin, 113(8), pp.976-995. https://doi.org/10.1130/0016-7606(2001)113<0976:ISAEOT>2.0.CO;2

De Souza, H.A.F., 1982. Age data from Scotland and the Carboniferous time scale. In: Odin, G.S. (ed.) *Numerical Dating in Stratigraphy*. Wiley, Chichester, pp. 455-465

Dewey, J.F., 1982. Plate tectonics and the evolution of the British Isles: Thirty-fifth William Smith Lecture. *Journal of the Geological Society*, *139*(4), pp.371-412. https://doi.org/10.1144/gsjgs.139.4.0371

Di Domenica, A., Bonini, L., Calamita, F., Toscani, G., Galuppo, C. and Seno, S., 2014. Analogue modeling of positive inversion tectonics along differently oriented pre-thrusting normal faults: an application to the Central-Northern Apennines of Italy. *Bulletin*, *126*(7-8), pp.943-955. https://doi.org/10.1130/B31001.1

Dimitropoulos, K. and Donato, J.A., 1981. The inner moray firth central ridge, a geophysical interpretation. *Scottish Journal of Geology*, *17*(1), pp.27-38. https://doi.org/10.1144/sjg17010027

Donato, J.A. and Tully, M.C., 1982. A proposed granite batholith along the western flank of the North Sea Viking Graben. *Geophysical Journal International*, *69*(1), pp.187-195. https://doi.org/10.1111/j.1365-246X.1982.tb04943.x

Donato, J.A., Martindale, W. and Tully, M.C., 1983. Buried granites within the mid North Sea High. *Journal of the Geological Society*, *140*(5), pp.825-837. https://doi.org/10.1144/gsjgs.140.5.0825

Donato, J.A. and Megson, J.B., 1990. A buried granite batholith beneath the East Midland Shelf of the Southern North Sea Basin. *Journal of the Geological Society*, *147*(1), pp.133-140. https://doi.org/10.1144/gsjgs.147.1.0133

Donato, J.A., 1993. A buried granite batholith and the origin of the Sole Pit Basin, UK Southern North Sea. *Journal of the Geological Society*, *150*(2), pp.255-258. https://doi.org/10.1144/gsjgs.150.2.0255

Donato, J.A., 2020. Gravity modelling across two postulated granite batholiths within the UK onshore East Midlands Shelf. *University of Oxford/UKOGL Beneath Britain Website.*

Donovan, R.N., 1982. Devonian calcretes (cornstones) near Tain. *Scottish Journal of Geology, 18*(2-3), pp.125-129. https://doi.org/10.1144/sjg18020125

Downing, R.A. and Gray, D.A., 1986a. Geothermal resources of the United Kingdom. *Journal of the Geological Society, 143*(3), pp.499-507. https://doi.org/10.1144/gsjgs.143.3.0499

Downing, R.A. and Gray, D.A., (eds.) 1986b. Geothermal Energy—the Potential in the United Kingdom. HMSO, London

Duffy, O.B., Brocklehurst, S.H., Gawthorpe, R.L., Leeder, M.R. and Finch, E., 2015. Controls on landscape and drainage evolution in regions of distributed normal faulting: Perachora Peninsula, Corinth Rift, Central Greece. *Basin Research, 27*(4), pp.473-494. https://doi.org/10.1111/bre.12084

Dunham, K.C., Johnson, G.A.L., Bott, M.H.P. and Hodge, B.L., 1961. Granite beneath the northern Pennines. *Nature, 190*(4779), pp.899-900. https://doi.org/10.1038/190899a0

Dunham, K.C. and Johnson, G.A.L., 1962. Sub-surface data on the Namurian strata of Allenheads, south Northumberland. *Proceedings of the Yorkshire Geological Society, 33*(3), pp.235-254. https://doi.org/10.1144/pygs.33.3.235

Dunham, K.C., Dunham, A.C., Hodge, B.L. and Johnson, G.A.L., 1965. Granite beneath Viséan sediments with mineralization at Rookhope, northern Pennines. *Quarterly Journal of the Geological Society, 121*(1-4), pp.383-414. https://doi.org/10.1144/gsjgs.121.1.0383

Dunham, K.C. 1990. *Geology of the Northern Pennine Orefield, Volume 1, Tyne to Stainmore,* 2nd edition. Economic Memoir of the British Geological Survey, sheets 19 and 25 and parts of 13, 24, 26, 31, 32 (England and Wales). HMSO, London.

Edel, J.B., Schulmann, K., Lexa, O. and Lardeaux, J.M., 2018. Late Palaeozoic palaeomagnetic and tectonic constraints for amalgamation of Pangea supercontinent in the European Variscan belt. Earth-science reviews, 177, pp.589-612. https://doi.org/10.1016/j.earscirev.2017.12.007

Egan, S.S., 1992. The flexural isostatic response of the lithosphere to extensional tectonics. *Tectonophysics, 202*(2-4), pp.291-308. https://doi.org/10.1016/0040-1951(92)90115-M

Egan, S.S. and Urquhart, J.M., 1993. Numerical modelling of lithosphere shortening: application to the Laramide erogenic province, western USA. *Tectonophysics, 221*(3-4), pp.385-411. https://doi.org/10.1016/0040-1951(93)90170-O

Egan, S.S., Kane, S., Buddin, T.S., Williams, G.D. and Hodgetts, D., 1999. Computer modelling and visualisation of the structural deformation caused by movement along geological faults. *Computers & Geosciences, 25*(3), pp.283-297. https://doi.org/10.1016/S0098-3004(98)00125-3

Egan, S.S. and Meredith, D.J., 2007. A kinematic modelling approach to lithosphere deformation and basin formation: application to the Black Sea. Geological Society, London, Special Publications, 282(1), pp.173-198. https://doi.org/10.1144/SP282.9

Ellen, R., Browne, M.A.E., Mitten, A.J., Clarke, S.M., Leslie, A.G. and Callaghan, E., 2019. Sedimentology, architecture and depositional setting of the fluvial Spireslack Sandstone of

the Midland Valley, Scotland: insights from the Spireslack surface coal mine. *Geological Society, London, Special Publications*, *488*(1), pp.181-204. https://doi.org/10.1144/SP488.2

Elliott, G.M., Jackson, C.A.L., Gawthorpe, R.L., Wilson, P., Sharp, I.R. and Michelsen, L., 2017. Late syn-rift evolution of the Vingleia Fault Complex, Halten Terrace, offshore Mid-Norway; a test of rift basin tectono-stratigraphic models. *Basin Research, 29*, pp.465-487. https://doi.org/10.1111/bre.12158

Elliott, T., 1976, Morphology, magnitude and regime of a Carboniferous fluvial distributary channel: *Journal of sedimentary petrology, 45*, p. 70-- 76.

Evans, D.J., Rowley, W.J., Chadwick, R.A., Kimbell, G.S. and Millward, D., 1994. Seismic reflection data and the internal structure of the Lake District batholith, Cumbria, northern England. *Proceedings of the Yorkshire Geological Society, 50*(1), pp.11-24. https://doi.org/10.1144/pygs.50.1.11

Everett, P. A., Lister, T. R., Fordyce, F. M., Ferreira, A. M. P. J., Donald, A. W., Gowing, C. J. B. and Lawley, R. S., 2019. Stream Sediment Geochemical Atlas of the United Kingdom. *British Geological Survey Open Report*, OR/18/048. 94 pp. http://nora.nerc.ac.uk/id/eprint/524956/1/OR18048.pdf

Ewing, C.J.C. and Francis, E.H., 1960. No. 1, 2 and 3 off-shore borings in the Firth of Forth 1955-1957. *Bulletin of the Geological Survey of Great Britain, 16*, pp.1-68.

Farey, J., 1815. General View of the Agriculture and Minerals of Derbyshire: With Observations on the Means of Their Improvement. Drawn Up for the Consideration of the Board of Agriculture and Internal Improvement.. (Vol. 2). B. McMillan.

Faulds, J.E. and Varga, R.J., 1998. The role of accommodation zones and transfer zones in the regional segmentation of extended terranes. *Geological Society of America Special Papers, 323*, pp.1-45.

Fazlikhani, H., Fossen, H., Gawthorpe, R.L., Faleide, J.I. and Bell, R.E., 2017. Basement structure and its influence on the structural configuration of the northern North Sea rift. *Tectonics, 36*(6), pp.1151-1177. https://doi.org/10.1002/2017TC004514

Fielding, C.R., 1984. Upper delta plain lacustrine and fluviolacustrine facies from the Westphalian of the Durham coalfield, NE England. *Sedimentology, 31*(4), pp.547-567. https://doi.org/10.1111/j.1365-3091.1984.tb01819.x

Fielding, C.R., Alexander, J. and Allen, J.P., 2018. The role of discharge variability in the formation and preservation of alluvial sediment bodies. *Sedimentary Geology, 365*, pp.1-20. https://doi.org/10.1016/j.sedgeo.2017.12.022

Flint, S., Aitken, J. and Hampson, G., 1995. Application of sequence stratigraphy to coal-bearing coastal plain successions: implications for the UK Coal Measures. Geological Society, London, Special Publications, 82(1), pp.1-16. https://doi.org/10.1144/GSL.SP.1995.082.01.01

Floyd, J.D., 1994. The derivation and definition of the 'Southern Upland Fault': a review of the Midland Valley–Southern Uplands terrane boundary. *Scottish Journal of Geology, 30*(1), pp.51-62. https://doi.org/10.1144/sjg30010051

Ford, M., Rohais, S., Williams, E.A., Bourlange, S., Jousselin, D., Backert, N. and Malartre, F., 2013. Tectono-sedimentary evolution of the western Corinth rift (Central Greece). *Basin Research, 25*(1), pp.3-25. https://doi.org/10.1111/j.1365-2117.2012.00550.x

Forsyth, I.H., Hall, I.H.S., and McMillan, A.A., 1996. Geology of the Airdrie district. *Memoir of the British Geological Survey, Sheet 31W* (Scotland).

Fraser, A.J. and Gawthorpe, R.L., 1990. Tectono-stratigraphic development and hydrocarbon habitat of the Carboniferous in northern England. *Geological Society, London, Special Publications, 55*(1), pp.49-86. https://doi.org/10.1144/GSL.SP.1990.055.01.03

Fraser, A.J. & Gawthorpe, R.L. 2003. An atlas of Carboniferous basin evolution in Northern England. *Geological Society Memoir 28.*

Freeman, B., Klemperer, S.L. and Hobbs, R.W., 1988. The deep structure of northern England and the Iapetus Suture zone from BIRPS deep seismic reflection profiles. *Journal of the Geological Society, 145*(5), pp.727-740. https://doi.org/10.1144/gsjgs.145.5.0727

Frost, D.V and Holliday, D.W., 1980. Geology of the country around Bellingham. *Memoir of the British Geological Survey, Sheet 13* (England & Wales).

Fuchs, S. and Balling, N., 2016. Improving the temperature predictions of subsurface thermal models by using high-quality input data. Part 1: Uncertainty analysis of the thermal-conductivity parameterization. *Geothermics, 64*, pp.42-54. https://doi.org/10.1016/j.geothermics.2016.04.010

Fuchs, S., Balling, N. and Mathiesen, A., 2020. Deep basin temperature and heat-flow field in Denmark–New insights from borehole analysis and 3D geothermal modelling. *Geothermics, 83*, p.101722. https://doi.org/10.1016/j.geothermics.2019.101722

Fullea, J., Afonso, J.C., Connolly, J.A.D., Fernandez, M., García-Castellanos, D. and Zeyen, H., 2009. LitMod3D: An interactive 3-D software to model the thermal, compositional, density, seismological, and rheological structure of the lithosphere and sublithospheric upper mantle. *Geochemistry, Geophysics, Geosystems, 10*(8). https://doi.org/10.1029/2009GC002391

Gale, N.H., Beckinsale, R.D. and Wadge, A.J., 1980. Discussion of a paper by McKerrow, Lambert and Chamberlain on the Ordovician, Silurian and Devonian Time Scales. *Earth and planetary science letters, 51*, pp. 9-17.

Gale, N.H., 1985. Numerical calibration of the Palaeozoic time-scale; Ordovician, Silurian and Devonian periods. *Geological Society, London, Memoirs, 10*(1), pp.81-88. https://doi.org/10.1144/GSL.MEM.1985.010.01.09

García-Mondéjar, J., 1996. Plate reconstruction of the Bay of Biscay. *Geology, 24*(7), pp.635-638. https://doi.org/10.1130/0091-7613(1996)024<0635:PROTBO>2.3.CO;2

Gawthorpe, R.L., 1984. *Sedimentation, tectonics and diagenesis: the Dinantian sequence of the Bowland Basin, northern England* (Doctoral dissertation, University of Leeds).

Gawthorpe, R.L. and Clemmey, H., 1985. Geometry of submarine slides in the Bowland Basin (Dinantian) and their relation to debris flows. *Journal of the Geological Society, 142*(3), pp.555-565. https://doi.org/10.1144/gsjgs.142.3.0555

Gawthorpe, R.L., 1986. Sedimentation during carbonate ramp-to-slope evolution in a tectonically active area: Bowland Basin (Dinantian), northern England. *Sedimentology, 33*(2), pp.185-206. https://doi.org/10.1111/j.1365-3091.1986.tb00531.x

Gawthorpe, R.L., 1987. Burial dolomitization and porosity development in a mixed carbonate-clastic sequence: an example from the Bowland Basin, northern England. *Sedimentology, 34*(4), pp.533-558. https://doi.org/10.1111/j.1365-3091.1987.tb00785.x

Gawthorpe, R.L. and Hurst, J.M., 1993. Transfer zones in extensional basins: their structural style and influence on drainage development and stratigraphy. *Journal of the Geological Society, 150*(6), pp.1137-1152. https://doi.org/10.1144/gsjgs.150.6.1137

Gawthorpe, R.L., Sharp, I., Underhill, J.R. & Gupta, S. 1997. Linked sequence stratigraphic and structural evolution of propagating normal faults. *Geology, 25*, 795-798. https://doi.org/10.1130/0091-7613(1997)025<0795:LSSASE>2.3.CO;2Gawthorpe, R.L. and Leeder, M.R., 2000. Tectono-sedimentary evolution of active extensional basins. *Basin Research, 12*(3-4), pp.195-218. https://doi.org/10.1111/j.1365-2117.2000.00121.x

George, T.N., 1958. Lower Carboniferous palaeogeography of the British Isles. *Proceedings of the Yorkshire Geological Society, 31*(3), pp.227-318. https://doi.org/10.1144/pygs.31.3.227

George, T.N., Johnson, G.A.L., Mitchell, M., Prentice, J.E., Ramsbottom, W.H.C., Sevastopulo, G.M. & Wilson, R.B. 1976. A correlation of Dinantian rocks in the British Isles. *Geological Society of London Special Report, 7*, 87 pp.

Ghinassi, M., Ielpi, A., Aldinucci, M. and Fustic, M., 2016. Downstream-migrating fluvial point bars in the rock record. *Sedimentary Geology, 334*, pp.66-96. https://doi.org/10.1016/j.sedgeo.2016.01.005

Gianni, G., Navarrete, C., Orts, D., Tobal, J., Folguera, A. and Giménez, M., 2015. Patagonian broken foreland and related synorogenic rifting: the origin of the Chubut Group Basin. *Tectonophysics, 649*, pp.81-99. https://doi.org/10.1016/j.tecto.2015.03.006

Gianni, G.M., Dávila, F.M., Echaurren, A., Fennell, L., Tobal, J., Navarrete, C., Quezada, P., Folguera, A. and Giménez, M., 2018. A geodynamic model linking Cretaceous orogeny, arc migration, foreland dynamic subsidence and marine ingression in southern South America. *Earth-Science Reviews, 185*, pp.437-462. https://doi.org/10.1016/j.earscirev.2018.06.016

Gibson, H., Stüwe, K., Seikel, R., FitzGerald, D., Calcagno, P., Guillen, A., and McInerney, P., 2008. Forward prediction temperature distribution direct from 3D geology models. In: *Proceedings of the Australian Geothermal Energy Conference*, Melbourne 2008.

Glennie, K.W., 2010. *Desert sedimentary environments*. Elsevier.

Glennie, K., 2005. Regional tectonics in relation to PermoCarboniferous hydrocarbon potential, Southern North Sea Basin: carboniferous hydrocarbon resources: the southern North Sea and surrounding areas. In: Collinson, J.D., Evans, D.J., Holliday, D.W. and Jones, N.S. (eds) *Carboniferous Hydrocarbon Geology: The Southern North Sea and Surrounding Onshore Areas.* Yorkshire Geological Society Occasional Publications, 7, pp.1–12.

Gochioco, L.M., 1990. Seismic surveys for coal exploration and mine planning. *The Leading Edge*, *9*(4), pp.25-28. https://doi.org/10.1190/1.1439738

Goodlet, G.A., 1959. Mid-Carboniferous sedimentation in the Midland Valley of Scotland. *Transactions of the Edinburgh Geological Society*, *17*(3), pp.217-240. https://doi.org/10.1144/transed.17.3.217

Grant, R.J., Booth, M.G., Underhill, J.R. and Bell, A., 2020. Structural evolution of the Breagh area: implications for carboniferous prospectivity of the Mid North Sea High, Southern North Sea. *Petroleum Geoscience*, *26*(2), pp.174-203. https://doi.org/10.1144/petgeo2019-100

Grayson, R.F., and Oldham, L., 1987. A new structural framework for the northern British Dinantian as a basis for oil, gas, and mineral exploration. In: *European Dinantian Environments* (Eds. J. Miller, A.E. Adams and V.P. Wright), pp. 31-59. Open University, Milton Keynes.

Green, P.F., 2002. Early Tertiary paleo-thermal effects in Northern England: reconciling results from apatite fission track analysis with geological evidence. *Tectonophysics*, *349*(1-4), pp.131-144. https://doi.org/10.1016/S0040-1951(02)00050-1

Greig, D.C., 1988. Geology of the Eyemouth district. *Memoir of the British Geological Survey*, Sheet 34 (Scotland). http://pubs.bgs.ac.uk/publications.html?pubID=B01888

Gudlaugsson, S.T., Faleide, J.I., Johansen, S.E. and Breivik, A.J., 1998. Late Palaeozoic structural development of the south-western Barents Sea. *Marine and Petroleum Geology*, *15*(1), pp.73-102. https://doi.org/10.1016/S0264-8172(97)00048-2

Gupta, S., Cowie, P.A., Dawers, N.H. and Underhill, J.R., 1998. A mechanism to explain rift-basin subsidence and stratigraphic patterns through fault-array evolution. *Geology*, *26*(7), pp.595-598. https://doi.org/10.1130/0091-7613(1998)026<0595:AMTERB>2.3.CO;2

Hall, I.H.S. and Chisholm, J.I., 1987. Aeolian sediments in the late Devonian of the Scottish Midland Valley. *Scottish Journal of Geology*, *23*(2), pp.203-208. https://doi.org/10.1144/sjg23020203

Hallsworth, C.R., Morton, A.C., Claoué-Long, J. and Fanning, C.M., 2000. Carboniferous sand provenance in the Pennine Basin, UK: constraints from heavy mineral and detrital zircon age data. *Sedimentary Geology*, *137*(3-4), pp.147-185. https://doi.org/10.1016/S0037-0738(00)00153-6

Hallsworth, C.R. and Chisholm, J.I., 2008. Provenance of late Carboniferous sandstones in the Pennine Basin (UK) from combined heavy mineral, garnet geochemistry and palaeocurrent

studies. *Sedimentary Geology, 203*(3-4), pp.196-212.
https://doi.org/10.1016/j.sedgeo.2007.11.002

Hallsworth, C.R. and Chisholm, J.I. 2017. Interplay of mid-Carboniferous sediment sources on the northern margin of the Wales-Brabant High. *Proceedings of the Yorkshire Geological Society, 61*, 285–309, https://doi.org/10.1144/pygs2017-382

Hantschel, T. and Kauerauf, A.I., 2009. Introduction to Basin modeling. In: *Fundamentals of Basin and Petroleum Systems Modeling* (pp. 1-30). Springer, Berlin, Heidelberg.

Hartley, A. and Evenstar, L., 2018. Fluvial architecture in actively deforming salt basins: Chinle Formation, Paradox Basin, Utah. *Basin Research, 30*(1), pp.148-166.
https://doi.org/10.1111/bre.12247

Hayward, A.B. and Graham, R.H., 1989. Some geometrical characteristics of inversion. *Geological Society, London, Special Publications, 44*(1), pp.17-39.
https://doi.org/10.1144/GSL.SP.1989.044.01.03

Heinemann, N., Alcalde, J., Johnson, G., Roberts, J.J., McCay, A.T. and Booth, M.G., 2019. Low-carbon GeoEnergy resource options in the Midland Valley of Scotland, UK. *Scottish Journal of Geology, 55*(2), pp.93-106. https://doi.org/10.1144/sjg2019-007

Hirst C.M., 2012. The geothermal potential of low enthalpy deep sedimentary basins in the UK. PhD Thesis, Durham University, UK.

Hodgson, A.V. and Gardiner, M.D., 1971. An investigation of the aquifer potential of the Fell Sandstone of Northumberland. *Quarterly Journal of Engineering Geology and Hydrogeology, 4*(2), pp.91-109. https://doi.org/10.1144/GSL.QJEG.1971.004.02.01

Holford, S.P., Green, P.F., Turner, J.P., Williams, G.A., Hillis, R.R., Tappin, D.R. and Duddy, I.R., 2008. Evidence for kilometre-scale Neogene exhumation driven by compressional deformation in the Irish Sea basin system. *Geological Society, London, Special Publications, 306*(1), pp.91-119. https://doi.org/10.1144/SP306.4

Holliday, D.W., Burgess, I.C. and Frost, D.V., 1975. A recorrelation of the Yoredale Limestones (Upper Viséan) of the Alston Block with those of the Northumberland Trough. *Proceedings of the Yorkshire Geological Society, 40*(3), pp.319-334. https://doi.org/10.1144/pygs.40.3.319

Holliday, D.W., Neves, R. and Owens, B., 1979. Stratigraphy and palynology of early Dinantian (Carboniferous) strata in shallow boreholes near Ravenstonedale, Cumbria. *Proceedings of the Yorkshire Geological Society, 42*(3), pp.343-356. https://doi.org/10.1144/pygs.42.3.343Holz, M., Vilas-Boas, D.B., Troccoli, E.B., Santana, V.C. and Vidigal-Souza, P.A., 2017. Conceptual models for sequence stratigraphy of continental rift successions. In: *Stratigraphy & Timescales* (Vol. 2, pp. 119-186). Academic Press.

Homewood, P., Allen, P.A. and Williams, G.D., 1986. Dynamics of the Molasse Basin of western Switzerland. In: *Foreland basins, Vol. 8*, pp. 199-217. Oxford, UK: Blackwell Scientific Publications.

Horton, B.K. and DeCelles, P.G., 2001. Modern and ancient fluvial megafans in the foreland basin system of the central Andes, southern Bolivia: Implications for drainage network evolution in fold-thrust belts. *Basin research*, *13*(1), pp.43-63. https://doi.org/10.1046/j.1365-2117.2001.00137.x

Howell, L., Egan, S., Leslie, G. and Clarke, S., 2019. Structural and geodynamic modelling of the influence of granite bodies during lithospheric extension: application to the Carboniferous basins of northern England. *Tectonophysics*, *755*, pp.47-63. https://doi.org/10.1016/j.tecto.2019.02.008

Howell, L.P., Besly, B.M., Sooriyathasan, S., Egan, S.S. and Leslie, A.G., 2020. Seismic and borehole-based mapping of the late Carboniferous succession in the Canonbie Coalfield, SW Scotland: evidence for a 'broken' Variscan foreland? *Scottish Journal of Geology*, *57*(1). https://doi.org/10.1144/sjg2020-007

Howell, L., Brown, C.S. and Egan, S.S., 2021. Deep geothermal energy in northern England: Insights from 3D finite difference temperature modelling. *Computers & Geosciences*, *147*, p.104661. https://doi.org/10.1016/j.cageo.2020.104661

Hughes, R.A., Evans, J.A., Noble, S.R. and Rundle, C.C., 1996. U–Pb chronology of the Ennerdale and Eskdale intrusions supports sub-volcanic relationships with the Borrowdale Volcanic Group (Ordovician, English Lake District). *Journal of the Geological Society*, *153*(1), pp.33-38. https://doi.org/10.1144/gsjgs.153.1.0033

Ingrams, S., McLean, D., Booth, M. and Bodman, D.J., 2020. Biostratigraphy and paleoecology of Asbian–Brigantian (Mississippian) miospores from Berwick-upon-Tweed, Northumberland, UK: Preliminary results. *Review of Palaeobotany and Palynology*, *276*, p.104206. https://doi.org/10.1016/j.revpalbo.2020.104206

Jackson, C.A.L., Gawthorpe, R.L., Carr, I.D. and Sharp, I.R., 2005. Normal faulting as a control on the stratigraphic development of shallow marine syn-rift sequences: the Nukhul and Lower Rudeis Formations, Hammam Faraun fault block, Suez Rift, Egypt. *Sedimentology*, *52*(2), pp.313-338. https://doi.org/10.1111/j.1365-3091.2005.00699.x

Jackson, C.L., Chua, S.T., Bell, R.E. and Magee, C., 2013. Structural style and early stage growth of inversion structures: 3D seismic insights from the Egersund Basin, offshore Norway. *Journal of Structural Geology*, *46*, pp.167-185. https://doi.org/10.1016/j.jsg.2012.09.005

Jackson, J.A. and White, N.J., 1989. Normal faulting in the upper continental crust: observations from regions of active extension. *Journal of Structural Geology*, *11*(1-2), pp.15-36. https://doi.org/10.1016/0191-8141(89)90033-3

Jackson, J. and Leeder, M., 1994. Drainage systems and the development of normal faults: an example from Pleasant Valley, Nevada. *Journal of Structural Geology*, *16*(8), pp.1041-1059. https://doi.org/10.1016/0191-8141(94)90051-5

Johannessen, E.P. and Steel, R.J., 1992. Mid-Carboniferous extension and rift-infill sequences in the Billefjorden Trough, Svalbard. *Norsk geologisk tidsskrift*, *72*(1), pp.35-48.

Johnson, G.A.L., 1967. Basement control of Carboniferous sedimentation in northern England. *Proceedings of the Yorkshire Geological Society, 36*(2), pp.175-194. https://doi.org/10.1144/pygs.36.2.175

Johnson, G.A.L. and Marshall, A.E., 1970. Tournaisian beds in Ravenstonedale, Westmorland. *Proceedings of the Yorkshire Geological Society, 38*(2), pp.261-280. https://doi.org/10.1144/pygs.38.2.261

Johnson, G.A.L., 1984. Subsidence and sedimentation in the Northumberland Trough. *Proceedings of the Yorkshire Geological Society, 45*(1-2), pp.71-83. https://doi.org/10.1144/pygs.45.1-2.71

Johnson, G.A.L. and Nudds, J.R., 1995. Carboniferous biostratigraphy of the Rookhope Borehole, Co. Durham. *Earth and Environmental Science Transactions of The Royal Society of Edinburgh, 86*(3), pp.181-226. https://doi.org/10.1017/S0263593300002224

Johnson, G.A.L., Somerville, I.D., Tucker, M.E. and Cózar, P., 2011, May. Carboniferous stratigraphy and context of the Seal Sands No. 1 Borehole, Teesmouth, NE England: the deepest onshore borehole in Great Britain. *Proceedings of the Yorkshire Geological Society, 58*(3), pp. 173-196. https://doi.org/10.1144/pygs.58.3.231

Jones, N.S., 1993. Stratigraphical and sedimentological characteristics of the 'Whitehaven Sandstone Series', Westphalian C, West Cumbrian Coalfield. *British Geological Survey Technical Report,* WH/93/102R. http://nora.nerc.ac.uk/id/eprint/7191/1/IR06043.pdf

Jones, N.S., Holloway, S., Creedy, D.P., Garner, K., Smith, N.J.P., Browne, M.A.E., Duncan, S., 2004. UK Coal Resource for New Exploration Technologies. British Geological Survey Commissioned Report. CR/04/015N. http://nora.nerc.ac.uk/id/eprint/509526/1/CR04015N.pdf

Jones, N.S. and Holliday, D.W., 2006. The stratigraphy and sedimentology of Upper Carboniferous Warwickshire Group red-bed facies in the Canonbie area of S.W. Scotland. *British Geological Survey Internal Report,* IR/06/043. 75pp. http://nora.nerc.ac.uk/id/eprint/7191/1/IR06043.pdf

Jones, N.S., 2007a. The West Lothian Oil-Shale Formation: Results of a sedimentological study. *British Geological Survey Internal Report,* IR/05/046. 63 pp. http://nora.nerc.ac.uk/id/eprint/11050/1/IR05046.pdf

Jones, N.S. 2007b. The Scremerston Formation: results of a sedimentological study of onshore outcrop sections and offshore Well 42/13-2. *British Geological Survey Commissioned Report,* CR/07/101. 70 pp. http://nora.nerc.ac.uk/id/eprint/512724/1/CR07101N.pdf

Jones, N.S., Holliday, D.W. and McKervey, J.A., 2011. Warwickshire Group (Pennsylvanian) red-beds of the Canonbie Coalfield, England–Scotland border, and their regional palaeogeographical implications. *Geological Magazine, 148*(1), pp.50-77. https://doi.org/10.1017/S001675681000035X

Jones, N.S. and Holliday, D.W., 2016. Intra-Carboniferous deformation and unconformity at Gilnockie Bridge, SW Scotland, reinterpreted as the result of multiple channel-bank collapse. *Scottish Journal of Geology, 52*(1), pp.43-54. https://doi.org/10.1144/sjg2015-009

Jutras, P., 2017. Climate fluctuations recorded in phreatic and vadose calcretes of the Lower Carboniferous Clyde Sandstone Formation of Machrihanish, Kintyre Peninsula, SW Scotland. *Journal of the Geological Society, 174*(4), pp.646-654. https://doi.org/10.1144/jgs2016-043

Kaiser, B.O., Cacace, M., Scheck-Wenderoth, M. and Lewerenz, B., 2011. Characterization of main heat transport processes in the Northeast German Basin: Constraints from 3-D numerical models. *Geochemistry, Geophysics, Geosystems, 12*(7). https://doi.org/10.1029/2011GC003535

Karner, G.D. and Watts, A.B., 1982. On isostasy at Atlantic-type continental margins. *Journal of Geophysical Research: Solid Earth, 87*(B4), pp.2923-2948. https://doi.org/10.1029/JB087iB04p02923

Karner, G.D. and Watts, A.B., 1983. Gravity anomalies and flexure of the lithosphere at mountain ranges. *Journal of Geophysical Research: Solid Earth, 88*(B12), pp.10449-10477. https://doi.org/10.1029/JB088iB12p10449

Kearsey, T.I., Millward, D., Ellen, R., Whitbread, K. and Monaghan, A.A., 2019. Revised stratigraphic framework of pre-Westphalian Carboniferous petroleum system elements from the Outer Moray Firth to the Silverpit Basin, North Sea, UK. *Geological Society, London, Special Publications, 471*(1), pp.91-113. https://doi.org/10.1144/SP471.11

Keller, J.V.A. and McClay, K.R., 1995. 3D sandbox models of positive inversion. *Geological Society, London, Special Publications, 88*(1), pp.137-146. https://doi.org/10.1144/GSL.SP.1995.088.01.09

Kelling, G., 1988. Silesian sedimentation and tectonics in the South Wales Basin: a brief review. In: *Sedimentation in a synorogenic basin complex. The Upper Carboniferous of Northwest Europe*, pp. 38-42.

Kimbell, G.S., Chadwick, R.A., Holliday, D.W. and Werngren, O.C., 1989. The structure and evolution of the Northumberland Trough from new seismic reflection data and its bearing on modes of continental extension. *Journal of the Geological Society, 146*(5), pp.775-787. https://doi.org/10.1144/gsjgs.146.5.0775

Kimbell, G.S., Carruthers, R.M., Walker, A.S.D., and Williamson, J.P., 2006. *Regional Geophysics of Southern Scotland and Northern England*. Version 1.0 on CD-ROM. British Geological Survey, Keyworth, Nottingham.

Kimbell, G.S., Young, B., Millward, D. and Crowley, Q.G., 2010. The North Pennine batholith (Weardale Granite) of northern England: new data on its age and form. *Proceedings of the Yorkshire Geological Society, 58*(2), pp.107-128. https://doi.org/10.1144/pygs.58.1.273

Kimbell, G.S., Williamson, J.P., 2015. A gravity interpretation of the Central North Sea. *British Geological Survey Commissioned Report*, CR/15/119. 75pp. http://nora.nerc.ac.uk/id/eprint/516759/1/CR15119.pdf

Kirby, E. and Whipple, K.X., 2012. Expression of active tectonics in erosional landscapes. Journal of *Structural Geology, 44,* pp.54-75. https://doi.org/10.1016/j.jsg.2012.07.009

Kombrink, H., 2008. The Carboniferous of the Netherlands and Surrounding Areas; a Basin Analysis (PhD Thesis: Utrecht University).

Kombrink, H., Van Lochem, H. and Van Der Zwan, K.J., 2010. Seismic interpretation of Dinantian carbonate platforms in the Netherlands; implications for the palaeogeographical and structural development of the Northwest European Carboniferous Basin. *Journal of the Geological Society, 167*(1), pp.99-108. https://doi.org/10.1144/0016-76492008-149

Kooi, H., Cloetingh, S. and Burrus, J., 1992. Lithospheric necking and regional isostasy at extensional basins 1. Subsidence and gravity modeling with an application to the Gulf of Lions margin (SE France). *Journal of Geophysical Research: Solid Earth, 97*(B12), pp.17553-17571. https://doi.org/10.1029/92JB01377

Kraus, M.J., Wells, T.M., Smith, N.D. and Rogers, J., 1999. Recognizing avulsion deposits in the ancient stratigraphical record. In: *Fluvial sedimentology VI* (Vol. 28, pp. 251-268). Special Publication 28: International Association of Sedimentologists. https://doi.org/10.1002/9781444304213.ch19

Kusznir, N.J. and Park, R.G., 1987. The extensional strength of the continental lithosphere: its dependence on geothermal gradient, and crustal composition and thickness. *Geological Society, London, Special Publications, 28*(1), pp.35-52. https://doi.org/10.1144/GSL.SP.1987.028.01.04

Kusznir, N.J. and Egan, S.S., 1989. Simple-Shear and Pure-Shear Models of Extensional Sedimentary Basin Formation: Application to the Jeanne d'Arc Basin, Grand Banks of Newfoundland: Chapter 20: North American Margins.

Kusznir, N.J., Marsden, G. and Egan, S.S., 1991. A flexural-cantilever simple-shear/pure-shear model of continental lithosphere extension: applications to the Jeanne d'Arc Basin, Grand Banks and Viking Graben, North Sea. *Geological Society, London, Special Publications, 56*(1), pp.41-60. https://doi.org/10.1144/GSL.SP.1991.056.01.04

Lancaster, P.J., Daly, J.S., Storey, C.D. and Morton, A.C., 2017. Interrogating the provenance of large river systems: multi-proxy in situ analyses in the Millstone Grit, Yorkshire. *Journal of the Geological Society, 174*(1), pp.75-87. https://doi.org/10.1144/jgs2016-069

Lee, M.K., 1986. A new gravity survey of the Lake District and three-dimensional model of the granite batholith. *Journal of the Geological Society, 143*(3), pp.425-435. https://doi.org/10.1144/gsjgs.143.3.0425

Lee, M.K., Brown, G.C., Webb, P.C., Wheildon, J. and Rollin, K.E., 1987. Heat flow, heat production and thermo-tectonic setting in mainland UK. *Journal of the Geological Society*, *144*(1), pp.35-42. https://doi.org/10.1144/gsjgs.144.1.0035

Leeder, M.R., 1972. *Upper Old Red Sandstone-Tournaisian sedimentology and the initiation and origin of the Northumberland basin* (Doctoral dissertation, University of Reading).

Leeder, M., 1973. Sedimentology and palaeogeography of the Upper Old Red Sandstone in the Scottish Border basin. *Scottish Journal of Geology*, *9*(2), pp.117-144. https://doi.org/10.1144/sjg09020117

Leeder, M.R., 1974. Lower Border Group (Tournaisian) fluvio-deltaic sedimentation and palaeogeography of the Northumberland Basin. *Proceedings of the Yorkshire Geological Society*, *40*(2), pp.129-180. https://doi.org/10.1144/pygs.40.2.129

Leeder, M.R., 1975. The origin of the Northumberland basin. *Scottish Journal of Geology*, *10*(4), pp.283-296. https://doi.org/10.1144/sjg10040283

Leeder, M.R., 1976. Palaeogeographic significance of pedogenic carbonates in the topmost upper Old Red Sandstone of the Scottish border basin. *Geological Journal*, *11*(1), pp.21-28. https://doi.org/10.1002/gj.3350110103

Leeder, M.R. and Bridges, P.H., 1978. Upper Old Red Sandstone near Kirkbean, Dumfries and Galloway. *Scottish Journal of Geology*, *14*(4), pp.267-272. https://doi.org/10.1144/sjg14040267

Leeder, M.R., 1982. Upper Palaeozoic basins of the British Isles—Caledonide inheritance versus Hercynian plate margin processes. *Journal of the Geological Society*, *139*(4), pp.479-491. https://doi.org/10.1144/gsjgs.139.4.0479

Leeder, M.R. and Gawthorpe, R.L., 1987. Sedimentary models for extensional tilt-block/half-graben basins. *Geological Society, London, Special Publications*, *28*(1), pp.139-152. https://doi.org/10.1144/GSL.SP.1987.028.01.11

Leeder, M.R. and McMahon, A.H., 1988. Upper Carboniferous (Silesian) bassin subsidence in northern Britain. In: *Sedimentation in a synorogenic basin complex. The Upper Carboniferous of Northwest Europe* (pp. 43-52).

Leeder, M.R. and Hardman, M., 1990. Carboniferous geology of the Southern North Sea Basin and controls on hydrocarbon prospectivity. *Geological Society, London, Special Publications*, *55*(1), pp.87-105. https://doi.org/10.1144/GSL.SP.1990.055.01.04

Lipsey, L., Pluymaekers, M., Goldberg, T., van Oversteeg, K., Ghazaryan, L., Cloetingh, S. and van Wees, J.D., 2016. Numerical modelling of thermal convection in the Luttelgeest carbonate platform, the Netherlands. *Geothermics*, *64*, pp.135-151. https://doi.org/10.1016/j.geothermics.2016.05.002

Littke, R., Buker, C., Luckge, A., Sachsenhofer, R.F. and Welte, D.H., 1994. A new evaluation of palaeoheat flows and eroded thicknesses for the Carboniferous Ruhr basin, western

Germany. *International Journal of Coal Geology, 26*, 155–183. https://doi.org/10.1016/0166-5162(94)90009-4

Littke, R., Buker, C., Hertle, M., Karg, H., Stroetmanheinen, V. and Oncken, O., 2000. Heat flow evolution, subsidence and erosion in the Rheno-Hercynian orogenic wedge of central Europe. In: Franke, W., Haak, V., Oncken, O. and Tanner, D. (eds) Orogenic Processes: Quantification and Modelling in the Variscan Belt. *Geological Society, London, Special Publications, 179*, 231–255, https://doi.org/10.1144/GSL.SP.2000. 179.01.15

López, M., García, M., Bucher, J., Funes, D.S., D'Elia, L., Bilmes, A., Naipauer, M., Sato, A.M., Valencia, V.A. and Franzese, J.R., 2019. Structural evolution of The Collón Cura basin: Tectonic implications for the north Patagonian Broken Foreland. *Journal of South American Earth Sciences, 93*, pp.424-438. https://doi.org/10.1016/j.jsames.2019.04.021

Lumsden, G.I. and Wilson, R.B., 1967. The Carboniferous Limestone Series of Douglas, Lanarkshire. *Bulletin of the Geological Survey of Great Britain, 26*, pp.1-22.

Lumsden, G.I., Tullock, W., Howells, M.F. and Davies, A., 1967. The geology of the neighbourhood of Langholm: explanation of one-inch geological sheet 11. *Memoirs of the Geological Survey of Scotland.* HMSO, Edinburgh. http://pubs.bgs.ac.uk/publications.html?pubID=B01863

Lundmark, A.M., Sæther, T. and Sørlie, R., 2014. Ordovician to Silurian magmatism on the Utsira High, North Sea: implications for correlations between the onshore and offshore Caledonides. *Geological Society, London, Special Publications, 390*(1), pp.513-523. https://doi.org/10.1144/SP390.21

Macgregor, A.G., 1960. Divisions of the Carboniferous on Geological Survey Scottish maps. *Bulletin of the Geological Survey of Great Britain, No. 16*, pp. 127–130.

Maclennan, J. and Lovell, B., 2002. Control of regional sea level by surface uplift and subsidence caused by magmatic underplating of Earth's crust. *Geology, 30*(8), pp.675-678. https://doi.org/10.1130/0091-7613(2002)030<0675:CORSLB>2.0.CO;2

Mahdi, S.A. and Butterworth, M.A., 1994. Palynology of the Dinantian Lower Border Group of the Solway Basin. Proceedings of the Yorkshire Geological Society, 50(2), pp.157-171. https://doi.org/10.1144/pygs.50.2.157

Majorowicz, J., Gosnold, W., Gray, A., Safanda, J., Klenner, R. and Unsworth, M., 2012. Implications of post-glacial warming for northern Alberta heat flow-correcting for the underestimate of the geothermal potential. *GRC Transactions, 36*(GRC1030303).

Manning, D.A.C., Younger, P.L., Smith, F.W., Jones, J.M., Dufton, D.J. and Diskin, S., 2007. A deep geothermal exploration well at Eastgate, Weardale, UK: a novel exploration concept for low-enthalpy resources. *Journal of the Geological Society, 164*(2), pp.371-382. https://doi.org/10.1144/0016-76492006-015

Marr, J.E., 1921. The rigidity of north-west Yorkshire. *Naturalist, 1921*, pp.63-72.

Marshak, S., Alkmim, F. and Jordt-Evangelista, H., 1992. Proterozoic crustal extension and the generation of dome-and-keel structure in an Archaean granite–greenstone terrane. *Nature, 357*(6378), pp.491-493. https://doi.org/10.1038/357491a0

Marshall, J.E., Reeves, E.J., Bennett, C.E., Davies, S.J., Kearsey, T.I., Millward, D., Smithson, T.R. and Browne, M.A., 2018. Reinterpreting the age of the uppermost 'Old Red Sandstone'and Early Carboniferous in Scotland. *Earth and Environmental Science Transactions of the Royal Society of Edinburgh, 109*(1-2), pp.265-278.

Martin, C.A. and Turner, B.R., 1998. Origins of massive-type sandstones in braided river systems. *Earth-Science Reviews, 44*(1-2), pp.15-38. https://doi.org/10.1016/S0012-8252(98)00019-1

Martinez Catalan, J.R., Arenas, R., Diaz Garcia, F., Gomez-Barreiro, J., Gonzalez Cuadra, P., Abati, J., Castineiras, P., Fernandez-Suarez, J., Sanchez Martınez, S., Andonaegui, P., Gonzalez Clavijo, E., Dıez Montes, A., Rubio Pascual, F.J. and Valle Aguado, B., 2007. Space and time in the tectonic evolution of the northwestern Iberian Massif. Implications for the Variscan belt. In: *4–D Framework of Continental Crust* (R.D. Hatcher Jr, M.P. Carlson, J.H. McBride and J.R. Martınez Catalan, eds). Geol. Soc. Am. Mem., 200, 403–423.

Maynard, J.R. and Leeder, M.R., 1992. On the periodicity and magnitude of Late Carboniferous glacio-eustatie sea-level changes. Journal of the Geological Society, 149(3), pp.303-311. https://doi.org/10.1144/gsjgs.149.3.0303

Maynard, J.R. and Dunay, R.E., 1999, January. Reservoirs of the Dinantian (Lower Carboniferous) play of the southern North Sea. In: *Geological Society, London, Petroleum Geology Conference Series, 5*(1), pp. 729-745). Geological Society of London. https://doi.org/10.1144/0050729

McKellar, Z., Hartley, A.J., Morton, A.C. and Frei, D., 2020. A multidisciplinary approach to sediment provenance analysis of the late Silurian–Devonian Lower Old Red Sandstone succession, northern Midland Valley Basin, Scotland. *Journal of the Geological Society, 177*(2), pp.297-314. https://doi.org/10.1144/jgs2019-063

McKenzie, D., 1978. Some remarks on the development of sedimentary basins. *Earth and Planetary science letters, 40*(1), pp.25-32. https://doi.org/10.1016/0012-821X(78)90071-7

McKerrow, W.S., Leggett, J.K. and Eales, M.H., 1977. Imbricate thrust model of the Southern Uplands of Scotland. *Nature, 267*(5608), pp.237-239.

McKerrow, W.S., Lambert, R.S.J. and Cocks, L.R.M., 1985. The Ordovician, Silurian and Devonian periods. *Geological Society, London, Memoirs, 10*(1), pp.73-80. https://doi.org/10.1144/GSL.MEM.1985.010.01.08

McLean, A.C., and Deegan, C.E., 1978, A synthesis of the solid geology of the Clyde region. *Institute of Geological Sciences Report, 78*(9), pp. 93-114.

McLean, D. and Murray, I., 1996. Subsurface correlation of Carboniferous coal seams and inter-seam sediments using palynology: application to exploration for coalbed methane. *Geological Society of London, Special Publications, 109*(1), pp.315-324. https://doi.org/10.1144/GSL.SP.1996.109.01.23

McLean, D. and Chisholm, J.I. 1996. Reworked palynomorphs as provenance indicators in the Yeadonian of the Pennine Basin. *Proceedings of the Yorkshire Geological Society, 51*, 141–151, https://doi.org/10.1144/pygs.51.2.141

McLean, W.S., 2018. Scottish coal seam names and correlations. *British Geological Survey Open Report Report*, OR/18/027. 19pp. http://nora.nerc.ac.uk/id/eprint/520887/1/OR18027.pdf

McMillan, A.A., Hamblin, R.J.O., Merritt, J.W., 2011. A lithostratigraphical framework for onshore Quaternary and Neogene (Tertiary) superficial deposits of Great Britain and the Isle of Man. *British Geological Survey Research Report*, RR/10/03. 343pp. http://nora.nerc.ac.uk/id/eprint/14531/1/RR10003.pdf

Menning, M., Alekseev, A.S., Chuvashov, B.I., Davydov, V.I., Devuyst, F.X., Forke, H.C., Grunt, T.A., Hance, L., Heckel, P.H., Izokh, N.G. and Jin, Y.G., 2006. Global time scale and regional stratigraphic reference scales of central and west Europe, east Europe, Tethys, south China, and North America as used in the Devonian–Carboniferous–Permian Correlation Chart 2003 (DCP 2003). *Palaeogeography, Palaeoclimatology, Palaeoecology, 240*(1-2), pp.318-372. https://doi.org/10.1016/j.palaeo.2006.03.058

Meredith, D.J. and Egan, S.S., 2002. The geological and geodynamic evolution of the eastern Black Sea basin: insights from 2-D and 3-D tectonic modelling. Tectonophysics, *350*(2), pp.157-179. https://doi.org/10.1016/S0040-1951(02)00121-X

Miall, A.D., 1977. A review of the braided-river depositional environment. *Earth-Science Reviews, 13*(1), pp.1-62. https://doi.org/10.1016/0012-8252(77)90055-1

Miall, A.D., 1985. Architectural-element analysis: a new method of facies analysis applied to fluvial deposits. *Earth-Science Reviews, 22*(4), pp.261-308. https://doi.org/10.1016/0012-8252(85)90001-7

Miall, A.D., 1988. Reservoir heterogeneities in fluvial sandstones: lessons from outcrop studies. *AAPG bulletin, 72*(6), pp.682-697. https://doi.org/10.1306/703C8F01-1707-11D7-8645000102C1865D

Mikesell, L.R., Weissmann, G.S. and Karachewski, J.A., 2010. Stream capture and piracy recorded by provenance in fluvial fan strata. *Geomorphology, 115*(3-4), pp.267-277. https://doi.org/10.1016/j.geomorph.2009.04.025

Millward, D., Keasrsey, T, Browne, M.A.E., 2013. Norham West Mains Farm Borehole: operations report. *British Geological Survey Internal Report*, IR/13/033. 39pp. http://nora.nerc.ac.uk/id/eprint/519306/1/IR13033.pdf

Millward, D., Davies, S.J., Brand, P.J., Browne, M.A., Bennett, C.E., Kearsey, T.I., Sherwin, J.E. and Marshall, J.E., 2019. Palaeogeography of tropical seasonal coastal wetlands in northern Britain during the early Mississippian Romer's Gap. Earth and Environmental Science *Transactions of the Royal Society of Edinburgh, 109*(1-2), pp.279-300. http://dx.doi.org/10.1017/S1755691018000737

Milton-Worssell, R., Smith, K., McGrandle, A., Watson, J. and Cameron, D., 2010, January. The search for a Carboniferous petroleum system beneath the Central North Sea. In: *Geological Society, London, Petroleum Geology Conference series* (Vol. 7, No. 1, pp. 57-75). Geological Society of London. https://doi.org/10.1144/0070057

Mitrovica, J.X., Beaumont, C. and Jarvis, G.T., 1989. Tilting of continental interiors by the dynamical effects of subduction. *Tectonics, 8*(5), pp.1079-1094. https://doi.org/10.1029/TC008i005p01079

Mitten, A.J., Howell, L.P., Clarke, S.M. and Pringle, J.K., 2020. Controls on the deposition and preservation of architectural elements within a fluvial multi-storey sandbody. *Sedimentary Geology, 401*, p.105629. https://doi.org/10.1016/j.sedgeo.2020.105629

Morton, A.C. and Whitham, A.G. 2002. The Millstone Grit of northern England: a response to tectonic evolution of a northern sourceland. *Proceedings of the Yorkshire Geological Society, 54*, 47–56, https://doi.org/10.1144/pygs.54.1.47

Morton, A., Hallsworth, C. and Moscariello, A. 2005. Interplay between northern and southern sediment sources during Westphalian deposition in the Silverpit Basin, southern North Sea. In: Collinson, J.D., Evans, D.J., Holliday, D.W. and Jones, N.S. (eds) *Carboniferous hydrocarbon geology: the southern North Sea and surrounding onshore areas.* Yorkshire Geological Society Occasional Publication, 7, 135–146.

Morton, A., Fanning, M. and Jones, N., 2010. Variscan sourcing of Westphalian (Pennsylvanian) sandstones in the Canonbie Coalfield, UK. *Geological Magazine, 147*(5), pp.718-727. https://doi.org/10.1017/S0016756810000014

Morton, A., Waters, C., Fanning, M., Chisholm, I. and Brettle, M. 2014. Origin of Carboniferous sandstones fringing the northern margin of the Wales-Brabant Massif: insights from detrital zircon ages. *Geological Journal, 50*, 553–574, https://doi.org/10.1002/gj.2572

Monaghan, A.A. and Pringle, M.S., 2004. 40Ar/39Ar geochronology of Carboniferous-Permian volcanism in the Midland Valley, Scotland. *Geological Society, London, Special Publications, 223*(1), pp.219-241. https://doi.org/10.1144/GSL.SP.2004.223.01.10

Monaghan, A.A. and Parrish, R.R., 2006. Geochronology of Carboniferous–Permian magmatism in the Midland Valley of Scotland: implications for regional tectonomagmatic evolution and the numerical time scale. *Journal of the Geological Society, 163*(1), pp.15-28. https://doi.org/10.1144/0016-764904-142

Monaghan, A.A. and Browne, M.A.E., 2010. Nine 40Ar/39Ar dates from Carboniferous igneous rocks of the Midland Valley of Scotland. British *Geological Survey Open Report*, OR/10/065. 46pp. http://nora.nerc.ac.uk/id/eprint/14172/3/OR10065.pdf

Monaghan, A.A. 2014. The Carboniferous shales of the Midland Valley of Scotland: geology and resource estimation. *British Geological Survey for Department of Energy and Climate Change*, London, UK. https://www.ogauthority.co.uk/media/2765/bgs_decc_mvs_2014_main_report.pdf

Monaghan, A.A., Arsenikos, S., Quinn, M.F., Johnson, K.R., Vincent, C.J., Vane, C.H., Kim, A.W., Uguna, C.N., Hannis, S.D., Gent, C.M.A. and Millward, D., 2017. Carboniferous petroleum systems around the Mid North Sea High, UK. *Marine and Petroleum Geology, 88*, pp.282-302. https://doi.org/10.1016/j.marpetgeo.2017.08.019

Monaghan, A., Starcher, V., Barron, H., Kuras, O., Abesser, C., Midgley, J., Dochartaigh, B.Ó., Fordyce, F., Burke, S., Taylor-Curran, H. and Luckett, R., 2019. A new Mine Water Geothermal Research Facility: the UK Geoenergy Observatory in Glasgow, Scotland. In *81st EAGE Conference and Exhibition 2019* (Vol. 2019, No. 1, pp. 1-5). European Association of Geoscientists & Engineers. https://doi.org/10.3997/2214-4609.201901602

Monro, M., 1986. *Sedimentology of the Carboniferous Fell Sandstone Group of Northumberland* (Doctoral dissertation, University of Newcastle upon Tyne).

Montenat, C., Barrier, P. and Hibsch, C., 2007. Seismites: An attempt at critical analysis and classification. *Sedimentary Geology, 196*(1-4), pp.5-30. https://doi.org/10.1016/j.sedgeo.2006.08.004

Moretti, I., Sakellariou, D., Lykousis, V. and Micarelli, L., 2003. The Gulf of Corinth: an active half graben? *Journal of Geodynamics, 36*(1-2), pp.323-340. https://doi.org/10.1016/S0264-3707(03)00053-X

Morley, C.K., 2010. Stress re-orientation along zones of weak fabrics in rifts: An explanation for pure extension in 'oblique'rift segments? *Earth and Planetary Science Letters, 297*(3-4), pp.667-673. https://doi.org/10.1016/j.epsl.2010.07.022

Morton, A.C., Claoué-Long, J.C. and Hallsworth, C.R., 2001. Zircon age and heavy mineral constraints on provenance of North Sea Carboniferous sandstones. *Marine and Petroleum Geology, 18*(3), pp.319-337. https://doi.org/10.1016/S0264-8172(00)00065-9

Mount, J.F., 1984. Mixing of siliciclastic and carbonate sediments in shallow shelf environments. *Geology, 12*(7), pp.432-435. https://doi.org/10.1130/0091-7613(1984)12<432:MOSACS>2.0.CO;2

Murchison, D., 2004. Aberrations in the coalification patterns of the offshore coalfields of Northumberland and Durham, United Kingdom. *International journal of coal geology, 58*(3), pp.133-146. https://doi.org/10.1016/j.coal.2003.10.005

Murphy, J.B., Braid, J.A., Quesada, C., Dahn, D., Gladney, E. and Dupuis, N., 2016. An eastern Mediterranean analogue for the Late Palaeozoic evolution of the Pangaean suture zone in SW Iberia. *Geological Society, London, Special Publications, 424*(1), pp.241-263. https://doi.org/10.1144/SP424.9

Mykura, W. 1960. The replacement of coal by limestone and the reddening of Coal Measures in the Ayrshire Coalfield. *Bulletin of the Geological Survey of Great Britain, No. 16,* pp. 69–109.

Mykura, W., 1965. The age of the lower part of the New Red Sandstone of South-West Scotland. *Scottish Journal of Geology, 1*(1), pp.9-18. https://doi.org/10.1144/sjg01010009

Mykura, W. 1967. The Upper Carboniferous rocks of south-west Ayrshire. *Bulletin of the Geological Survey of Great Britain, No. 26*, pp. 23–48.

Nairn, A.E.M., 1956. IV.—The Lower Carboniferous Rocks between the Rivers Esk and Annan, Dumfriesshire. *Transactions of the Geological Society of Glasgow, 22*(1), pp.80-93. https://doi.org/10.1144/transglas.22.1.80

Nemec, W. and Postma, G., 1993. Quaternary alluvial fans in southwestern Crete: sedimentation processes and geomorphic evolution. In: *Alluvial sedimentation* (Vol. 17, pp. 235-276). Oxford: International Association of Sedimentologists. https://doi.org/10.1002/9781444303995.ch18

Neves, R., Gueinn, K.J., Clayton, G., Ioannides, N.S., Neville, R.S. and Kruszewska, K.R.I.S.T.I.N.A., 1973. 2.—Palynological Correlations within the Lower Carboniferous of Scotland and Northern England. Earth and Environmental Science *Transactions of The Royal Society of Edinburgh, 69*(2), pp.23-70.

Neves, R., 1974. Palynology of the Spilmersford Borehole. *Bulletin of the Geological Survey of Great Britain, 12*, pp.73-97.

Newport, S.M., Jerrett, R.M., Taylor, K.G., Hough, E. and Worden, R.H., 2018. Sedimentology and microfacies of a mud-rich slope succession: in the Carboniferous Bowland Basin, NW England (UK). *Journal of the Geological Society, 175*(2), pp.247-262. https://doi.org/10.1144/jgs2017-036

Nicol, A., Walsh, J.J., Manzocchi, T. and Morewood, N., 2005. Displacement rates and average earthquake recurrence intervals on normal faults. *Journal of Structural Geology, 27*(3), pp.541-551. https://doi.org/10.1016/j.jsg.2004.10.009

Noack, V., Cherubini, Y., Scheck-Wenderoth, M., Lewerenz, B., Höding, T., Simon, A. and Moeck, I., 2010. Assessment of the present-day thermal field (NE German Basin)—inferences from 3D modelling. *Geochemistry, 70*, pp.47-62. https://doi.org/10.1016/j.chemer.2010.05.008

Norden, B. and Forster, A., 2006. Thermal conductivity and radiogenic heat production of sedimentary and magmatic rocks in the Northeast German Basin. *AAPG bulletin, 90*(6), pp.939-962. https://doi.org/10.1306/01250605100

Norden, B., Förster, A. and Balling, N., 2008. Heat flow and lithospheric thermal regime in the Northeast German Basin. *Tectonophysics, 460*(1-4), pp.215-229. https://doi.org/10.1016/j.tecto.2008.08.022

Norden, B., Förster, A., Förster, H.J. and Fuchs, S., 2020. Temperature and pressure corrections applied to rock thermal conductivity: impact on subsurface temperature prognosis and heat-flow determination in geothermal exploration. *Geothermal Energy, 8*(1), pp.1-19. https://doi.org/10.1186/s40517-020-0157-0

Nøttvedt, A., Cecchi, M., Gjelberg, J.G., Kristensen, S.E., Lønøy, A., Rasmussen, A., Rasmussen, E., Skott, P.H. and Van Veen, P.M., 1993. Svalbard-Barents Sea correlation: a short review.

Norwegian Petroleum Society Special Publications, 2, pp.363-375.
https://doi.org/10.1016/B978-0-444-88943-0.50027-7

O'Mara, P.T. and Turner, B.R., 1999. Sequence stratigraphy of coastal alluvial plain Westphalian B Coal Measures in Northumberland and the southern North Sea. *International Journal of Coal Geology*, *42*(1), pp.33-62. https://doi.org/10.1016/S0166-5162(99)00028-2

Oncken, O., Von Winterfeld, C. and Dittmar, U., 1999. Accretion of a rifted passive margin: the Late Paleozoic Rhenohercynian fold and thrust belt (Middle European Variscides). *Tectonics*, *18*(1), pp.75-91. https://doi.org/10.1029/98TC02763

Osagiede, E.E., Rotevatn, A., Gawthorpe, R., Kristensen, T.B., Jackson, C.A. and Marsh, N., 2020. Pre-existing intra-basement shear zones influence growth and geometry of non-colinear normal faults, western Utsira High–Heimdal Terrace, North Sea. *Journal of Structural Geology*, *130*, p.103908. https://doi.org/10.1016/j.jsg.2019.103908

Oxburgh, E.R., Richardson, S.W., Turcotte, D.L. and Hsui, A., 1972. Equilibrium bore hole temperatures from observation of thermal transients during drilling. *Earth and Planetary Science Letters*, *14*(1), pp.47-49. https://doi.org/10.1016/0012-821X(72)90077-5

Painter, C.S. and Carrapa, B., 2013. Flexural versus dynamic processes of subsidence in the North American Cordillera foreland basin. *Geophysical Research Letters*, *40*(16), pp.4249-4253. https://doi.org/10.1002/grl.50831

Parsons, B. and Sclater, J.G., 1977. An analysis of the variation of ocean floor bathymetry and heat flow with age. *Journal of geophysical research*, *82*(5), pp.803-827. https://doi.org/10.1029/JB082i005p00803

Paterson, I.B. and Hall, I.H.S., 1986. Lithostratigraphy of the late Devonian and early Carboniferous rocks in the Midland Valley of Scotland. *British Geological Survey Report*, *18*(3). http://pubs.bgs.ac.uk/publications.html?pubID=B01299

Paulillo, A., Cotton, L., Law, R., Striolo, A. and Lettieri, P., 2020. Geothermal energy in the UK: the life-cycle environmental impacts of electricity production from the United Downs Deep Geothermal Power project. *Journal of Cleaner Production*, *249*, p.119410. https://doi.org/10.1016/j.jclepro.2019.119410

Peace, G.R. and Besly, B.M., 1997. End-Carboniferous fold-thrust structures, Oxfordshire, UK: implications for the structural evolution of the late Variscan foreland of south-central England. *Journal of the Geological Society*, *154*(2), pp.225-237. https://doi.org/10.1144/gsjgs.154.2.0225

Pearce, T.J., Besly, B.M., Wray, D.S. and Wright, D.K., 1999. Chemostratigraphy: a method to improve interwell correlation in barren sequences—a case study using onshore Duckmantian/Stephanian sequences (West Midlands, UK). *Sedimentary Geology*, *124*(1-4), pp.197-220. https://doi.org/10.1016/S0037-0738(98)00128-6

Pearce, T.J., Wray, D.S., Ratcliffe, K.T., Wright, D.K. and Moscariello, A., 2005. Chemostratigraphy of the upper carboniferous schooner formation, southern North Sea. Carboniferous

hydrocarbon geology: the southern North Sea and surrounding onshore areas. *Yorkshire Geological Society, Occasional Publications Series, 7*, pp.47-164.

Pérez-Zárate, D., Santoyo, E., Acevedo-Anicasio, A., Díaz-González, L. and García-López, C., 2019. Evaluation of artificial neural networks for the prediction of deep reservoir temperatures using the gas-phase composition of geothermal fluids. *Computers & Geosciences, 129*, pp.49-68. https://doi.org/10.1016/j.cageo.2019.05.004

Perrier, R. and Quiblier, J., 1974. Thickness changes in sedimentary layers during compaction history; methods for quantitative evaluation. *AAPG Bulletin, 58*(3), pp.507-520. https://doi.org/10.1306/83D9142A-16C7-11D7-8645000102C1865D

Pharaoh, T., England, R. and Lee, M., 1995. The concealed Caledonide basement of eastern England and the southern North Sea—a review. *Studia geophysica et geodaetica, 39*(3), pp.330-346. https://doi.org/10.1007/BF02295826

Pharaoh, T., Haslam, R., Hough, E., Kirk, K., Leslie, G., Schofield, D. and Heafford, A., 2020. The Môn–Deemster–Ribblesdale fold–thrust belt, central UK: a concealed Variscan inversion belt located on weak Caledonian crust. *Geological Society, London, Special Publications, 490*(1), pp.153-176. https://doi.org/10.1144/SP490-2018-109

Phillips, T.B., Fazlikhani, H., Gawthorpe, R.L., Fossen, H., Jackson, C.A.L., Bell, R.E., Faleide, J.I. and Rotevatn, A., 2019. The Influence of Structural Inheritance and Multiphase Extension on Rift Development, the NorthernNorth Sea. *Tectonics, 38*(12), pp.4099-4126. https://doi.org/10.1029/2019TC005756

Pickard, N.A., Rees, J.G., Strogen, P., Somerville, I.D. and Jones, G.L., 1994. Controls on the evolution and demise of Lower Carboniferous carbonate platforms, northern margin of the Dublin Basin, Ireland. *Geological Journal, 29*(2), pp.93-117. https://doi.org/10.1002/gj.3350290202

Picken, G.S., 1988. The concealed coalfield at Canonbie: an interpretation based on boreholes and seismic surveys. *Scottish Journal of Geology, 24*(1), pp.61-71. https://doi.org/10.1144/sjg24010061

Poole, E.G., 1988. The concealed coalfield of Canonbie: Comment. *Scottish Journal of Geology, 24*(3), pp.305-306. https://doi.org/10.1144/sjg24030305

Porter, R.J. and Gallois, R.W., 2008. Identifying fluvio–lacustrine intervals in thick playa-lake successions: An integrated sedimentology and ichnology of arenaceous members in the mid–late Triassic Mercia Mudstone Group of south-west England, UK. *Palaeogeography, Palaeoclimatology, Palaeoecology, 270*(3-4), pp.381-398. https://doi.org/10.1016/j.palaeo.2008.07.020

Poulsen, S.E., Balling, N., Bording, T.S., Mathiesen, A. and Nielsen, S.B., 2017. Inverse geothermal modelling applied to Danish sedimentary basins. *Geophysical Journal International, 211*(1), pp.188-206. https://doi.org/10.1093/gji/ggx296

Powell, J H, Chisholm, JI, Bridge, D M, Rees, J G, Glover, B W and Besly, B M. 1999. Stratigraphical framework for Westphalian to Early Permian red-bed successions of the Pennine Basin. *British Geological Survey Technical Report*, WA/99/10. http://nora.nerc.ac.uk/id/eprint/3242/1/RR00001.pdf

Pratt, J.H., 1858. The deflection of the plumb-line in India and the compensatory effect of a deficiency of matter below the Himalaya mountains. *Philosophical Transactions of the Royal Society London, 149*, pp.745-778.

Quirk, D.G. and Aitken, J.F., 1997. The structure of the Westphalian in the northern part of the southern North Sea. *Geological Society, London, Special Publications, 123*(1), pp.143-152. https://doi.org/10.1144/GSL.SP.1997.123.01.09

Ramos, E., Busquets, P. and Vergés, J., 2002. Interplay between longitudinal fluvial and transverse alluvial fan systems and growing thrusts in a piggyback basin (SE Pyrenees). *Sedimentary Geology, 146*(1-2), pp.105-131. https://doi.org/10.1016/S0037-0738(01)00169-5

Ramsbottom, W.H.C., 1979. Rates of transgression and regression in the Carboniferous of NW Europe. *Journal of the Geological Society, 136*(2), pp.147-153. https://doi.org/10.1144/gsjgs.136.2.0147

Read, W.A., 1981. Facies breaks in the Scottish Passage Group and their possible correlation with the Mississippian—Pennsylvanian hiatus. *Scottish Journal of Geology, 17*(4), pp.295-300. https://doi.org/10.1144/sjg17040295

Read, W.A., 1988. Controls on Silesian sedimentation in the Midland Valley of Scotland. In: Besly, B.M., Kelling, G. (Eds.), *Sedimentation in a Synorogenic Basin Complex: the Upper Carboniferous of Northwest Europe*. Blackie and Son, Glasgow, pp. 222–241.

Read, W.A. and Forsyth, I.H., 1989. Allocycles and autocycles in the upper part of the Limestone Coal Group (Pendleian E1) in the Glasgow–Stirling region of the Midland Valley of Scotland. *Geological Journal, 24*(2), pp.121-137. https://doi.org/10.1002/gj.3350240205

Reineck, H.E. and Wunderlich, F., 1968. Classification and origin of flaser and lenticular bedding. Sedimentology, 11(1-2), pp.99-104. https://doi.org/10.1111/j.1365-3091.1968.tb00843.x

Rickards, R.B. and Woodcock, N.H., 2005. Stratigraphical revision of the Windermere Supergroup (Late Ordovician–Silurian in the southern Howgill Fells, NW England. *Proceedings of the Yorkshire Geological Society, 55*(4), pp.263-285. https://doi.org/10.1144/pygs.55.4.263

Ridd, M.F., Walker, D.B. and Jones, J.M., 1970. A deep borehole at Harton on the margin of the Northumbrian Trough. *Proceedings of the Yorkshire Geological Society, 38*(1), pp.75-103. https://doi.org/10.1144/pygs.38.1.75

Ring, U., 1994. The influence of preexisting structure on the evolution of the Cenozoic Malawi rift (East African rift system). *Tectonics, 13*(2), pp.313-326. https://doi.org/10.1029/93TC03188

Rippon, J., Read, W.A. and Park, R.G., 1996. The Ochil Fault and the Kincardine basin: key structures in the tectonic evolution of the Midland Valley of Scotland. *Journal of the Geological Society, 153*(4), pp.573-587. https://doi.org/10.1144/gsjgs.153.4.0573

Ritchie, J.D., Johnson, H., Browne, M.A.E. and Monaghan, A.A., 2003. Late Devonian–Carboniferous tectonic evolution within the Firth of Forth, Midland Valley; as revealed from 2D seismic reflection data. *Scottish Journal of Geology, 39*(2), pp.121-134. https://doi.org/10.1144/sjg39020121

Roberts, S. and Jackson, J., 1991. Active normal faulting in central Greece: an overview. Geological Society, *London, Special Publications, 56*(1), pp.125-142. https://doi.org/10.1144/GSL.SP.1991.056.01.09

Robson, A.G., King, R.C. and Holford, S.P., 2017. Structural evolution of a gravitationally detached normal fault array: Analysis of 3D seismic data from the Ceduna Sub-Basin, Great Australian Bight. *Basin Research, 29*(5), pp.605-624. https://doi.org/10.1111/bre.12191

Robson, D.A., 1977. The structural history of the Cheviot and adjacent regions. *Scottish Journal of Geology, 13*(3), pp.255-262. https://doi.org/10.1144/sjg13030255

Røe, S.L. and Steel, R., 1985. Sedimentation, sea-level rise and tectonics at the Triassic-Jurassic boundary (Statfjord Formation), Tampen Spur, northern North Sea. *Journal of Petroleum Geology, 8*(2), pp.163-186. https://doi.org/10.1111/j.1747-5457.1985.tb01009.x

Rollin, K.E., 1995. A simple heat-flow quality function and appraisal of heat-flow measurements and heat-flow estimates from the UK Geothermal Catalogue. *Tectonophysics, 244*(1-3), pp.185-196. https://doi.org/10.1016/0040-1951(94)00227-Z

Royden, L. and Keen, C.E., 1980. Rifting process and thermal evolution of the continental margin of eastern Canada determined from subsidence curves. Earth and Planetary Science Letters, 51(2), pp.343-361. https://doi.org/10.1016/0012-821X(80)90216-2

Rybach, L. 1981. Geothermal systems, conductive heat flow, geothermal anomalies. *In*: Rybach, L. and Muffler, L.J.P. (eds.), *Geothermal Systems: Principles and Case Histories.* Wiley, Chichester, 3-36.

Sánchez, M.A., García, H.P., Acosta, G., Gianni, G.M., Gonzalez, M.A., Ariza, J.P., Martinez, M.P. and Folguera, A., 2019. Thermal and lithospheric structure of the Chilean-Pampean flat-slab from gravity and magnetic data. In: *Andean Tectonics*, pp. 487-507. Elsevier.

Scheck-Wenderoth, M., Cacace, M., Maystrenko, Y.P., Cherubini, Y., Noack, V., Kaiser, B.O., Sippel, J. and Björn, L., 2014. Models of heat transport in the Central European Basin System: Effective mechanisms at different scales. *Marine and Petroleum Geology, 55*, pp.315-331. https://doi.org/10.1016/j.marpetgeo.2014.03.009

Schlische, R.W., 1991. Half-graben basin filling models: new constraints on continental extensional basin development. *Basin Research, 3*(3), pp.123-141. https://doi.org/10.1111/j.1365-2117.1991.tb00123.x

Sclater, J.G. and Christie, P.A., 1980. Continental stretching: An explanation of the post-mid-Cretaceous subsidence of the central North Sea basin. *Journal of Geophysical Research: Solid Earth, 85*(B7), pp.3711-3739. https://doi.org/10.1029/JB085iB07p03711

Shail, R.K. and Leveridge, B.E., 2009. The Rhenohercynian passive margin of SW England: Development, inversion and extensional reactivation. *Comptes Rendus Geoscience, 341*(2-3), pp.140-155. https://doi.org/10.1016/j.crte.2008.11.002

Sharp, I.R., Gawthorpe, R.L., Armstrong, B. and Underhill, J.R., 2000. Propagation history and passive rotation of mesoscale normal faults: implications for synrift stratigraphic development. *Basin Research, 12*(3-4), pp.285-305. https://doi.org/10.1111/j.1365-2117.2000.00132.x

Shaw, J., Johnston, S.T., Gutiérrez-Alonso, G. and Weil, A.B., 2012. Oroclines of the Variscan orogen of Iberia: Paleocurrent analysis and paleogeographic implications. *Earth and Planetary Science Letters, 329*, pp.60-70. https://doi.org/10.1016/j.epsl.2012.02.014

Shiells, K.A.G., 1963. XVIII.—The Geological Structure of North-East Northumberland. *Earth and Environmental Science Transactions of The Royal Society of Edinburgh, 65*(18), pp.449-481.

Sippel, J., Fuchs, S., Cacace, M., Braatz, A., Kastner, O., Huenges, E. and Scheck-Wenderoth, M., 2013. Deep 3D thermal modelling for the city of Berlin (Germany). *Environmental Earth Sciences, 70*(8), pp.3545-3566. https://doi.org/10.1007/s12665-013-2679-2

Slagstad, T., Balling, N., Elvebakk, H., Midttømme, K., Olesen, O., Olsen, L. and Pascal, C., 2009. Heat-flow measurements in Late Palaeoproterozoic to Permian geological provinces in south and central Norway and a new heat-flow map of Fennoscandia and the Norwegian–Greenland Sea. *Tectonophysics, 473*(3-4), pp.341-361. https://doi.org/10.1016/j.tecto.2009.03.007

Somerville, D.J., Mountney, N.P., Colombera, L. and Collier, R.E.L., 2019. Impact of a pre-existing transverse drainage system on active rift stratigraphy: An example from the Corinth Rift, Greece. *Basin Research, 32*(4), pp. 764-788. https://doi.org/10.1111/bre.12396

Sonder, L.J., 1990. Effects of density contrasts on the orientation of stresses in the lithosphere: Relation to principal stress directions in the Transverse Ranges, California. *Tectonics, 9*(4), pp.761-771. https://doi.org/10.1029/TC009i004p00761

Soper, N.J., England, R.W., Snyder, D.B. and Ryan, P.D., 1992. The Iapetus suture zone in England, Scotland and eastern Ireland: a reconciliation of geological and deep seismic data. *Journal of the Geological Society, 149*(5), pp.697-700. https://doi.org/10.1144/gsjgs.149.5.0697

Southern, S.J., Mountney, N.P. and Pringle, J.K., 2014. The Carboniferous Southern Pennine Basin, UK. *Geology Today, 30*(2), pp.71-78. https://doi.org/10.1111/gto.12044

Smith, K., Smith, N.J.P. and Holliday, D.W., 1985. The deep structure of Derbyshire. *Geological Journal, 20*(3), pp.215-225. https://doi.org/10.1002/gj.3350200303

Smith, N.J.P.; Kirby, G.A.; Pharaoh, T.C., 2005. *Structure and evolution of the south-west Pennine Basin and adjacent areas: subsurface memoir*. Nottingham, UK, British Geological Survey, 129 pp.

Smith, N.T., 1999. Variscan inversion within the Cheshire Basin, England: Carboniferous evolution north of the Variscan Front. *Tectonophysics*, *309*(1-4), pp.211-225. https://doi.org/10.1016/S0040-1951(99)00140-7Smith, S.A. and Holliday, D.W., 1991. The sedimentology of the middle and upper border groups (Viséan) in the stonehaugh borehole, Northumberland. *Proceedings of the Yorkshire Geological Society*, *48*(4), pp.435-446. https://doi.org/10.1144/pygs.48.4.435

Smith, T.E., 1968. The Upper Old Red Sandstone-Carboniferous junction at Burnmouth, Berwickshire. *Scottish Journal of Geology*, *4*(4), pp.349-354. https://doi.org/10.1144/sjg04040349

Song, T., 1997. Inversion styles in the Songliao basin (northeast China) and estimation of the degree of inversion. *Tectonophysics*, *283*(1-4), pp.173-188. https://doi.org/10.1016/S0040-1951(97)00147-9

Sosio, G., Campana, A., Braham, R.O., Spyrou, C., Burachok, O., Mandiuc, A., Baujard, C. and Genter, A., 2019. Mitigating risk in geothermal projects with an integrated modelling approach: A case study in France. *First Break*, *37*(7), pp.71-79. https://doi.org/10.3997/1365-2397.n0042

Spears, D.A., 2012. The origin of tonsteins, an overview, and links with seatearths, fireclays and fragmental clay rocks. *International Journal of Coal Geology*, *94*, pp.22-31. https://doi.org/10.1016/j.coal.2011.09.008

Stone, P. 2008. *Bedrock Geology UK North*. British Geological Survey 88pp. ISBN 978 085272 585 6 http://nora.nerc.ac.uk/3709/

Stone, P., Millward, D., Young, B., Merritt, J., Clarke, S., McCormac, M. and Lawrence, D., 2010. *British regional geology: Northern England. Fifth edition*. Keyworth, Nottingham: British Geological Survey.

Stone, P., McMillan, A.A., Floyd, J.D., Barnes, R.P. and Phillips, E.R., 2012. *British Regional Geology: South of Scotland. Fourth edition*. Keyworth, Nottingham: British Geological Survey.

Stein, S., Cloetingh, S., Sleep, N.H. and Wortel, R., 1989. Passive margin earthquakes, stresses and rheology. In: *Earthquakes at North-Atlantic Passive Margins: Neotectonics and Postglacial Rebound*. pp. 231-259. Springer, Dordrecht. https://doi.org/10.1007/978-94-009-2311-9_14

Stephenson, D., Loughlin, S.C., Millward, D., Waters, C.N., and Williamson, I.T., 2003. Carboniferous and Permian Igneous Rocks of Great Britain North of the Variscan Front. *Geological Conservation Review Series Number 27*, Joint Nature Conservation Committee, Peterborough.

Stow, D.A. and Shanmugam, G., 1980. Sequence of structures in fine-grained turbidites: comparison of recent deep-sea and ancient flysch sediments. *Sedimentary Geology*, *25*(1-2), pp.23-42. https://doi.org/10.1016/0037-0738(80)90052-4

Strachey, J., 1719. IV. A curious description of the strata observ'd in the coal-mines of Mendip in Somersetshire; being a letter of John Strachey Esq; to Dr. Robert Welsted, MD and RS Soc. and by him communicated to the Society. *Philosophical Transactions of the Royal Society of London*, 30(360), pp.968-973. https://doi.org/10.1098/rstl.1717.0054

Strecker, M.R., Cerveny, P., Bloom, A.L. and Malizia, D., 1989. Late Cenozoic tectonism and landscape development in the foreland of the Andes: Northern Sierras Pampeanas (26–28 S), Argentina. *Tectonics*, 8(3), pp.517-534. https://doi.org/10.1029/TC008i003p00517

Strecker, M.R., Hilley, G.E., Bookhagen, B. and Sobel, E.R., 2011. Structural, geomorphic, and depositional characteristics of contiguous and broken foreland basins: examples from the eastern flanks of the central Andes in Bolivia and NW Argentina. *Tectonics of sedimentary basins: Recent advances*, pp.508-521. https://doi.org/10.1002/9781444347166.ch25

Suriano, J., Limarino, C.O., Tedesco, A.M. and Alonso, M.S., 2015. Sedimentation model of piggyback basins: Cenozoic examples of San Juan Precordillera, Argentina. *Geological Society, London, Special Publications*, 399(1), pp.221-244. https://doi.org/10.1144/SP399.17

Ter Borgh, M.M., Eikelenboom, W. and Jaarsma, B., 2019. Hydrocarbon potential of the Visean and Namurian in the northern Dutch offshore. *Geological Society, London, Special Publications*, 471(1), pp.133-153. https://doi.org/10.1144/SP471.5

Terrington, R.L. and Thorpe, S., 2014. Metadata report for the Northumberland and Solway Basin 1:250 000 geological model. British Geological Survey Open Report, OR/13/049. 20pp. http://nora.nerc.ac.uk/id/eprint/507069/1/OR13049.pdf

Thirlwall, M.F., 1988. Geochronology of Late Caledonian magmatism in northern Britain. *Journal of the Geological Society*, 145(6), pp.951-967. https://doi.org/10.1144/gsjgs.145.6.0951

Trewin, N.H. and Holdsworth, B.K., 1973. Sedimentation in the lower Namurian rocks of the North Staffordshire Basin. *Proceedings of the Yorkshire Geological Society*, 39(3), pp.371-408. https://doi.org/10.1144/pygs.39.3.371

Trotter, F.M. and Hollingworth, S.E., 1928. The Alston Block. *Geological Magazine*, 65(10), pp.433-448. https://doi.org/10.1017/S0016756800108337

Tucker, M.E., 2003. Mixed clastic–carbonate cycles and sequences: Quaternary of Egypt and Carboniferous of England. *Geologia Croatica*, 56(1), pp.19-37.

Turner, B.R. and Monro, M., 1987. Channel formation and migration by mass-flow processes in the Lower Carboniferous fluviatile Fell Sandstone Group, northeast England. *Sedimentology*, 34(6), pp.1107-1122. https://doi.org/10.1111/j.1365-3091.1987.tb00595.x

Turner, B.R., Younger, P.L. and Fordham, C.E., 1993. Fell Sandstone lithostratigraphy south-west of Berwick-upon-Tweed: implications for the regional development of the Fell Sandstone. *Proceedings of the Yorkshire Geological Society*, 49(4), pp.269-281. https://doi.org/10.1144/pygs.49.4.269

Turner, B.R., Dewey, C. and Fordham, C.E., 1997. Marine ostracods in the Lower Carboniferous fluviatile Fell Sandstone Group: evidence for base level change and marine flooding of the central graben, Northumberland Basin. *Proceedings of the Yorkshire Geological Society, 51*(4), pp.297-306. https://doi.org/10.1144/pygs.51.4.297

Underhill, J.R., Gayer, R.A., Woodcock, N.H., Donnelly, R., Jolley, E. & Stimpson, I.G. 1988. The Dent Fault, northern England - reinterpreted as a major oblique slip fault zone. Journal of the Geological Society, 145, 313-316.

Underhill, J.R. and Brodie, J.A., 1993. Structural geology of Easter Ross, Scotland: implications for movement on the Great Glen fault zone. *Journal of the Geological Society, 150*(3), pp.515-527. https://doi.org/10.1144/gsjgs.150.3.0515

Underhill, J.R., Monaghan, A.A. and Browne, M.A., 2008. Controls on structural styles, basin development and petroleum prospectivity in the Midland Valley of Scotland. Marine and *Petroleum Geology, 25*(10), pp.1000-1022. https://doi.org/10.1016/j.marpetgeo.2007.12.002

Upton, B.G.J., Stephenson, D., Smedley, P.M., Wallis, S.M. and Fitton, J.G., 2004. Carboniferous and Permian magmatism in Scotland. *Geological Society, London, Special Publications, 223*(1), pp.195-218. https://doi.org/10.1144/GSL.SP.2004.223.01.09

Varker, W.J. and Higgins, A.C., 1979. Conodont evidence for the age of the Pinskey Gill Beds of Ravenstonedale, north-west England. *Proceedings of the Yorkshire Geological Society, 42*(3), pp.357-369. https://doi.org/10.1144/pygs.42.3.357

Verrall, P., 1982. Structural interpretation with applications to North Sea problems: Geological Society of London Course Notes No 3. *JAPEC* (UK).

Vilà, M., Fernández, M. and Jiménez-Munt, I., 2010. Radiogenic heat production variability of some common lithological groups and its significance to lithospheric thermal modeling. *Tectonophysics*, 490(3-4), pp.152-164. https://doi.org/10.1016/j.tecto.2010.05.003

Vincent, C.J., 2015. Maturity modelling of selected wells in the Central North Sea. *British Geological Survey Internal Report*, CR/15/122. 193pp. http://nora.nerc.ac.uk/id/eprint/516764/1/CR15122.pdf

Wagner, R.H., 1983. A lower Rotliegend flora from Ayrshire. *Scottish Journal of Geology, 19*(2), pp.135-155. https://doi.org/10.1144/sjg19020135

Waldron, J.W., Giles, P.S. and Thomas, A.K., 2017. Correlation chart for Late Devonian to Permian stratified rocks of the Maritimes Basin, Atlantic Canada. *Nova Scotia Department of Energy Open File Report*, 2017-02.

Waltham, A.C., 1970. Shale units in the Great Scar Limestone of the southern Askrigg Block. *Proceedings of the Yorkshire Geological Society, 38*(2), pp.285-292. https://doi.org/10.1144/pygs.38.2.285

Ward, J., 1997. Early Dinantian evaporites of the Easton-1 well, Solway basin, onshore, Cumbria, England. *Geological Society, London, Special Publications, 124*(1), pp.277-296. https://doi.org/10.1144/GSL.SP.1997.124.01.17

Waschbusch, P. and Beaumont, C., 1996. Effect of a retreating subduction zone on deformation in simple regions of plate convergence. *Journal of Geophysical Research: Solid Earth*, *101*(B12), pp.28133-28148. https://doi.org/10.1029/96JB02482

Waters, C N, Browne, M A E, Dean, M T, and Powell, J H, 2007. Lithostratigraphical framework for Carboniferous successions of Great Britain (Onshore). *British Geological Survey Research Report*, RR/07/01. 60pp. http://nora.nerc.ac.uk/id/eprint/3235/1/RR07001.pdf

Waters, C.N., Somerville, I.D., Jones, N.S., Cleal, C.J., Collinson, J.D., Waters, R.A., Besly, B.M., Dean, M.T., Stephenson, M.H., Davies, J.R. and Freshney, E.C., 2011. A revised correlation of Carboniferous rocks in the British Isles. *Geological Society of London Special Report*, No. 26.

Waters, C.N., Holliday, D.W. and Chisholm, J.I., 2020. The contribution of publications of the Yorkshire Geological Society to the understanding of the geological development of the Carboniferous Pennine Basin, northern England. *Proceedings of the Yorkshire Geological Society*, *63*(1), pp.1-32. https://doi.org/10.1144/pygs2018-019

Watts, A.B., 1978. An analysis of isostasy in the world's oceans 1. Hawaiian-Emperor seamount chain. *Journal of Geophysical Research: Solid Earth*, *83*(B12), pp.5989-6004. https://doi.org/10.1029/JB083iB12p05989

Watts, A.B., Bodine, J.H. and Steckler, M.S., 1980. Observations of flexure and the state of stress in the oceanic lithosphere. *Journal of Geophysical Research: Solid Earth*, *85*(B11), pp.6369-6376. https://doi.org/10.1029/JB085iB11p06369

Watts, A.B. and Zhong, S., 2000. Observations of flexure and the rheology of oceanic lithosphere. *Geophysical Journal International*, *142*(3), pp.855-875. https://doi.org/10.1046/j.1365-246x.2000.00189.x

Watts, A.B., 2001. *Isostasy and Flexure of the Lithosphere*. Cambridge University Press.

Weissmann, G.S., Hartley, A.J., Nichols, G.J., Scuderi, L.A., Olson, M., Buehler, H. and Banteah, R., 2010. Fluvial form in modern continental sedimentary basins: distributive fluvial systems. *Geology*, *38*(1), pp.39-42. https://doi.org/10.1130/G30242.1

Wernicke, B., 1985. Uniform-sense normal simple shear of the continental lithosphere. *Canadian Journal of Earth Sciences*, *22*(1), pp.108-125. https://doi.org/10.1139/e85-009

Whitbread, K., Ellen, R., Callaghan, E., Gordon, J.E. and Arkley, S., 2015. East Lothian Geodiversity Audit. *British Geological Survey Open Report*, OR/14/063. 192pp. http://nora.nerc.ac.uk/id/eprint/509518/1/OR14063.pdf

White, N.J., Jackson, J.A. and McKenzie, D.P., 1986. The relationship between the geometry of normal faults and that of the sedimentary layers in their hanging walls. *Journal of Structural Geology*, *8*(8), pp.897-909. https://doi.org/10.1016/0191-8141(86)90035-0

White, N. and McKenzie, D., 1988. Formation of the" steer's head" geometry of sedimentary basins by differential stretching of the crust and mantle. Geology, 16(3), pp.250-253. https://doi.org/10.1130/0091-7613(1988)016<0250:FOTSSH>2.3.CO;2

Whittaker, A.C., Attal, M. and Allen, P.A., 2010. Characterising the origin, nature and fate of sediment exported from catchments perturbed by active tectonics. *Basin Research*, *22*(6), pp.809-828. https://doi.org/10.1111/j.1365-2117.2009.00447.x

Wignall, P.B. and Best, J.L., 2000. The western Irish Namurian basin reassessed. Basin Research, 12(1), pp.59-78. https://doi.org/10.1046/j.1365-2117.2000.00113.x

Williams, G.D., Powell, C.M. and Cooper, M.A., 1989. Geometry and kinematics of inversion tectonics. *Geological Society, London, Special Publications*, *44*(1), pp.3-15. https://doi.org/10.1144/GSL.SP.1989.044.01.02

Wilson, R.B., 1974. A study of the Dinantian marine faunas of south-east Scotland. *Bulletin of the Geological Survey of Great Britain 46*, 35-65

Woodcock, N.H. and Strachan, R.A., 2009. *Geological history of Britain and Ireland*. John Wiley & Sons.

Wright, V.P., 1986. Facies sequences on a carbonate ramp: the Carboniferous Limestone of South Wales. *Sedimentology*, *33*(2), pp.221-241. https://doi.org/10.1111/j.1365-3091.1986.tb00533.x

Young, G.M. and Caldwell, W.G.E., 2011. Early Carboniferous stratigraphy in the Firth of Clyde area: new information from the Isle of Bute. *Scottish Journal of Geology*, *47*(2), pp.143-156. https://doi.org/10.1144/0036-9276/01-431

Young, G.M. and Caldwell, W.G.E., 2019. The South Kintyre Basin: its role in the stratigraphical and structural evolution of the Firth of Clyde region during the Devonian–Carboniferous transition. *Scottish Journal of Geology*, *55*(2), pp.141-154. https://doi.org/10.1144/sjg2019-001

Younger, P.L., Manning, D.A., Millward, D., Busby, J.P., Jones, C.R. and Gluyas, J.G., 2016. Geothermal exploration in the Fell Sandstone Formation (Mississippian) beneath the city centre of Newcastle upon Tyne, UK: the Newcastle Science Central deep geothermal borehole. *Quarterly Journal of Engineering Geology and Hydrogeology*, *49*(4), pp.350-363. https://doi.org/10.1144/qjegh2016-053

Zervos, F., 1987. A compilation and regional interpretation of the northern North Sea gravity map. *Geological Society, London, Special Publications*, *28*(1), pp.477-493. https://doi.org/10.1144/GSL.SP.1987.028.01.30

Zhang, X., Lyu, D., Li, P., Jin, X., Liaw, P.K. and Keer, L.M., 2019. A closed-form solution for the horizontally aligned thermal-porous spheroidal inclusion in a half-space and its applications in geothermal reservoirs. *Computers & Geosciences*, *122*, pp.15-24. https://doi.org/10.1016/j.cageo.2018.10.001

Ziegler, P. A., and van Hoom, B., 1989. Evolution of North Sea rift system, In: *Extensional tectonics and stratigraphy of North Atlantic margins: American Association of Petroleum Geologists Memoir 46*, p. 471-501.

Ziegler, P.A., 1990. Tectonic and palaeogeographic development of the North sea rift system. In: Blundell, D. J. and Gibbs, A. D. (eds.) *Tectonic Evolution of the North Sea Rifts*. Oxford Science Publications, Oxford 1-36.

Ziegler, P.A., 1992. North Sea rift system. *Tectonophysics, 208*(1-3), pp.55-75. https://doi.org/10.1016/0040-1951(92)90336-5

Ziegler, P.A., Cloetingh, S. and van Wees, J.D., 1995. Dynamics of intra-plate compressional deformation: the Alpine foreland and other examples. *Tectonophysics, 252*(1-4), pp.7-59. https://doi.org/10.1016/0040-1951(95)00102-6

Ziegler, P.A. and Cloetingh, S., 2004. Dynamic processes controlling evolution of rifted basins. *Earth-Science Reviews, 64*(1-2), pp.1-50. https://doi.org/10.1016/S0012-8252(03)00041-2

Zoback, M.L., 1992. First-and second-order patterns of stress in the lithosphere: The World Stress Map Project. *Journal of Geophysical Research: Solid Earth, 97*(B8), pp.11703-11728. https://doi.org/10.1029/92JB00132

Appendices

Supplementary data table 1: Major element geochemical (XRF) data for Chapter 5

Sample	Basin	Ba (ppm) Meas.	Error +/-	Nb (ppm) Meas.	Error +/-	Zr (ppm) Meas.	Error +/-	Sr (ppm) Meas.	Error +/-	Rb (ppm) Meas.	Error +/-
SC-01	Tweed	309	122	bdl		106	2	9	3	bdl	
SC-02	Tweed	323	113	bdl		62	1	8	4	bdl	
SC-03	Tweed	326	109	bdl		43	1	8	3	8	2
SC-04	Tweed	310	120	bdl		41	1	9	2	bdl	
SC-05	Tweed	313	120	3	1	202	2	12	2	bdl	
SC-06	Tweed	311	125	bdl		117	2	13	2	6	2
SC-07	Tweed	326	103	bdl		104	1	7	4	bdl	
SC-08	Tweed	303	147	bdl		138	2	8	3	bdl	
SC-09	Tweed	313	126	bdl		138	2	9	3	bdl	
SC-10	Tweed	326	106	bdl		123	2	5		bdl	
SC-11	Tweed	302	137	bdl		80	1	9	3	bdl	
SC-12	Tweed	320	124	bdl		215	2	9	3	bdl	
SC-13	Tweed	296	132	bdl		97	1	8	3	bdl	
SC-14	Tweed	321	107	bdl		80	1	8	4	bdl	
SC-15	Tweed	334	94	bdl		75	1	9	3	bdl	
MUR-01	Tweed	343	91	bdl		53	1	12	2	10	2
MUR-02	Tweed	334	104	2	1	102	2	9	3	9	2
MUR-03	Tweed	350	89	bdl		57	1	11	2	8	2
MUR-04	Tweed	373	79	bdl		87	1	14	2	10	2
MUR-05	Tweed	381	79	bdl		82	1	14	2	11	1
MUR-06	Tweed	319	118	bdl		79	1	8	3	6	2
MUR-07	Tweed	311	122	bdl		58	1	8	3	5	3
MUR-08	Tweed	434	67	3	1	237	2	17	1	25	1

MUR-09	Tweed	347	92	bdl		74	1	11	2	8	2
MUR-10	Tweed	318	49	bdl	1	46	2	12	1	7	1
MUR-11	Tweed	349	66	bdl	1	101	2	12	1	8	1
MUR-12	Tweed	419	113	bdl		52	1	16	2	17	2
DR-01	Northumberland	650	96	2		121	1	42	2	37	2
DR-02	Northumberland	460	68	5		227	1	31	2	23	1
DR-03	Northumberland	374	78	bdl		180	2	13	2	9	2
DR-04	Northumberland	424	77	4	1	79	1	22	1	15	1
DR-05	Northumberland	445	70	bdl		48	1	22	1	18	1
DR-06	Northumberland	460	63	bdl		65	1	29	1	19	1
DR-07	Northumberland	423	72	bdl		63	1	23	1	12	1
ST-1309	Northumberland	363	92	bdl		46	1	32	1	5	3
ST-1380	Northumberland	348	95	bdl		103	2	45	1	6	2
ST-1406	Northumberland	341	93	bdl		37	1	20	1	bdl	
ST-1412	Northumberland	350	87	bdl		44	1	28	1	5	3
ST-1420	Northumberland	337	95	bdl		39	1	27	1	bdl	
ST-1434	Northumberland	292	145	3	1	168	2	29	1	bdl	
ST-1436	Northumberland	342	94	bdl		91	1	23	1	bdl	
ST-1447	Northumberland	356	84	bdl		48	1	26	1	5	3
ST-1454	Northumberland	369	82	2	1	68	1	49	1	bdl	
ST-1461	Northumberland	457	64	4	1	416	3	47	1	14	1
ST-1466	Northumberland	348	89	bdl		42	1	25	1	6	2
ST-1525	Northumberland	541	54	4		293	3	55	1	24	1
ST-1545	Northumberland	345	89			37	1	22	1	bdl	
ST-1553	Northumberland	440	62	bdl		56	1	43	1	7	2
ST-1579	Northumberland	383	74	2	1	150	2	23	1	5	2
ST-1719	Northumberland	430	65	bdl		136	2	34	1	6	2
ST-1924	Northumberland	5029	56	bdl		36	1	190	2	5	3
HA-4922	Alston	400	72	bdl		66	1	20	1	20	1
HA-5651	Alston	466	67	2	1	23	1	44	1	7	2
HA-5658	Alston	404	76	bdl		101	2	58	2	13	1

HA-5697	Alston	457	61	bdl	37	1	39	1	21	1
HA-5703	Alston	686	47	bdl	35	1	30	1	29	1
HA-5719	Alston	407	76	bdl	40	1	46	1	14	1
HA-5752	Alston	368	82	bdl	64	1	20	1	11	1
HA-5764	Alston	432	69	bdl	36	1	32	1	29	1
HA-5774	Alston	284	163	bdl	42	1	42	1	13	1
HA-5783	Alston	474	61	bdl	28	1	40	1	20	1
HA-5793	Alston	370	84	bdl	151	2	23	1	11	1
HA-5798	Alston	401	72	2	1	204	2	40	1	14	1

Supplementary data table 1: Concentrations of selected elements in parts per million (ppm) for sandstone samples belonging to the Fell Sandstone

Formation across the northern Pennine Basin. Bdl = below limit of detection.

Supplementary data table 2: Trace elemental geochemical (XRF) data for Chapter 5

		Fe2O3 (wt. %)		TiO2 (wt. %)		CaO (wt. %)		K2O (wt. %)		Al2O3 (wt. %)		SiO2 (wt. %)	
			Error		Error		Error		Error		Error		Error
Sample	Basin	Meas.	+/-	Meas.	+/-	Meas.	+/-	Meas.	+/-	Meas.	+/-	Meas.	+/-
SC-01	Tweed	0.08	0.00	0.10	0.00	0.08	0.01	bdl		3.98	0.19	69.98	0.24
SC-02	Tweed	0.09	0.00	0.07	0.00	bdl		bdl		2.52	0.21	78.66	0.25
SC-03	Tweed	2.24	0.01	0.08	0.00	bdl		0.04	0.00	5.27	0.19	68.16	0.23
SC-04	Tweed	0.03	0.00	0.07	0.00	bdl		bdl		5.42	0.19	74.91	0.24
SC-05	Tweed	0.04	0.00	0.11	0.00	bdl		bdl		2.76	0.20	80.23	0.24
SC-06	Tweed	1.13	0.01	0.14	0.00	bdl		0.01	0.00	6.31	0.20	61.83	0.23
SC-07	Tweed	0.18	0.00	0.11	0.00	bdl		bdl		4.99	0.19	79.07	0.24
SC-08	Tweed	0.09	0.00	0.17	0.00	bdl		bdl		3.69	0.20	60.37	0.25
SC-09	Tweed	0.21	0.01	0.17	0.00	bdl		bdl		4.11	0.19	63.24	0.24
SC-10	Tweed	0.68	0.01	0.13	0.00	bdl		bdl		9.33	0.22	61.11	0.23
SC-11	Tweed	0.06	0.00	0.09	0.00	bdl		bdl		4.29	0.18	76.94	0.24

SC-12	Tweed	0.16	0.00	0.10	0.00	bdl		bdl		3.69	0.19	73.96	0.24
SC-13	Tweed	0.03	0.00	0.09	0.00	bdl		bdl		3.91	0.18	80.37	0.23
SC-14	Tweed	0.04	0.00	0.10	0.00	bdl		bdl		6.84	0.19	68.14	0.23
SC-15	Tweed	0.27	0.01	0.11	0.00	bdl		bdl		5.24	0.18	77.13	0.24
MUR-01	Tweed	0.18	0.00	0.05	0.00	bdl		0.33	0.01	7.01	0.20	69.80	0.23
MUR-02	Tweed	0.33	0.01	0.16	0.00	bdl		0.04	0.00	7.59	0.21	64.75	0.24
MUR-03	Tweed	0.19	0.00	0.10	0.00	bdl		0.30	0.01	4.15	0.18	73.15	0.24
MUR-04	Tweed	0.18	0.00	0.10	0.00	bdl		0.25	0.01	5.12	0.18	74.28	0.24
MUR-05	Tweed	0.14	0.00	0.13	0.00	bdl		0.25	0.01	4.65	0.19	74.24	0.24
MUR-06	Tweed	0.07	0.00	0.18	0.00	bdl		bdl		5.61	0.20	72.65	0.25
MUR-07	Tweed	0.42	0.01	0.09	0.00	bdl		bdl		7.14	0.20	67.73	0.24
MUR-08	Tweed	1.14	0.01	0.21	0.00	0.03	0.00	0.50	0.01	6.27	0.20	68.75	0.24
MUR-09	Tweed	0.16	0.00	0.15	0.00	bdl		0.34	0.01	4.19	0.18	74.27	0.25
MUR-10	Tweed	0.29	0.00	0.08	0.00	bdl		0.09	0.02	4.39	0.22	70.22	0.24
MUR-11	Tweed	0.19	0.01	0.16	0.00	bdl		0.12	0.02	3.24	0.21	69.34	0.24
MUR-12	Tweed	0.55	0.01	0.08	0.00	bdl		0.94	0.00	9.46	0.18	61.57	0.24
DR-01	Northumberland	0.17	0.00	0.16	0.00	bdl		1.55	0.00	7.16	0.20	70.73	0.24
DR-02	Northumberland	0.62	0.01	0.21	0.00	bdl		1.26	0.01	5.88	0.23	59.34	0.23
DR-03	Northumberland	0.04	0.00	0.13	0.00	bdl		0.37	0.01	7.56	0.21	71.39	0.25
DR-04	Northumberland	0.50	0.01	0.15	0.00	bdl		0.62	0.01	4.04	0.21	56.97	0.25
DR-05	Northumberland	0.46	0.01	0.06	0.00	bdl		0.92	0.01	7.15	0.23	61.18	0.24
DR-06	Northumberland	0.08	0.00	0.12	0.00	bdl		0.91	0.01	6.19	0.20	71.38	0.24
DR-07	Northumberland	0.53	0.01	0.15	0.00	bdl		0.46	0.01	5.00	0.19	69.29	0.24
ST-1309	Northumberland	0.60	0.01	0.04	0.00	3.13	0.03	bdl		2.73	0.23	93.54	0.24
ST-1380	Northumberland	0.56	0.01	0.08	0.00	3.48	0.04	bdl		2.71	0.24	90.46	0.25
ST-1406	Northumberland	0.29	0.01	0.05	0.00	0.44	0.01	bdl		2.47	0.23	99.77	0.24
ST-1412	Northumberland	0.30	0.01	0.11	0.00	0.29	0.01	bdl		4.50	0.19	95.92	0.24
ST-1420	Northumberland	0.28	0.01	0.02	0.00	0.73	0.02	bdl		3.70	0.20	90.67	0.24
ST-1434	Northumberland	0.44	0.01	0.06	0.00	0.19	0.01	bdl		4.86	0.19	92.26	0.24
ST-1436	Northumberland	0.40	0.01	0.08	0.00	0.56	0.01	bdl		3.36	0.19	88.19	0.25
ST-1447	Northumberland	0.20	0.00	0.03	0.00	0.25	0.01	bdl		3.57	0.19	89.56	0.24

ST-1454	Northumberland	0.95	0.01	0.05	0.00	2.64	0.03	bdl		2.80	0.23	91.19	0.24
ST-1461	Northumberland	1.39	0.01	0.19	0.00	0.99	0.02	0.23	0.01	5.41	0.21	87.75	0.25
ST-1466	Northumberland	0.45	0.01	0.03	0.00	0.93	0.02	bdl		3.69	0.20	97.69	0.24
ST-1525	Northumberland	0.69	0.01	0.19	0.00	1.15	0.02	0.56	0.01	5.63	0.20	85.98	0.25
ST-1545	Northumberland	0.22	0.01	0.03	0.00	0.39	0.01	bdl		3.60	0.19	93.10	0.24
ST-1553	Northumberland	0.27	0.01	0.03	0.00	0.58	0.01	0.02	0.00	5.53	0.20	91.91	0.24
ST-1579	Northumberland	0.49	0.01	0.13	0.00	0.39	0.01	bdl		2.85	0.21	95.57	0.24
ST-1719	Northumberland	0.43	0.01	0.06	0.00	0.84	0.02	bdl		3.99	0.20	92.27	0.24
ST-1924	Northumberland	0.96	0.01	0.07	0.01	2.36	0.03	bdl		2.47	0.25	96.94	0.24
HA-4922	Alston	0.69	0.01	0.02	0.00	0.16	0.01	0.48	0.01	3.78	0.20	94.35	0.24
HA-5651	Alston	0.39	0.01	0.04	0.00	9.14	0.06	0.24	0.01	3.19	0.24	66.98	0.24
HA-5658	Alston	0.29	0.01	0.06	0.00	0.38	0.01	0.71	0.01	4.62	0.20	74.31	0.25
HA-5697	Alston	0.16	0.00	0.03	0.00	0.40	0.01	0.79	0.01	4.00	0.20	87.00	0.24
HA-5703	Alston	0.25	0.01	0.01	0.00	0.05	0.01	1.03	0.01	4.17	0.20	96.41	0.25
HA-5719	Alston	1.04	0.01	0.03	0.00	5.52	0.05	0.56	0.01	4.05	0.23	72.21	0.24
HA-5752	Alston	0.47	0.01	0.06	0.00	1.32	0.02	0.36	0.01	3.51	0.21	85.63	0.24
HA-5764	Alston	0.55	0.01	0.03	0.00	0.43	0.02	1.88	0.02	5.10	0.21	76.43	0.24
HA-5774	Alston	0.33	0.01	0.02	0.00	3.19	0.03	0.31	0.01	3.32	0.22	94.43	0.24
HA-5783	Alston	0.49	0.01	0.03	0.00	2.00	0.03	0.88	0.01	4.55	0.22	80.44	0.24
HA-5793	Alston	0.27	0.01	0.09	0.00	0.76	0.02	0.39	0.01	3.74	0.21	81.79	0.24
HA-5798	Alston	0.51	0.01	0.09	0.00	2.23	0.03	0.24	0.01	3.27	0.21	93.56	0.24

Supplementary data table 2: Concentrations of selected element oxides in weight per cent (wt. %) for sandstone samples belonging to the Fell Sandstone Formation across the northern Pennine Basin. Bdl = below limit of detection.